

2016

Catalytically active metal complexes supported by cyclopentadiene and mesoporous silica

Naresh Eedugurala
Iowa State University

Follow this and additional works at: <https://lib.dr.iastate.edu/etd>

 Part of the [Chemistry Commons](#)

Recommended Citation

Eedugurala, Naresh, "Catalytically active metal complexes supported by cyclopentadiene and mesoporous silica" (2016). *Graduate Theses and Dissertations*. 16714.
<https://lib.dr.iastate.edu/etd/16714>

This Dissertation is brought to you for free and open access by the Iowa State University Capstones, Theses and Dissertations at Iowa State University Digital Repository. It has been accepted for inclusion in Graduate Theses and Dissertations by an authorized administrator of Iowa State University Digital Repository. For more information, please contact digirep@iastate.edu.

Catalytically active metal complexes supported by cyclopentadiene and mesoporous silica

by

Naresh Eedugurala

A dissertation submitted to the graduate faculty
in partial fulfillment of the requirements for the degree of

DOCTOR OF PHILOSOPHY

Major: Chemistry

Program of Study Committee:
Aaron D. Sadow, Major Professor
Marek Pruski
Javier Vela-Becerra
L. Keith Woo
Levi M. Stanley

Iowa State University

Ames, Iowa

2016

Copyright © Naresh Eedugurala, 2016. All rights reserved.

To my dad, mom, wife and daughter

TABLE OF CONTENTS

	Page
ACKNOWLEDGMENTS	v
ABSTRACT.....	vii
CHAPTER 1. GENERAL INTRODUCTION	1
CHAPTER 2. MESOPOROUS SILICA-SUPPORTED AMIDOZIRCONIUM-CATALYZED CARBONYL HYDROBORATION.....	9
Abstract	9
Introduction	10
Results and discussion	13
Conclusion	46
Experimental	48
References	64
CHAPTER 3. β -SiH-CONTAINING TRIS(SILAZIDO) RARE EARTH COMPLEXES AS HOMOGENEOUS AND GRAFTED SINGLE-SITE CATALYST PRECURSORS FOR HYDROAMINATION.....	67
Abstract	67
Introduction	68
Results and discussion	72
Conclusion	94
Experimental	97
References	112
CHAPTER 4. CYCLOPENTADIENYL BIS(OXAZOLINE) MAGNESIUM AND ZIRCONIUM COMPLEXES IN AMINOALKENE HYDROAMINATION.....	114
Abstract	114
Introduction	115
Results and discussion	118
Conclusion	136
Experimental	138
References	147

CHAPTER 5. SYNTHESIS AND CHARACTERIZATION OF TRIS(OXAZOLINYL) BORATO COPPER(II) AND COPPER(I) COMPLEXES.	150
Abstract	150
Introduction	150
Results and discussion	152
Conclusion	165
Experimental	166
References	172
 CHAPTER 6. GENERAL CONCLUSIONS.....	 174

ACKNOWLEDGMENTS

I deeply appreciate many individuals who have supported and continually encouraged me throughout my PhD life at Iowa State University. Without their time, attention, encouragement, and patience, I would not have been able to see it through.

First, I would like to wholeheartedly thank my Ph.D. advisor Prof. Aaron D. Sadow, for giving me an opportunity to work in his research group under his guidance, with suggestions throughout all my years of graduate school. You have set an example of excellence as a researcher, mentor, instructor and role model. I am also very grateful to Aaron for his scientific advice, knowledge and many insightful discussions and suggestions. His guidance helped me in all the time of research and writing this thesis. I could not have imagined having a better advisor and mentor for my PhD study.

Beside my advisor, I would like to thank all of my POS committee members Prof. Marek Pruski, Prof. Javier Vela, Prof. Keith Woo, Prof. Levi Stanley and Prof. Andreja Bakac for their valuable support, advice and time.

I would also like to thank my past and present group members in the Sadow group: Especially, I am grateful to James, Kuntal, Isaac and Kaking for their valuable suggestions during my initial days of Ph.D life in the Sadow group. Special thanks to Dr. Dunne for helping me setup a new Schlenk line and Dr. Ho for teaching me how to use the Schlenk line and for his assistance in helping perform my first and successful reaction in the Sadow Group. I thank undergraduate students Alexander Porter and Erik burton Schiferle, who had conducted research with me in Sadow lab.

I thank all the members of the CBS catalysis program in Ames Laboratory. I enjoyed working as part of this collaborative research project under the CBS Catalysis program. I would like to thank Dr. Igor I. Slowing and the Slowing group members for our collaboration for the synthesis of heterogeneous catalysts supported by mesoporous silica. Thanks to Dr. Takeshi Kobayashi and Zhuoran Wang for their valuable time spent collecting solid-state NMR data for my samples for our collaboration project. I also thank Prof. Marek Pruski for our collaboration.

I thank all the chemical instrument services, glass shop, Chemistry Stores and machine shop in the chemistry department. Thanks to Dr. Shu Xu and Dr. Sarah Cady for helping me with several NMR experiments and EPR experiments for my research. I would like to thank the Ames Laboratory and Iowa State University for funding and support of my research. I would also like to thank the funding sources with the research being supported by the U.S. Department of Energy, Office of Basic Energy Science Division of Chemical Science, Geoscience, and Bioscience through Ames Laboratory.

Last, but not least, I would like to thank my family, starting with my wife Anupama Burra for her understanding and love during the past few years. Her support and encouragement was in the end what made this dissertation possible. I thank my parents Sulochana and Ramachandram for the love, understanding, and support throughout my education. It was under their watchful eye that I gained inspiration and an ability to tackle challenges head on.

Finally, I would like to thank my four-year-old princess and sweet daughter Ashritha and please forgive me for not being with you these four years.

ABSTRACT

In this work, a new class of cyclopentadiene-bis(oxazoline) compounds and their piano-stool-type organometallic compounds are prepared as catalysts for hydroamination of aminoalkenes. The two compounds $\text{MeC}(\text{Ox}^{\text{Me}_2})_2\text{C}_5\text{H}_5$ ($\text{Bo}^{\text{M}}\text{CpH}$; Ox^{Me_2} = 4,4-dimethyl-2-oxazoline) and $\text{MeC}(\text{Ox}^{\text{Me}_2})_2\text{C}_5\text{Me}_4\text{H}$ ($\text{Bo}^{\text{M}}\text{Cp}^{\text{tet}}\text{H}$) are synthesized from $\text{C}_5\text{R}_4\text{HI}$ ($\text{R} = \text{H}, \text{Me}$) and $\text{MeC}(\text{Ox}^{\text{Me}_2})_2\text{Li}$. Synthesis of $\{\text{Bo}^{\text{M}}\text{Cp}\}\text{MgMe}$, $\{\text{Bo}^{\text{M}}\text{Cp}^{\text{tet}}\}\text{MgMe}$ and $\{\text{Bo}^{\text{M}}\text{Cp}^{\text{tet}}\}\text{Zr}(\text{NMe}_2)_2$ and their catalysis for the hydroamination/cyclization of aminoalkenes under mild conditions are presented. Also, the heterogeneous catalysts for hydroboration of carbonyl compounds and hydroamination/cyclization of aminoalkenes are discussed. The catalysts are prepared by the reaction of metal amides and mesoporous silica (MSN, 10nm). The catalysts are further characterized by stoichiometry of synthesis through quantification of byproducts, FTIR, ^{13}C -CP/MAS, ^{13}C -DP/MAS, ^{29}Si -CP, DP/MAS and elemental analysis (ICP-OES and CHN). Efficiency of newly developed catalysts in the hydroboration carbonyl compounds and hydroamination of aminoalkenes is discussed in detail. Finally, a comparative study between homogeneous and heterogeneous is presented.

CHAPTER 1: GENERAL INTRODUCTION

Industrial chemical processes depend on homogeneous and heterogeneous catalysis. During homogeneous catalysis the catalyst and the reactants are in the same phase while in heterogeneous catalysis the catalyst and the reactants are in a different phase. Homogeneous transition-metal catalysts are chemically well-defined, active at lower temperatures and afford higher selectivity. Additionally, all the active sites are known and the uniform structure allows developing more stable catalysts. However the widespread applicability of homogeneous catalysts is limited by factors such as the low stability of metal complexes during catalysis and difficulties in catalyst separation from the reaction mixture. On the other hand, heterogeneous catalysts are easy to separate and recover from the reaction mixture (Figure 1.1). However, heterogeneous catalysts are limited by the underutilization of the active metal components during catalysis, as only a small fraction of the available active sites are accessible on the surface of the catalyst to the substrates. Hence considerable efforts have been directed to combine the best aspects of homogeneous and heterogeneous catalysts in order to generate heterogeneous catalysts with well-defined active sites (so-called “single-site catalysts”). A major goal of the work described in this thesis is to explore the facile synthesis and efficient recyclability of single site catalysts. A second goal, which represents the second part of this thesis, is to control the coordination environment of soluble catalysts with new ligands and in new complexes, and develop their chemistry. This introduction focuses on the single-site catalyst and catalysis development.

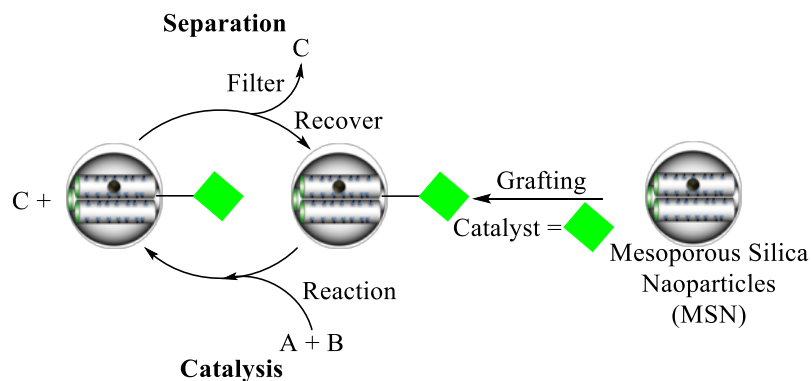


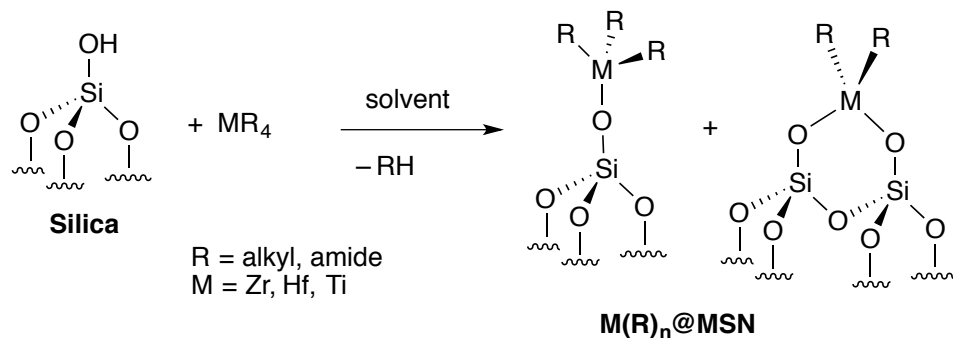
Figure 1.1. Synthesis of a single-site heterogeneous catalyst and possible separation technique.

In heterogeneous catalysis, development of catalysts that influence selectivity in catalysis remains a challenge. Additionally, heterogeneous catalysts have not achieved optimum performance primarily due to leaching of active metal species from the support leading to inefficient recycling. Overcoming these obstacles are necessary for applying heterogeneous catalysts to large-scale chemical applications.¹ Our target is the facile synthesis of heterogeneous catalysts with effective recyclability via strong interactions between the catalytically active sites and their intended supports. Polymeric and hybrid organic-inorganic materials can serve as ideal supports to realize these goals. There are few heterogeneous catalysts reported using polymer supports, which has disadvantages such as swelling and leaching in organic solvents.^{2a,b,c} Organic-inorganic hybrid materials such as mesoporous materials are used as an alternative support that have many advantages over organic polymer based catalysts. These materials show excellent stability in organic solvents, in which hybrid materials do not swell, and leaching can be avoided. Mesoporous materials are porous materials with unidimensional mesopores (2-50 nm in diameter) and their large surface areas make them useful as adsorbents or catalysts. Mesoporous materials are useful

solid supports for transition metal complexes, due to architectural properties such as optimum pore sizes, high surface area, stability and reactive isolated/hydrogen bonded surface silanol (-OH) groups.^{3a,b} Thus, mesoporous material were selected as solid supports for the synthesis of surface organometallic catalysts.

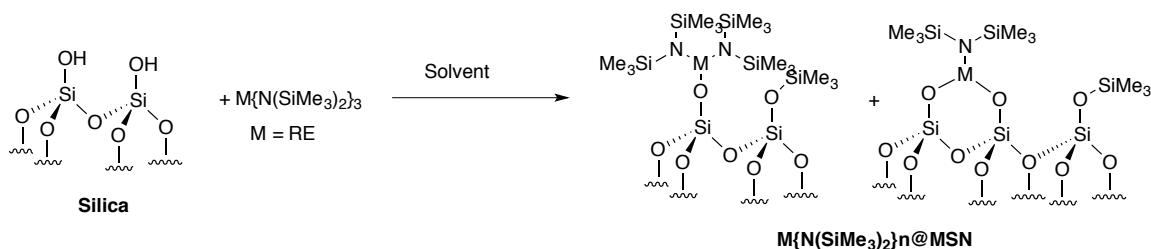
Surface organometallic chemistry (SOMC) is a powerful approach to post-synthetically incorporate metal centers on the surface by grafting of organometallic complexes.^{4,5,6,7} In general, SOMC is performed on a dehydroxylated silanol rich surface and the method requires air and moisture free conditions to prevent hydrolysis and aggregation of metal complexes. Organometallic complexes containing reactive metal—carbon bonds react with surface silanol groups of support pretreated at 500 °C under vacuum resulting in surface organometallic component with covalently bound $\equiv\text{SiO-M}$ and including the release of alkane. Trisneopentylzirconium monografted to silica surface [$\equiv\text{SiOZr}(\text{CH}_2\text{tBu})_3$] was the first surface complex to be fully characterized by spectroscopic methods (Scheme 1.1).⁸

Thermal pretreatment of silica supports has significant effect on the distribution of isolated surface hydroxyl groups and the formation of mono-, bi- and tri-podal surface complexes. The use of silica pretreated under vacuum at >500 °C allows the generation of isolated surface silanol groups and therefore leads to the formation of mono-podal surface complexes ($\equiv\text{SiOMR}_{n-1}$). In contrast, the use of silica pretreated at intermediate or lower temperatures results in a mixture of bi-podal ($(\equiv\text{SiO})_2\text{MR}_{n-2}$) and tri-podal ($(\equiv\text{SiO})_3\text{MR}_{n-3}$) due to partially dehydroxylated silica.⁹



Scheme 1.1: Possible surface supported early transition metal alkyl or amide compounds formed in the immobilization.

More recently, several studies have reported the grafting of methyl, neosilyl and benzyl derivatives of early transition metals on solid supports.^{10,11,12} Alternatively, the reaction of early transition metal amides with partially dehydroxylated solid supports results in the formation of amine (HNR_2) and heterogeneous equivalents ($\text{=SiOM}(\text{NR}_2)_{n-1}$) similar to the alkyl complexes.^{13,14,15} The reaction of supported early transition metal alkyls and amides with H_2 at 100 – 200 °C results in the formation of metal hydrides.^{16,17,18,19} Surface-supported early transition metal hydrides are highly active towards C–H bond activations,^{17,20} and catalytic conversions such as alkane metathesis and hydrogenolysis of polyethylene.²¹



Scheme 1.2: Possible surface supported homoleptic silazido rare earth compounds formed in the immobilization of $\text{M}\{\text{N}(\text{SiMe}_2)_2\}_3$.

Similar to transition metal amides, rare earth amides supported by disilazido ligands are starting materials for the rare earth chemistry including synthesis of single site catalysts.

The reaction of silyl amide derivatives $M\{N(\text{SiMe}_n\text{H}_{3-n})_2\}_3$ with surface $-\text{OH}$ results in the formation of $\equiv\text{SiOM}\{N(\text{SiMe}_n\text{H}_{3-n})_2\}_{3-x}$ and the disilazane $\text{HN}(\text{SiMe}_n\text{H}_{3-n})_2$ (Scheme 1.2).^{22,23,24} Rare earth single site catalysts catalyze alkyne dimerization,²⁵ Tischenko aldehyde dimerization,²⁶ and hydroamination.²⁷

Hydroamination is the process of formation C-N bonds by the addition of a nitrogen-hydrogen bond to carbon-carbon multiple bonds. Particularly intramolecular hydroamination is an efficient route for the synthesis of N-heterocycles, which have significant importance in pharmaceutical and natural products synthesis.²⁸ Although much progress has been made over the last decades, there is room for exploration because most catalysts employed for the reaction have been homogeneous while heterogeneous catalysis is relatively rare. One of our goals is the synthesis of single-site metal amide catalysts active for the hydroamination of aminoalkenes.

This thesis contributes to the utilization of surface organometallic chemistry (SOMC) to synthesize single site heterogeneous catalysts and demonstrates their utilization in hydroboration and hydroamination. A heterogeneous zirconium catalyst was prepared by grafting $\text{Zr}(\text{NMe}_2)_4$ on mesoporous silica (MSN) and the catalyst was used in the hydroboration of carbonyl compounds. Furthermore, rare earth silylamides of type $\text{RE}\{N(t\text{Bu})(\text{SiHMe}_2)\}_3\text{Solv}$ (RE = Sc, Y, La, Ce, Pr, Nd and Lu) have been prepared and transformed into their heterogeneous equivalents via grafting onto mesoporous silica (MSN). Additionally, homogeneous and heterogeneous catalysts are shown to be efficient catalysts for the hydroamination/cyclization of aminoalkenes and aminodienes under mild conditions.

Thesis organization:

This thesis contains six chapters that include both published manuscripts and manuscripts in preparation towards publication. A general introduction to the motivation to develop single-site catalysts for the heterogeneous catalysis is given in Chapter 1. The synthesis of mesoporous silica-supported amidozirconium catalyst and its catalysis in hydroboration of carbonyls are described in Chapter 2. The mesoporous silica used in this work was synthesized by Umesh Chaudhary and Kapil Kandel and solid state NMR was measured by Zhuoran Wang and Takeshi Kobayashi. The synthesis of metal (Y, Sc and Ln) silazides as starting materials for the synthesis of heterogeneous catalysts through the grafting reactions is described in Chapter 3. The synthesis of ligand and homoleptic silazanes is also discussed. Mesoporous silica nanoparticles are synthesized by Umesh Chowdary solid state NMR is measured by Zhuoran Wang and Takeshi Kobayashi.

The synthesis of achiral cyclopentadienyl-bis(oxazoline) ligands and followed by the synthesis of magnesium, zirconium complexes and studies of these complexes catalytic activity in hydroaminations of aminoalkenes are presented in Chapter 4. Finally, chapter 5 describes the synthesis of tris(oxazolanyl) borate copper(II) and copper(I) compounds and their reactivity. The reduction of tris(oxazolanyl) borate copper(II) to copper(I) with hydride sources is also discussed in Chapter 5. The general conclusion and future direction for the work demonstrated in this thesis are given in Chapter 6.

References:

1. Leadbeater, N. E.; Marco, M. *Chem. Rev.* **2002**, *102*, 3217-3274.
2. (a) Buchmeiser, M. R. *Chem. Rev.* **2009**, *109*, 303-321; (b) Sherrington, D. C. *J. Polym. Sci. Part A: Polym. Chem.* **2001**, *39*, 2364; (c) Anzenbacher, P., Jr.; Kral, V.; Jursikova, K.; Gunterova, J.; Kasal, A. *J. Mol. Catal. A: Chem.* **1997**, *118*, 63.
3. (a). Beck, J. S.; Vartuli, J. C.; Roth, W. J.; Leonowicz, M. E.; Kresge, C. T. *J. Am. Chem. Soc.* **1992**, *114*, 10834; (b) Choudary, B. M.; Valli, V. L. K.; Prasad, A. D. *Chem. Commun.* **1990**, 1186.
4. Marks, T. J. *Acc. Chem. Res.* **1992**, *25*, 57-65.
5. Coperet, C.; Chabanas, M.; Petroff Saint-Arroman, R.; Basset, J.-M. *Angew. Chem., Int. Ed.* **2003**, *42*, 156-181.
6. Coperet, C.; Comas-Vives, A.; Conley, M. P.; Estes, D. P.; Fedorov, A.; Mougel, V.; Nagae, H.; Nuñez-Zarur, F.; Zhizhko, P. A. *Chem. Rev.* **2016**, *116*, 323-421.
7. Rascon, F.; Wischert, R.; Coperet, C. *Chem. Sci.* **2011**, *2*, 1449-1456.
8. (a) F. Quignard, A. Choplin, J.-M. Basset, *J. Chem. Soc. Chem. Commun.* **1991**, 1589; (b) S. A. King, J. Schwartz, *Inorg. Chem.* **1991**, *30*, 3771; (c) F. Quignard, C. Lécuyer, C. Bougault, F. Lefebvre, A. Choplin, D. Olivier, J.-M. Basset, *Inorg. Chem.* **1992**, *31*, 928.
9. Coperet, C.; Comas-Vives, A.; Conley, M. P.; Estes, D. P.; Fedorov, A.; Mougel, V.; Nagae, H.; Nunez-Zarur, F.; Zhizhko, P. A. *Chem. Rev.* **2016**, *116*, 323-421
10. Chen, Y.; Abou-Hamad, E.; Hamieh, A.; Hamzaoui, B.; Emsley, L.; Basset, J.-M. *J. Am. Chem. Soc.* **2015**, *137*, 588-591.
11. Amor Nait Ajjou, J.; Scott, S. L. *Organometallics* **1997**, *16*, 86-92.
12. Popoff, N.; Espinas, J.; Pelletier, J.; Macqueron, B.; Szeto, K. C.; Boyron, O.; Boisson, C.; Del Rosal, I.; Maron, L.; De Mallmann, A. *Chem. - Eur. J.* **2013**, *19*, 964-973.
13. Lappert, M.; Protchenko, A.; Power, P.; Seeber, A. Metal Amide Chemistry; *John Wiley & Sons, Ltd: New York*, **2008**.
14. Bouh, A. O.; Rice, G. L.; Scott, S. L. *J. Am. Chem. Soc.* **1999**, *121*, 7201-7210.
15. Eter, M. E.; Hamzaoui, B.; Abou-Hamad, E.; Pelletier, J. D.; Basset, J. M. *Chem. Commun.* **2013**, *49*, 4616-4618.
16. Rosier, C.; Niccolai, G. P.; Basset, J.-M. *J. Am. Chem. Soc.* **1997**, *119*, 12408-12409.
17. Corker, J.; Lefebvre, F.; Lecuyer, C.; Dufaud, V.; Quignard, F.; Choplin, A.; Evans, J.; Basset, J. M. *Science* **1996**, *271*, 966-969.
18. Dufaud, V.; Basset, J.-M. *Angew. Chem., Int. Ed.* **1998**, *37*, 806-810.
19. Rataboul, F.; Baudouin, A.; Thieuleux, C.; Veyre, L.; Coperet, C.; Thivolle-Cazat, J.; Basset, J. M.; Lesage, A.; Emsley, L. *J. Am. Chem. Soc.* **2004**, *126*, 12541-12550.
20. Thieuleux, C.; Quadrelli, E. A.; Basset, J.-M.; Dobler, J.; Sauer, J. *Chem. Commun.* **2004**, 1729-1731.
21. Basset, J.-M.; Coperet, C.; Soulivong, D.; Taoufik, M.; Cazat, J. T. *Acc. Chem. Res.* **2009**, *43*, 323-334.
22. Liang, Y.; Anwander, R. *Dalton Trans.* **2013**, *42*, 12521-12545.
23. Nagl, I.; Widenmeyer, M.; Herdtweck, E.; Raudaschl-Sieber, G.; Anwander, R. *Microporous Mesoporous Mater.* **2001**, *44*, 311-319.
24. Gerstberger, G.; Palm, C.; Anwander, R. *Chem. - Eur. J.* **1999**, *5*, 997-1005.

25. Gauvin, R. M.; Delevoye, L.; Hassan, R. A.; Keldenich, J.; Mortreux, A., *Inorganic Chemistry* **2007**, *46*, 1062-1070;
26. Gauvin, R. M.; Chenal, T.; Hassan, R. A.; Addad, A.; Mortreux, A., *Journal of Molecular Catalysis A: Chemical* **2006**, *257*, 31-40;
27. Roux, E. L.; Liang, Y.; Storz, M. P.; Anwender, R., *J. Am. Chem. Soc.* **2010**, *132*, 16368-16371;
28. Hultsch, K. C. *Org. Biomol. Chem.* **2005**, *3*, 1819–1824.

CHAPTER 2

**MESOPOROUS SILICA-SUPPORTED AMIDOZIRCONIUM-CATALYZED
CARBONYL HYDROBORATION**

Modified from a paper published in *ACS Catalysis*, **2015**, 5, 7399 – 7414

Naresh Eedugurala, Zhuoran Wang, Umesh Chaudhary, Nicholas Nelson, Kapil Kandel,
Takeshi Kobayashi, Igor I. Slowing, Marek Pruski, and Aaron D. Sadow

US Department of Energy Ames Laboratory and Department of Chemistry, Ames IA 50011

Abstract. The hydroboration of aldehydes and ketones using a silica-supported zirconium catalyst is reported. Reaction of $Zr(NMe_2)_4$ and mesoporous silica nanoparticles (MSN) provides the catalytic material $Zr(NMe_2)_n@MSN$. Characterization of $Zr(NMe_2)_n@MSN$ with solid-state (SS)NMR and infrared spectroscopy, elemental analysis, powder X-ray diffraction, electron microscopy, and reactivity studies suggests its surface structure is primarily $=SiOZr(NMe_2)_3$, with smaller amounts of the bis(amido)amine zirconium site $(=SiO)_2Zr(NMe_2)_2(NHMe_2)$ and the bis(amido) zirconium $(=SiO)_2Zr(NMe_2)_2$. The presence of these nitrogen-containing zirconium sites is supported by ^{15}N NMR spectroscopy, including natural abundance ^{15}N NMR measurements using dynamic nuclear polarization (DNP) SSNMR. The $Zr(NMe_2)_n@MSN$ material reacts with pinacolborane (HBpin) to provide Me_2NBpin and a material $ZrH/Bpin@MSN$ that is composed of interacting surface-bonded zirconium hydride and surface bonded borane $=SiOBpin$ moieties in an approximately 1:1 ratio, as well as a zirconium sites coordinated by dimethylamine. The $ZrH/Bpin@MSN$ is characterized by 1H SSNMR and infrared spectroscopy through its reactivity with D_2 , as well as by elemental analysis. The interaction of Zr and $=SiOBpin$ surface sites in $ZrH/Bpin@MSN$ is also characterized by ^{11}B NMR SSNMR spectroscopy. A small amount of nitrogen-based ligand remains bonded to zirconium sites, and this

component of the material is also characterized by ^{15}N SSNMR, elemental analysis, and reaction stoichiometry. The zirconium hydride material or the zirconium amide precursor $\text{Zr}(\text{NMe}_2)_n@ \text{MSN}$ catalyze the hydroboration of aldehydes and ketones with HBpin. The catalytic reduction is selective for carbonyl groups in the presence of functional groups that are often reduced under hydroboration conditions or are sensitive to metal hydrides, including olefins, alkynes, nitro groups, halides, and ethers. Remarkably, this catalytic material may be recycled without any loss of activity at least eight times, and air-exposed materials are catalytically active. These results show that these supported zirconium centers are robust catalytic sites for carbonyl reduction, and that surface-supported, catalytically reactive zirconium hydride may be generated from zirconium-amide or zirconium alkoxide sites.

Introduction

Surface-supported early transition metal hydrides^{1,2} are highly reactive toward C–H bond breaking reactions that allow stoichiometric methane metalation³ and catalytic conversions such as olefin polymerization,⁴ hydrogenation,⁵ H/D exchange,⁶ alkane metathesis and hydrogenolysis of polyethylene and other alkanes.⁷⁻¹⁰ Although the surface provides kinetic stabilization of metal hydrides against multi-metallic decomposition reactions, solution-phase early metal and rare earth hydrides are implicated in a range of catalytic chemistry including hydrosilylation,¹¹⁻¹⁷ hydrogenation,¹⁸ dehydrocoupling and dehydrogenative polymerization,¹⁹⁻²¹ and hydroboration.^{22,23} Often, the metal hydrides in these reactions are generated and used *in situ* or are proposed as intermediates in catalytic cycles. This *in situ* generation could also be an advantageous approach for the application of surface-supported metal hydrides in catalysis. Moreover, a surface-supported hydride such as

(=SiO)₃ZrH could tolerate harsher conditions (e.g., higher temperature) than soluble analogues in catalytic addition chemistry thereby permitting more difficult conversions as well as a straightforward means for recycling the catalytic materials.

We recently reported a homogeneous magnesium-catalyzed cleavage and hydroboration of esters using an *in situ* generated magnesium hydridoborate catalyst.²⁴ Despite the oxophilicity of the magnesium center, the catalytic site could be generated by reaction of pinacolborane (HBpin) and magnesium alkoxide. Similarly, [{Nacnac}MgH]₂ (Nacnac = ((2,6-*i*Pr₂C₆H₃)NCMe)₂HC) is a highly active catalyst for hydroboration of pyridines, ketones and aldehydes.^{22,25} A related zwitterionic magnesium catalyst is sufficiently reactive to reduce carbon dioxide to a methanol equivalent.²⁶ Hydroboration of aldehydes and ketones is catalyzed by soluble titanium,²⁷ molybdenum,²⁸ as well as few late metal catalysts.^{29,30} Recently, divalent germanium and tin compounds were also shown to catalyze this reaction, and hydrides were postulated intermediates.³¹ Group 4 catalyzed carbonyl hydrosilylations and hydrogenations are also known,^{11,32-35} and although Schwartz's reagent catalyzes hydroboration of alkynes,³⁶ we are not aware of previous reports of zirconium-catalyzed hydroboration of carbonyls. In addition, the reaction of Zr(NMe₂)₄ and SBA-15 was recently reported to give an azazirconocyclopropane surface species,³⁷ as does a titanium amide on silica en route to a titanium imido.³⁸ Notably, the azazirconocyclopropane species reacts with hydrogen to give a zirconium hydride that catalyzes hydrogenation of olefins.³⁹ The catalytic C–H and C–C bond breaking and forming reactions of surface-supported zirconium hydride are notoriously sensitive to oxygen-containing impurities, which give irreversible deactivation of the catalytic sites.

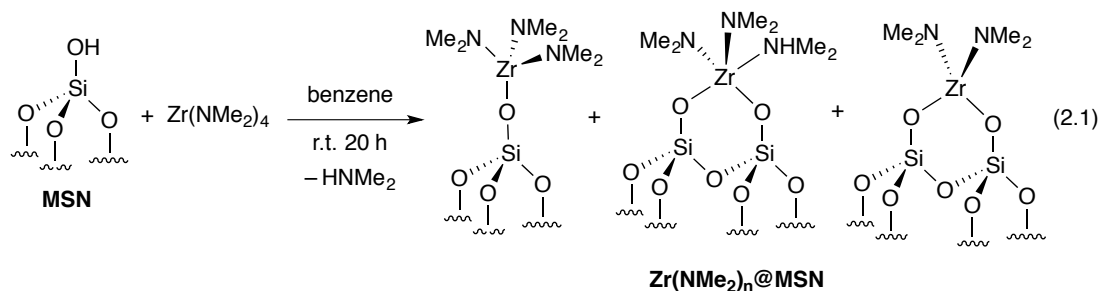
As a possible solution to these deactivation processes, we envisioned that surface-supported oxophilic metal complexes with oxygen- or nitrogen-containing ligand precursors could be activated with reducing reagents such as boranes. Such transformations could potentially allow access to highly reactive surface-supported zirconium hydride sites under mild conditions and also provide a means for reactivating deactivated catalytic sites. On the basis of these ideas and the known chemistry of $(\equiv\text{SiO})_3\text{ZrH}$,^{1,3,40,41} the hydroboration of carbonyls appears to be an appropriate choice for testing the surface-supported Zr–OR bond cleavage steps in a catalytic cycle. Reductions of ketones and aldehydes are readily achieved with stoichiometric boron-containing reagents such as $\text{BH}_3\cdot\text{THF}$ or NaBH_4 or highly reactive metal hydrides such as LiAlH_4 .^{42,43} However, selectivity for carbonyls vs olefins and other functional groups including organohalides and nitro groups are limited with these reagents, these reagents are easily hydrolyzed by adventitious moisture, and their reactions produce substantial amounts of salt waste. Thus, alternative catalytic methods for selective carbonyl reductions, employing earth abundant catalysts, are desirable. In this context, supported single-site hydroboration catalysts based on earth abundant zirconium would represent a significant conceptual advance in the field. In addition, a heterogeneous catalyst could offer advantages in sustainable synthesis through recyclable catalytic materials and in flow chemistry.

Here we report the synthesis and characterization of a mesoporous silica nanoparticle (MSN)-supported zirconium amide complex identified as $\text{Zr}(\text{NMe}_2)_n@MSN$. In the first section of this paper we describe the details supporting the assigned surface structures of this material. In the second section, we describe the reactivity of $\text{Zr}(\text{NMe}_2)_n@MSN$ with pinacolborane, and the nature of the surface species $\text{ZrH/Bpin}@MSN$ produced from that

reaction. Finally, we present the catalytic activity of $\text{Zr}(\text{NMe}_2)_n@MSN$ as a recyclable catalyst for the reduction of carbonyls by catalytic hydroboration.

Results and Discussion

Synthesis and characterization of $\text{Zr}(\text{NMe}_2)_n@MSN$. Tetrakis(dimethylamido)zirconium was grafted on high surface area mesoporous silica to give $\text{Zr}(\text{NMe}_2)_n@MSN$. The silica support, in the form of SBA-15 type MSN characterized by a hexagonal array ($p6mm$) of 9.7 nm diameter pores and a surface area of 385 m^2/g , was produced by hydrolysis-condensation of tetramethylorthosilicate using the Pluronic P104 template, calcined at 550 °C, washed with water, then heated at 550 °C under vacuum, and subsequently stored in a glovebox away from ambient air and moisture.⁴⁴ The SiOH group surface concentration of 1.7 mmol/g was determined by measuring the concentration of toluene produced in a titration with $\text{Mg}(\text{CH}_2\text{Ph})_2(\text{O}_2\text{C}_4\text{H}_8)_2$ ⁵³ and by spin counting of Q³-sites with ²⁹Si DPMAS NMR spectroscopy (1.6 mmol/g). Thus-prepared MSN and $\text{Zr}(\text{NMe}_2)_4$ react in benzene at room temperature for 20 h producing $\text{Zr}(\text{NMe}_2)_n@MSN$, a grafted material that we will contend is primarily monopodal tris(dimethylamido)zirconium, with smaller amounts of bipodal species bis(dimethylamido)zirconium and bis(dimethylamido)(dimethylamino)zirconium (eq. 2.1).



Upon scale-up, the $\text{Zr}(\text{NMe}_2)_n@MSN$ is purified from excess $\text{Zr}(\text{NMe}_2)_4$ by pentane and benzene washes. The structural morphology of the material was characterized by powder

XRD and TEM. The zirconium sites were identified and characterized by the mass-balance implied by stoichiometry from the synthesis, quantitative metals analysis using ICP-OES, combustion analysis, infrared spectroscopy, and SSNMR spectroscopy, as well as the stoichiometry and observed products of its reactions with HBpin and D_2 .

A TEM image (Figure 2.1A) of $Zr(NMe_2)_n@MSN$ showed that the ordered mesoporous nature of the SBA-15-type material is maintained after its treatment with $Zr(NMe_2)_4$. There was no evidence for large zirconium clusters formed in the grafting experiments in the images produced by TEM and HAADF-STEM (Figure 2.1B). Likewise, the EDX analysis (Figure 1C) suggested that zirconium is well dispersed over the silica. In addition, a powder XRD measurement of $Zr(NMe_2)_n@MSN$ showed diffraction peaks assigned to the periodic channels of the mesoporous silica support.

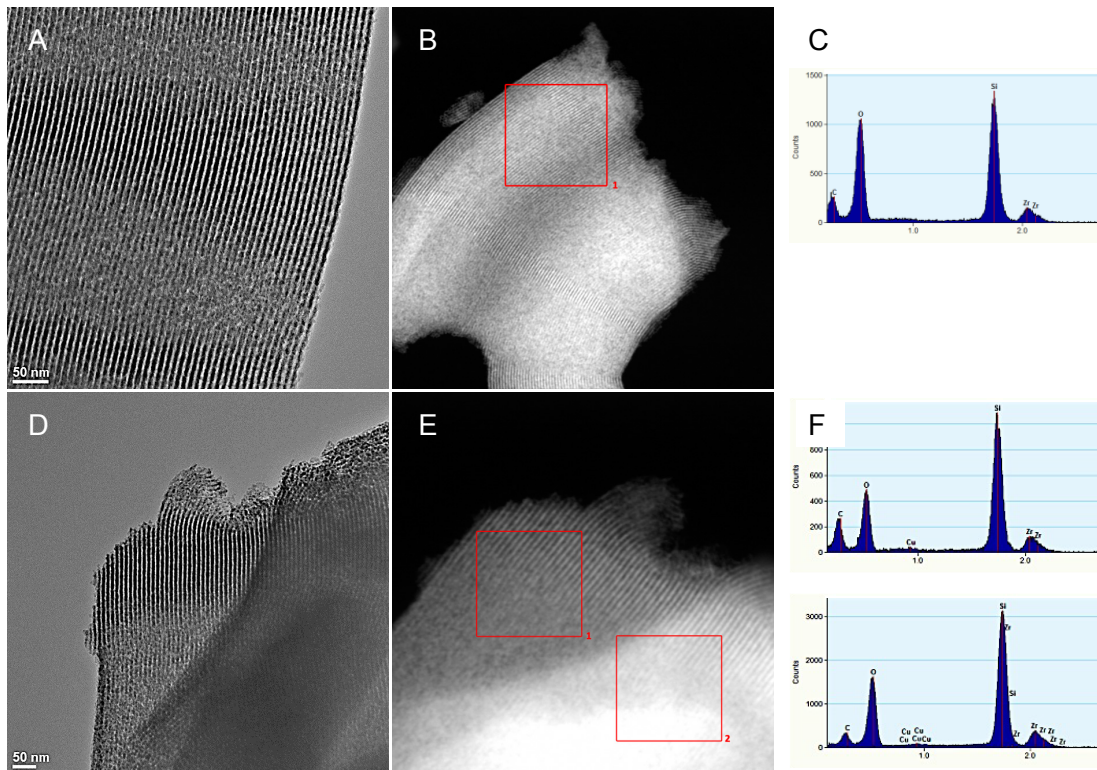


Figure 2.1. (A) TEM of $\text{Zr}(\text{NMe}_2)_n@MSN$, (B) HAADF-STEM of $\text{Zr}(\text{NMe}_2)_n@MSN$, (C) EDX analysis of the region enclosed in the red square in the HAADF-STEM image of $\text{Zr}(\text{NMe}_2)_n@MSN$, (D) TEM of $\text{Zr}(\text{NMe}_2)_n@MSN + \text{HBpin}$, (E) HAADF-STEM of $\text{Zr}(\text{NMe}_2)_n@MSN + \text{HBpin}$, and (F) EDX analysis of the regions enclosed in the red squares in the HAADF-STEM image showing consistent Zr:Si ratios throughout the material.

Next, the amount of $\text{Zr}(\text{NMe}_2)_4$ grafted onto MSN was approximated by quantifying the soluble zirconium amide before and after its reaction with the silica. A benzene solution of excess $\text{Zr}(\text{NMe}_2)_4$ (1.78 mmol) stirred with 1 g of MSN resulted in the consumption of 1 mmol of $\text{Zr}(\text{NMe}_2)_4$, indicating that the loading is ca. 1 mmol Zr per gram of MSN. In this reaction, approximately 1.2 mmol of HNMe_2 was produced per gram of silica. These amounts were determined by integration of the reactant and product resonances in ^1H NMR spectra of the reaction mixtures, which contained a known concentration of $\text{Si}(\text{SiMe}_3)_4$ as an internal standard. This loading was further supported by ICP-OES analysis that indicated the presence of 8.4 ± 0.1 weight % Zr in $\text{Zr}(\text{NMe}_2)_n@MSN$ (0.91 ± 0.1 mmol Zr/g; Table 2.1). The ICP-OES analysis involved 10 measurements performed over several days on samples of $\text{Zr}(\text{NMe}_2)_n@MSN$ and established the stability of the zirconium-supported material and the reproducibility of the method for the comparison of the series of materials derived from $\text{Zr}(\text{NMe}_2)_n@MSN$. Heating of $\text{Zr}(\text{NMe}_2)_n@MSN$ at $60\text{ }^\circ\text{C}$ in benzene did not affect the material's weight %.

Table 2.1. Zirconium loading of $Zr(NMe_2)_n@MSN$ materials obtained by ICP-OES analysis.

Material preparation	conditions ^a	weight Zr ^b	% Zr/g
$Zr(NMe_2)_4 + MSN \rightarrow Zr(NMe_2)_n@MSN$	20 h, r.t.	8.4±0.1	0.91
$Zr(NMe_2)_n@MSN$ heated at 60 °C	2 h, 60 °C	8.4±0.1	0.92
$Zr(NMe_2)_n@MSN + 10 HBpin \rightarrow ZrH/Bpin@MSN$	2 h, 60 °C	8.2±0.1	0.89
$Zr(NMe_2)_n@MSN + 10 HBpin + 10 PhMeC=O$	2 h, 60 °C	8.2±0.1	0.89

^aBenzene solvent. ^bDetermined by ICP-OES analysis.

The Zr:NMe₂ ratio in $Zr(NMe_2)_n@MSN$, as well as the carbon (5.91%, 4.9 mmol/g), hydrogen (1.08%, 10.8 mmol/g), and nitrogen (3.44%, 2.5 mmol/g) loadings were measured using combustion analysis. From these data, the Zr:C:N ratio is 1:5.4:2.7 corresponding to a Zr:NMe₂ ratio of 1:2.7. These results, corroborated by the measurements of the stoichiometry of the grafting reactions, imply that the material contains primarily zirconium sites with three nitrogen-containing ligands and a smaller amount (up to 30%) of sites with two nitrogen-containing ligands.

The presence of NMe₂ groups in $Zr(NMe_2)_n@MSN$ was identified through infrared spectroscopy. An IR spectrum of MSN (calcined, washed with water, and then dried at 550 °C under vacuum) contained an absorption at 3747 cm⁻¹ assigned to isolated SiOH groups (Figure 2.2A).⁵⁴ Also, for comparison, the infrared spectrum of $Zr(NMe_2)_4$ contained bands at 2942, 2869, 2773 and 1457 cm⁻¹ (Figure 2.2B).

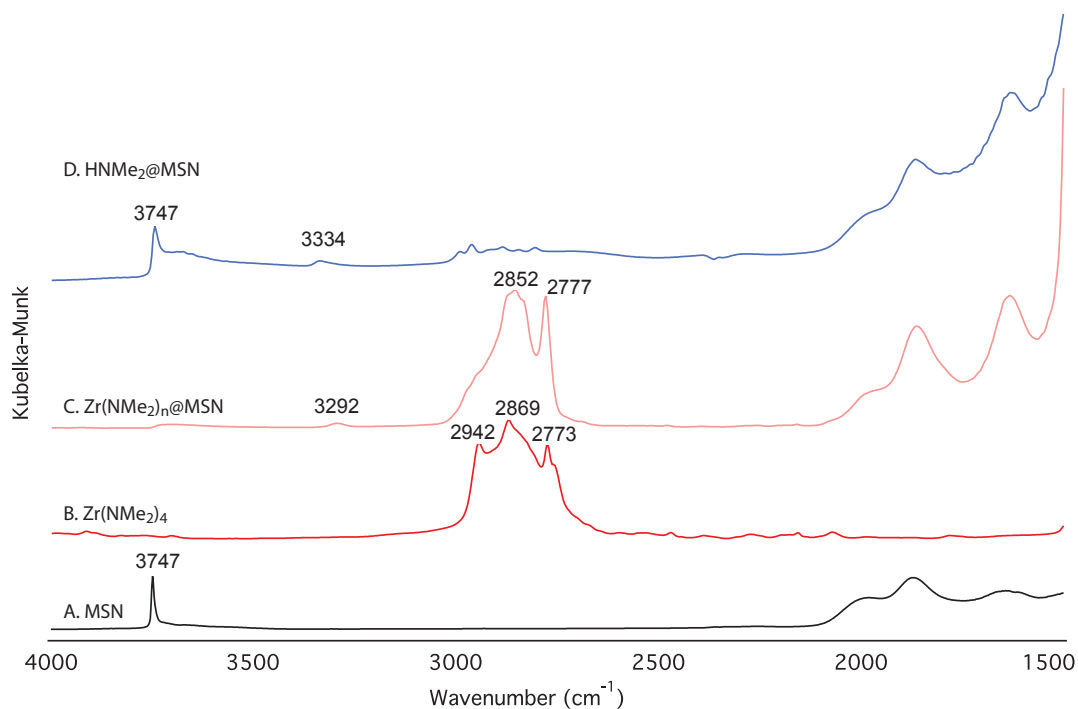


Figure 2.2. Diffuse reflectance infrared spectra of (A) MSN, (B) $Zr(NMe_2)_4$, (C) $Zr(NMe_2)_n@MSN$, and (D) MSN + $HNMe_2$.

After the reaction between MSN and $Zr(NMe_2)_4$, several new signals associated with organic groups were observed at 2852, 2777 and 1457 cm^{-1} . These signals are similar to those observed for $Zr(NMe_2)_4$, as can be seen through comparison of Figures 2.2B and 2.2C. After the grafting reaction, the IR band associated with isolated surface SiOH moieties was diminished, and it is likely that some unreacted SiOH groups are still present on the surface. These groups, as well as likely NH containing species, are difficult to detect as a result of their low concentration and possible broadening due to hydrogen bonding.

The $HNMe_2$ reaction byproduct might be expected to interact with the acidic silica surface. To test for this possibility, MSN and $HNMe_2$ were allowed to react in benzene, pentane, or under solid-gas conditions (Figure 2.2D) in three independent experiments, followed by evacuation. In all cases, a small signal at 1457 cm^{-1} and even weaker intensity

signals typically attributed to ν_{CH} or ν_{NH} (at 3334 cm^{-1}) were observed in the infrared spectra. The peak at 3747 cm^{-1} assigned to isolated SiOH groups was observed after the HNMe₂ treatments. In addition, a weak, yet sharp signal was observed in the ¹³C CPMAS spectrum (not shown), with the chemical shift very close to neat dimethylamine (~35 ppm) and the intensity corresponding to less than 0.1 mmol/g. From these experiments, we conclude that only a small amount of HNMe₂ associates with the MSN material in physisorbed form. Moreover, these sites may be blocked once zirconium amide is grafted to the silica surface.

The ¹³C CPMAS SSNMR spectrum of Zr(NMe₂)_n@MSN (Figure 2.3, top) showed two strongly overlapping signals with the chemical shifts of ~36 and ~39 ppm, which are similar to that of Zr(NMe₂)₄ dissolved in benzene-*d*₆ (42 ppm). No other resonances were detected, even after 76,000 acquisitions. The completeness of the CPMAS spectrum was confirmed by the ¹³C DPMAS experiment (Figure 2.3, bottom), which yielded the same line shape. These ¹³C spectra contrast with those reported earlier by El Eter et al., in which ≡SiOZr(η²-CH₂NMe)(NMe₂)(NHMe₂), formed from the reaction of SBA-15₇₀₀ (i.e., mesoporous silica pretreated at 700 °C) and Zr(NMe₂)₄ in pentane for 1 h, produced three signals at 36, 47 and 85 ppm.³⁷

DFT calculations showed that the chemical shifts of all methyl carbons in dimethylamido zirconium model surface moieties, including ≡SiOZr(NMe₂)₃ and (≡SiO)₂Zr(NMe₂)₂, are expected between 36 and 43 ppm, strongly supporting the hypothesis that both resonances observed in Zr(NMe₂)_n@MSN represent the Zr-bound NMe₂ functionalities. The DFT calculations were based on the gauge-including projector-augmented wave (GIPAW) method.⁵⁵ The observed nonequivalence of methyl groups can be attributed to differences in local geometries and mobilities (see eq. 2.1).

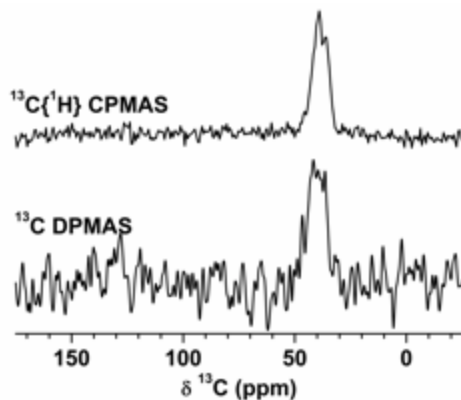


Figure 2.3. ^{13}C CPMAS (top) and DPMAS (bottom) spectra of $\text{Zr}(\text{NMe}_2)_n@ \text{MSN}$ obtained under 25 kHz MAS with ^1H TPPM heteronuclear decoupling at $\nu_{\text{RF}}(^1\text{H}) = 100$ kHz. The CPMAS spectrum was measured using $\nu_{\text{RF}}(^1\text{H}) = 60$ kHz and $\nu_{\text{RF}}(^{13}\text{C}) = 100$ kHz during CP, $\tau_{\text{CP}} = 4.5$ ms, $\tau_{\text{RD}} = 1.5$ s, and 76,000 scans. The DPMAS spectrum resulted from 360 scans with $\tau_{\text{RD}} = 60$ s.

Spin counting, using a ^{13}C DPMAS NMR experiment, quantified the NMe_2 loading in $\text{Zr}(\text{NMe}_2)_n@ \text{MSN}$ at $2.7 (\pm 0.5)$ mmol/g. Considering the fact that the Zr loading measured with ICP-OES was 0.91 mmol/g, the Zr: NMe_2 ratio is estimated at close to 1:3. This value and the value obtained from combustion analysis (1:2.7) described above are in sufficient agreement to suggest the surface species in $\text{Zr}(\text{NMe}_2)_n@ \text{MSN}$ primarily comprises three nitrogen-containing ligands, although some quantity of bipodal $(\equiv\text{SiO})_2\text{Zr}(\text{NMe}_2)_2$ (up to 30%) is likely to be present. The former species may be either the monopodal $\equiv\text{SiOZr}(\text{NMe}_2)_3$ or a dipodal diamido amine adduct $(\equiv\text{SiO})_2\text{Zr}(\text{NMe}_2)_2(\text{NHMe}_2)$. The monopodal stoichiometry would imply that $\sim 0.7\text{--}0.8$ mmol/g of $\equiv\text{SiOH}$ remained intact, and indeed, the experiments with pinacolborane described below suggest that accessible $\equiv\text{SiOH}$

groups remain on the silica surface. In contrast, the diffuse reflectance FTIR spectrum does not contain signals in the expected region for isolated SiOH. That is, neither the IR peak at 3747 cm^{-1} , associated with isolated silanols, nor a broad signal for hydrogen-bonded silanols are observed. However, a weak signal at 3292 cm^{-1} may be assigned to an NH stretching band of a possible zirconium-coordinated dimethylamine, and this signal is slightly shifted from the signal of physisorbed HNMe_2 on MSN. On the basis of the residual nitrogen loading after treatment of $\text{Zr}(\text{NMe}_2)_n@MSN$ with HBpin (see below), the amount of zirconium-coordinated dimethylamine is estimated to be less than 10%.

Because $\equiv\text{SiOZr}(\text{NMe}_2)_3$, $(\equiv\text{SiO})_2\text{Zr}(\text{NMe}_2)_2(\text{NHMe}_2)$, or $(\equiv\text{SiO})_2\text{Zr}(\text{NMe}_2)_2$ are not conclusively distinguished as surface structures by ^{13}C SSNMR, IR, and elemental analysis, we turned to ^{15}N SSNMR measurements to further characterize the nitrogen-containing ligands bonded to zirconium. At natural ^{15}N abundance, NMR signals could not be detected either in 1D ^{15}N spectra or in 2D ^1H - ^{15}N correlation experiments. We thus resorted the newly developed DNP method, which enhances the sensitivity of SSNMR of surface species by ~ 2 orders magnitude via excitation of the exogenously introduced biradicals (here TEKPol dissolved in 1,1,2,2-tetrachloroethane) at their ESR resonance frequency, followed by transfer of magnetization to the nuclear spins.^{50,51} A high quality DNP-enhanced ^{15}N CPMAS spectrum of $\text{Zr}(\text{NMe}_2)_n@MSN$ was indeed acquired under natural abundance in just over 2 hours (Figure 2.4A, top spectrum). The spectrum features a single, fairly broad signal at -355 ppm, which we assign to Zr-bound NMe_2 groups. To further investigate their nature, a series of DNP-enhanced CPMAS ^{15}N NMR spectra were measured as a function of τ_{CP} contact time. The build-up of ^1H - ^{15}N cross-polarization, which is governed by the heteronuclear dipolar coupling, and thus can be used to evaluate the ^1H - ^{15}N distance,⁵⁶ indicates that the

^{15}N nuclei are polarized primarily by ^1H nuclei at a distance of about 2 Å, which is consistent with protons in NMe_2 groups being the source. Interestingly, the local maxima in the curve (which were reproducibly measured several times, and evaluated using equation 20c in reference 49), suggest that a small fraction of the ^1H - ^{15}N pairs reside at a distance of ~ 1.0 Å, as would be expected in zirconium amine species. This finding implies that the resonance centered at -355 ppm can be assigned to dimethylamide groups and a small amount of dimethylamine coordinated to surface-bonded zirconium sites.

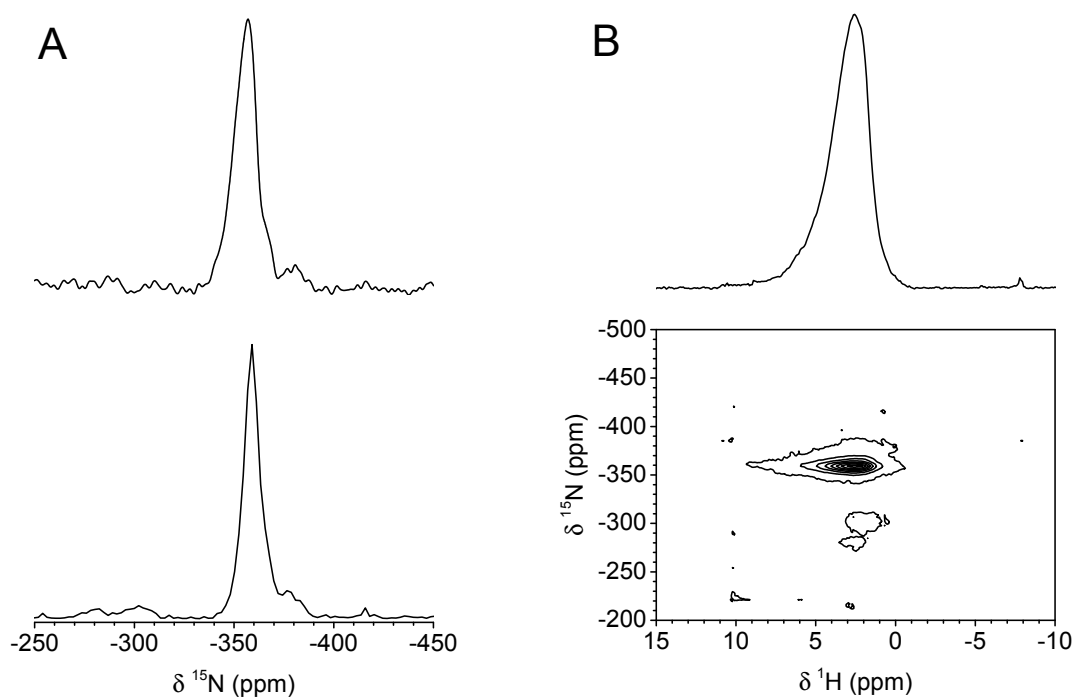
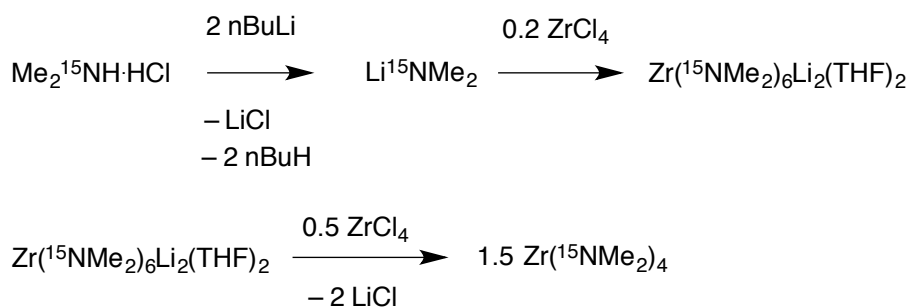


Figure 2.4. (A) Top spectrum: DNP-enhanced ^{15}N CPMAS spectrum of $\text{Zr}(\text{NMe}_2)_n@MSN$ under natural ^{15}N abundance. The spectrum was obtained at ~ 100 K using $\nu_R = 10$ kHz; $\nu_{\text{RF}}(^1\text{H}) = 100$ kHz, 107 kHz, and 100 kHz during hard pulse, cross polarization and SPINAL ^1H decoupling; $\nu_{\text{RF}}(^{15}\text{N}) = \sim 87$ kHz during cross polarization; $\tau_{\text{cp}} = 4$ ms; 2048 scans; and $\tau_{\text{RD}} = 4$ s. Lower spectrum: skyline ^{15}N projection of the 2D ^{15}N - ^1H idHetcor spectrum in figure (B). (B) 2D ^{15}N - ^1H idHetcor spectrum of ^{15}N -enriched $\text{Zr}(^{15}\text{NMe}_2)_n@MSN$. The spectrum

was obtained at 14.1 T, using $\nu_R = 34$ kHz; $\nu_{RF}(^1\text{H}) = 91$ kHz during 90° pulse and CP, and 10 kHz during SPINAL-64 ^1H decoupling; $\nu_{RF}(^{15}\text{N}) = 57$ kHz during CP and 90° pulses, and 10 kHz during SPINAL-64 ^{15}N decoupling; 128 rows with $\Delta t_1 = 30$ μs ; 64 scans per row, and STATES-TPPI acquisition with $\tau_{RD} = 2$ s.

We decided to verify that the surface Zr species observed by DNP did not result from the reaction with the solvent or the nitroxide radicals. To this end, we synthesized labeled $\text{Zr}(^{15}\text{NMe}_2)_4$ from isotopically enriched $\text{Me}_2^{15}\text{NH}\cdot\text{HCl}$ through the sequence shown in Scheme 2.1. The intermediate species $\text{Zr}(\text{NMe}_2)_6\text{Li}_2\text{THF}_2$ was previously reported from the reaction of $\text{Zr}(\text{NMe}_2)_4$ and 2 equiv. of LiNMe_2 .⁵² Here it is synthesized directly from ZrCl_4 and LiNMe_2 , and we report its ^{15}N NMR chemical shift at -295 ppm.



Scheme 2.1. Synthesis of labeled $\text{Zr}(^{15}\text{NMe}_2)_4$.

The reaction of $\text{Zr}(^{15}\text{NMe}_2)_6\text{Li}_2\text{THF}_2$ and 0.5 equiv. of ZrCl_4 gives pure $\text{Zr}(^{15}\text{NMe}_2)_4$ as its ^{15}N labeled isotopomer (^{15}N NMR in benzene- d_6 : -306 ppm). The grafting reaction was repeated with the labeled $\text{Zr}(^{15}\text{NMe}_2)_4$ sample to produce $\text{Zr}(^{15}\text{NMe}_2)_n@MSN$ and $\text{H}^{15}\text{NMe}_2$ (^{15}N NMR in benzene- d_6 : -366 ppm). A 2D ^{15}N - ^1H correlation spectrum of $\text{Zr}(^{15}\text{NMe}_2)_n@MSN$ was acquired under fast (35 kHz) MAS using the indirect detection of ^{15}N nuclei for sensitivity enhancement (^{15}N - ^1H idHetcor, see Figure 2.4B).⁵⁷ In agreement

with the DNP-based experiment, the idHetcor measurement showed a dominant correlation between the ^1H NMR signal at ~ 2.4 ppm and NMe_2 groups resonating at around -355 ppm. A minor peak at -370 ppm most likely represents small concentration of free HNMe_2 left within the pores.

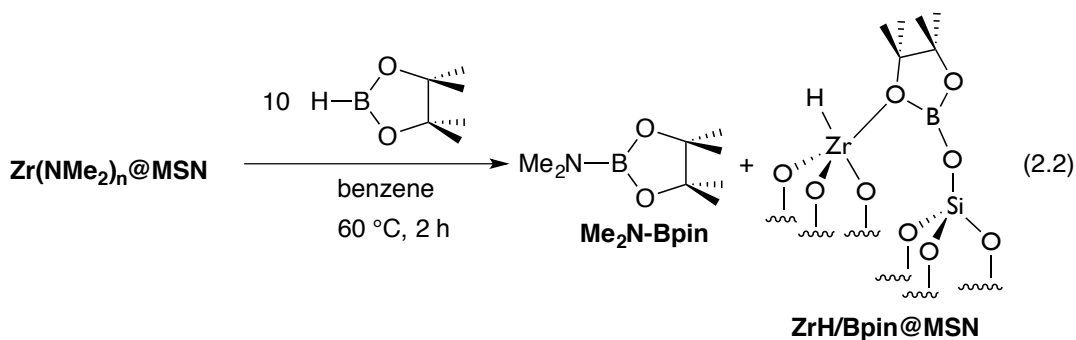
In addition, note that $\text{Zr}(\text{NMe}_2)_n@MSN$ features close to 1 mmol of functional groups per 385 m^2 of surface, which corresponds to the coverage of $\sim 70\%$. Thus, the grafting reaction provides the maximum zirconium amide loading. We may further speculate that the distinction between $\equiv\text{SiOZr}(\text{NMe}_2)_3$, $(\equiv\text{SiO})_2\text{Zr}(\text{NMe}_2)_2(\text{NHMe}_2)$, and $(\equiv\text{SiO})_2\text{Zr}(\text{NMe}_2)_2$ may relate to steric effects controlled by this surface coverage. The distinction between the surface species obtained in our grafting experiments vs the cyclometalated $\equiv\text{OSiZr}(\eta^2\text{-NMeCH}_2)(\text{NMe}_2)(\text{NHMe}_2)$ may also relate to these intersite steric effects. In particular, silica₇₀₀, which is dehydroxylated at $700 \text{ }^\circ\text{C}$ under vacuum to give isolated silanols, reacts to provide only monopodal surface structures. In the $550 \text{ }^\circ\text{C}$ calcined MSN used in our study, a bipodal zirconium-surface interaction relieves the intersite steric pressure rather than β -abstraction that would give the zirconacyclopropane structure.

The ^{15}N NMR experiments also rule out the presence of $\equiv\text{SiNMe}_2$ surface groups, which could form by addition of Zr-NMe_2 across a strained Si-O-Si surface site. This conclusion is based on the featureless region of the ^{15}N NMR experiments from -300 to -350 ppm. The ^{15}N NMR signal for $\equiv\text{SiNMe}_2$ is expected to be ca. -330 ppm based on the ^{15}N NMR chemical shift of the model compound $(\text{EtO})_3\text{SiNMe}_2$ (^{15}N NMR, benzene-*d*₆: -326 ppm). A summary of all findings that support the composition of $\text{Zr}(\text{NMe}_2)_n@MSN$ as a primarily $\equiv\text{SiOZr}(\text{NMe}_2)_3$, with smaller amounts of $(\equiv\text{SiO})_2\text{Zr}(\text{NMe}_2)_2$ and $(\equiv\text{SiO})_2\text{Zr}(\text{NMe}_2)_2(\text{NHMe}_2)$ is given in Table 2.2.

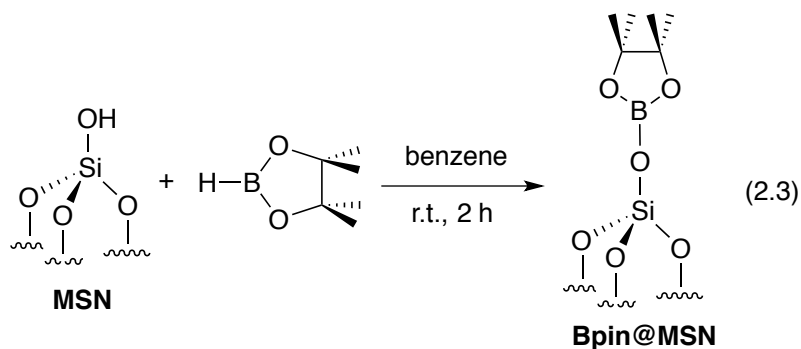
Table 2.2. Characterization Experiments and Conclusions Regarding the Nature of $\text{Zr}(\text{NMe}_2)_n@MSN$.

Experiment	Observation	Interpretation
Electron microscopy/EDX	well-dispersed Zr	no Zr or ZrO_2 clusters formed
Reaction stoichiometry	1.2 mmol HNMe_2 detected/g MSN 1.0 mmol $\text{Zr}(\text{NMe}_2)_4$ consumed/g MSN	
ICP-OES	0.91 mmol Zr/g	zirconium loading established
C, N combustion analysis	4.9 mmol C/g, 2.5 mmol N/g	Zr:NMe ₂ ~ 1:2.7 suggests a 3:7 mixture of $\text{Zr}(\text{NMe}_2)_2$ and $\text{Zr}(\text{NMe}_2)_3$ groups
¹³ C DPMAS/spin counting	2.7 mmol NMe ₂ /g	Zr:NMe ₂ ~ 1:3 suggests primarily three NMe ₂ -containing ligands/Zr
IR	new ν_{CH} bands at ~2900 cm^{-1} ν_{OH} band at 3747 cm^{-1} not detected	NMe ₂ groups present on surface isolated silanols have reacted with $\text{Zr}(\text{NMe}_2)_4$
¹⁵ N SSNMR:	strong signal at -355 ppm polarized by Me groups, weakly by H	nitrogen is primarily present as dimethylamide groups
MSN + HNMe_2 , ¹³ C NMR: IR analysis:	weak peak at 36 ppm ν_{OH} band at 3747 cm^{-1} and weak intensity NH and CH bands are detected	only a small amount of HNMe_2 physisorbs to calcined MSN
Reaction with HBpin (below)	2.5 mmol Me_2NBpin formed/g $\text{Zr}(\text{NMe}_2)_n@MSN$	ca. 2.7 reactive NMe ₂ groups per Zr center

Synthesis and characterization of ZrH/Bpin@MSN. The reaction of $\text{Zr}(\text{NMe}_2)_n@MSN$ and HBpin, which produces the zirconium hydride surface species discussed below, also further characterizes the zirconium amide sites by quantification of reactive NMe_2 groups (eq. 2.2). A micromolar scale reaction of $\text{Zr}(\text{NMe}_2)_n@MSN$ and excess HBpin affords 2.5 mmol of Me_2NBpin per gram of material, which was quantified by integration of product signals with respect to a known concentration of $\text{Si}(\text{SiMe}_3)_4$ as an internal standard. In the ^1H NMR spectrum of the soluble portion of the reaction mixture, a resonance at 2.62 ppm was assigned to the NMe_2 moiety of Me_2NBpin . In the corresponding solution-phase ^{11}B NMR spectrum, a singlet at 24.2 ppm was assigned to Me_2NBpin ⁵⁸ and a doublet at 28.5 ppm ($^1J_{\text{BH}} = 174$ Hz) represented unreacted HBpin. The reaction of ^{15}N -labeled $\text{Zr}(^{15}\text{NMe}_2)_n@MSN$ yields an isotopically-enriched sample of $\text{Me}_2^{15}\text{NBpin}$. The ^{15}N NMR chemical shift of this material appears at -350 ppm, and this value will be used to assign surface species (see below). The amount of Me_2NBpin quantified by integration suggests that approximately 2.8 NMe_2 groups are accessible per zirconium center, again indicating that the predominant surface species in $\text{Zr}(\text{NMe}_2)_n@MSN$ contains three NMe_2 groups per zirconium. Finally, this experiment rules out the presence of any cyclometalated amide in this sample because the interaction of two equivalents of HBpin and the $\equiv\text{OSiZr}(\text{NMeCH}_2)(\text{NMe}_2)(\text{NHMe}_2)$ surface moiety would give $\text{pinB-NMeCH}_2\text{-Bpin}$, and that species was not detected in the solution-phase ^{11}B NMR spectrum.



The ZrH/Bpin@MSN sample was synthesized following the reaction given by equation 2.2. To facilitate the ensuing discussion of this product, whose identification proved to be very challenging, we first consider an independent reaction 2.3 of HBpin on calcined MSN. The ICP measurement of the resulting material, referred to as Bpin@MSN, indicates a boron loading of 1.33 mmol/g.



A ^{11}B DPMAS experiment on Bpin@MSN revealed a single resonance, which, based on the observed NMR shift ($\delta \approx 19$ ppm, see Figure 5A, dashed line) must be attributed to trigonally coordinated boron species. We note that the MAS NMR spectra of half-integer quadrupolar nuclei, such as ^{11}B , are broadened by the quadrupolar interaction, and that the NMR shifts (δ) observed in such spectra consist of contributions from the dominant chemical shifts (δ_{CS}) and the so-called quadrupole induced shifts. Based on the discussion below, we estimate the δ_{CS} value for the boron species in Bpin@MSN to be around 21 ppm, which is close to one measured in the solution NMR spectrum of PhCH₂OBpin (23 ppm), suggesting

that the $\equiv\text{SiOBpin}$ groups are indeed a product of the reaction of equation 2.3. This conclusion is supported by two additional findings. First, the ^1H DPMAS spectrum of Bpin@MSN features a dominant resonance at 1 ppm, consistent with one observed in the solution ^1H NMR spectrum of $\text{PhCH}_2\text{O-Bpin}$ for the pinacol moiety (1.04 ppm). Second, as in the case of ^{15}N CPMAS, by measuring the build-up of $^1\text{H} \rightarrow ^{11}\text{B}$ CP signal as a function of τ_{CP} , we estimated the $^1\text{H} - ^{11}\text{B}$ internuclear distance in Bpin@MSN at $\sim 3.4 \text{ \AA}$ (Figure S7A in SI), in good agreement with the average distance between the ^{11}B and methyl protons in Bpin .⁵⁶

We now return to ZrH/Bpin@MSN produced by the reaction given by equation 2.2. First, ICP-OES measurements show similar zirconium loading (0.89 mmol/g) and boron loading (0.86 mmol/g), and that the loading of Zr from $\text{Zr(NMe}_2)_n\text{@MSN}$ is unaffected by the treatment with HBpin . The ^{11}B spin counting experiment yielded 0.9 (± 0.1) mmol/g of boron in ZrH/Bpin@MSN , in excellent agreement with the ICP-OES analysis. In the ^{11}B DPMAS spectrum of this sample, a broad signal appeared whose NMR shift ($\delta \approx 18 \text{ ppm}$) is similar, but not identical with that of Bpin@MSN discussed above (compare solid and dashed lines in Figure 2.5A). The 2D MQMAS experiment on this sample (Figure 2.5B), which removes the anisotropic broadening due to the second-order quadrupolar interaction and allows for determination of the pure chemical shift (δ_{CS}),^{59,60} shows that the ^{11}B chemical shift for this boron site is the same as in Bpin@MSN ($\delta_{\text{CS}} \approx 21 \text{ ppm}$). The so-called isotropic (vertical) dimension of this spectrum revealed a small shoulder representing an additional resonance with $\delta_{\text{CS}} \approx 23 \text{ ppm}$ (*vide infra*), which most likely represents residual Me_2NBpin trapped within the MSN pores.

We also measured the ^1H DPMAS and 2D ^1H - ^{11}B Hetcor spectra of ZrH/Bpin@MSN (Figure 2.5C and 2.5D). Note that the ^1H projection of the Hetcor spectrum is very similar to the ^1H DPMAS spectrum. The dominant ^1H peak at ~ 1 ppm is easily assigned to the protons of the methyl groups of Bpin, whereas one at ~ 2.4 ppm corresponds to ^1H of a small amount of Me_2N moiety. These results imply that $\equiv\text{SiOBpin}$ is the dominant boron-containing structure found in ZrH/Bpin@MSN. However, in addition to small difference in the observed shifts (Figure 2.5A), the chemical environments of this moiety in Bpin@MSN and in ZrH/Bpin@MSN samples are not identical. Indeed, the $^1\text{H} \rightarrow ^{11}\text{B}$ CP dynamics indicated that the nearest ^1H - ^{11}B internuclear distance is considerably shorter (~ 2.1 Å) in the zirconium-containing sample. Note that these experiments do not establish the identity of the polarizing spin.

The ^{11}B NMR signals for Me_2NBpin and ZrH/Bpin@MSN are unresolved under MAS alone and thus cannot be discerned in the Hetcor spectrum. Most likely, the correlation between the ^{11}B NMR signal and ^1H NMR signal at 2.4 ppm is assigned to the intermolecular interaction between the ^{11}B of abundant $\equiv\text{Si-O-Bpin}$ and ^1H of Me_2NBpin , as well as intramolecular interactions within Me_2NBpin or ZrH/Bpin@MSN species.

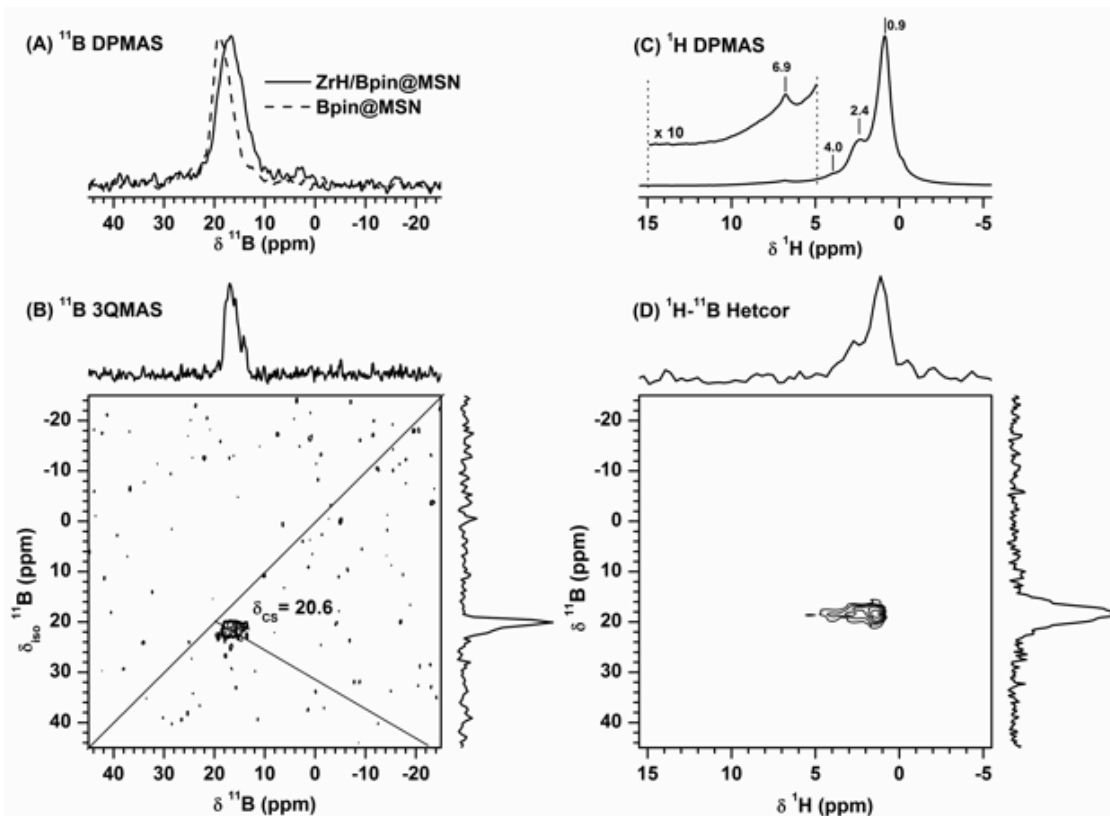
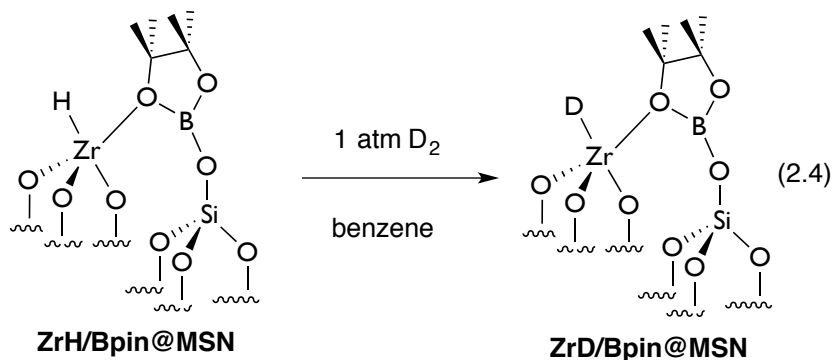


Figure 2.5. (A) ^{11}B DPMAS spectra of Bpin@MSN (dashed line) and ZrH/Bpin@MSN (solid line), (B) 2D ^{11}B 3QMAS spectrum of ZrH/Bpin@MSN, (C) ^1H DPMAS spectrum of ZrH/Bpin@MSN, and (D) 2D ^1H - ^{11}B Hetcor spectrum of ZrH/Bpin@MSN. The spectra were obtained using $\nu_R = 25$ kHz, with (A) $\nu_{\text{RF}}(^{11}\text{B}) = 125$ kHz during hard pulse (corresponding to $\sim 10^\circ$ flip angle), $\nu_{\text{RF}}(^1\text{H}) = 100$ kHz during TPPM ^1H decoupling, 8000 scans, and $\tau_{\text{RD}} = 1$ s; (B) $\nu_{\text{RF}}(^{11}\text{B}) = 125$ kHz and 15 kHz during hard and soft (z-filter) pulses, respectively, $\nu_{\text{RF}}(^1\text{H}) = 100$ kHz during TPPM ^1H decoupling, 64 rows with $\Delta t_1 = 10$ μs , 72 scans per row, and $\tau_{\text{RD}} = 1.5$ s; (C) $\nu_{\text{RF}}(^1\text{H}) = 100$ kHz during hard pulse, 4 scans, and $\tau_{\text{RD}} = 1$ s; and (D) $\nu_{\text{RF}}(^1\text{H}) = 125$ kHz, 75 kHz, and 100 kHz during hard pulse, CP, and TPPM ^1H decoupling, $\nu_{\text{RF}}(^{11}\text{B}) = 50$ kHz during CP, $\tau_{\text{CP}} = 2$ ms, 64 rows with $\Delta t_1 = 20$ μs , 96 scans per row, and $\tau_{\text{RD}} = 1$ s.

Although we propose the surface organometallic species to be a zirconium hydride (eq. 2.3), ^1H NMR resonances at >10 ppm that were previously assigned as $(\equiv\text{SiO})_3\text{ZrH}$ and $(\equiv\text{SiO})_2\text{ZrH}_2$ ⁴¹ were notably absent from the ^1H NMR spectrum of the product from $\equiv\text{SiOZr}(\text{NMe}_2)_3$ and HBpin. Despite the absence of those downfield ^1H resonances, a zirconium hydride species, albeit with a modified coordination sphere from $(\equiv\text{SiO})_3\text{ZrH}$ and $(\equiv\text{SiO})_2\text{ZrH}_2$, is a proposed product of the reaction of $\text{Zr}(\text{NMe}_2)_n@MSN$ and HBpin. In fact, the room temperature, solution-solid interfacial reaction conditions of the hydroboration are mild with respect to the gas-solid $150\text{ }^\circ\text{C}$ reaction of $\equiv\text{SiOZr}(\text{CH}_2\text{CMe}_3)_3$ that gives $(\equiv\text{SiO})_3\text{ZrH}$ and $(\equiv\text{SiO})_2\text{ZrH}_2$. That is, HBpin as a hydride source may provide access to new zirconium-hydride surface structures. Unfortunately, we are unaware of any reliable chemical shift information on structures such as $\equiv\text{SiOZrH}_3$; however on the basis of the chemical shift trend for $(\equiv\text{SiO})_3\text{ZrH}$ and $(\equiv\text{SiO})_2\text{ZrH}_2$, the ^1H NMR signal for $\equiv\text{SiOZrH}_3$ might be expected to be at least >12 ppm. In contrast to that trend, a small resonance at around 6.9 ppm is present in our sample (Figure 2.5C). This signal is not observed in the sample from the reaction of MSN and HBpin. The zirconium-bound hydrogen chemical shifts in $\text{Cp}^*_2\text{ZrH}_2$, $(\text{Cp}^*_2\text{ZrH})_2\text{O}$, and $\text{Cp}^*_2\text{ZrH}(\text{NH}_2)$ ($\text{Cp}^* = \text{C}_5\text{Me}_5$) were reported to be 7.46, 5.5 and 4.82 ppm respectively,^{61,62} and even further upfield ZrH resonances were reported for $\text{Cp}^*_2\text{ZrH}(\text{NH}_2\text{BH}_3)$.⁶³ That is, association of pinacolborane or borate groups or amide moieties with a surface-bonded zirconium hydride might result in upfield chemical shifts with respect to $(\equiv\text{SiO})_3\text{ZrH}$ and $(\equiv\text{SiO})_2\text{ZrH}_2$. To test for the presence of a surface-supported zirconium hydride that is distinct from $(\equiv\text{SiO})_3\text{ZrH}$ and $(\equiv\text{SiO})_2\text{ZrH}_2$ and assign the ^1H NMR signal at 6.9 ppm, the HBpin-treated solid was allowed to react with D_2 gas in benzene (eq. 2.4).



Upon treatment with 1 atm of D_2 , the signal at 6.9 ppm diminished 50%, and after 3 cycles with 1 atm of D_2 , the signal disappeared entirely (Figure 2.6). Interestingly, the 2H NMR spectrum from the reaction of $ZrH/Bpin@MSN$ and D_2 gives only a signal at ~ 2.5 ppm, suggesting that deuterium is incorporated in methyl groups. Unfortunately, a signal at ~ 7 ppm could not be unambiguously identified above the noise. However, 2H DPMAS spectrum of $ZrD/Bpin@MSN$ from the reaction of $DBpin$ and $Zr(NMe_2)_n@MSN$ contains signals at 7.3, 4.0, 2.5 (as a shoulder), and 1.5 ppm corresponding to deuterium incorporation into ZrH , NMe_2 , and $Bpin$ groups. On the basis of these facile H/D exchange reactions, this resonance is assigned as a zirconium hydride. Spin counting experiments indicate that the ZrH loading is ca. 0.5 mmol per gram, and thus surface ZrH sites account for $> 50\%$ of the zirconium in the sample.

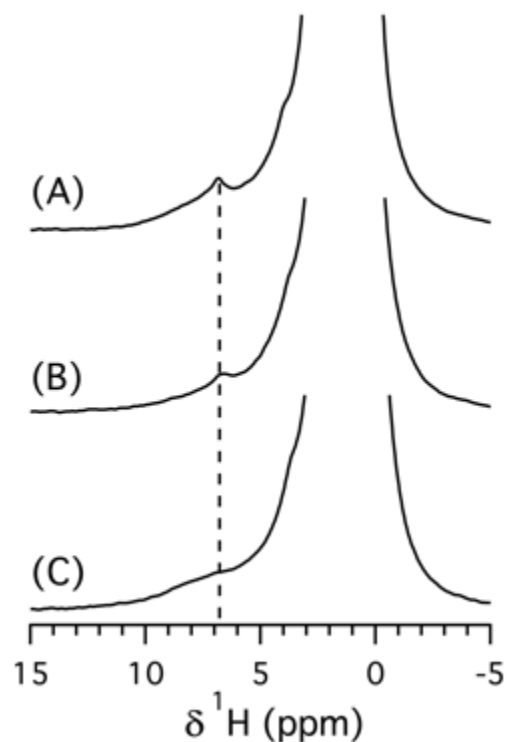


Figure 2.6. ^1H DPMAS spectra of $\text{Zr}(\text{NMe})_n@MSN + 10 \text{ HBpin}$, (A) as synthesized, (B) 1 time of D_2 exchange, (C) 3 times of D_2 exchange. The spectra are normalized to the sample amount and show the absolute intensities. The spectra were obtained using $\nu_R = 40 \text{ kHz}$, $\nu_{\text{RF}}(^1\text{H}) = 125 \text{ kHz}$, and $\tau_{\text{RD}} = 20 \text{ s}$.

The infrared spectrum of the $\text{ZrH/Bpin}@MSN$ solid product further supported this assignment (Figure 2.7B) on the basis of a band centered at 1592 cm^{-1} that we assigned to a ν_{ZrH} . The IR spectrum of MSN treated with HBpin does not contain signals in this region (Figure 2.7A). Previously, a signal at 1638 cm^{-1} was assigned to the ν_{ZrH} in $(\equiv\text{SiO})_3\text{ZrH}$.⁴¹ Importantly, the 1592 cm^{-1} peak was not detected in the IR spectrum of the $\text{ZrH/Bpin}@MSN$ exposed to D_2 , and this change is taken as evidence for the formation of $\text{ZrD/Bpin}@MSN$ (Figure 2.7C). Unfortunately, the expected location of a ν_{ZrD} at 1125 cm^{-1} overlaps with the silica absorptions, and that signal could not be detected. However, the signal at 1592 cm^{-1}

reappears upon addition of H_2 to $ZrD/Bpin@MSN$ (Figure 2.7D). Interestingly, new broad signals at $\sim 2395\text{ cm}^{-1}$ appear in the sample treated with D_2 . Similar bands were observed in the spectrum resulting from treatment of $Zr(NMe_2)_n@MSN$ with DBpin (Figure 2.7E); in that IR spectrum, the signal at 1592 cm^{-1} was also not detected. These lower energy bands $\sim 2395\text{ cm}^{-1}$ may be attributed to H/D exchange reactions catalyzed by a surface zirconium hydride and correspond to signals of deuterium-exchanged pinacol and amido methyls. These observations are consistent with the 1H SSNMR results and support the characterization of this material as containing a zirconium hydride, including the expected H/D exchange reactivity.⁶

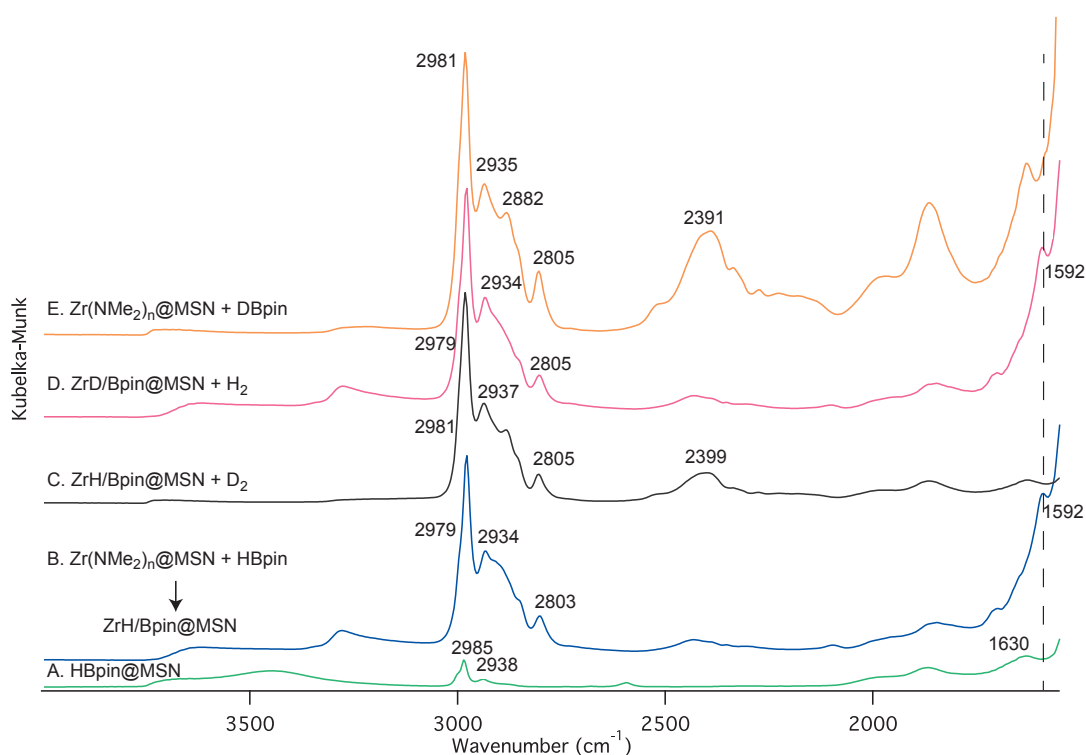


Figure 2.7. Diffuse reflectance IR spectra of (A) Bpin@MSN, (B) ZrH/Bpin@MSN, (C) ZrH/Bpin@MSN + D_2 , and (D) ZrD/Bpin@MSN + H_2 .

Finally, additional experiments were performed to account for the small amount of NMe_2 groups in the reaction of HBpin and $Zr(NMe_2)_n@MSN$ (which produced only 2.5

mmol of Me₂NBpin vs 2.7 mmol per gram of Zr(NMe₂)₃@MSN). Combustion analysis of ZrH/Bpin@MSN revealed 0.4 ± 0.05 mmol of nitrogen per gram of material. This value is significantly reduced in comparison to the Zr(NMe₂)_n@MSN starting sample. Therefore, a ¹⁵N-¹H idHetcor experiment was used to probe the identity of the nitrogen species (Figure 2.8). There is a correlation from a ¹⁵N NMR signal at -355 ppm to a ¹H NMR resonance at 2.4 ppm. On the basis of the similarity of this chemical shift to Me₂NBpin and the ¹¹B NMR signal at 24 ppm, we attribute the residual ¹⁵N SSNMR signal partly to surface-absorbed Me₂NBpin. Furthermore, there is also a correlation between the ¹⁵N SSNMR signal at -355 ppm and a signal in the ¹H NMR dimension at 7.9 ppm. These chemical shifts, as well as the ¹H-¹⁵N correlation suggests that some of the remaining surface nitrogen is present as Zr-NHMe₂.

The evidence supporting the identity of ZrH/Bpin@MSN, formed from reaction of Zr(NMe₂)_n@MSN and HBpin as a zirconium hydride is given in Table 2.3, and a description of the spectroscopy and structural assignment is summarized in the conclusion.

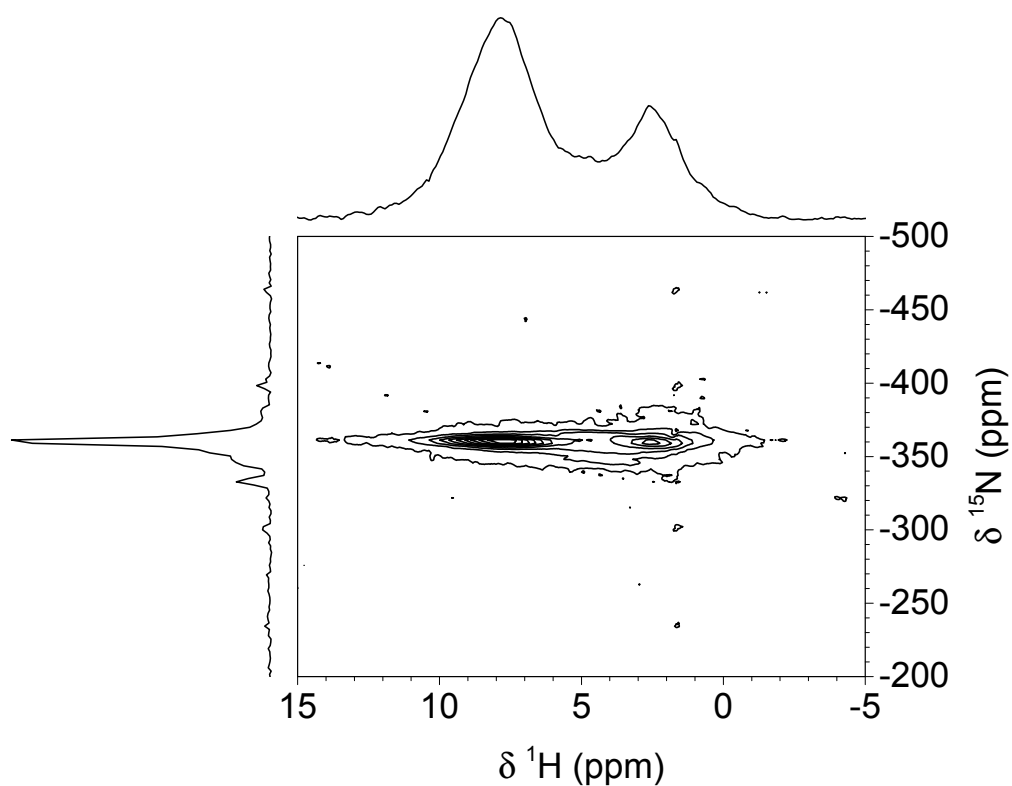


Figure 2.8. 2D ^{15}N - ^1H idHetcors spectrum of ^{15}N -enriched ZrH/Bpin@MSN. The spectrum was obtained at 14.1 T, using $\nu_R = 34$ kHz; $\nu_{\text{RF}}(^1\text{H}) = 91$ kHz during 90° pulse and CP, and 10 kHz during SPINAL-64 ^1H decoupling; $\nu_{\text{RF}}(^{15}\text{N}) = 57$ kHz during CP and 90° pulses, and 10 kHz during SPINAL-64 ^{15}N decoupling; 128 rows with $\Delta t_1 = 30$ μs ; 64 scans per row, and STATES-TPPI acquisition with $\tau_{\text{RD}} = 2$ s.

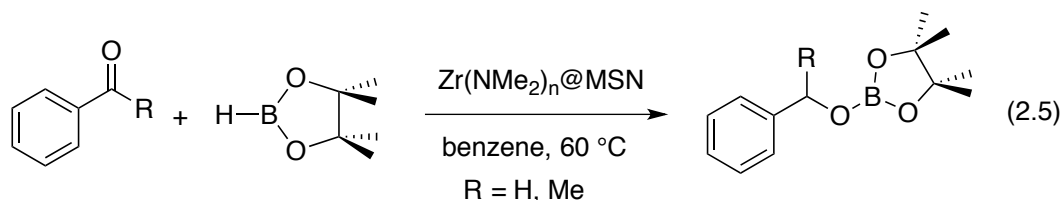
Table 2.3. Characterization Experiments and Conclusions Regarding the Nature of ZrH/Bpin@MSN.

Experiments	Observations	Interpretations
Reaction stoichiometry: Zr(NMe ₂) _n @MSN + HBpin	2.5 mmol Me ₂ NBpin formed/g Zr(NMe ₂) _n @MSN	all but ca. 0.2 mmol NMe ₂ /g are desorbed from the material
Reaction side products:		
Zr(NMe ₂) _n @MSN + HBpin	small amount of H ₂ formed	few reactive silanols or NH groups present in Zr(NMe ₂) _n @MSN
MSN + HBpin	large amount of H ₂ formed	
ICP-OES:		the Zr:B ratio is ~ 1:1.
Zr(NMe ₂) _n @MSN + HBpin:	0.89 mmol Zr/g material 0.86 mmol B/g material	HBpin treatment does not leach Zr from MSN
MSN + HBpin:	1.33 mmol B/g material	Bpin is grafted to the material
IR	ν_{ZrH} observed at 1592 cm ⁻¹	zirconium hydride formed using HBpin that is distinct from (=SiO) ₃ ZrH
Reaction with D ₂ , then H ₂	band at 1592 cm ⁻¹ disappears upon D ₂ addition, then reappears upon H ₂ addition	exchangable zirconium hydride
¹ H SSNMR: treatment with D ₂	δ_{ZrH} at 6.9 ppm, 0.5 mmol H/g Signal disappears upon D ₂ addition	the zirconium hydride surface species is distinct from (=SiO) ₃ ZrH
¹¹ B SSNMR:		
MSN + HBpin	$\delta \approx 19$ ppm; $\delta_{\text{CS}} \approx 21$ ppm; ¹ H- ¹¹ B distance ~3.4 Å	the =SiOBpin chemical environment is influenced by surface Zr species
Zr(NMe ₂) _n @MSN + HBpin	$\delta \approx 18$ ppm; $\delta_{\text{CS}} \approx 21$ ppm; ¹ H- ¹¹ B distance ~2.1 Å	
¹¹ B NMR spin count	0.9 mmol B/g	

Table 2.3. Continued

^1H - ^{15}N Hetcor	-355 ppm ^{15}N signal correlates with 7.9 ppm ^1H signal	residual NMe ₂ groups unreactive due to zirconium-coordination and H-bonding
---------------------------------------	-----------------------------------------------------------------------------	-----------------------------------------------------------------------------------------

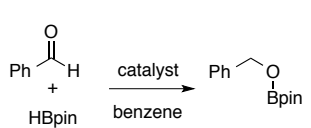
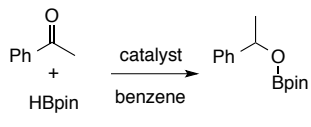
Catalytic hydroboration of carbonyls. On the basis of the facile reaction of $\text{Zr}(\text{NMe}_2)_n@ \text{MSN}$ and HBpin, this material was investigated as a catalyst for the hydroboration of carbonyl compounds with pinacolborane. Initially, benzaldehyde was used as a test substrate to compare the reactivity of supported zirconium with possible background reactions and homogeneous analogues. With grafted tris(amido)zirconium as the precatalyst (5 mol %, based on ICP-OES-determined zirconium loading), quantitative conversion of benzaldehyde to its pinacolborane ester is accomplished at room temperature after 2 h in benzene-*d*₆, as determined by ^1H NMR spectroscopy (eq. 2.5). Control experiments, in which PhCHO and HBpin are mixed in benzene at room temperature with or without MSN give only trace quantities of product (Table 2.4). In addition, conversion of PhCHO and HBpin occur to the same extent with the zirconium-free material $\equiv\text{SiOBpin}$, obtained from the reaction of MSN and HBpin, as the slow, uncatalyzed background reaction. Thus, the zirconium sites present in the $\text{Zr}(\text{NMe}_2)_n@ \text{MSN}$ material are responsible for catalytic activity.



Further support for this idea is provided by related homogeneous catalysis. The compound $\text{Zr}(\text{NMe}_2)_4$ is an effective catalyst for this carbonyl hydroboration reaction, as is

$\{\text{PhB}(\text{Ox}^{\text{Me}2})_2\text{C}_5\text{H}_4\}\text{Zr}(\text{NMe}_2)_2$.⁴⁶ In the presence of 5 mol % of either soluble complex, quantitative conversion of PhCHO to PhCH₂OBpin is observed after 30 min in benzene-*d*₆ at 60 °C. The faster conversion obtained with homogeneous vs heterogeneous catalysts may result from the effect of diffusion, a lower percentage of active sites or slower site activation in the supported catalyst, or simply the effect of silica as a ligand for zirconium in this catalysis.

Table 2.4. Catalytic hydroboration of benzaldehyde and acetophenone with pinacolborane.^a

Reaction	Catalyst (5 mol %)	Temp. (°C)	Time (h)	Conv. (%) ^b
	No cat	25	1	Trace
	MSN	25	1	0
	Zr(NMe ₂) ₄	25	0.5	>99
	Zr(NMe ₂) _n @MSN	25	2	>99
	$\{\text{PhB}(\text{Ox}^{\text{Me}2})_2\text{C}_5\text{H}_4\}\text{Zr}(\text{NMe}_2)_2$	25	0.5	>99
	No cat	25-100	2	0
	MSN	25-100	2	0
	Zr(NMe ₂) ₄	25	1	>99
	Zr(NMe ₂) ₄	60	0.5	>99
	Zr(NMe ₂) _n @MSN	25	24	>99
	Zr(NMe ₂) _n @MSN	60	2	>99
	$\{\text{PhB}(\text{Ox}^{\text{Me}2})_2\text{C}_5\text{H}_4\}\text{Zr}(\text{NMe}_2)_2$	25	10	>99
	$\{\text{PhB}(\text{Ox}^{\text{Me}2})_2\text{C}_5\text{H}_4\}\text{Zr}(\text{NMe}_2)_2$	60	1	>99

^a5 mol % catalyst in benzene-*d*₆ using 1.3 equiv. of HBpin. ^bObtained by integration of product signal in comparison to Si(SiMe₃)₄ as an internal standard.

The hydroboration using $Zr(NMe_2)_n@MSN$ as the catalyst is selective in the presence of a number of functional groups, as determined by conversion of substituted benzaldehydes shown in Table 2.5. Aldehyde substrates containing ethers (*p*-methoxy-benzaldehyde and furfural), nitro groups (*p*-nitrobenzaldehyde), halides (*p*-chlorobenzaldehyde), alkyl substitution (*p*-tolualdehyde), an aliphatic aldehyde (cyclohexanecarboxaldehyde) and ferrocene substitution (ferrocene-2-carboxaldehyde) are readily reduced, although *para*-chlorobenzaldehyde required 5× greater reaction time than benzaldehyde. *Para*-substitution by formyl or pinacolborane ester groups does not impact the reacting moiety as assessed by the hydroboration of *p*-phthaldialdehyde which gives 1,4-bis(pinacolborane ester)benzene. Equivalent amounts of the solvent, reactants, and catalysts are used in each experiment for consistency and straightforward comparisons between substrates.

Table 2.5. $Zr(NMe_2)_n@MSN$ -catalyzed hydroboration of aldehydes with pinacolborane.^a


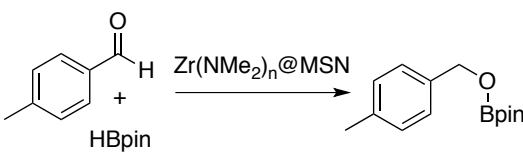
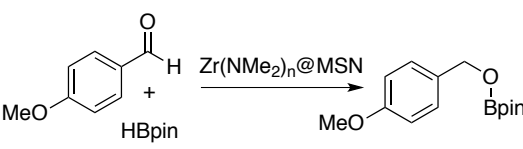
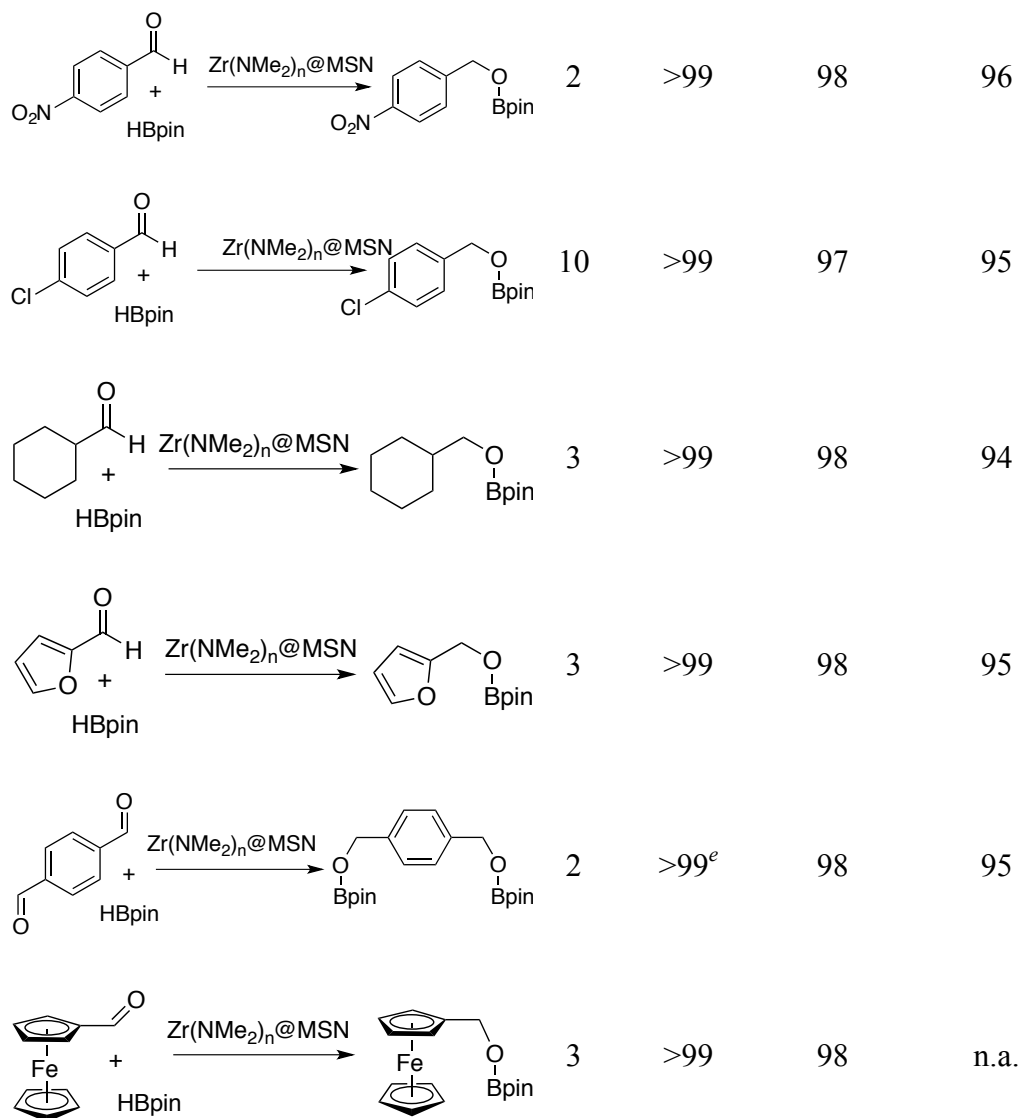
Catalytic Conversion	Time (h)	Conv. (%) ^b	Boronate Yield (%) ^c	Alcohol Yield (%) ^d
	2	>99	98	95
	2	>99	97	95
	2	>99	98	95

Table 2.5. Continued



^aAll the reactions are carried with 5 mol % $\text{Zr}(\text{NMe}_2)_n@MSN$ in benzene- d_6 at room temperature using 1.3 equiv. of HBpin. ^bObtained by integration of RCH_2OBpin signal against $\text{Si}(\text{SiMe}_3)_4$ as an internal standard. ^cIsolated yields for RCH_2OBpin product. ^dIsolated yield of RCH_2OH product after hydrolysis with NaOH. ^e2 equiv. HBpin used.

The hydroboration of ketones is also efficiently catalyzed by $\text{Zr}(\text{NMe}_2)_n@MSN$. A background screen of catalyst-free conditions, calcined MSN, or $=\text{SiOBpin}$ as catalysts for the addition of acetophenone and pinacolborane only returned unreacted acetophenone, even with heating to 100 °C (see Table 2.3). A loading of 5 mol % $\text{Zr}(\text{NMe}_2)_n@MSN$ catalyzes

quantitative formation of 1-phenylethoxyborane ester after 24 h at room temperature in benzene. However, 60 °C appears to be a generally appropriate temperature for convenient rates of conversion. As in the aldehyde hydroboration examples, reactions of acetophenone and HBpin with 5 mol % $\text{Zr}(\text{NMe}_2)_4$ or $\{\text{PhB}(\text{Ox}^{\text{Me}_2})_2\text{C}_5\text{H}_4\}\text{Zr}(\text{NMe}_2)_2$ (under homogeneous conditions) is accomplished in shorter times than with 5 mol % $\text{Zr}(\text{NMe}_2)_n@MSN$.

As in the aldehyde hydroboration, aliphatic substituents with α -hydrogen are reduced without production of pinacolborane enolate ester side products that might form through substrate deprotonation (Table 2.6). Linear aliphatic ketones are reduced more rapidly than cyclic aliphatic or aryl-substituted ketones. Ketones containing nitroarene or trifluoromethyl groups are readily reduced without affecting the functionality. In addition, α,β -unsaturated ketones are reduced selectively at the carbonyl, leaving the carbon-carbon double-bond intact. Benzophenone and fluorenone are also reduced in good yield, with fluorenone showing faster conversion under equivalent conditions.

Table 2.6. $\text{Zr}(\text{NMe}_2)_n@MSN$ -catalyzed hydroboration of ketones with pinacolborane.^a

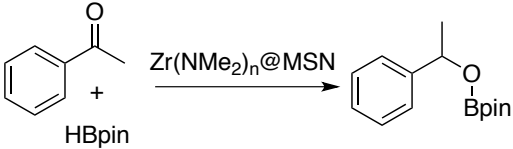
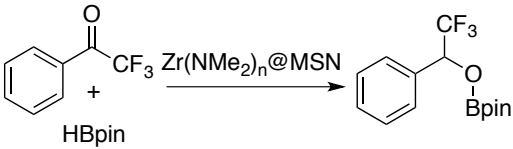
Reaction	Time (h)	Conv. (%) ^b	Boronate Yield (%) ^c	Alcohol Yield (%) ^d
	2	>99	97	91
	2	>99	97	92

Table 2.6. Continued

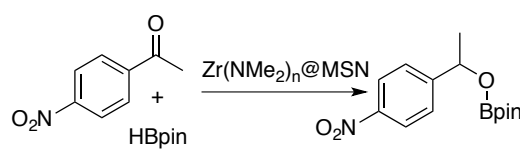
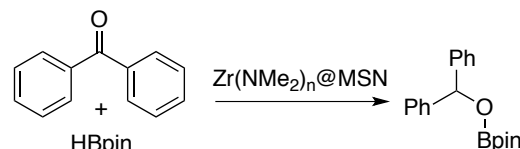
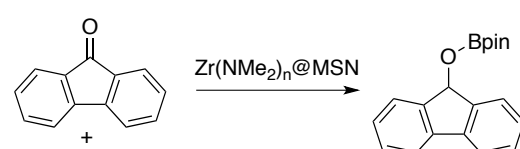
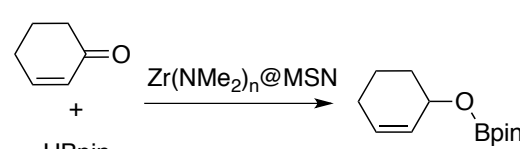
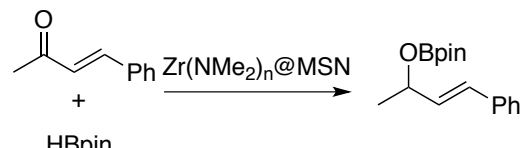
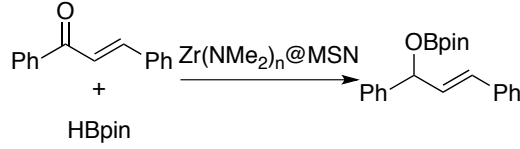
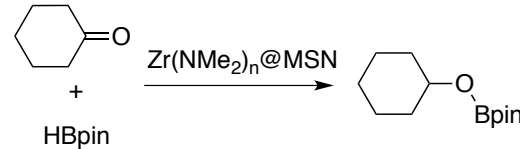
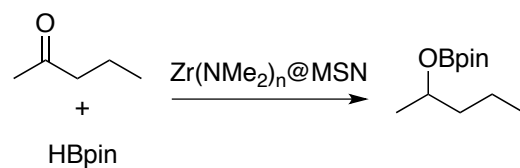
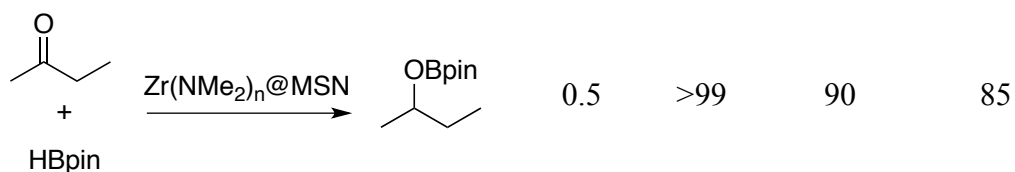
	2	>99	95	92
	4	>99	97	94
	2	>99	98	93
	1	>99	98	92
	3	>99	95	90
	7	>99	96	91
	1	>99	98	92
	0.5	>99	91	87

Table 2.6. Continued

^aAll the reactions are carried with 5 mol % catalyst in benzene-*d*₆ at 60 °C using 1.3 equiv. of HBpin. ^bObtained by integration of R₂CHOBpin signal against Si(SiMe₃)₄ as an internal standard. ^cIsolated yields for R₂CHOBpin. ^dIsolated yield for R₂CHOH

A possible intermediate in the zirconium-catalyzed carbonyl hydroboration is a zirconium alkoxy moiety of the type [Zr]–OCHRR'. The reaction of such an intermediate with pinacolborane to form a B–O bond is not necessarily straightforward given the oxophilicity of zirconium. We should note, however, that our recently proposed boron-centered zwitterionic mechanism for a magnesium-catalyzed hydroboration of esters avoids the magnesium alkoxide intermediate.²⁴ A related mechanism could bypass the Zr–O bond in the current catalysis. Despite this possibility, magnesium alkoxides and HBpin react to give pinacolborane esters. Moreover, the surface-supported zirconium amide and HBpin react to give Me₂NBpin.

Thus, the intermediacy of [Zr]OCHRR' is not ruled out, and there are (at least) two types of Zr–O bonds present in a possible (≡SiO)_nX_{3-n}Zr–OCHRR' intermediate, a siloxide-zirconium bond and an alkoxide-zirconium bond. Both moieties might be capable of reaction with HBpin, with the reaction of ≡SiOZr bonds potentially resulting in catalyst leaching. In order to test for this possibility, the Zr(NMe₂)_n@MSN was reacted with excess HBpin and the MSN product was analyzed. Low angle powder XRD and TEM measurements (Figure 2.1D-E) indicated that the pore structure and particle morphology were not affected by the pinacolborane. In addition, EDX measurements (Figure 2.1F) show that the well-distributed

zirconium remains unchanged after treatment with HBpin. Thus the zirconium-surface interaction and the silica wall structure is maintained in the presence of HBpin.

A number of additional experiments also were performed to test for zirconium leaching. First, the catalytic material was isolated by filtration, washed with benzene, dried under vacuum, and reused in hydroboration of benzaldehyde or acetophenone. This sequence was performed eight times with both PhCHO and PhC(O)Me as substrates without apparent loss of catalytic activity (Figure 2.9). The reactions were monitored during the conversion, verifying that ~2 h are required for full conversion in the first and eighth cycles. Moreover, plots of acetophenone concentration versus time roughly follow exponential decay, with the observed pseudo first-order rate constants after 1, 4, and 8 recycles being $4 \times 10^{-4} \text{ s}^{-1}$, $4 \times 10^{-4} \text{ s}^{-1}$, and $3 \times 10^{-4} \text{ s}^{-1}$. Thus, the rates of catalysis are not significantly diminished with repeated catalysts recycling. In the first cycle with $\text{Zr}(\text{NMe}_2)_n@ \text{MSN}$ as the precatalyst, the Me_2NBpin byproduct of catalyst activation is present in the crude $\text{RR}'\text{HCO-Bpin}$ product. This substance was not observed during subsequent cycles, and pure boronate ester product is obtained after filtration and evaporation of volatile materials.

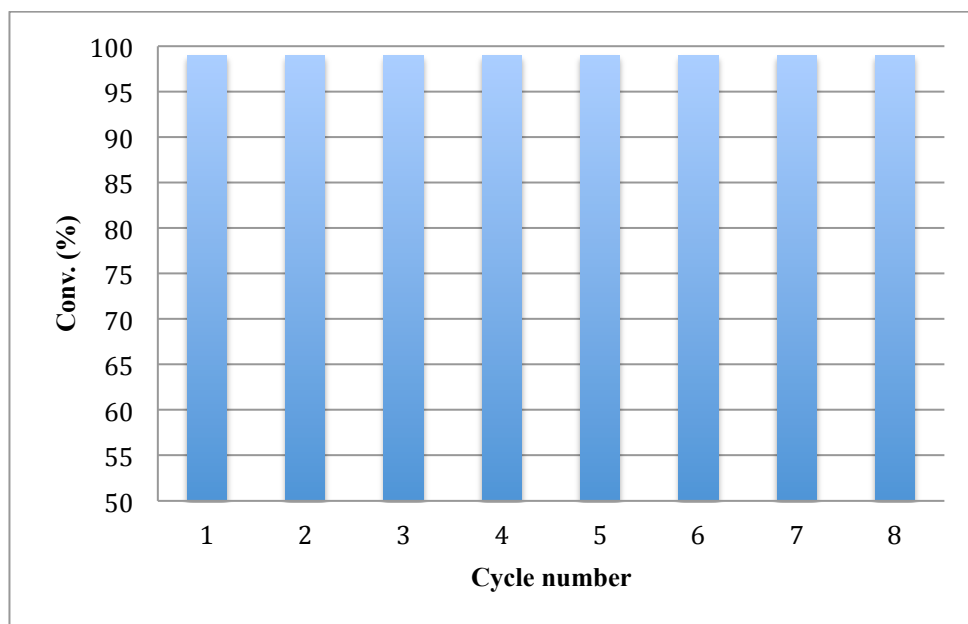


Figure 2.9. Catalyst recycling experiments. Quantitative conversion and >99% selectivity for acetophenone hydroboration is observed after reisolation and reapplication of the catalyst for at least 8 cycles. In situ monitoring of the catalytic reactions indicated that ~2 h is required for full conversion in each recycle experiment.

Secondly, the zirconium loading on MSN after catalysis, as determined by ICP-OES, is identical within error after grafting of $Zr(NMe_2)_4$ on calcined MSN and after heating at 60 °C in benzene. The same weight % Zr is obtained for the ZrH/Bpin@MSN material as obtained from the reaction of HBpin and $Zr(NMe_2)_n@MSN$ and after catalytic hydroboration reactions (Table 2.1). In addition, a catalytic reaction mixture was filtered after 50% conversion to give a mixture of PhCOMe, HBpin, and PhMeHCO-Bpin, and the soluble portion of the reaction mixture was heated at 60 °C. The ratio of starting material and product in this separated solution-phase portion is invariant over 1 h (i.e., no further conversion), while full conversion to PhMeHCO-Bpin is observed in an unfiltered parallel experiment. Finally, the supernatant was evaporated after a catalytic reaction and only trace amount of

zirconium (0.001 mM) was detected by ICP-OES. These experiments reinforce the robust nature of the supported zirconium catalyst and the supported nature of the hydroboration catalyst.

Conclusion

The reaction of $\text{Zr}(\text{NMe}_2)_4$ and calcined mesoporous silica provides $\text{Zr}(\text{NMe}_2)_n@MSN$, a material containing zirconium sites with a $\text{Zr}:\text{NMe}_2$ ratio of $\sim 1:2.7$. Detailed SSNMR studies, particularly ^{15}N Hetcor experiments and DNP-enhanced CPMAS ^{15}N NMR spectra, reveal that zirconium is primarily bonded to dimethylamide groups, with a small amount of coordinated dimethylamine. These data, together with quantitative ^{13}C SSNMR and elemental analysis, characterize the surface zirconium species as containing three sites: primarily (more than 70%) coordinated by three nitrogen-containing ligands, with the remaining sites (up to 30%) as the dipodal $(\equiv\text{SiO})_2\text{Zr}(\text{NMe}_2)_2$. Moreover, the former sites are a mixture of mainly monopodal $\equiv\text{SiOZr}(\text{NMe}_2)_3$ (more than 90%) with the small remaining amount as diamido amine $(\equiv\text{SiO})_2\text{Zr}(\text{NMe}_2)_2(\text{NHMe}_2)$. The basis for this conclusion is the reactivity of $\text{Zr}(\text{NMe}_2)_n@MSN$ with HBpin. Around 85-90% of the surface NMe_2 groups react with HBpin to give Me_2NBpin , and the remaining nitrogen groups are likely present as either zirconium-coordinated and hydrogen-bond species or physisorbed Me_2NBpin . This assignment is supported by the characteristic ^{15}N SSNMR chemical shift (-355 ppm), the nitrogen correlation with a broad downfield hydrogen signal in $^{15}\text{N}-^1\text{H}$ Hetcor experiments, and the high reactivity of both dimethylamine and dimethyl amidozirconium groups toward pinacolborane. The latter observations suggest that the unreactive NMe_2 are in chemically distinct environments from free HNMe_2 and ZrNMe_2 moieties, and coordination

to zirconium and the involvement of the NMe_2 groups in hydrogen-bonding to the silica surface may explain their inert nature.

The surface species formed in the reaction of $\text{Zr}(\text{NMe}_2)_n@MSN$ and HBpin, namely $\text{ZrH/Bpin}@MSN$, was characterized by ^1H and ^{11}B SSNMR and infrared spectroscopies. In this MSN system, the reaction of HBpin and silanol groups provides $\equiv\text{SiOBpin}$, and the interaction of these groups and surface zirconium species perturbs the chemical environment of the surface Bpin groups. ^1H NMR and infrared spectroscopies reveal signals assigned to zirconium hydride, and these assignments are supported by selective H/D exchange reactions of zirconium hydride and D_2 or zirconium deuteride with H_2 . Thus, the reaction of HBpin and $\text{Zr}(\text{NMe}_2)_n@MSN$ provides a zirconium hydride that shows the anticipated reactivity of such a species in H/D exchange reactions.

The present work has demonstrated that surface-supported, catalytically active zirconium hydrides are accessible from amides and likely from metal alkoxides or hydroxides using HBpin as the hydride source. That notion is advanced by characterization data and the catalytic hydroboration studies, which may involve the zirconium hydride and zirconium alkoxides as catalytic intermediates. The zirconium sites on MSN are active in carbonyl hydroboration even after exposure of the catalytic materials to air. For example, reaction of $\text{Zr}(\text{NMe}_2)_n@MSN$ and air produces detectable amounts of HNMe_2 , but the addition reaction of HBpin and acetophenone is readily catalyzed by the hydrolyzed material under the conditions of Table 4. Thus, this MSN-supported early transition metal system is a capable, robust catalyst for the reduction of oxygenated organic compounds.

Although the catalytic reduction of oxygenates by early transition metal sites has previously been demonstrated with homogeneous catalysis, zirconium hydrides are typically

associated with extreme sensitivity to air and moisture. This list of highly sensitive species includes silica surface-supported zirconium hydrides, which have previously shown high reactivity toward inert substrates such as methane.^{1,3,6,40} Although the apparent rate of hydroboration with surface-supported $\text{Zr}(\text{NMe}_2)_n@MSN$ is lower than the homogeneous zirconium catalysts, the accessibility of a catalytically active species even after air exposure and the recyclability of the surface-supported catalyst provide appealing advantages for the heterogeneous system. We are currently exploring other hydride sources to access surface-supported hydrides for new catalytic applications.

Experimental

General. All reactions were performed under a dry argon atmosphere using standard Schlenk techniques or under a nitrogen atmosphere in a glovebox, unless otherwise indicated. Dry, oxygen-free solvents were used throughout. Benzene, toluene, pentane, methylene chloride, and tetrahydrofuran were degassed by sparging with nitrogen, filtered through activated alumina columns, and stored under nitrogen. Benzene- d_6 was heated to reflux over Na/K alloy and vacuum-transferred. SBA-15 type MSNs were synthesized according to the literature,⁴⁴ calcined at 550 °C, washed with water, and then heated to 550 °C under vacuum. The materials were characterized by N_2 sorption/desorption, powder XRD, TEM, solid-state ^1H , ^{11}B , ^{13}C and ^{15}N (SS)NMR spectroscopy, ^{15}N SSNMR spectroscopy enhanced by dynamic nuclear polarization (DNP), and infrared spectroscopy. $\text{Zr}(\text{NMe}_2)_4$,⁴⁵ $\{\text{PhB}(\text{Ox}^{\text{Me}_2})_2\text{C}_5\text{H}_4\}\text{Zr}(\text{NMe}_2)_2$ (Ox^{Me_2} = 4,4-dimethyl-2-oxazoline),⁴⁶ $\text{Si}(\text{SiMe}_3)_4$ ^{47,48} and DBpin⁴⁹ were synthesized according to literature procedures. Pinacolborane (used as received) and 98% ^{15}N -labeled $[\text{H}_2^{15}\text{NMe}_2]\text{Cl}$ (dried under vacuum at 120 °C for 2 h) were

purchased from Aldrich. Solution-phase ^1H , $^{13}\text{C}\{^1\text{H}\}$ and ^{11}B NMR spectra were collected either on a Bruker DRX 400 MHz spectrometer, Bruker Avance III 600 MHz spectrometer or a Varian MR 400 MHz spectrometer. ^{11}B NMR spectra were referenced to an external sample of $\text{BF}_3 \cdot \text{Et}_2\text{O}$. Infrared spectra were recorded on neat MSN samples using a Bruker Vertex 80 spectrometer using a Harrick Praying Mantis Diffuse Reflection Accessory in a reaction chamber with ZnSe windows. These samples were prepared and maintained under an inert N_2 atmosphere. Elemental analyses were performed using a Perkin-Elmer 2400 Series II CHN/S in the Iowa State Chemical Instrumentation Facility.

Inductively coupled plasma-optical emission spectroscopy (ICP-OES) was performed on ten samples to measure the zirconium loading in $\text{Zr}(\text{NMe}_2)_n@MSN$ and zirconium and boron loading in $\text{ZrH/Bpin}@MSN$. The samples (2.0 – 4.0 mg each) were digested for 24 h in aqueous HF and HCl solution (0.18% and 5% respectively) and analyzed in a Perkin Elmer Optima 2100 DV ICP-OES instrument.

N_2 sorption isotherms were measured in a Micromeritics Tristar surface area analyzer. Samples were previously degassed for 6 h under a N_2 flow at 393 K, and the isotherms were determined at 77 K. The surface area was calculated using the Brunauer-Emmett-Teller equation, and the pore size distribution was obtained from analysis of the adsorption branch of the isotherm using the Barrett-Joyner-Halenda method.

Powder X-ray diffraction (XRD) patterns were obtained with a Rigaku Ultima IV diffractometer using a Cu target at 40 kV and 44 mA. $\text{K}\beta$ was removed with a monochromator, and the data were collected from 0.7 to $8\ 2\theta^\circ$ with a resolution of $0.02\ 2\theta^\circ$.

Transmission electron microscopy (TEM) and high angle annular dark field scanning TEM (HAADF-STEM) images were acquired in a Tecnai G2 F20 electron microscope

operated at 200 kV. Samples were prepared by dispersion into benzene, deposition of a single drop in a copper grid coated with lacey carbon, and evaporation at room temperature. Energy dispersive X-ray (EDX) spectra were collected on representative areas to probe for homogeneity of elemental composition.

SSNMR measurements were performed on a 600 MHz Varian NMR System spectrometer, equipped with a 1.6-mm magic-angle spinning (MAS) probe. Several one-dimensional (1D) and two-dimensional (2D) experiments were used, including 1D ^1H , ^2H , ^{13}C , and ^{11}B MAS with direct polarization (DPMAS), 1D $^1\text{H} \rightarrow ^{13}\text{C}$ cross-polarization under MAS (^{13}C CPMAS), ^{15}N CPMAS, ^{11}B CPMAS, 2D ^{11}B triple-quantum (3Q)MAS, as well as 2D ^1H - ^{11}B heteronuclear correlation (Hetcor) NMR and indirectly detected ^{15}N - ^1H (id)Hetcor NMR. The samples were packed in zirconia MAS rotors in a glovebox under nitrogen atmosphere. NMR experiments were carried out under N_2 atmosphere, as well.

The ^{15}N DNP-enhanced CPMAS experiments were performed at 9.4 T on a 400 MHz Bruker DNP SSNMR spectrometer equipped with a low-temperature (~ 100 K) MAS probe. The sample was prepared by impregnating the MSNs with a 16 mM solution of TEKPol in 1,1,2,2-tetrachloroethane (predried by stirring overnight with CaCl_2 followed by distillation under N_2), and then packed into a 3.2-mm sapphire MAS rotor.^{50,51}

The SSNMR experimental parameters are given in the figure captions using the following symbols: ν_R denotes the MAS rate, $\nu_{\text{RF}}(\text{X})$ is the magnitude of the RF field applied to X nuclei, τ_{CP} is the cross-polarization contact time, τ_{RD} is the recycle delay, Δt_1 is the time interval of t_1 during 2D acquisition.

Zr(NMe₂)₄. Labeled $\text{H}^{15}\text{NMe}_2$ was only available as $\text{Me}_2^{15}\text{NH}\cdot\text{HCl}$, so the synthesis of $\text{Zr}(\text{NMe}_2)_4$ from $\text{Me}_2\text{NH}\cdot\text{HCl}$ was developed, first with unlabeled starting material and then

on small scale with the isotopically enriched material. Dried $\text{Me}_2\text{NH}\cdot\text{HCl}$ (0.500 g, 6.133 mmol) was suspended in tetrahydrofuran (50 mL) and cooled to $-78\text{ }^\circ\text{C}$, and $n\text{BuLi}$ (4.9 mL, 12.3 mmol) was added. The mixture was stirred at this temperature for 2 h and then warmed to room temperature and stirred for 12 h. The volatile components were evaporated under reduced pressure to give a solid residue, which was washed with pentane (3 \times) and dried under vacuum to yield a white solid mixture of LiNMe_2 , LiCl and a sub-stoichiometric amount of coordinated tetrahydrofuran. ^1H NMR ($\text{THF-}d_8$, 600 MHz): δ 3.63 (br, 1 H, THF), 2.70 (s, 6 H, NMe_2), 1.77 (br, 1 H, THF). $^{13}\text{C}\{^1\text{H}\}$ NMR ($\text{THF-}d_8$, 151 MHz): δ 68.3 (THF), 49.1 (NMe_2), 26.5 (THF). $^{15}\text{N}\{^1\text{H}\}$ NMR ($\text{THF-}d_8$, 59.2 MHz): δ - 375.9.

The mixture of LiNMe_2 (0.370 g, 3.332 mmol of LiNMe_2) and LiCl was suspended in toluene. ZrCl_4 (0.110 g, 0.472 mmol) was added at room temperature, and the reaction mixture was stirred for 12 h. The solution was filtered, and the solvent was evaporated under reduced pressure to yield $\text{Zr}(\text{NMe}_2)_6\text{Li}_2\text{THF}_2$ (0.231 g, 0.449 mmol, 96%). ^1H NMR ($\text{benzene-}d_6$, 600 MHz): δ 3.35 (br, 8 H, THF), 3.19 (s, 36 H, NMe_2), 1.18 (br, 8 H, THF). $^{13}\text{C}\{^1\text{H}\}$ NMR ($\text{benzene-}d_6$, 151 MHz): δ 68.8 (THF), 46.9 (NMe_2), 25.7 (THF). $^{15}\text{N}\{^1\text{H}\}$ NMR ($\text{benzene-}d_6$, 59.2 MHz): δ - 295.1.

$\text{Zr}(\text{NMe}_2)_6\text{Li}_2\text{THF}_2$ (0.200 g, 0.390 mmol) was dissolved in benzene. ZrCl_4 (0.045 g, 0.195 mmol) was added at room temperature, and the reaction mixture was stirred for 10 min. The solution was filtered, and the solvent was evaporated under reduced vacuum to yield $\text{Zr}(\text{NMe}_2)_4$ (0.180 g, 0.673 mmol, 86%). The ^1H and $^{13}\text{C}\{^1\text{H}\}$ NMR spectra matched the reported literature values.⁵² ^1H NMR ($\text{benzene-}d_6$, 600 MHz): δ 2.97 (s, 6 H, NMe_2).

$\text{Zr}(^{15}\text{NMe}_2)_4$. The above procedure, employing $\text{Me}_2^{15}\text{NH}\cdot\text{HCl}$ (0.123 g, 1.12 mmol) and ZrCl_4 (0.036 g, 0.155 mmol), afforded $\text{Zr}(^{15}\text{NMe}_2)_6\text{Li}_2\text{THF}_2$ (0.074 g, 0.142 mmol, 93%).

Reaction of this material with ZrCl_4 (0.033 g, 0.141 mmol) provided $\text{Zr}(\text{}^{15}\text{NMe}_2)_4$ (0.061 g, 0.225 mmol, 79%). ^1H NMR (benzene- d_6 , 600 MHz): δ 2.98 (s, 6 H, NMe_2). $^{15}\text{N}\{^1\text{H}\}$ NMR (benzene- d_6 , 59.2 MHz): δ -306.2.

$\text{Zr}(\text{NMe}_2)_n@MSN$. A benzene solution of $\text{Zr}(\text{NMe}_2)_4$ (0.095 g, 0.355 mmol, 5 mL) was added to MSN (0.20 g, 0.34 mmol of $-\text{OH}$ groups) suspended in benzene (15 mL). The suspension was stirred for 20 h at ambient temperature, the mixture was centrifuged, and the solvent was decanted. The unreacted $\text{Zr}(\text{NMe}_2)_4$ was removed from the solid material by washing with benzene (3×5 mL) and then pentane (2×5 mL). The solid material was dried under vacuum yielding a white solid (0.253 g). IR (KBr, cm^{-1}): 2852 (m), 2777 (m), 1457 (m), 1084 (s, $\nu_{\text{Si-O}}$), 950 (m). Elemental analysis: Found: C, 5.91; H, 1.08; N, 3.44; Zr, 8.3 wt % (0.91 mmol).

$\text{Bpin}@MSN$. Pinacolborane (0.075 g, 0.594 mmol) dissolved in benzene was added to a suspension of calcined MSN (0.20 g, 0.34 mmol of SiOH) in benzene (5 mL). Vigorous bubbling was observed immediately. After 2 h of stirring, no more bubbling was observed, the mixture was centrifuged, and the solvent was decanted. The unreacted HBpin was removed from the solid material by washing with benzene (3×5 mL) and then pentane (2×5 mL). The solid material was dried under reduced pressure yielding a white solid (0.226 g). IR (KBr, cm^{-1}): 2985 (m), 2938 (w), 1480 (m), 1456 (w), 1375 (m), 1223 (m), 1156 (m), 1086 (s, $\nu_{\text{Si-O}}$), 950 (m). Elemental analysis: Found: C, 9.99; H, 0.98; N, 0.03; B, 14.3 wt % (1.33 mmol).

$\text{ZrH/Bpin}@MSN$. Pinacolborane (0.691 g, 5.40 mmol) dissolved in benzene was added to $\text{Zr}(\text{NMe}_2)_3@MSN$ (0.200 g, 0.182 mmol of Zr, 0.540 mmol of NMe_2 , 5 mL) suspended in benzene. Slow evolution of a small amount of bubbles was observed, and this bubbling was

significantly reduced compared to the Bpin@MSN sample. The mixture was stirred at 60 °C for 2 h, the mixture was centrifuged, and the solvent was decanted. The unreacted HBpin and Me₂NBpin were removed from the solid material by washing with benzene (3 × 5 mL) and pentane (2 × 5 mL). The solid material was dried under reduced pressure yielding a white solid (0.207 g). IR (KBr, cm⁻¹): 2979 (m), 2934 (w), 2805 (w), 1592 (w, Zr-H), 1479 (m), 1376 (w), 1095 (s, ν_{Si-O}), 950 (m). Elemental analysis: Found: C, 8.09; H, 1.00; N, 0.51; Zr, 8.1 wt % (0.89 mmol); B, 9.3 wt % (0.86 mmol). Companion *in situ* micromolar scale reactions were performed in a J. Young-style Teflon-sealable NMR tube with 0.013 g Zr(NMe₂)₃@MSN, 0.041 g HBpin, and benzene-*d*₆ as solvent with a 7.48 mM Si(SiMe₃)₄ standard. From the integrated values of the Me₂NBpin and Si(SiMe₃)₄ resonances, 0.102 mmol of Me₂NBpin was formed.

General procedure for the catalytic hydroboration of carbonyls (aldehydes and ketones) using Zr(NMe₂)_n@MSN. A mixture of the carbonyl substrate (1 mmol) and HBpin (1.3 mmol) was added to Zr(NMe₂)_n@MSN (0.05 mmol Zr) that was suspended in benzene (10 mL). The reaction mixture was stirred for 10 h at room temperature for aldehydes or at 60 °C for ketones. The catalyst was removed from the reaction mixture by filtration, and then the boronic esters were isolated by evaporation of the solvent under reduced pressure. The boronic esters were quenched with 1 M aqueous NaOH solution, and the alcohol product was extracted with diethyl ether. The Et₂O solution was dried by stirring over Na₂SO₄ for 2 h, and the solvent was evaporated under reduced pressure to give the pure alcohol product.

Recycling studies. The initial reaction mixture was prepared and allowed to react as above. The catalyst was separated from the reaction mixture by filtration. The recycled catalyst was

washed with benzene and pentane to remove residual organics and dried under vacuum. Then, this material was resubjected to catalytic hydroboration conditions (60 °C, 2 h). Separation of the catalyst and reaction product was again accomplished by filtration, and the soluble portion of the reaction mixture was analyzed by ^1H NMR spectroscopy. This procedure was repeated 8 times without loss of yield.

Spectroscopic data of aldehyde and ketone hydroboration products.

2-(benzyloxy)-4,4,5,5-tetramethyl-1,3,2-dioxaborolane. 98% isolated yield. ^1H NMR (benzene- d_6 , 600 MHz): δ 7.31 (d, $^3J_{\text{HH}} = 7.4$ Hz, 2 H, *ortho*- C_6H_5), 7.14 (t, $^3J_{\text{HH}} = 7.3$ Hz, 2 H, *meta*- C_6H_5), 7.05 (t, $^3J_{\text{HH}} = 7.1$ Hz, 1 H, *para*- C_6H_5), 4.96 (s, 2 H, OCH_2), 1.04 (s, 12 H, $\text{BO}_2\text{C}_2\text{Me}_4$). $^{13}\text{C}\{^1\text{H}\}$ NMR (benzene- d_6 , 150 MHz): δ 139.7 (*ipso*- C_6H_5), 128.2 (*ortho*- C_6H_5), 127.2 (*para*- C_6H_5), 126.7 (*meta*- C_6H_5), 82.4 ($\text{BO}_2\text{C}_2\text{Me}_4$), 66.6 (OCH_2), 24.3 ($\text{BO}_2\text{C}_2\text{Me}_4$). ^{11}B NMR (benzene- d_6 , 128 MHz): δ 22.8.

4,4,5,5-tetramethyl-2-((4-methylbenzyl)oxy)-1,3,2-dioxaborolane. 97% isolated yield. ^1H NMR (benzene- d_6 , 600 MHz): δ 7.27 (d, $^3J_{\text{HH}} = 7.3$ Hz, 2 H, *ortho*- $\text{C}_6\text{H}_4\text{Me}$), 6.97 (d, $^3J_{\text{HH}} = 7.4$ Hz, 2 H, *meta*- $\text{C}_6\text{H}_4\text{Me}$), 4.97 (s, 2 H, OCH_2), 2.08 (s, 3 H, $\text{C}_6\text{H}_4\text{Me}$), 1.04 (s, 12 H, $\text{BO}_2\text{C}_2\text{Me}_4$). $^{13}\text{C}\{^1\text{H}\}$ NMR (benzene- d_6 , 150 MHz): δ 136.8 (*ipso*- $\text{OCH}_2\text{C}_6\text{H}_4\text{Me}$), 136.6 (*para*- $\text{OCH}_2\text{C}_6\text{H}_4\text{Me}$), 128.9 (*ortho*- $\text{OCH}_2\text{C}_6\text{H}_4\text{Me}$), 126.9 (*meta*- $\text{OCH}_2\text{C}_6\text{H}_4\text{Me}$), 82.3 ($\text{BO}_2\text{C}_2\text{Me}_4$), 66.6 (OCH_2), 24.3 ($\text{BO}_2\text{C}_2\text{Me}_4$), 20.7 ($\text{C}_6\text{H}_4\text{Me}$). ^{11}B NMR (benzene- d_6 , 128 MHz): δ 22.8.

2-((4-methoxybenzyl)oxy)-4,4,5,5-tetramethyl-1,3,2-dioxaborolane. 98% isolated yield. ^1H NMR (benzene- d_6 , 600 MHz): δ 7.27 (d, $^3J_{\text{HH}} = 8.1$ Hz, 2 H, *ortho*- $\text{OCH}_2\text{C}_6\text{H}_4\text{OMe}$), 6.76 (d, $^3J_{\text{HH}} = 8.1$ Hz, 2 H, *meta*- $\text{OCH}_2\text{C}_6\text{H}_4\text{OMe}$), 4.95 (s, 2 H, OCH_2), 3.28 (s, 3 H, $\text{C}_6\text{H}_4\text{OMe}$), 1.05 (s, 12 H, $\text{BO}_2\text{C}_2\text{Me}_4$). $^{13}\text{C}\{^1\text{H}\}$ NMR (benzene- d_6 , 150 MHz): δ 159.3 (*ipso*-

OCH₂C₆H₄OMe), 131.8 (*para*-OCH₂C₆H₄OMe), 128.5 (*ortho*-OCH₂C₆H₄OMe), 113.7 (*meta*-OCH₂C₆H₄OMe), 82.3 (BO₂C₂Me₄), 66.4 (OCH₂), 54.4 (C₆H₄OMe), 24.4 (BO₂C₂Me₄). ¹¹B NMR (benzene-*d*₆, 128 MHz): δ 22.8.

4,4,5,5-tetramethyl-2-((4-nitrobenzyl)oxy)-1,3,2-dioxaborolane. 98% isolated yield. ¹H NMR (benzene-*d*₆, 600 MHz): δ 7.78 (d, ³J_{HH} = 8.4 Hz, 2 H, *ortho*-OCH₂C₆H₄NO₂), 6.88 (d, ³J_{HH} = 8.1 Hz, 2 H, *meta*-C₆H₄NO₂), 4.68 (s, 2 H, OCH₂), 1.03 (s, 12 H, BO₂C₂Me₄). ¹³C{¹H} NMR (benzene-*d*₆, 150 MHz): δ 147.2 (*ipso*-C₆H₄NO₂), 146.1 (*para*-C₆H₄NO₂), 126.4 (*ortho*-C₆H₄NO₂), 123.2 (*meta*-C₆H₄NO₂), 82.7 (BO₂C₂Me₄), 65.3 (OCH₂), 24.3 (BO₂C₂Me₄). ¹¹B NMR (benzene-*d*₆, 128 MHz): δ 22.7.

2-((4-chlorobenzyl)oxy)-4,4,5,5-tetramethyl-1,3,2-dioxaborolane. 97% isolated yield. ¹H NMR (benzene-*d*₆, 600 MHz): δ 7.06 (d, ³J_{HH} = 7.8 Hz, 2 H, *ortho*-C₆H₄Cl), 6.99 (d, ³J_{HH} = 7.6 Hz, 2 H, *meta*-C₆H₄Cl), 4.76 (s, 2 H, OCH₂), 1.03 (s, 12 H, BO₂C₂Me₄). ¹³C{¹H} NMR (benzene-*d*₆, 150 MHz): δ 138.1 (*para*-C₆H₄Cl), 133.0 (*ipso*-C₆H₄Cl), 128.4 (*ortho*-C₆H₄Cl), 128.0 (*meta*-C₆H₄Cl), 82.5 (BO₂C₂Me₄), 65.7 (OCH₂), 24.3 (BO₂C₂Me₄). ¹¹B NMR (benzene-*d*₆, 128 MHz): δ 22.8.

2-(cyclohexylmethoxy)-4,4,5,5-tetramethyl-1,3,2-dioxaborolane. 98% isolated yield. ¹H NMR (benzene-*d*₆, 600 MHz): δ 3.80 (d, ³J_{HH} = 6.3 Hz, 2 H, OCH₂), 1.73 (m, 2 H, C₆H₁₁), 1.61 (m, 2 H, C₆H₁₁), 1.53 (m, 2 H, C₆H₁₁), 1.13 (m, 3 H, C₆H₁₁), 1.02 (s, 12 H, BO₂C₂Me₄), 0.92 (m, 2 H, C₆H₁₁). ¹³C{¹H} NMR (benzene-*d*₆, 150 MHz): δ 82.0 (BO₂C₂Me₄), 70.3 (OCH₂), 39.5 (C₆H₁₁), 29.4 (C₆H₁₁), 26.5 (C₆H₁₁), 25.8 (C₆H₁₁), 24.4 (BO₂C₂Me₄). ¹¹B NMR (benzene-*d*₆, 128 MHz): δ 22.6.

2-(furan-2-ylmethoxy)-4,4,5,5-tetramethyl-1,3,2-dioxaborolane. 98% isolated yield. ¹H NMR (benzene-*d*₆, 600 MHz): δ 7.05 (br, 1 H, 5H-OC₄H₃), 6.13 (br, 1 H, 3H-OC₄H₃), 6.01

(br, 1 H, 4H-OC₄H₃), 4.85 (s, 2 H, OCH₂), 1.03 (s, 12 H, BO₂C₂Me₄). ¹³C{¹H} NMR (benzene-*d*₆, 150 MHz): δ 153.0 (2C-OC₄H₃), 142.2 (5C-OC₄H₃), 110.1 (3C-OC₄H₃), 108.1 (4C-OC₄H₃), 82.5 (BO₂C₂Me₄), 59.1 (OCH₂), 24.3 (BO₂C₂Me₄). ¹¹B NMR (benzene-*d*₆, 128 MHz): δ 22.8.

1,4-bis(((4,4,5,5-tetramethyl-1,3,2-dioxaborolan-2-yl)oxy)methyl)benzene. 98% isolated yield. ¹H NMR (benzene-*d*₆, 600 MHz): δ 7.27 (s, 4 H, C₆H₄), 4.93 (s, 2 H, OCH₂), 1.03 (s, 12 H, BO₂C₂Me₄). ¹³C{¹H} NMR (benzene-*d*₆, 150 MHz): δ 138.8 (*ipso*-C₆H₄), 126.8 (3C-C₆H₄), 82.3 (BO₂C₂Me₄), 66.4 (OCH₂), 24.3 (BO₂C₂Me₄). ¹¹B NMR (benzene-*d*₆, 128 MHz): δ 22.9.

2-(ferrocenylmethoxy) 4,4,5,5-tetramethyl-1,3,2-dioxaborolane. 98% isolated yield. ¹H and ¹³C{¹H} NMR spectroscopic data are identical to literature values.⁶⁴ ¹H NMR (benzene-*d*₆, 600 MHz): δ 4.77 (s, 2 H, OCH₂), 4.22 (br, 2 H, C₅H₄), 3.98 (s, 5 H, C₅H₅), 3.95 (br, 2 H, C₅H₄), 1.08 (s, 12 H, BO₂C₂Me₄). ¹³C{¹H} NMR (benzene-*d*₆, 150 MHz): δ 85.7 (C₅H₄), 82.2 (BO₂C₂Me₄), 68.7 (C₅H₄), 68.4 (C₅H₅), 68.2 (C₅H₄), 63.1 (OCH₂), 24.4 (BO₂C₂Me₄). ¹¹B NMR (benzene-*d*₆, 128 MHz): δ 22.7.

4,4,5,5-tetramethyl-2-(1-phenylethoxy)-1,3,2-dioxaborolane. 97% isolated yield. ¹H NMR (benzene-*d*₆, 600 MHz): δ 7.37 (d, ³J_{HH} = 7.3 Hz, 2 H, *ortho*-C₆H₅), 7.14 (t, ³J_{HH} = 8.0 Hz, 2 H, *meta*-C₆H₅), 7.05 (t, ³J_{HH} = 7.2 Hz, 1 H, *para*-C₆H₅), 5.42 (q, ³J_{HH} = 6.2 Hz, 1 H, OCHMe) 1.46 (d, ³J_{HH} = 6.4 Hz, 3 H, OCHMe), 1.03 s, 6 H, BO₂C₂Me₄), 1.00 (s, 6 H, BO₂C₂Me₄). ¹³C{¹H} NMR (benzene-*d*₆, 150 MHz): δ 145.0 (*ipso*-C₆H₅), 128.2 (*ortho*-C₆H₅), 127.0 (*para*-C₆H₅), 125.3 (*meta*-C₆H₅), 82.2 (BO₂C₂Me₄), 72.6 (OCHMe), 25.4 (OCHMe), 24.3 (BO₂C₂Me₄), 24.2 (BO₂C₂Me₄). ¹¹B NMR (benzene-*d*₆, 128 MHz): δ 22.6.

4,4,5,5-tetramethyl-2-(2,2,2-trifluoro-1-phenylethoxy)-1,3,2-dioxaborolane. 97% isolated yield. ^1H NMR (chloroform- d_1 , 600 MHz): δ 7.50 (m, 2 H, *ortho*- C_6H_5), 7.40 (m, 3 H, *para*- C_6H_5 , *meta*- C_6H_5), 5.39 (q, $^3J_{\text{HH}} = 6.7$ Hz, 1 H, OCH), 1.27 s, 6 H, $\text{BO}_2\text{C}_2\text{Me}_4$), 1.23 (s, 6 H, $\text{BO}_2\text{C}_2\text{Me}_4$). $^{13}\text{C}\{^1\text{H}\}$ NMR (chloroform- d_1 , 150 MHz): δ 133.4 (*ipso*- C_6H_5), 129.3 (*ortho*- C_6H_5), 128.4 (*para*- C_6H_5), 127.6 (*meta*- C_6H_5), 124.6 (q, $^1J_{\text{CF}} = 282$ Hz, CF_3), 83.8 ($\text{BO}_2\text{C}_2\text{Me}_4$), 74.2 (q, $^2J_{\text{CF}} = 32$ Hz, OCH), 24.5 ($\text{BO}_2\text{C}_2\text{Me}_4$), 24.4 ($\text{BO}_2\text{C}_2\text{Me}_4$). ^{11}B NMR (chloroform- d_1 , 128 MHz): δ 22.6. ^{19}F NMR (chloroform- d_1 , 376 MHz): δ -78.1 (d, $^3J_{\text{HF}} = 6.9$ Hz).

4,4,5,5-tetramethyl-2-((4-nitrobenzyl)oxy)-1,3,2-dioxaborolane. 95% isolated yield. ^1H NMR (benzene- d_6 , 600 MHz): δ 7.80 (d, $^3J_{\text{HH}} = 8.4$ Hz, 2 H, *ortho*- C_6H_4), 6.98 (d, $^3J_{\text{HH}} = 8.3$ Hz, 2 H, *meta*- C_6H_4), 5.20 (q, $^3J_{\text{HH}} = 6.6$ Hz, 1 H, OCHMe) 1.25 (d, $^3J_{\text{HH}} = 6.4$ Hz, 3 H, OCHMe), 1.03 (s, 6 H, $\text{BO}_2\text{C}_2\text{Me}_4$), 1.00 (s, 6 H, $\text{BO}_2\text{C}_2\text{Me}_4$). $^{13}\text{C}\{^1\text{H}\}$ NMR (benzene- d_6 , 175 MHz): δ 151.3 (*ipso*- C_6H_4), 147.1 (*para*- C_6H_4), 125.7 (*ortho*- C_6H_4), 123.3 (*meta*- C_6H_4), 82.5 ($\text{BO}_2\text{C}_2\text{Me}_4$), 71.6 (OCHMe), 24.9 (OCHMe), 24.2 ($\text{BO}_2\text{C}_2\text{Me}_4$). ^{11}B NMR (benzene- d_6 , 128 MHz): 23.0 (s, B-O).

2-(benzhydryloxy)-4,4,5,5-tetramethyl-1,3,2-dioxaborolane. 97% isolated yield. ^1H NMR (benzene- d_6 , 600 MHz): δ 7.45 (d, $^3J_{\text{HH}} = 7.7$ Hz, 4 H, *ortho*- C_6H_5), 7.09 (t, $^3J_{\text{HH}} = 7.4$ Hz, 4 H, *meta*- C_6H_5), 7.01 (t, $^3J_{\text{HH}} = 7.3$ Hz, 2 H, *para*- C_6H_5), 6.44 (s, 1 H, OCH), 0.98 (s, 12 H, $\text{BO}_2\text{C}_2\text{Me}_4$). $^{13}\text{C}\{^1\text{H}\}$ NMR (benzene- d_6 , 150 MHz): δ 143.5 (*ipso*- C_6H_5), 128.2 (*ortho*- C_6H_5), 127.2 (*para*- C_6H_5), 126.6 (*meta*- C_6H_5), 82.5 ($\text{BO}_2\text{C}_2\text{Me}_4$), 78.2 (OCH), 24.2 ($\text{BO}_2\text{C}_2\text{Me}_4$). ^{11}B NMR (benzene- d_6 , 128 MHz): δ 23.0.

2-((9H-fluoren-9-yl)oxy)-4,4,5,5-tetramethyl-1,3,2-dioxaborolane. 98% isolated yield. ^1H NMR (benzene- d_6 , 600 MHz): δ 7.69 (d, $^3J_{\text{HH}} = 7.2$ Hz, 2 H, 3*H*- C_{13}H_9), 7.40 (d, $^3J_{\text{HH}} = 7.3$

Hz, 2 H, 6*H*-C₁₃H₉), 7.16 (m, 4 H, 4*H* and 5*H*-C₁₃H₉), 6.24 (s, 1 H, OCH), 1.11 (s, 12 H, BO₂C₂Me₄). ¹³C{¹H} NMR (benzene-*d*₆, 150 MHz): δ 144.9 (2*C*-C₁₃H₉), 140.5 (7*C*-C₁₃H₉), 128.8 (3*C*-C₁₃H₉), 127.5 (6*C*-C₁₃H₉), 125.3 (4*C*-C₁₃H₉), 119.8 (5*C*-C₁₃H₉), 82.8 (BO₂C₂Me₄), 76.6 (OCH), 24.4 (BO₂C₂Me₄). ¹¹B NMR (benzene-*d*₆, 128 MHz): δ 23.5.

2-(cyclohex-2-en-1-yloxy)-4,4,5,5-tetramethyl-1,3,2-dioxaborolane. 98% isolated yield. ¹H and ¹³C{¹H} NMR spectroscopic data are identical to literature values.⁶⁹ ¹H NMR (benzene-*d*₆, 600 MHz): δ 5.96 (d, ³J_{HH} = 10.0 Hz, 1 H, OCHCH), 5.67 (d, ³J_{HH} = 9.8 Hz, 1 H, OCHCHCH), 4.83 (br, 1 H, OCH) 1.80 (m, 3 H, C₆H₉), 1.68 (m, 2 H, C₆H₉), 1.36 (m, 1 H, C₆H₉), 1.07 (s, 12 H, BO₂C₂Me₄). ¹³C{¹H} NMR (benzene-*d*₆, 150 MHz): δ 129.7 (1*C*-C₆H₉), 129.4 (2*C*-C₆H₉), 82.0 (BO₂C₂Me₄), 68.1 (OCH), 31.0 (3*C*-C₆H₉), 24.8 (5*C*-C₆H₉), 24.4 (BO₂C₂Me₄), 19.0 (4*C*-C₆H₉). ¹¹B NMR (benzene-*d*₆, 128 MHz): δ 22.6.

(*E*)-4,4,5,5-tetramethyl-2-((4-phenylbut-3-en-2-yl)oxy)-1,3,2-dioxaborolane. 95% isolated yield. ¹H NMR (C₆D₆, 600 MHz): δ 7.23 (d, ³J_{HH} = 7.6 Hz, 2 H, *ortho*-C₆H₅), 7.10 (t, ³J_{HH} = 7.5 Hz, 2 H, *meta*-C₆H₅), 7.03 (t, ³J_{HH} = 7.4 Hz, 1 H, *para*-C₆H₅), 6.68 (d, ³J_{HH} = 15.9 Hz, C₆H₅CH), 6.23 (dd, ³J_{HH} = 15.9 Hz, 5.9 Hz, C₆H₅CHCH) 5.44 (p, ³J_{HH} = 6.9 Hz, 1 H, OCH) 1.35 (d, ³J_{HH} = 6.5 Hz, 3 H, OCHCH₃), 1.07 (s, 6 H, BO₂C₂Me₄), 1.06 (s, 6 H, BO₂C₂Me₄). ¹³C{¹H} NMR (C₆D₆, 150 MHz): δ 137.4 (C₆H₅CHCH), 132.7 (C₆H₅CH), 129.5 (*ipso*-C₆H₅), 128.7 (*ortho*-C₆H₅), 127.6 (*para*-C₆H₅), 126.9 (*meta*-C₆H₅), 82.5 (BO₂C₂Me₄), 71.5 (OCH), 24.8 (BO₂C₂Me₄), 24.6 (BO₂C₂Me₄), 23.4 (OCHCH₃). ¹¹B NMR (C₆D₆, 128 MHz): δ 22.7.

(*E*)-2-((1,3-diphenylallyl)oxy)-4,4,5,5-tetramethyl-1,3,2-dioxaborolane. 96% isolated yield. ¹H NMR (C₆D₆, 600 MHz): δ 7.49 (d, ³J_{HH} = 7.6 Hz, 2 H, C₆H₅), 7.15 (m, 4 H, C₆H₅), 7.11 (m, 4 H, C₆H₅), 6.78 (d, ³J_{HH} = 15.8 Hz, C₆H₅CH), 6.37 (dd, ³J_{HH} = 15.9 Hz, 6.4 Hz,

C_6H_5CHCH) 5.98 (d, $^3J_{HH} = 6.3$ Hz, 1 H, OCH), 1.01 (s, 6 H, $BO_2C_2Me_4$), 1.00 (s, 6 H, $BO_2C_2Me_4$). $^{13}C\{^1H\}$ NMR (C_6D_6 , 150 MHz): δ 143.0 (C_6H_5CHCH), 137.5 (C_6H_5CH), 131.8 (C_6H_5), 130.7 (C_6H_5), 129.1 (C_6H_5), 127.4 (C_6H_5), 127.1 (C_6H_5), 83.2 ($BO_2C_2Me_4$), 77.8 (OCH), 25.0 ($BO_2C_2Me_4$), 25.0 ($BO_2C_2Me_4$). ^{11}B NMR (C_6D_6 , 128 MHz): δ 23.1.

2-(cyclohexyloxy)-4,4,5,5-tetramethyl-1,3,2-dioxaborolane. 98% isolated yield. 1H NMR (benzene- d_6 , 600 MHz): δ 4.24 (br, 1 H, OCH) 1.91 (m, 2 H, C_6H_{11}), 1.61 (m, 2 H, C_6H_{11}), 1.49 (m, 2 H, C_6H_{11}), 1.29 (m, 1 H, C_6H_{11}), 1.14 (m, 2 H, C_6H_{11}), 1.08 (s, 12 H, $BO_2C_2Me_4$). $^{13}C\{^1H\}$ NMR (benzene- d_6 , 150 MHz): δ 81.8 ($BO_2C_2Me_4$), 72.4 (OCH), 34.4 (C_6H_{11}), 25.4 (C_6H_{11}), 24.4 ($BO_2C_2Me_4$), 23.7 (C_6H_{11}). ^{11}B NMR (benzene- d_6 , 128 MHz): δ 22.5.

2-(sec-butoxy)-4,4,5,5-tetramethyl-1,3,2-dioxaborolane. 91% isolated yield. 1H NMR (benzene- d_6 , 600 MHz): δ 4.26 (m, 1 H, OCH), 1.55 (m, 1 H, OCHCH₂Me), 1.39 (m, 1 H, OCHCH₂Me), 1.18 (d, $^3J_{HH} = 6.2$ Hz, 3 H, OCHMe), 1.07 (s, 12 H, $BO_2C_2Me_4$), 0.88 (t, $^3J_{HH} = 6.0$ Hz, 3 H, CH₂Me). $^{13}C\{^1H\}$ NMR (benzene- d_6 , 150 MHz): δ 81.8 ($BO_2C_2Me_4$), 71.9 (OCHMe), 31.1 (OCHMe), 24.3 ($BO_2C_2Me_4$), 22.0 (CH₂Me), 9.8 (CH₂Me). ^{11}B NMR (benzene- d_6 , 128 MHz): δ 22.5.

4,4,5,5-tetramethyl-2-(pentan-2-yloxy)-1,3,2-dioxaborolane. 90% isolated yield. 1H NMR (benzene- d_6 , 600 MHz): δ 4.36 (m, 1 H, OCH), 1.55 (m, 1 H, CH₂CH₂Me), 1.39 (m, 1 H, CH₂CH₂Me), 1.32 (m, 2 H, CH₂CH₂Me), 1.20 (d, $^3J_{HH} = 6.1$ Hz, 3 H, OCHMe), 1.07 (s, 12 H, $BO_2C_2Me_4$), 0.85 (t, $^3J_{HH} = 7.1$ Hz, 3 H, CH₂Me). $^{13}C\{^1H\}$ NMR (benzene- d_6 , 150 MHz): δ 81.8 ($BO_2C_2Me_4$), 70.3 (OCH), 40.5 (OCHMe), 24.3 ($BO_2C_2Me_4$), 22.6 (CH₂Et), 18.8 (CH₂CH₂Me), 13.8 (CH₂CH₂Me). ^{11}B NMR (benzene- d_6 , 128 MHz): δ 22.4.

Zr(NMe₂)_n@MSN. A benzene solution of Zr(NMe₂)₄ (0.095 g, 0.355 mmol, 5 mL) was added to MSN (0.20 g, 0.34 mmol of –OH groups) suspended in benzene (15 mL). The

suspension was stirred for 20 h at ambient temperature, and then the mixture was centrifuged and the solvent was decanted. The unreacted $\text{Zr}(\text{NMe}_2)_4$ was removed from the solid material by washing with benzene (3×5 mL) and then pentane (2×5 mL). The solid material was dried under vacuum yielding a white solid (0.253 g). IR (KBr, cm^{-1}): 2972 (m), 2853 (m) 2779 (m), 1466 (m), 1084 (s, $\nu_{\text{Si-O}}$), 950 (m), 902 (m), 807 (s), 480 (s). Elemental analysis: Found: C, 5.91; H, 1.08; N, 3.44; Zr, 8.3 wt % (0.91 mmol).

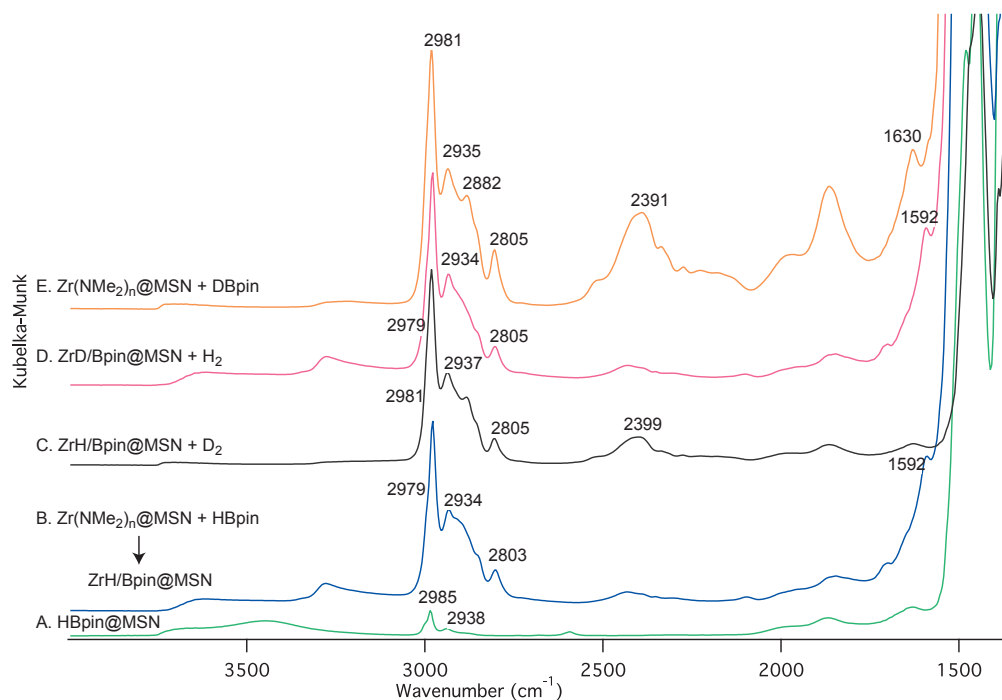


Figure 2.10. Diffuse reflectance IR spectra from 1350 to 4000 cm^{-1} for (A) Bpin@MSN, (B) ZrH/Bpin@MSN, (C) ZrH/Bpin@MSN + D_2 , and (D) ZrD/Bpin@MSN + H_2 .

Bpin@MSN. Pinacolborane (0.075 g, 0.594 mmol) dissolved in benzene was added to a suspension of calcined MSN (0.20 g, 0.34 mmol of SiOH) in benzene (5 mL). Vigorous bubbling was observed immediately. After 2 h of stirring, no more bubbling was observed, the mixture was centrifuged, and the solvent was decanted. The unreacted HBpin was removed from the solid material by washing with benzene (3×5 mL) and then pentane (2×5 mL). The solid material was dried under reduced pressure yielding a white solid (0.226 g). IR (KBr, cm^{-1}): 2980 (m), 2921 (w), 2851 (w), 1480 (m), 1456 (w), 1375 (m), 1223 (m), 1156

(m), 1086 (s, $\nu_{\text{Si-O}}$), 950 (m), 902 (m), 854 (w), 804 (m), 480 (s). Elemental analysis: Found: C, 9.99; H, 0.98; N, 0.03; B, 14.3 wt % (1.33 mmol).

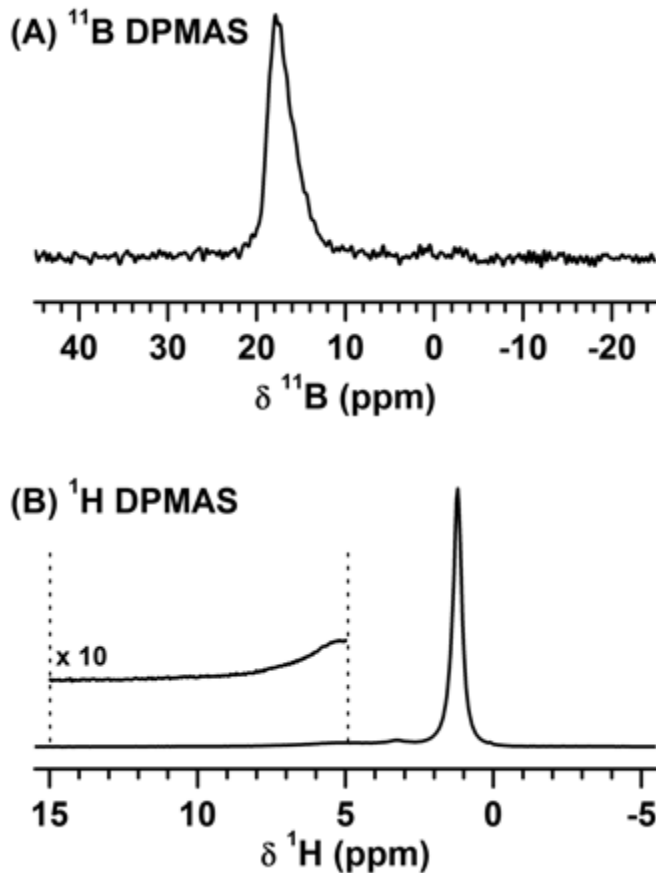


Figure 2.11. (A) ^{11}B DPMAS and (B) ^1H DPMAS spectra of Bpin@MSN.

ZrH/Bpin@MSN. Pinacolborane (0.691 g, 5.40 mmol) dissolved in benzene was added to $\text{Zr}(\text{NMe}_2)_3\text{@MSN}$ (0.200 g, 0.182 mmol of Zr, 0.540 mmol of NMe_2 , 5 mL) suspended in benzene. A slow evolution of a small amount of bubbles was observed, and this was significantly reduced compared to the Bpin@MSN sample. This mixture was stirred at 60 °C for 2 h, the mixture was centrifuged, and the solvent was decanted. The unreacted HBpin and Me_2NBpin were removed from the solid material by washing with benzene (3×5 mL) and pentane (2×5 mL). The solid material was dried under reduced pressure yielding a white solid (0.207 g). IR (KBr, cm^{-1}): 2979 (m), 2933 (w), 2869 (w), 1628 (w, Zr-H), 1478 (m), 1376 (w), 1095 (s, $\nu_{\text{Si-O}}$), 950 (m), 902 (m), 809 (s), 480 (s). Elemental analysis: Found: C, 8.09; H, 1.00; N, 0.51; Zr, 8.1 wt % (0.89 mmol); B, 9.3 wt % (0.86 mmol). Companion *in*

situ micromolar scale reactions were performed in a J. Young-style Teflon-sealable NMR tube with 0.013 g $\text{Zr}(\text{NMe}_2)_3@MSN$, HBpin (0.041 g) 7.48 mM $\text{Si}(\text{SiMe}_3)_4$, and benzene- d_6 as solvent. From the integrated values of the Me_2NBpin and $\text{Si}(\text{SiMe}_3)_4$ resonances, 0.102 mmol of Me_2NBpin was formed.

Reaction of $\text{ZrH}@MSN$ and D_2 . A 100 mL resealable Teflon-valved flask was charged with $\text{ZrH}@MSN$ (0.050 g), and benzene (5 mL) was added to give a suspension. The mixture was degassed with freeze-pump-thaw cycles (3 \times) and sealed under an atmosphere of D_2 . The suspension was stirred at room temperature for 2 h. The mixture was degassed and then resealed under a fresh atmosphere of D_2 . This sequence was repeated for one addition cycle. The mixture was centrifuged, and the solvent was decanted. The solid material was dried under reduced pressure yielding a white solid. IR (KBr, cm^{-1}): 2980 (m), 2934 (w), 1477 (m), 1456 (m), 1375 (w), 1095 (s, $\nu_{\text{Si-O}}$), 950 (m), 902 (m), 809 (s), 480 (s).

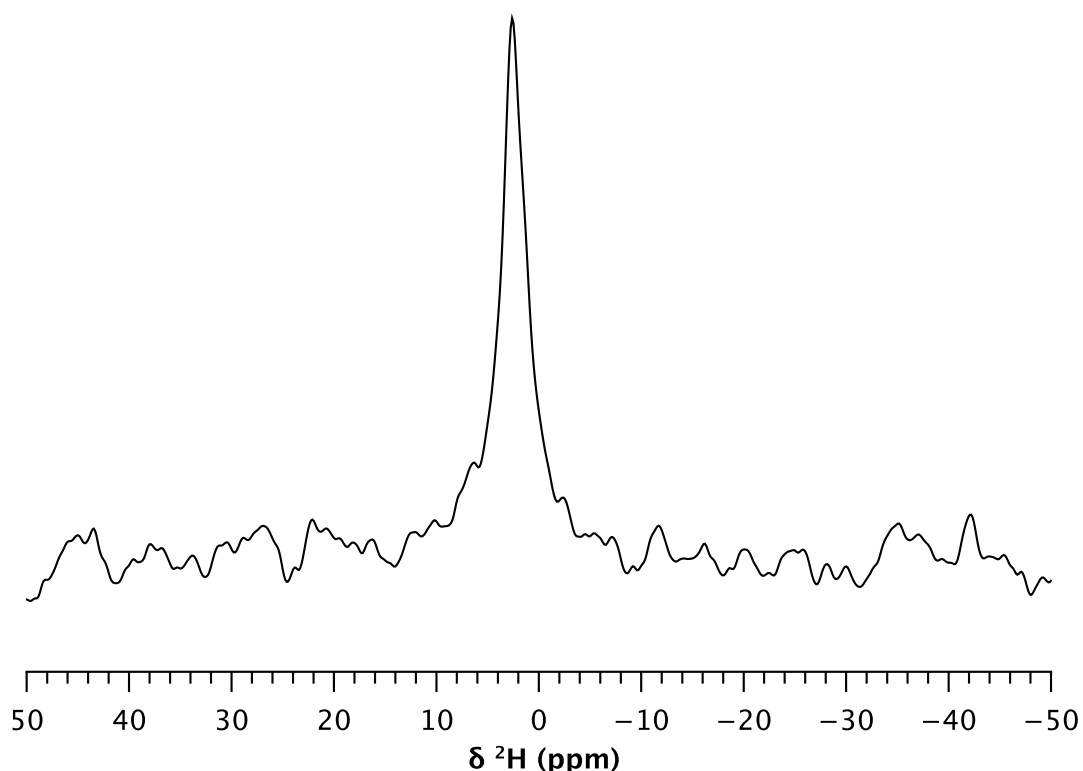


Figure 2.12. ^2H SSNMR spectrum from the reaction of ZrH/Bpin@MSN and D_2 . Experimental parameters: $B_0 = 14.1$ T, $B_1 = 125$ kHz (2 μs excitation), 2 s for recycle delay, 20.48 ms acquisition, 8000 scans, using 1.6 mm rotor, 30 kHz for MAS, data is processed with 30 Hz linebroadening.

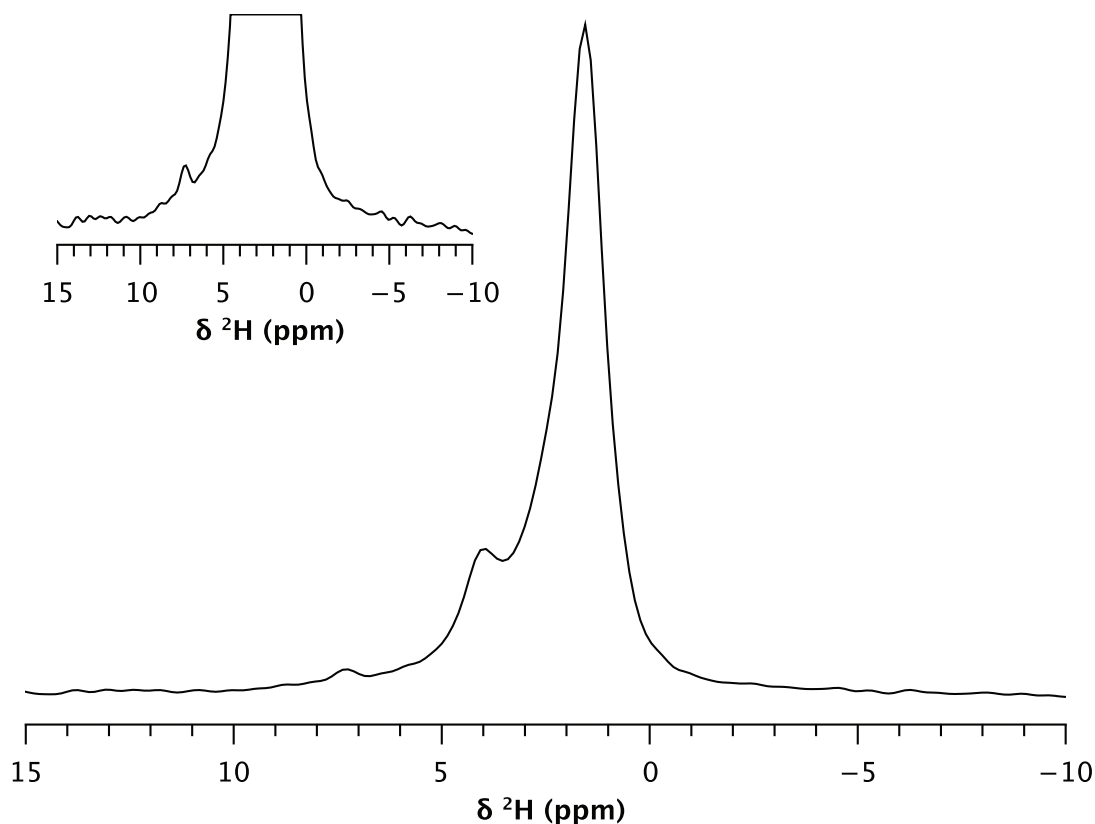


Figure 2.13. ^2H DPMAS spectrum from the reaction of $\text{Zr(NMe}_2)_3\text{@MSN}$ and DBpin. Experimental parameters: $B_0 = 14.1$ T, $B_1 = 125$ kHz (2 μs excitation), 2 s for recycle delay, 20.48 ms acquisition, 8000 scans, using 1.6 mm rotor, 30 kHz for MAS, data is processed with 30 Hz linebroadening.

References:

1. Quignard, F.; Choplin, A.; Basset, J.-M. *J. Chem. Soc., Chem. Commun.* **1991**, 1589-1590.
2. Zakharov, V. A.; Dudchenko, V. K.; Paukshtis, E. A.; Karakchiev, L. G.; Yermakov, Y. I. *J. Mol. Catal.* **1977**, *2*, 421-435.
3. Thieuleux, C.; Quadrelli, E. A.; Basset, J.-M.; Dobler, J.; Sauer, J. *Chem. Commun.* **2004**, 1729-1731.
4. Zakharov, V. A.; Yermakov, Y. I. *Catal. Rev. -Sci. Eng.* **1979**, *19*, 67-103.
5. Yermakov, Y. I.; Ryndin, Y. A.; Alekseev, O. S.; Kochubey, D. I.; Shmachkov, V. A.; Gergert, N. I. *J. Mol. Catal.* **1989**, *49*, 121-132.
6. Casty, G. L.; Matturro, M. G.; Myers, G. R.; Reynolds, R. P.; Hall, R. B. *Organometallics* **2001**, *20*, 2246-2249.
7. Basset, J.-M.; Coperet, C.; Soulivong, D.; Taoufik, M.; Cazat, J. T. *Acc. Chem. Res.* **2009**, *43*, 323-334.
8. Copéret, C.; Chabanas, M.; Petroff Saint-Arroman, R.; Basset, J.-M. *Angew. Chem. Int. Ed.* **2003**, *42*, 156-181.
9. Lécuyer, C.; Quignard, F.; Choplin, A.; Olivier, D.; Basset, J.-M. *Angew. Chem. Int. Ed. Engl.* **1991**, *30*, 1660-1661.
10. Quignard, F.; Lécuyer, C.; Choplin, A.; Olivier, D.; Basset, J.-M. *J. Mol. Catal.* **1992**, *74*, 353-363.
11. Carter, M. B.; Schiott, B.; Gutierrez, A.; Buchwald, S. L. *J. Am. Chem. Soc.* **1994**, *116*, 11667-11670.
12. Fu, P.-F.; Brard, L.; Li, Y.; Marks, T. J. *J. Am. Chem. Soc.* **1995**, *117*, 7157-7168.
13. Gountchev, T. I.; Tilley, T. D. *Organometallics* **1999**, *18*, 5661-5667.
14. Molander, G. A.; Julius, M. *J. Org. Chem.* **1992**, *57*, 6347-6351.
15. Molander, G. A.; Retsch, W. H. *Organometallics* **1995**, *14*, 4570-4575.
16. Takahashi, T.; Hasegawa, M.; Suzuki, N.; Saburi, M.; Rousset, C. J.; Fanwick, P. E.; Negishi, E. *J. Am. Chem. Soc.* **1991**, *113*, 8564-8566.
17. Xin, S. X.; Harrod, J. F. *Can. J. Chem.* **1995**, *73*, 999-1002.
18. Jeske, G.; Lauke, H.; Mauermann, H.; Schumann, H.; Marks, T. J. *J. Am. Chem. Soc.* **1985**, *107*, 8111-8118.
19. Tilley, T. D. *Acc. Chem. Res.* **1993**, *26*, 22-29.
20. Gauvin, F.; Harrod, J. F.; Woo, H. G. *Adv. Organomet. Chem.* **1998**, *42*, 363-405.
21. Waterman, R. *Organometallics* **2013**, *32*, 7249-7263.
22. Arrowsmith, M.; Hadlington, T. J.; Hill, M. S.; Kociok-Kohn, G. *Chem. Commun.* **2012**, *48*, 4567-4569.
23. Harrison, K. N.; Marks, T. J. *J. Am. Chem. Soc.* **1992**, *114*, 9220-9221.
24. Mukherjee, D.; Ellern, A.; Sadow, A. D. *Chem. Sci.* **2014**, *5*, 959-964.
25. Arrowsmith, M.; Hill, M. S.; Hadlington, T.; Kociok-Kohn, G.; Weetman, C. *Organometallics* **2011**, *30*, 5556-5559.
26. Anker, M. D.; Arrowsmith, M.; Bellham, P.; Hill, M. S.; Kociok-Kohn, G.; Liptrot, D. J.; Mahon, M. F.; Weetman, C. *Chem. Sci.* **2014**, *5*, 2826-2830.
27. Oluyadi, A. A.; Ma, S.; Muhoro, C. N. *Organometallics* **2012**, *32*, 70-78.
28. Khalimon, A. Y.; Farha, P.; Kuzmina, L. G.; Nikonov, G. I. *Chem. Commun.* **2012**, *48*, 455-457.

29. Koren-Selfridge, L.; Query, I. P.; Hanson, J. A.; Isley, N. A.; Guzei, I. A.; Clark, T. B. *Organometallics* **2010**, *29*, 3896-3900.
30. Evans, D. A.; Fu, G. C. *J. Org. Chem.* **1990**, *55*, 5678-5680.
31. Hadlington, T. J.; Hermann, M.; Frenking, G.; Jones, C. *J. Am. Chem. Soc.* **2014**, *136*, 3028-3031.
32. Verdagner, X.; Lange, U. E. W.; Reding, M. T.; Buchwald, S. L. *J. Am. Chem. Soc.* **1996**, *118*, 6784-6785.
33. Willoughby, C. A.; Buchwald, S. L. *J. Am. Chem. Soc.* **1994**, *116*, 11703-11714.
34. Willoughby, C. A.; Buchwald, S. L. *J. Am. Chem. Soc.* **1994**, *116*, 8952-8965.
35. Yun, J.; Buchwald, S. L. *J. Am. Chem. Soc.* **1999**, *121*, 5640-5644.
36. Pereira, S.; Srebnik, M. *Organometallics* **1995**, *14*, 3127-3128.
37. Eter, M. E.; Hamzaoui, B.; Abou-Hamad, E.; Pelletier, J. D. A.; Basset, J.-M. *Chem. Commun.* **2013**, *49*, 4616-4618.
38. Beaudoin, M.; Scott, S. L. *Organometallics* **2000**, *20*, 237-239.
39. Hamzaoui, B.; Eter, M. E.; Abou-hamad, E.; Chen, Y.; Pelletier, J. D. A.; Basset, J.-M. *Chem. Eur. J.* **2015**, *21*, 4294-4299.
40. Pasha, F. A.; Bendjeriou-Sedjerari, A.; Huang, K.-W.; Basset, J.-M. *Organometallics* **2014**, *33*, 3320-3327.
41. Rataboul, F.; Baudouin, A.; Thieuleux, C.; Veyre, L.; Coperet, C.; Thivolle-Cazat, J.; Basset, J. M.; Lesage, A.; Emsley, L. *J. Am. Chem. Soc.* **2004**, *126*, 12541-12550.
42. Brown, H. C. *Hydroboration*; W. A. Benjamin: New York, 1962.
43. Gaylord, N. G. *Reduction with Complex Metal Hydrides*; Interscience: New York, 1956.
44. Kandel, K.; Frederickson, C.; Smith, E. A.; Lee, Y.-J.; Slowing, I. I. *ACS Catal.* **2013**, *3*, 2750-2758.
45. Diamond, G. M.; Jordan, R. F.; Petersen, J. L. *J. Am. Chem. Soc.* **1996**, *118*, 8024-8033.
46. Manna, K.; Ellern, A.; Sadow, A. D. *Chem. Commun.* **2010**, *46*, 339-341.
47. Gutekunst, G.; G. Brook, A. *J. Organomet. Chem.* **1982**, *225*, 1-3.
48. Gilman, H.; Smith, C. L. *J. Organomet. Chem.* **1967**, *8*, 245-253.
49. Wu, J. Y.; Moreau, B.; Ritter, T. *J. Am. Chem. Soc.* **2009**, *131*, 12915-12917.
50. Lesage, A.; Lelli, M.; Gajan, D.; Caporini, M. A.; Vitzthum, V.; Miéville, P.; Alauzun, J.; Roussey, A.; Thieuleux, C.; Mehdi, A.; Bodenhausen, G.; Coperet, C.; Emsley, L. *J. Am. Chem. Soc.* **2010**, *132*, 15459-15461.
51. Zagdoun, A.; Casano, G.; Ouari, O.; Schwarzwälder, M.; Rossini, A. J.; Aussenac, F.; Yulikov, M.; Jeschke, G.; Copéret, C.; Lesage, A.; Tordo, P.; Emsley, L. *J. Am. Chem. Soc.* **2013**, *135*, 12790-12797.
52. Chisholm, M. H.; Hammond, C. E.; Huffman, J. C. *Polyhedron* **1988**, *7*, 2515-2520.
53. Furdala, K. L.; Tilley, T. D. *J. Am. Chem. Soc.* **2001**, *123*, 10133-10134.
54. Quignard, F.; Lecuyer, C.; Bougault, C.; Lefebvre, F.; Choplin, A.; Olivier, D.; Basset, J. M. *Inorg. Chem.* **1992**, *31*, 928-930.
55. Troullier, N.; Martins, J. L. *Phys. Rev. B* **1991**, *43*, 1993-2006.
56. Amoureux, J. P.; Pruski, M. *Mol. Phys.* **2002**, *100*, 1595-1613.
57. Althaus, S. M.; Mao, K.; Stringer, J. A.; Kobayashi, T.; Pruski, M. *Solid State Nucl. Magn. Reson.* **2014**, *57-58*, 17-21.
58. Solé, C.; Fernández, E. *Angew. Chem. Int. Ed.* **2013**, *52*, 11351-11355.

59. Medek, A.; Harwood, J. S.; Frydman, L. *J. Am. Chem. Soc.* **1995**, *117*, 12779-12787.
60. Fernandez, C.; Pruski, M. *Solid State NMR*; Chan, J. C. C., Ed.; Springer Berlin: 2012; 306, 119-188.
61. Manriquez, J. M.; McAlister, D. R.; Sanner, R. D.; Bercaw, J. E. *J. Am. Chem. Soc.* **1976**, *98*, 6733-6735.
62. Hillhouse, G. L.; Bercaw, J. E. *J. Am. Chem. Soc.* **1984**, *106*, 5472-5478.
63. Almqvist, F.; Torstensson, L.; Gudmundsson, A.; Frejd, T. *Angew. Chem. Int. Eng. Ed.* **1997**, *36*, 376-377.

CHAPTER 3
 **β -SiH-CONTAINING TRIS(SILAZIDO) RARE EARTH COMPLEXES AS
 HOMOGENEOUS AND GRAFTED SINGLE-SITE CATALYST PRECURSORS FOR
 HYDROAMINATION**

Naresh Eedugurala, Zhuoran Wang, KaKing Yan, Kasuni Boteju, Umesh Chaudhary,
 Takeshi Kobayashi, Arkady Ellern, Igor I. Slowing, Marek Pruski, and Aaron D. Sadow

Department of Chemistry and U.S. Department of Energy Ames Laboratory, 1605 Gilman
 Hall, Iowa State University, Ames IA 50011

Abstract. Trivalent tris(silazido) rare earth compounds $\text{Ln}\{\text{N}(\text{SiHMe}_2)t\text{Bu}\}_3\text{L}$ ($\text{M} = \text{Sc}, \text{Y}, \text{Lu}, \text{La}, \text{Ce}, \text{Pr}, \text{Nd}$) have been prepared in high yield by salt metathesis reactions between three equiv. of $[\text{LiN}(\text{SiHMe}_2)t\text{Bu}]$ and LnCl_3 , $\text{LnCl}_3\text{THF}_n$, or LnI_3THF_n in tetrahydrofuran or diethyl ether. The complexes have been characterized by NMR and IR spectroscopy, as well as single-crystal X-ray diffraction studies to reveal bridging $\text{Ln}\text{---}\text{H}\text{---}\text{Si}$ bonding motifs. The homoleptic complex $\text{Sc}\{\text{N}(\text{SiHMe}_2)t\text{Bu}\}_3$ (**1**) has a distorted trigonal planar structure in the solid state with three short Sc-H and Sc-Si interactions. A low $^1J_{\text{SiH}}$ value in the ^1H NMR spectrum and a low energy ν_{SiH} band in the IR spectrum suggest these interactions are maintained in solution. The structurally-characterized, distorted tetrahedral complexes $\text{Y}\{\text{N}(\text{SiHMe}_2)t\text{Bu}\}_3\text{L}$ ($\text{L} = \text{Et}_2\text{O}$ (**2·Et₂O**), THF (**2·THF**)) and $\text{Lu}\{\text{N}(\text{SiHMe}_2)t\text{Bu}\}_3\text{THF}$ (**3**) retained the $\text{Ln}\text{---}\text{H}\text{---}\text{Si}$ features, while the spectroscopic values varied with solvent and rare earth center. The ν_{SiH} bands in the infrared spectra of $\text{Ln}\{\text{N}(\text{SiHMe}_2)t\text{Bu}\}_3\text{THF}$ ($\text{Ln} = \text{La}$ (**4**), Ce (**5**), Pr (**6**), Nd (**7**)) appeared at higher energy than scandium, yttrium, and lutetium analogues. Scandium **1** and yttrium **2·THF** were grafted onto mesoporous silica nanoparticles (MSN) pre-treated under vacuum at 550 °C (MSN₅₅₀) or 700 °C (MSN₇₀₀). The surface species were characterized by multinuclear, multidimensional solid-state nuclear magnetic resonance (SSNMR) spectroscopic techniques, as well as diffuse reflectance FTIR,

elemental analysis, and the reaction stoichiometry. These data indicate that a mixture of monopodal and bipodal species are obtained from MSN₅₅₀, whereas MSN₇₀₀ primarily provides the monopodal surface species. Both scandium **1** and yttrium **2**·THF homoleptic amides and their heterogeneous M{N(SiHMe₂)tBu}_n@MSN (M = Y, Sc) counterparts efficiently catalyze the intramolecular hydroamination/cyclization of aminoalkenes and bicyclization of aminodialkenes. Both interfacial and solution phase conditions provide the bicyclized product with equivalent cis/trans ratio. The catalytic activity of heterogeneous catalysts is found to be slower compared to molecular precursors, and the recycling ability of heterogeneous catalyst is demonstrated.

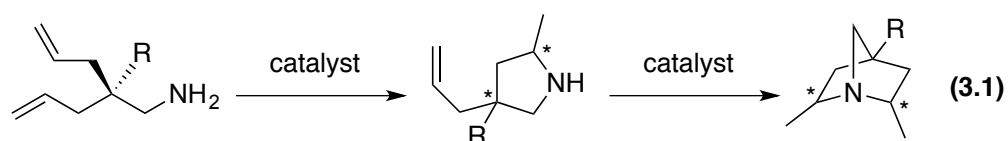
Introduction

Complexes containing only one type of ligand, known as homoleptic compounds (MX_n), represent the simplest systems for characterizing the nature of metal-ligand interactions because all ligands equivalently contribute to electronic and structural effects. The resulting complexes often have intriguing structural and spectroscopic features that are associated with secondary metal-ligand interactions and non-VSEPR geometries.¹ In addition, high oxidation state homoleptic compounds often have electronic and coordinative unsaturation giving highly electrophilic sites, which may also contribute to geometric distortions. The nature of the M–X bond in homoleptic compounds is important to their reactivity; for example, selective substitution of these X groups with ancillary ligands (LX) through protonolysis provides routes to reactive complexes, including catalysts. In rare earth chemistry, homoleptic organometallic and pseudo-organometallic compounds are particularly important starting materials, but the large ionic radii and low numbers of X-type ligands

(either 2 or 3) add to the challenge of preparing homoleptic and monometallic rare earth compounds.²

As a result, few types of ligands, most commonly disilazido ligands such as hexamethyldisilazide $N(SiMe_3)_2$ and tetramethyldisilazide $N(SiHMe_2)_2$, support monometallic homoleptic rare earth compounds. Trivalent $Ln\{N(SiMe_3)_2\}_3$ ³ and $Ln\{N(SiHMe_2)_2\}_3$ ⁴ and divalent $Ln\{N(SiMe_3)_2\}_2$ and $Ln\{N(SiHMe_2)_2\}_2$ ^{4b} compounds are prevalent starting materials for a range of rare earth chemistries, including as catalysts⁵ and as precursors for single-site supported rare earth catalysts.^{4a,6} Such surface-grafted materials catalyze alkyne dimerization,^{6a} Tishchenko aldehyde dimerization,^{6a,6b} hydroamination,^{6c} and polymerization.^{6b,7} Despite the potential synthetic efficiency of hydroamination (the addition of amines and olefins) and the high reactivity of rare earth silazides as catalysts for this process,⁸ examples of grafted single-site rare earth hydroamination catalysts are limited.^{6c} Moreover, those examples suggested that silica-supported catalysts are diminished in activity compared to homogeneous analogues. A number of challenges face catalytic hydroamination reactions including functional group tolerance, catalytic efficiency for intermolecular additions, and control over selectivity. In this context, the effect of surface and pore-localized catalytic sites on selectivity is poorly defined.

The selectivity and activity in catalytic conversions of aminodialkenes could provide a means for examining the effect of surface and pore environment on hydroamination, because both mono- and di-cyclization products are possible, and each product has cis and trans diastereomers (eq 3.1), and the diastereoselectivity is sensitive to reaction conditions.



For example, we recently reported that substrate concentration affected the cis/trans ratio in a enantioselective Zr-catalyzed monocyclization reaction of aminodialkenes and aminodialkynes to optically active pyrrolidines.⁹ Although a few zirconium catalysts give hydroamination/bicyclization products,¹⁰ rare earth compounds tend to provide the pyrrolizidines bicyclization products a two-step process in which the second cyclization requires more forcing conditions than the first cyclization.¹¹ To the best of our knowledge, the hydroamination of aminodialkenes by heterogeneous or single-site supported catalysts is not yet described, and this approach could provide additional control over selectivity. In fact, controlling selectivity in these reactions has synthetic value as monocyclization pyrrolidine¹² and azabicyclo heptane products contain motifs found in natural products and biological active substances.¹³

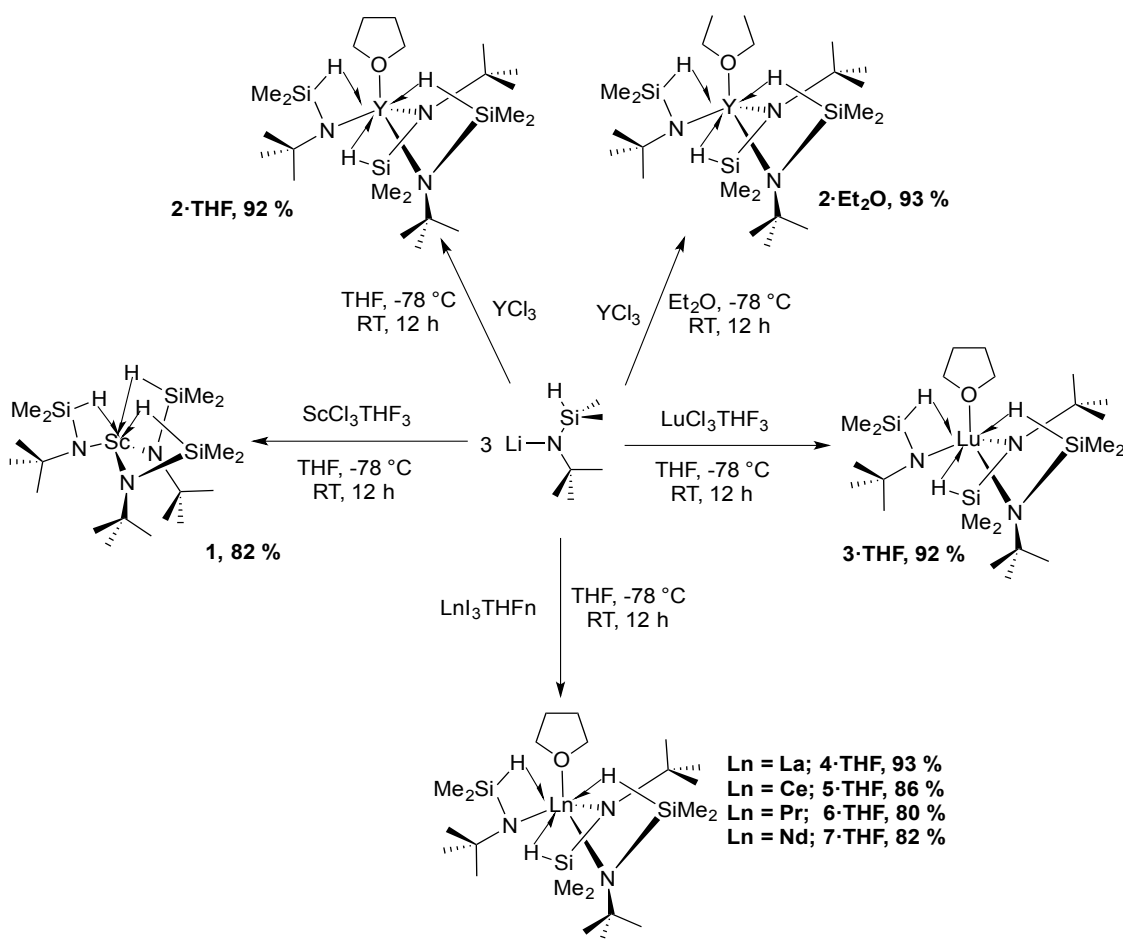
We began to compare surface-supported and homogeneous rare earth catalysts in stereoselective catalytic hydroamination as a possible strategy to control C–N bond forming chemistry. However, a downside of the reported disilazido complexes for this catalysis is that $\text{HN}(\text{SiMe}_3)_2$ and especially $\text{HN}(\text{SiHMe}_2)_2$ can be poor leaving groups due to their relatively high acidity, with pKa values of 25.7 and 22.6, respectively.¹⁴ Disilazanes, particularly $\text{HN}(\text{SiHMe}_2)_2$, are effective silylating agents, and grafting of $\text{Ln}\{\text{N}(\text{SiHMe}_2)_2\}_3$ on silica results in significant surface silylation that may affect active-site loadings. In addition, compounds containing the smaller $\text{N}(\text{SiHMe}_2)_2$ ligand are often multimetallic (e.g., $[\text{La}\{\text{N}(\text{SiHMe}_2)_2\}_3]_2$).¹⁵ Moreover, the basicity of the bulkier silazido ligand $\text{N}(\text{SiMe}_3)t\text{Bu}$ was invoked in its facile substitution in $\text{Ln}\{\text{N}(\text{SiMe}_3)t\text{Bu}\}_3$ ($\text{Ln} = \text{Y}, \text{La}$), as a precursor to hydroamination catalysts.^{11c} Still, the SiH group provides a valuable spectroscopic handle for both NMR and IR analysis,^{4a} potential stabilization of coordinatively and electronically

unsaturated metal centers through secondary interactions,^{4a,14,16} as well as a site for reactivity.¹⁷ The silazide $\text{N}(\text{SiHMe}_2)t\text{Bu}$ provides enhanced steric protection and a more basic amide while including the SiH moiety. This silazido ligand has been underutilized as a supporting ligand in homoleptic compounds compared to the disilazido ligands, despite the early promise of the homoleptic $\text{Er}\{\text{N}(\text{SiHMe}_2)t\text{Bu}\}_3$,¹⁸ and the rich chemistry of $\text{Cp}_2\text{Zr}\{\text{N}(\text{SiHMe}_2)t\text{Bu}\}\text{X}$ ($\text{X} = \text{hydride, halide, alkyl}$).^{16,19} Both of these systems, as well as the main group compound $[\text{Mg}\{\text{N}(\text{SiHMe}_2)t\text{Bu}\}_2]_2$,²⁰ show structural and spectroscopic features associated with multicenter $\text{M}\cdots\text{H}\cdots\text{Si}$ interactions, including short $\text{M}\cdots\text{H}$ distances and acute $\angle\text{M}\cdots\text{N}\cdots\text{Si}$ angles in X-ray diffraction studies, low energy ν_{SiH} bands in infrared spectra, upfield δ_{SiH} in ^1H NMR spectra, and low $^1J_{\text{SiH}}$ in ^{29}Si (and ^1H) NMR spectra. The latter properties, however, have not been evaluated for the homoleptic compound $\text{Er}\{\text{N}(\text{SiHMe}_2)t\text{Bu}\}_3$ because of its paramagnetism, although the solid-state structure and infrared spectra established that all three SiH interact with the rare earth center.¹⁸

Thus, homoleptic monometallic compounds of the type $\text{Ln}\{\text{N}(\text{SiHMe}_2)t\text{Bu}\}_3$ may be effective precatalysts and precursors for single-site heterogeneous catalysts. The present study describes our efforts to synthesize and characterize a series of rare earth compounds of this type including the NMR properties of diamagnetic analogues, our studies of surface grafting and characterization of mesoporous silica (MSN) supported rare earth silazido materials, and a comparison of activity and selectivity of solution-phase vs. grafted catalysts in hydroamination/cyclization of aminoalkenes and aminodialkenes.

Results and Discussion

Synthesis and spectroscopic characterization of $\text{Ln}\{\text{N}(\text{SiHMe}_2)\text{tBu}\}_3\text{L}_x$. Reactions of three equiv. of $[\text{LiN}(\text{SiHMe}_2)\text{tBu}]$ and LnCl_3 ($\text{Ln} = \text{Y}$), $\text{LnCl}_3\text{THF}_3$ ($\text{Ln} = \text{Sc}, \text{Lu}$), or LnI_3THF_n ($\text{Ln} = \text{La}, \text{Ce}, n = 4$; $\text{Ln} = \text{Pr}, \text{Nd}; n = 3$) in THF or Et_2O provide $\text{Ln}\{\text{N}(\text{SiHMe}_2)\text{tBu}\}_3$ or $\text{Ln}\{\text{N}(\text{SiHMe}_2)\text{tBu}\}_3\text{L}$ as outlined in Scheme 3.1 ($\text{Ln} = \text{Sc}$ (**1**); Y (**2**· Et_2O); Y (**2**· THF); Lu (**3**· THF); La (**4**· THF); Ce (**5**· THF); Pr (**6**· THF); Nd (**7**· THF)).



Scheme 3.1. Synthesis of homoleptic silazido rare earth compounds

Compound **1** is isolated as a light yellow sticky solid, and neither Et_2O nor THF are retained in the scandium's coordination sphere. The complexes **2**· Et_2O , **2**· THF , and **3**· THF are isolated as white sticky solids. The La compound **4**· THF is an off-white gel, cerium

analogue **5·THF** is a yellow gel, Pr complex **6·THF** is a pale green oil, and neodymium tris(silazido) **7·THF** is a light blue oil. These compounds form analytically pure (La, Ce and Lu) or nearly analytically pure (Sc, Y) materials from pentane crystallization or precipitation, although the very oily Pr and Nd were impure. Sublimation of the sticky solids of **2·THF**, **3·THF**, **6·THF**, **7·THF** affords the materials as analytically pure powders. However, the coordinated ether is not removed during the sublimation. While the ^1H NMR spectrum of **2·THF** does not change after sublimation, the ν_{SiH} region of the infrared spectra are slightly sharper after sublimation. The La compound did not sublime under vacuum below 130 °C.

Syntheses were attempted in toluene to access solvent-free analogues, on the basis of syntheses of related THF-free homoleptic alkyls from LnCl_3 or LnI_3 and potassium alkyl $\text{KC}(\text{SiHMe}_2)_3$ that occur readily in toluene.²¹ However, only starting materials are observed in reactions of $[\text{LiN}(\text{SiHMe}_2)t\text{Bu}]$ and LnCl_3 ($\text{Ln} = \text{Y}, \text{La}$), while THF-containing precursors LnX_3THF_x react to give THF-containing products.

The infrared spectra of compounds **1**, **2·Et₂O**, and **2-7·THF** contained bands ranging from 2135 to 1865, which encompassed the region typically assigned to Si-H stretching modes (Figure 3.1 and Table 3.1). Spectra for **1** and **2·Et₂O** revealed a single strong band assigned to bridging $\text{Ln}\text{--H}\text{--Si}$ groups, with the tricoordinated scandium complex's peak appearing at higher energy than the signal for the ether-coordinated yttrium species. In contrast, the ν_{SiH} region for unsublimed **2·THF** contained two peaks at 2019 and 1967 cm^{-1} at notably higher energy than **1** and **2·Et₂O**; once sublimed, the signal at 2117 cm^{-1} , which is present in **1** and **2·Et₂O** was detected. The signals for lutetium, lanthanum, cerium, praseodymium, and neodymium complexed appeared around 2000 cm^{-1} , and increase in energy in that order. For comparison, the SiH stretching frequencies of the silazane

HN(SiHMe₂)*t*Bu (2104 and 2055 cm⁻¹) and lithium silazido [LiN(SiHMe₂)*t*Bu] (2135 cm⁻¹) appeared at higher energy than the rare earth silazido compounds.

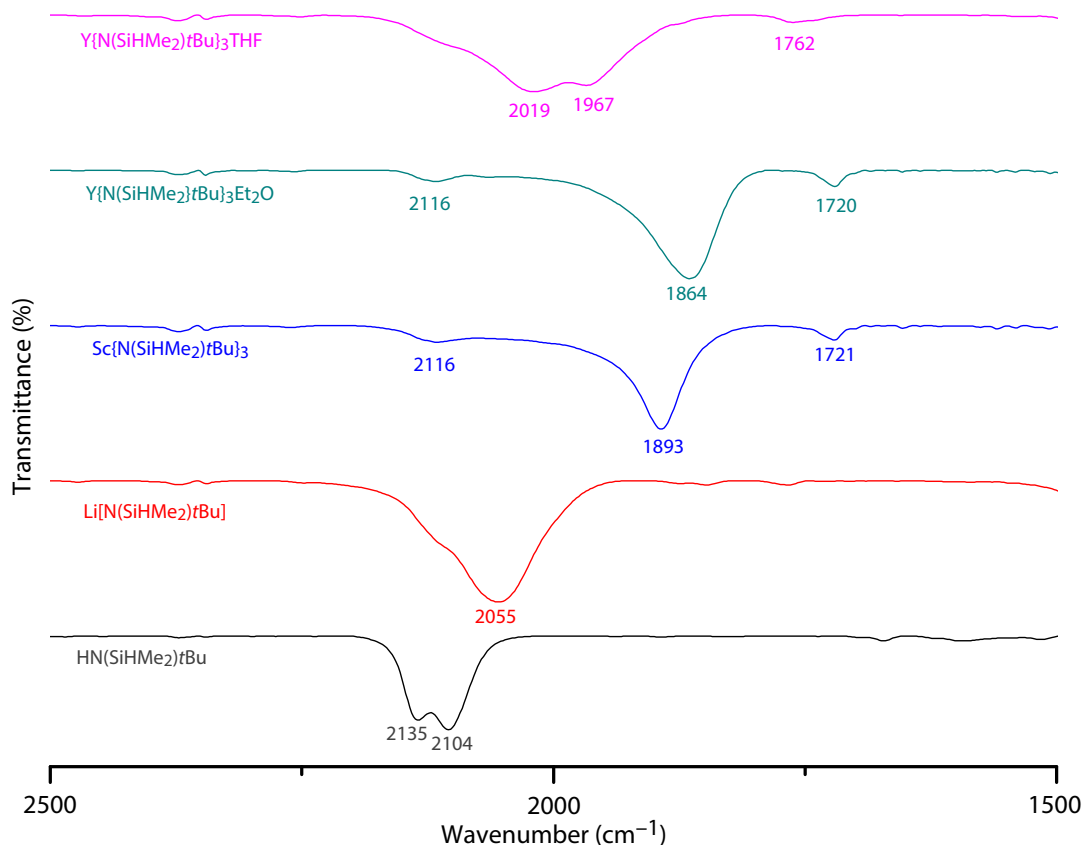


Figure 1. Infrared spectra of HN(SiHMe₂)*t*Bu, [LiN(SiHMe₂)*t*Bu], Sc{N(SiHMe₂)*t*Bu}₃ (**1**), Y{N(SiHMe₂)*t*Bu}₃Et₂O (**2·Et₂O**), and Y{N(SiHMe₂)*t*Bu}₃THF (**2·THF**, before sublimation).

The room temperature ¹H NMR spectra of the series of diamagnetic compounds suggested the homoleptic rare earth species are C_{3v} symmetric on the basis of three resonances, which were assigned to the SiH, SiMe₂, and *t*Bu groups in equivalent silazido ligands. The ³J_{HH} coupling in SiHMe₂ is small and resolved clearly as doublets for the Me only in **2·THF** (3.0 Hz), **3·THF** (3.1 Hz), and **4·THF** (3.2 Hz). The ¹J_{SiH} values (Table 3.1)

vary depending on the rare earth element and the coordinated THF or Et₂O ligands, but are generally low and suggest the Ln←H-Si bonding motifs. The (room temperature) ¹J_{SiH} values in HN(SiHMe₂)*t*Bu (193 Hz) and [LiN(SiHMe₂)*t*Bu] (168 Hz) are larger than in the rare earth compounds. At low temperature (190 K), the SiMe₂ signals in the ¹H NMR spectra of **1**, **2**·THF and **3**·THF appeared as two signals of equal intensity, implying low temperature C₃-symmetric structures. Interestingly, the SiH chemical shift and coupling constants were identical in spectra acquired from room temperature down to 190 K. In a further contrast, the ¹H NMR spectra of **2**·Et₂O and **4**·THF merely broadened as the temperature was lowered.

The ²⁹Si NMR spectra of the diamagnetic compounds vary from -22.9 to -33.7 ppm depending on the identity of the rare earth element, and these chemical shifts appeared slightly upfield compared to HN(SiHMe₂)*t*Bu. A similar trend was observed in the ²⁹Si NMR spectra of the homoleptic rare earth disilazido compounds Ln{N(SiHMe₂)₃THF_n}, which are ca. 10 ppm upfield compared to the disilazane HN(SiHMe₂)₂ (-11.1 ppm). In addition, ¹H-¹⁵N HMQC experiments at natural abundance revealed crosspeaks between N and *t*Bu signals but not to the SiHMe₂ group. The ¹⁵N NMR chemical shifts varied from -192 to -232 ppm, and these are downfield compared to HN(SiHMe₂)*t*Bu and [LiN(SiHMe₂)*t*Bu] (see Table 3.1). The same trend was also discovered in the ¹⁵N NMR chemical shifts for Sc{N(SiHMe₂)₂}₃THF (-252.6 ppm) and Y{N(SiMe₃)₂}₃ (-243.1 ppm), which are downfield of HN(SiHMe₂)₂ (-365.3 ppm) and HN(SiMe₃)₂ (-354.3 ppm). Likewise, the ¹⁵N NMR chemical shifts for Cp₂Zr{N(SiHMe₂)*t*Bu}H (-259.5 ppm) and Cp₂Zr{N(SiHMe₂)₂}H (-292.4 ppm) are downfield with respect to HN(SiHMe₂)*t*Bu (-329.2 ppm) and HN(SiHMe₂)₂ (-365.3 ppm).^{17a}

Table 3.1. Spectroscopic data for t-butyl(dimethylsilyl)amido compounds.

Compound	δ_{SiH} (ppm)	$^1J_{\text{SiH}}$ (Hz)	^{29}Si (ppm)	^{15}N (ppm)	ν_{SiH} (cm^{-1})
Sc{N(SiHMe ₂)tBu} ₃ (1)	4.18	125	-22.9	-208	1893
Y{N(SiHMe ₂)tBu} ₃ OEt ₂ (2 ·OEt ₂)	4.3	126	-25.9	-222	1865
Y{N(SiHMe ₂)tBu} ₃ THF (2 ·THF)	4.59	143	-30.5	-231	2020,1969
Lu{N(SiHMe ₂)tBu} ₃ THF (3 ·THF)	4.63	137	-28.7	-232	1988
La{N(SiHMe ₂)tBu} ₃ THF (4 ·THF)	4.66	146	-33.7	-196	2003, 1941
Ce{N(SiHMe ₂)tBu} ₃ THF (5 ·THF) ^a	-----	-----	-----	-----	2003
Pr{N(SiHMe ₂)tBu} ₃ THF (6 ·THF) ^a	-----	-----	-----	-----	2009
Nd{N(SiHMe ₂)tBu} ₃ THF (7 ·THF) ^a	-----	-----	-----	-----	2010
HN(SiHMe ₂)tBu	4.83	192	-18.8	-329	2135, 2104
LiN(SiHMe ₂)tBu	4.87	168	-23.1	-301	2054

^aNMR parameters for these paramagnetic compounds were not determined.

X-ray Crystallography. Single crystal X-ray diffraction studies provided solid-state structures of Sc{N(SiHMe₂)tBu}₃ (**1**), Y{N(SiHMe₂)tBu}₃OEt₂ (**2**·Et₂O), Y{N(SiHMe₂)tBu}₃THF (**2**·THF), and Lu{N(SiHMe₂)tBu}₃THF (**3**·THF) for comparison to Er{N(SiHMe₂)tBu}₃.¹⁸ The molecular structures of **1** and Er{N(SiHMe₂)tBu}₃ are similar: the overall symmetry is pseudo-C₃ with the N(SiHMe₂)tBu ligands adopting a propeller-like configuration with all three SiH groups on the same face of the the ScN₃ core. The methyl groups in the SiMe₂ are inequivalent in this structure, and this is consistent with the low temperature ¹H NMR spectrum described above.

The ScN₃ core adopts a pyramidalized trigonal geometry ($\sum_{\text{NScN}} = 348.62(9)$ vs. $\sum_{\text{NErN}} = 350.42$), and there are three short Sc \cdots H and three short Sc \cdots Si distances. Remarkably, the scandium-silicon distances (Sc1-Si1, 2.8603(3); Sc1-Si2, 2.8343(4); Sc1-Si3, 2.8557(4) Å) are similar to the distances in scandium silyl compounds Cp₂ScSi(SiMe₃)₃THF (2.863(2) Å)²² and only slightly longer than Cp*₂ScSiH₂SiPh₃ (2.797(1) Å),²³ both of which contain bona fide 2 center-2 electron Sc–Si bonds. Taking into consideration the short distances to N and Si, the N₃Si₃ atoms form a twisted trigonal prism, with the smaller N₃ end-capping triangle twisted from the triangular face composed of Si₃ vertices. The Sc center is 0.41 and 1.02 Å from the N₃ and Si₃ planes, respectively. The scandium-hydrogen distances (Sc1-H1s, 2.26(1); Sc1-H2s, 2.20(2); Sc1-H3s, 2.23(1) Å), however, are significantly longer than the calculated distance in ScH₃ (1.82 Å).²⁴ The only comparable homoleptic, solvent-free tris(amido)scandium compound Sc{N(SiMe₃)₂}₃, is pyramidal in the solid state ($\sum_{\text{NScN}} = 346.5$, D₃ symmetry) but planar in the gas-phase.²⁵ In that compound, the solid-state and gas-phase Sc–N distance (2.047(2) and 2.02(3) Å, respectively) are slightly shorter than in **1** (Sc1-N1, 2.0656(6); Sc1-N2, 2.063(1); Sc1-N3, 2.071(2) Å). The Sc–N distances in **1**, however, are similar to those in four-coordinate THF-adduct Sc{N(SiHMe₂)₂}₃THF.^{4a}

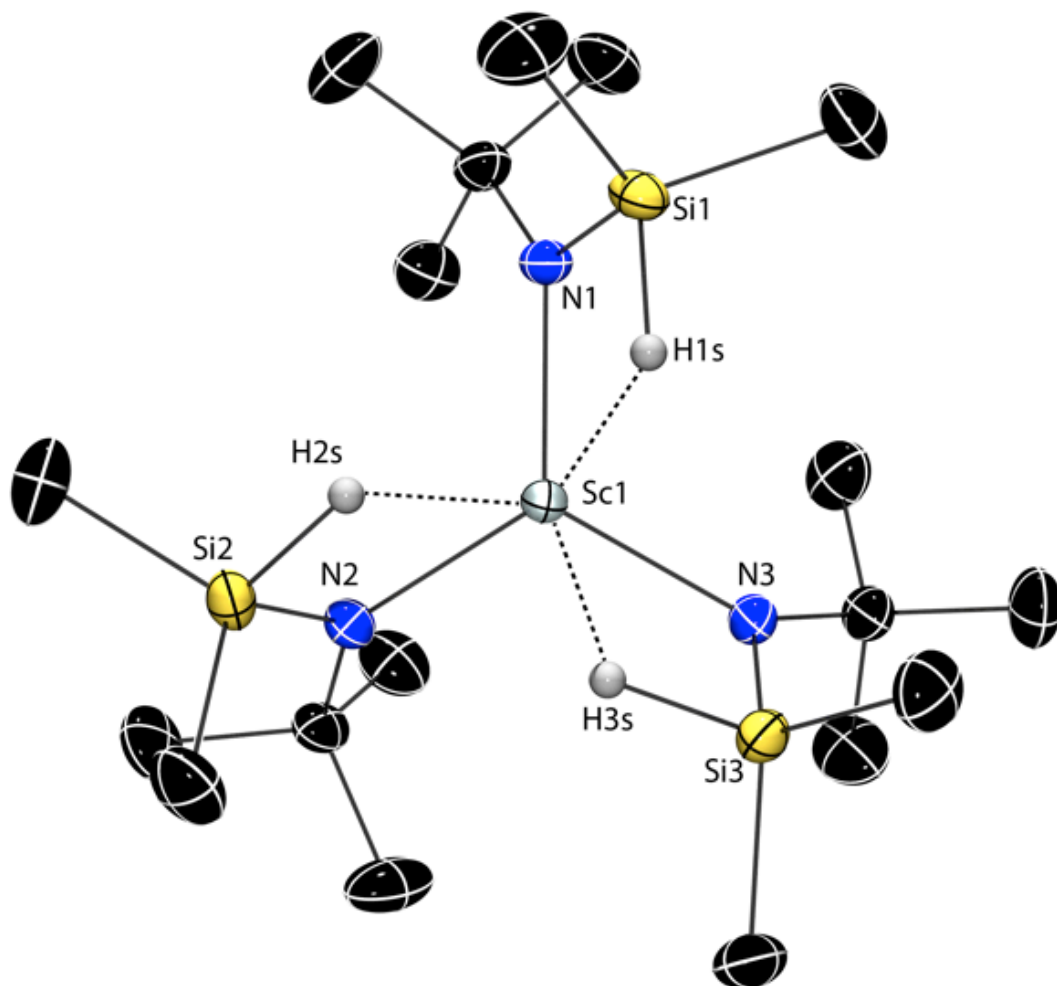


Figure 3.2. Thermal ellipsoid plot of $\text{Sc}\{\text{N}(\text{SiHMe}_2)_2\}_3$ (**1**). Selected interatomic distances (Å): Sc1-N1, 2.0656(6); Sc1-N2, 2.063(8); Sc1-N3, 2.071(9); Sc1-H1s, 2.26(1); Sc1-H2s, 2.20(2); Sc1-H3s, 2.23(1); Sc1-Si1, 2.8603(3); Sc1-Si2, 2.8343(4); Sc1-Si3, 2.8557(4). Selected interatomic angles (°): N1-Sc1-N2, 117.89(3); N1-Sc1-N3, 116.92(3); N2-Sc1-N3, 113.81(3); Sc1-N1-Si1, 98.47(4); Sc1-N2-Si2, 97.39(4); Sc1-N3-Si3, 97.98(4).

The two yttrium compounds **2**· Et_2O and **2**· THF were studied by single crystal X-ray diffraction because distinct ν_{SiH} bands in their IR spectra and $^1J_{\text{SiH}}$ values suggested inequivalent structures. Both compounds crystallize in the $P2_1/c$, but **2**· THF contains two crystallographically unique molecules ($Z = 8$) per unit cell, whereas **2**· Et_2O crystallizes with

only one ($Z = 4$). All three molecules of **2·L** are four coordinate based on the YN_3O core, with the YN_3 part flattened ($\sum_{NYN} = 344.7(3)^\circ$ (**2·OEt₂**), $346.4(3)$, and $347.9(3)$ (**2·THF**) compared to that of an ideal tetrahedron ($\sum = 327^\circ$). In addition, one of the N-Y-O angles is ca. 90° in each of the structures (i.e., the molecules lack even a pseudo- C_3 axis). All three Si-H groups point toward the Y center, and each of these H atoms is pseudo-trans to either a silazide or ether ligand (e.g., in **2·Et₂O** H1s-Y1-N2 is $175(1)^\circ$, H2s-Y1-N3 is $152(1)^\circ$ and H3s-Y1-O1 is $153(1)^\circ$). The conformations, as well as the metrical features associated with Y-N-Si-H structural motifs, are similar across the yttrium structures, contrasting the distinguishing IR spectroscopic features noted above. The geometry of the lutetium analogue $Lu\{N(SiHMe_2)tBu\}_3THF$ (Figure 3.3) is similar to **2·Et₂O** and **2·THF** yet SiH-centered spectroscopic features are in between (Table 3.1). Thus, the Ln-H and Ln-Si distances trends do not correlated one-to-one with energies and coupling constants indicated by the spectroscopic signatures, although the features are consistently present in all the compounds.

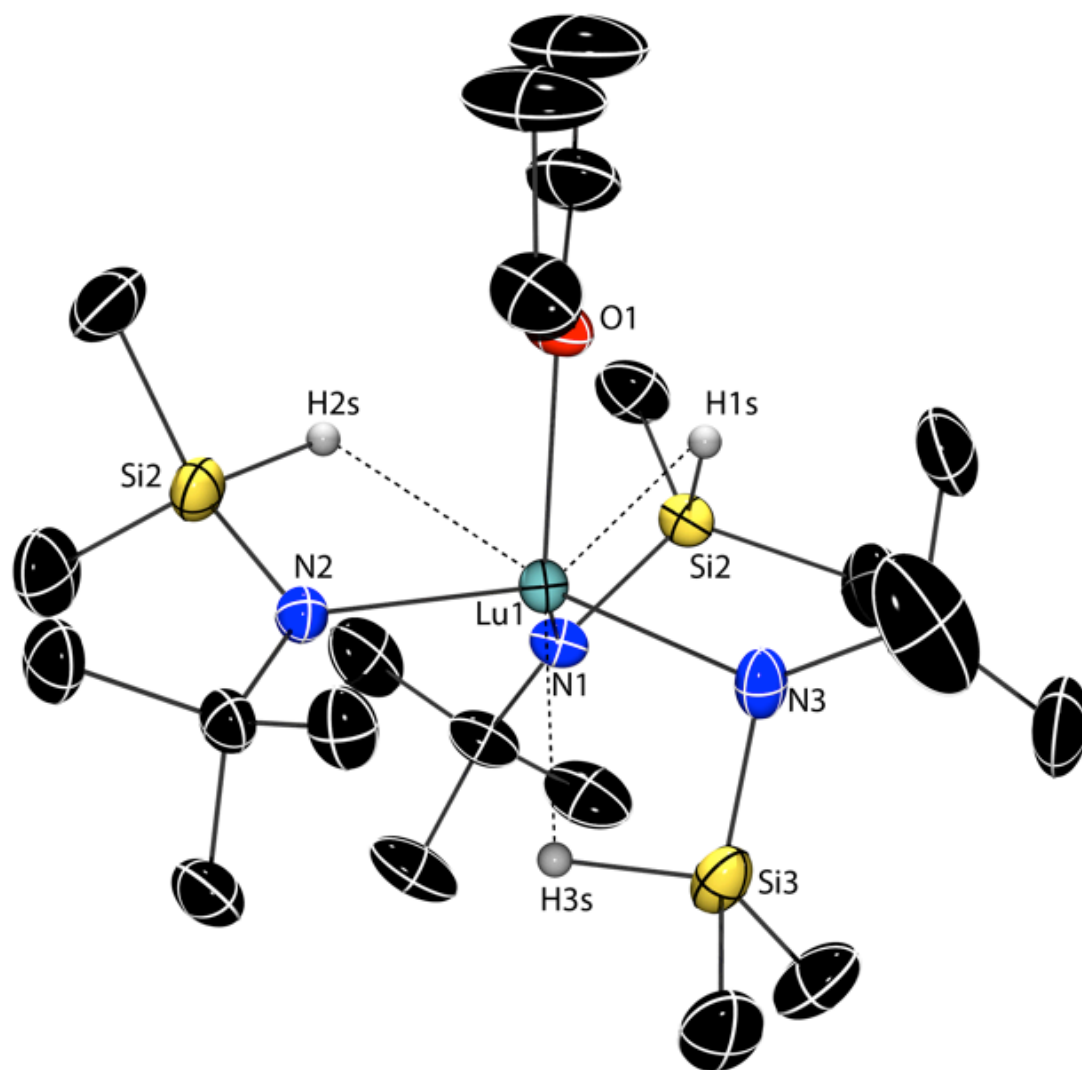
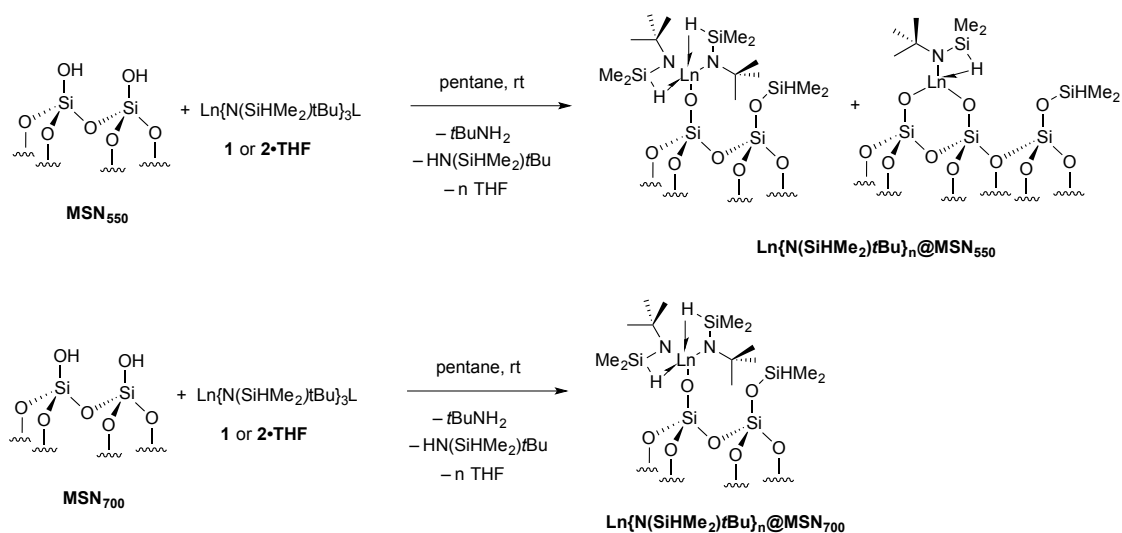


Figure 3.3. Thermal ellipsoid plot of $\text{Lu}\{\text{N}(\text{SiHMe}_2)_2\}_3\text{THF}$ (**3·THF**). Selected interatomic distances (Å): Lu1-N1, 2.199(2); Lu1-N2, 2.214(2); Lu1-N3, 2.219(2); Lu1-O1, 2.338(2); Lu1-Si1, 2.9969(8); Lu1-H1s, 2.36(2); Lu1-Si2, 3.070(1); Lu1-H2s, 2.53(3); Lu1-Si3, 2.9831(9); Lu1-H3s, 2.35(3). Selected interatomic angles (°): N1-Lu1-N2, 114.79(7); N1-Lu1-N3, 107.64(7); N2-Lu1-N3, 121.31(7); N2-Lu1-H1s, 147.4(6); N3-Lu1-H2s, 170.5(6); O1-Lu1-H3s, 149.9(6).

Synthesis and characterization of $\text{M}\{\text{N}(\text{SiHMe}_2)_2\text{tBu}\}_n@ \text{MSN}$. Compounds **1** or **2·THF** were stirred with SBA-type mesoporous silica nanoparticles (MSN) previously heated under

vacuum either at 550 °C (MSN₅₅₀, 1.5 mmol OH/g) or 700 °C (MSN₇₀₀, 0.9 mmol OH/g) to graft the rare earth species on the material, as depicted in Scheme 3.2. The smaller rare earth elements were initially studied because Anwender and co-workers showed that grafted yttrium complexes are more active in hydroamination/cyclization than lanthanide catalysts,^{6c} and we wished to compare mild conditions for cyclization with diastereoselective Zr-catalyzed hydroamination.⁹ Micromole-scale grafting reactions were performed in benzene-*d*₆ and monitored by ¹H NMR spectroscopy, while preparative-scale syntheses were performed in pentane at room temperature for 20 h. The former experiments provided an initial estimate of loading and possible surface species species based on reaction stoichiometry (Table 3.2). For example, a micromole-scale reaction in benzene-*d*₆ consumed 0.480 mmol of **2·THF** and produced 0.330 mmol of *t*BuNH₂ and 0.350 mmol of HN(SiHMe₂)*t*Bu per g of MSN₅₅₀. These experiments provide a rough estimate of the yttrium loading (see Table 3.2, 0.48 mmol/g in this example), the average podality (~ 1:1 monopodal and dipodal in this example), and the quantity of surface silylation in the grafting experiments. Notably, less rare earth amide is consumed, and less *t*BuNH₂ and HN(SiHMe₂)*t*Bu are formed in reactions with MSN₇₀₀, while the ratio of *t*BuNH₂:HN(SiHMe₂)*t*Bu also decreased in experiments with the high temperature-treated silica. Moreover, the ratio of consumed rare earth silazide to amine produced in reactions with MSN₇₀₀ suggest that the grafted species are primarily monopodal in those cases. Systematic and corroborative characterization with quantitative analysis with inductively coupled plasma optical emission spectroscopy (ICP-OES) and CHN combustion analysis and spectroscopically using IR and solid-state (SS)NMR spectroscopy support the initial estimates.



Scheme 3.2. Surface grafting reactions and proposed surface-supported homoleptic silazido rare earth compounds formed from MSN_{550} or MSN_{700} and $\text{Sc}\{\text{N}(\text{SiHMe}_2)\text{tBu}\}_3$ (**1**) or $\text{Y}\{\text{N}(\text{SiHMe}_2)\text{tBu}\}_3\text{THF}$ (**2·THF**).

Table 3.2. Stoichiometry of surface grafting reactions.^a

Preparation	mmol Ln consumed/g	mmol tBuNH_2 measured/g MSN	mmol $\text{HN}(\text{SiHMe}_2)\text{tBu}$ measured/g MSN
$\text{Sc}\{\text{N}(\text{SiHMe}_2)\text{tBu}\}_3 + \text{MSN}_{550}$	0.54 ± 0.01	0.37 ± 0.02	0.46 ± 0.03
$\text{Sc}\{\text{N}(\text{SiHMe}_2)\text{tBu}\}_3 + \text{MSN}_{700}$	0.35 ± 0.01	0.14 ± 0.02	0.21 ± 0.03
$\text{Y}\{\text{N}(\text{SiHMe}_2)\text{tBu}\}_3\text{THF} + \text{MSN}_{550}$	0.48 ± 0.01	0.33 ± 0.02	0.35 ± 0.03
$\text{Y}\{\text{N}(\text{SiHMe}_2)\text{tBu}\}_3\text{THF} + \text{MSN}_{700}$	0.22 ± 0.01	0.05 ± 0.02	0.15 ± 0.03

^aStandard deviation was estimated by measuring one example in triplicate.

The loading of grafted metal species was quantified by ICP-OES, while the loading of $\text{N}(\text{SiHMe}_2)\text{tBu}$ ligands was measured by CHN combustion analysis (Table 3). The N:Sc ratio of 1.35:1 for $\text{Sc}\{\text{N}(\text{SiHMe}_2)\text{tBu}\}_n@ \text{MSN}_{550}$ suggested a mixture of mono(silazido)scandium ($\equiv\text{SiO}-\text{ScN}(\text{SiHMe}_2)\text{tBu}$) and bis(silazido)scandium ($\equiv\text{SiO}-\text{Sc}\{\text{N}(\text{SiHMe}_2)\text{tBu}\}_2$) surface

species. As in the above experiments that measure stoichiometry, these values average the composition of the surface species rather than provide a precise structure. Alternatively, the N:Sc ratio for $\text{Sc}\{\text{N}(\text{SiHMe}_2)t\text{Bu}\}_n@MSN_{700}$ implied bis(silazido) scandium $\equiv\text{SiO}-\text{Sc}\{\text{N}(\text{SiHMe}_2)t\text{Bu}\}_2$ is the dominant surface species.

Table 3.3. Quantification of Ln, N, and C using ICP-OES and CHN (combustion) analysis.

Preparation	weight % Ln	mmol Ln/g	mmol N/g	N:Ln	mmol C/g	C:N
$\text{Sc}\{\text{N}(\text{SiHMe}_2)t\text{Bu}\}_3 + MSN_{550}$	2.5±0.1	0.556±0.002	0.749±0.009	1.35±0.01	6.111±0.004	8.15±0.01
$\text{Sc}\{\text{N}(\text{SiHMe}_2)t\text{Bu}\}_3 + MSN_{700}$	1.5±0.1	0.334±0.002	0.635±0.009	1.90±0.01	4.321±0.004	6.81±0.01
$\text{Y}\{\text{N}(\text{SiHMe}_2)t\text{Bu}\}_3\text{THF} + MSN_{550}$	4.2±0.1	0.467±0.001	0.864±0.009	1.86±0.01	6.389±0.004	7.39±0.01
$\text{Y}\{\text{N}(\text{SiHMe}_2)t\text{Bu}\}_3\text{THF} + MSN_{700}$	2.3±0.1	0.259±0.001	0.535±0.009	2.05±0.01	3.430±0.004	6.41±0.01

In addition, an excess of carbon is present on the surface. The C:N ratio in a $\text{N}(\text{SiHMe}_2)t\text{Bu}$ ligand is 5.15:1, whereas the grafted materials' measured C:N ratios are higher (e.g. $\text{Sc}\{\text{N}(\text{SiHMe}_2)t\text{Bu}\}_n@MSN_{550}$, C:N = 8.16:1). This higher carbon loading is readily rationalized by a silylation of surface silanols, similarly to surface silylation agents known for disilazanes $\text{HN}(\text{SiMe}_3)_2$ and $\text{HN}(\text{SiHMe}_2)_2$,^{4a,26} and the high carbon ratio and observation of $t\text{BuNH}_2$ in the supernatant is consistent with such a process. Less surface silylation occurs in grafting reactions involving MSN_{700} than MSN_{550} .

Diffuse reflectance IR spectra of the rare earth silazide-treated materials, compared to pristine MSN₅₅₀ and MSN₇₀₀ and precursors **1** and **2·THF**, revealed that isolated silanols are consumed in the grafting reactions and the new surface species contain CH and SiH groups. In all reactions of MSN and rare earth silazides, the absorption band at 3747 cm⁻¹ assigned to isolated silanol groups²⁷ disappeared upon grafting, however a broad signal from 3740 to 3280 cm⁻¹ assigned to hydrogen-bonded silanols was apparent in the grafted materials' spectra.²⁷⁻²⁸ These remaining SiOH groups were not readily accessible for reactivity, as demonstrated by the trace amounts of toluene detected upon addition of Mg(CH₂Ph)₂(O₂C₄H₈)₂. The SiH region of the diffuse reflectance IR spectrum of Y{N(SiHMe₂)*t*Bu}_n@MSN₅₅₀ and Y{N(SiHMe₂)*t*Bu}_n@MSN₇₀₀ contained a sharp signal at 2149 cm⁻¹ and a broad signal from 2080 to 1780 cm⁻¹ with a maximum at 1924 cm⁻¹. The former signal was assigned to ≡SiO–SiHMe₂ surface groups on the basis of comparison with MSN treated with HN(SiHMe₂)*t*Bu or HN(SiHMe₂)₂ (at 2152 cm⁻¹, see Figure 3.4D) and literature reports.^{4a} This functionality is expected from the reaction of silanols and HN(SiHMe₂)*t*Bu, the byproduct from grafting of **1** or **2·THF**. The broad signals were assigned to terminal Si–H and bridging Y–H–Si groups in surface-grafted Y{N(SiHMe₂)*t*Bu}_n@MSN. Similarly, diffuse reflectance IR spectra of the scandium material Sc{N(SiHMe₂)*t*Bu}_n@MSN contained a sharp signal at 2149 cm⁻¹ assigned to ≡SiO–SiHMe₂ and a broad signal from 2070 to 1820 cm⁻¹ with a maximum of 1867 cm⁻¹, suggesting that the majority of surface scandium silazido species are bridging Sc–H–Si groups.

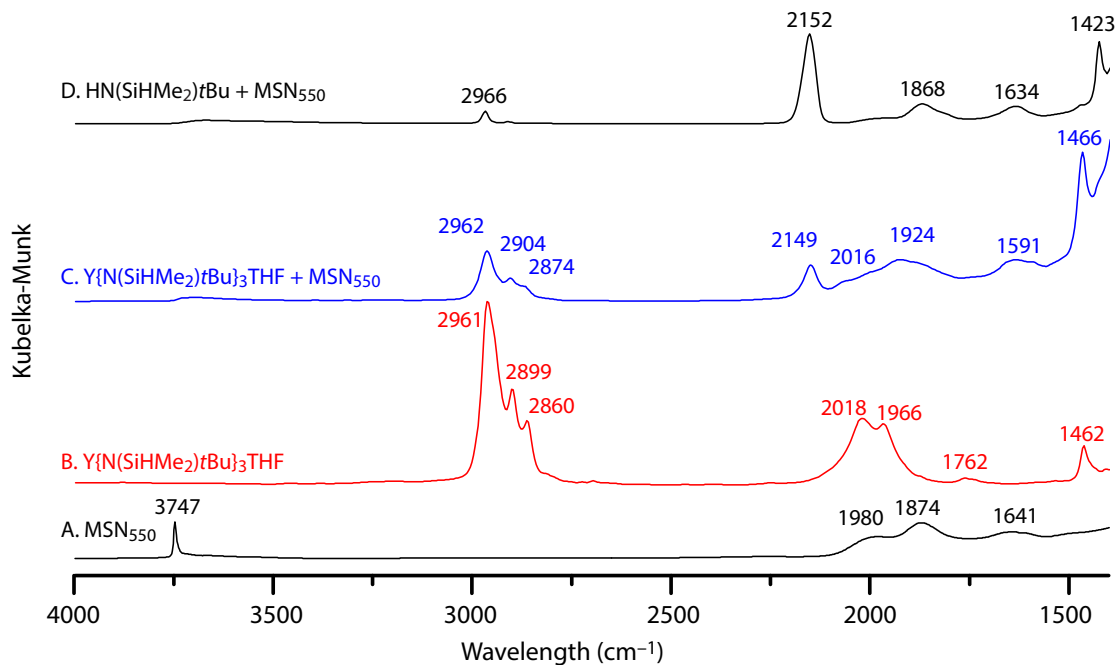


Figure 3.4. Diffuse reflectance infrared spectra of (A) MSN_{550} , (B) $\text{Y}\{\text{N}(\text{SiHMe}_2)\text{tBu}\}_3\text{THF}$, (C) $\text{Y}\{\text{N}(\text{SiHMe}_2)\text{tBu}\}_3 + \text{MSN}_{550}$ and (D) $\text{HN}(\text{SiHMe}_2)\text{tBu} + \text{MSN}_{550}$.

^1H CPMAS SSNMR spectra of $\text{Sc}\{\text{N}(\text{SiHMe}_2)\text{tBu}\}_n@ \text{MSN}_{550}$ and $\text{Y}\{\text{N}(\text{SiHMe}_2)\text{tBu}\}_n@ \text{MSN}_{550}$ contained broad, yet resolved signals at 4.4, 1.0, and -0.1 ppm assigned to SiH, tBu, and SiMe. The signals for $\equiv\text{SiO}-\text{SiHMe}_2$ and $\equiv\text{SiO}-\text{Ln}\{\text{N}(\text{SiHMe}_2)\text{tBu}\}_n$ are not distinguished in the ^1H NMR spectra for either scandium or yttrium derivatives on MSN_{550} , however, two partly resolved signals at 4.0 and 4.5 ppm were observed in $\text{Sc}\{\text{N}(\text{SiHMe}_2)\text{tBu}\}_n@ \text{MSN}_{700}$.

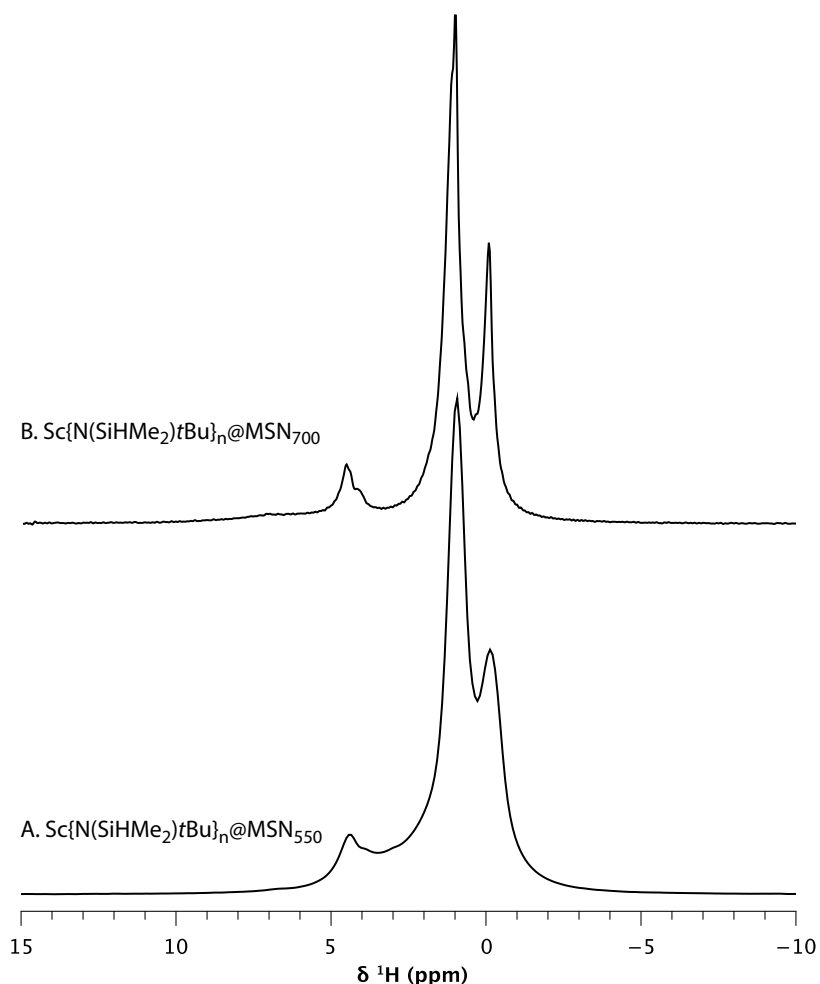


Figure 3.5. The ^1H Hahn echo spectra of (A) $\text{Sc}\{\text{N}(\text{SiHMe}_2)\text{tBu}\}_n@ \text{MSN}_{550}$ (echo delay 40 μs , recycle delay 10 s, 8 scans, MAS 25 kHz, $B_1 = 100$ kHz) and (B) $\text{Sc}\{\text{N}(\text{SiHMe}_2)\text{tBu}\}_n@ \text{MSN}_{700}$. (echo delay 666.6 μs , recycle delay 10s, 16 scans, MAS 18kHz, $B_1(^1\text{H}) = 125$ kHz (to remove severe probe background)).

$^{29}\text{Si}\{^1\text{H}\}$ CPMAS spectra of $\text{Sc}\{\text{N}(\text{SiHMe}_2)\text{tBu}\}_n@ \text{MSN}_{550}$ and $\text{Sc}\{\text{N}(\text{SiHMe}_2)\text{tBu}\}_n@ \text{MSN}_{700}$ reveal three types of SiHMe_2 groups (Figure 6A,C), including $\equiv\text{SiO}-\text{SiHMe}_2$ (M sites, -2.9 ppm), bipodal $(\equiv\text{SiO})_2\text{ScN}(\text{SiHMe}_2)\text{tBu}$ (-17.9 ppm), and monopodal $\equiv\text{SiO}-\text{Sc}\{\text{N}(\text{SiHMe}_2)\text{tBu}\}_2$ (-29.9 ppm), as well as and silica Q sites (-106.6

ppm) from the support. Assignment of the upfield signal at -29.9 ppm is supported by the ^{29}Si NMR chemical shift of $\text{Sc}\{\text{N}(\text{SiHMe}_2)_2\}_3$ (**1**) of -24.0 ppm (CPMAS) and -22.9 ppm (benzene- d_6). The ratio of these SiHMe_2 signals in $\text{Sc}\{\text{N}(\text{SiHMe}_2)t\text{Bu}\}_n@MSN_{550}$ and $\text{Sc}\{\text{N}(\text{SiHMe}_2)t\text{Bu}\}_n@MSN_{700}$ are inequivalent, with the latter sample showing diminished intensity of signals assigned to $\equiv\text{SiO}-\text{SiHMe}_2$ and dipodal $(\equiv\text{SiO}-)_2\text{ScN}(\text{SiHMe}_2)t\text{Bu}$ (-17.9 ppm).

In order to probe the SiHMe_2 structures associated with signals at -29.9 and -17.9 ppm, a DNP-enhanced ^{29}Si CPMAS spectrum was acquired (Figure 3.6B). Under DNP-conditions (i.e., in the presence of Tekpol at 100 K), the signal at -29.9 was not observed. Remarkably, the resonances at -17.9 ppm as well as the $\equiv\text{SiO}-\text{SiHMe}_2$ site are still detected, even though the former is tentatively assigned as a scandium silazido species. That assignment is supported by CP build-up curves for signals at -2.9 ($424 \mu\text{s}$, $\equiv\text{SiO}-\text{SiHMe}_2$) and -29.9 ($638 \mu\text{s}$, $\equiv\text{SiO}-\text{Sc}\{\text{N}(\text{SiHMe}_2)t\text{Bu}\}_2$), which further supports the presence of a $\text{Sc}\leftarrow\text{H}-\text{Si}$ interaction on the surface-grafted site.

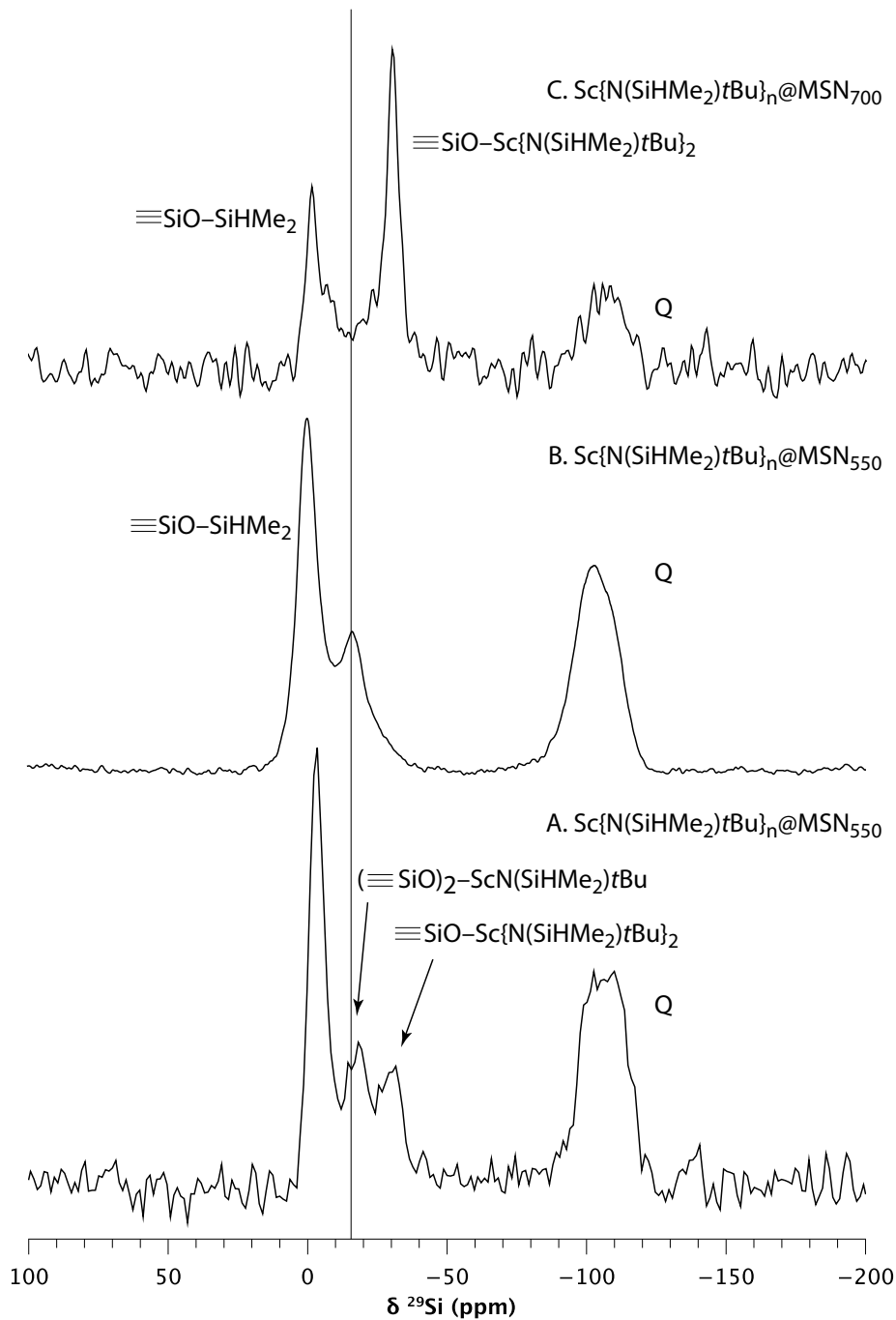


Figure 3.6. (A) $^{29}\text{Si}\{^1\text{H}\}$ CPMAS spectrum of $\text{Sc}\{\text{N}(\text{SiHMe}_2)\text{tBu}\}_n@MSN_{550}$, (B) DNP-CPMAS spectrum of $\text{Sc}\{\text{N}(\text{SiHMe}_2)\text{tBu}\}_n@MSN_{550}$, and (C) $^{29}\text{Si}\{^1\text{H}\}$ CPMAS spectrum of $\text{Sc}\{\text{N}(\text{SiHMe}_2)\text{tBu}\}_n@MSN_{700}$. The CPMAS spectra were obtained using a 400 MHz spectrometer, 3.2 mm rotor, 83 kHz (^1H CP) and 63 kHz (^{29}Si CP), 1 ms contact time, 1.3 s

recycle delay, 10000 scans, 83 kHz SPINAL-64 ^1H decoupling. DNP-CPMAS spectra were acquired with MAS=7.5 kHz, $B_1(^1\text{H}) = 75\text{kHz}$, $B_1(^{29}\text{Si}) = 60\text{kHz}$.

The $^{13}\text{C}\{^1\text{H}\}$ CPMAS spectrum of $\text{Sc}\{\text{N}(\text{SiHMe}_2)t\text{Bu}\}_n@\text{MSN}_{700}$ contained the expected signals assigned to SiMe_2 (0 ppm) and $t\text{Bu}$ (47.4 and 32.6 ppm). The relative intensity of SiMe_2 and $t\text{Bu}$ signals favors the latter signal in the spectrum of $\text{Sc}\{\text{N}(\text{SiHMe}_2)t\text{Bu}\}_n@\text{MSN}_{700}$, while the material grafted on MSN heated to 550 °C contained a more intense SiMe_2 signal. Support for these assignments was provided by a $^{13}\text{C}\{^1\text{H}\}$ idHetcor experiment.

Catalytic hydroamination/cyclization and bicyclization of aminodialkenes. The bicyclization of aminodialkenes requires C–N bond formation first from a primary amine and then from a secondary amine, and each step generates diastereomers (see eq. 3.1). This reaction provides a test to compare the relative reactivity and selectivity of homoleptic homogeneous compounds and their mesoporous silica-grafted analogues.

First, the intramolecular hydroamination of 2,2-diphenylpent-4-enyl-amine (**8a**) was examined to compare conditions for cyclization of primary aminoalkenes. With **1** or **2**·THF, quantitative conversion to 4,4-diphenyl-5-methylpyrrolidine (**8b**) is completed within 10 min. at ambient temperature. Although supported $\text{Ln}\{\text{N}(\text{SiHMe}_2)t\text{Bu}\}_n@\text{MSN}$ ($\text{Ln} = \text{Sc}, \text{Y}$) requires 2 h at 60 °C for quantitative conversion, 5 mol % of either homogeneous or heterogeneous catalyst gives the cyclized product in high isolated yield (84 - 88 %, Table 3.4, entries 1-6). Moreover, kinetic studies, in which NMR yields of pyrrolidine were determined every 30 min., revealed similar rates (per mole rare earth element) for all four combinations

of Sc and Y, on MSN₅₅₀ and MSN₇₀₀. We also noted a roughly linear relationship between time and yield, indicating zero-order rate dependence on substrate concentration.

Table 3.4. Catalytic hydroamination of aminoalkenes and aminodialkenes.^a

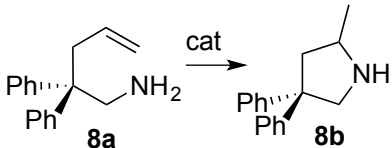
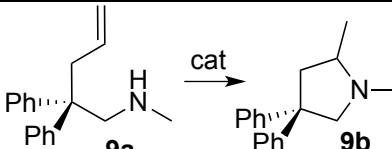
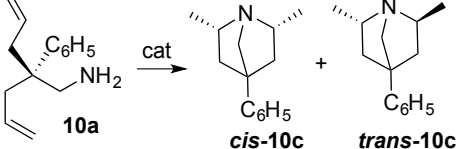
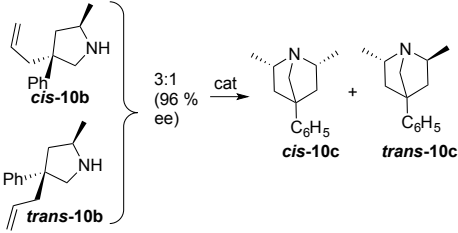
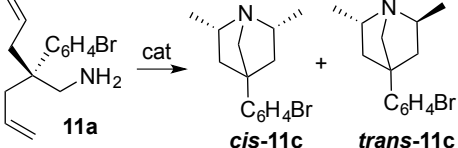
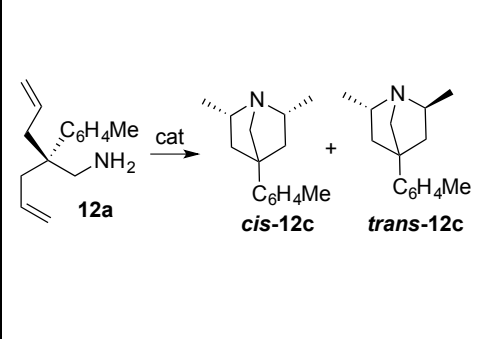
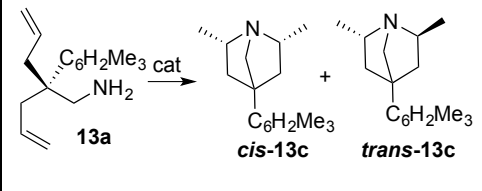
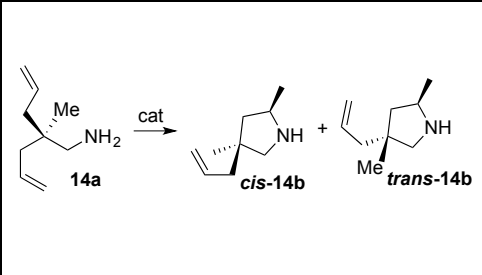
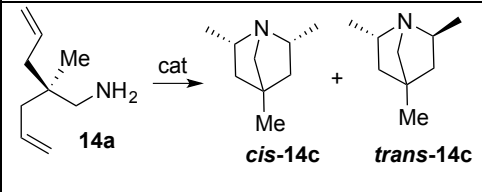
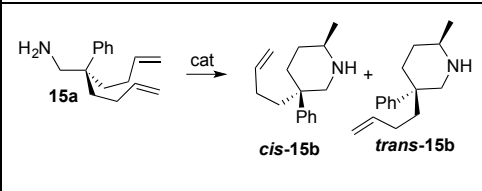
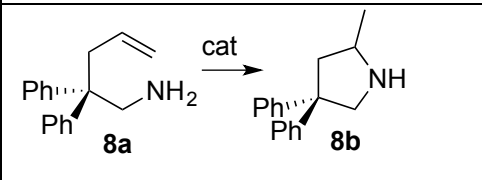
Reaction	Catalyst	Temp (°C)	Time (h)	Yield (%) ^b	dr ^c
	1	25	0.1	85	n.a
	2•THF	25	0.1	88	
	1@MSN ₅₅₀	60	2	84	
	2•THF@MSN ₅₅₀	60	2	84	
	1@MSN ₇₀₀	60	2	88	
	2•THF@MSN ₇₀₀	60	2	86	
	1	25	2	83	n.a
	2•THF	25	2	85	
	1@MSN ₅₅₀	60	12	85	
	2•THF@MSN ₅₅₀	60	12	84	
	2•THF@MSN ₅₅₀	60	12	84	
	1	25	2	88	2:1
	2•THF	25	2	92	2:1
	1@MSN ₅₅₀	60	12	92	2:1
	2•THF@MSN ₅₅₀	60	12	90	2:1
	2•THF@MSN ₅₅₀	60	12	90	2:1
	1	25	2	82	2:1
	2•THF	25	2	81	2:1
	1@MSN ₅₅₀	60	12	83	2:1
	2•THF@MSN ₅₅₀	60	12	83	2:1
	1	25	2	85	2:1
	2•THF	25	2	89	2:1
	1@MSN ₅₅₀	60	12	87	2:1
	2•THF@MSN ₅₅₀	60	12	87	2:1
	2•THF@MSN ₅₅₀	60	12	87	2:1

Table 3.4. Continued

 <p>12a</p> <p><i>cis</i>-12c</p> <p><i>trans</i>-12c</p>	<p>1</p> <p>2•THF</p> <p>1@MSN₅₅₀</p> <p>2•THF@MSN₅₅₀</p>	<p>25</p> <p>25</p> <p>60</p> <p>60</p>	<p>2</p> <p>2</p> <p>12</p> <p>12</p>	<p>83</p> <p>90</p> <p>89</p> <p>89</p>	<p>2.5:</p> <p>1</p> <p>2.5:</p> <p>1</p> <p>2.5:</p> <p>1</p> <p>2.5:</p> <p>1</p>
 <p>13a</p> <p><i>cis</i>-13c</p> <p><i>trans</i>-13c</p>	<p>1</p> <p>2•THF</p> <p>1@MSN₅₅₀</p> <p>2•THF@MSN₅₅₀</p>	<p>25</p> <p>25</p> <p>60</p> <p>60</p>	<p>2</p> <p>2</p> <p>12</p> <p>12</p>	<p>86</p> <p>89</p> <p>88</p> <p>89</p>	<p>7:1</p> <p>7:1</p> <p>7:1</p> <p>7:1</p>
 <p>14a</p> <p><i>cis</i>-14b</p> <p><i>trans</i>-14b</p>	<p>1</p> <p>2•THF</p> <p>1@MSN₅₅₀</p> <p>2•THF@MSN₅₅₀</p>	<p>25</p> <p>25</p> <p>60</p> <p>60</p>	<p>2</p> <p>2</p> <p>12</p> <p>12</p>	<p>81</p> <p>81</p> <p>88</p> <p>84</p>	<p>1:1.</p> <p>2</p> <p>1:1.</p> <p>21:</p> <p>1.2</p> <p>1:1.</p> <p>2</p>
 <p>14a</p> <p><i>cis</i>-14c</p> <p><i>trans</i>-14c</p>	<p>1</p> <p>2•THF</p> <p>1@MSN₅₅₀</p> <p>2•THF@MSN₅₅₀</p>	<p>60</p> <p>60</p> <p>80</p> <p>80</p>	<p>6</p> <p>6</p> <p>24</p> <p>24</p>	<p>81</p> <p>81</p> <p>88</p> <p>84</p>	<p>1:1</p> <p>1:1</p> <p>1:1</p> <p>1:1</p>
 <p>15a</p> <p><i>cis</i>-15b</p> <p><i>trans</i>-15b</p>	<p>1</p> <p>2•THF</p> <p>1@MSN₅₅₀</p> <p>2•THF@MSN₅₅₀</p>	<p>25</p> <p>25</p> <p>60</p> <p>60</p>	<p>2</p> <p>2</p> <p>12</p> <p>12</p>	<p>86</p> <p>88</p> <p>92</p> <p>90</p>	<p>3:1</p> <p>3:1</p> <p>3:1</p> <p>3:1</p>
 <p>8a</p> <p>8b</p>	<p>2•THF@MSN₇₀₀</p> <p>1st cycle</p> <p>2nd cycle</p> <p>3rd cycle</p>	<p>60</p> <p>60</p> <p>60</p> <p>60</p>	<p>2</p> <p>2</p> <p>2</p> <p>2</p>	<p>96^c</p> <p>94^c</p> <p>82^c</p> <p>70^c</p>	<p>n.a</p>

^aCatalytic conditions: 0.1 mmol of catalyst (5 mol % metal basis), 2.0 mmol of aminoalkene, 5 mL benzene. Only one enantiomer of the (racemic) product is illustrated in mixtures of diastereomers. ^bisolated yield, ^cdr = cis:trans.

Conversion of the soluble or supported rare earth silazido precatalyst into an active species involves protonolytic substitution of $\text{N}(\text{SiHMe}_2)t\text{Bu}$ by an aminoalkene reactant. Accordingly, $\text{HN}(\text{SiHMe}_2)t\text{Bu}$ was observed in the reaction mixtures and quantified. For example, 2.5 equiv. of $\text{HN}(\text{SiHMe}_2)t\text{Bu}$ was measured with respect to the $\text{Y}\{\text{N}(\text{SiHMe}_2)t\text{Bu}\}_3\text{THF}$ precatalyst after addition of **8a**, whereas 1.1 and 1.5 equiv. of $\text{HN}(\text{SiHMe}_2)t\text{Bu}$ were observed for the $\text{Y}\{\text{N}(\text{SiHMe}_2)t\text{Bu}\}_n@MSN_{550}$ and $\text{Y}\{\text{N}(\text{SiHMe}_2)t\text{Bu}\}_n@MSN_{700}$ materials, respectively. Note that the greater number of equiv. with yttrium supported on MSN_{700} vs. MSN_{550} is consistent with the former's formulation as primarily monopodal $\equiv\text{SiO}-\text{Y}\{\text{N}(\text{SiHMe}_2)t\text{Bu}\}_2$.

The second step of the bicyclization sequence requires a hydroamination of secondary amines, and this reaction was decoupled from the first hydroamination step using the secondary aminoalkene *N*-methyl-2,2-diphenylpent-4-enyl-amine (**9a**). The desired tertiary amine product forms in 2 h at room temperature using **1** or **2**·**THF** as catalysts or 12 h at 60 °C using the supported catalysts.

On the basis of the above primary and secondary aminoalkene cyclizations studies, the reactivity of supported and homogeneous catalysts for the mono- and bicyclization of a series of aminodialkenes was investigated. As shown in Table 3.4, reactions with aminodialkenes provide pyrrolizidines in good yields with both homogeneous and heterogeneous catalysts. As in the monocyclization of primary and secondary aminoalkenes, the supported catalysts require longer reaction times at higher temperatures than homogeneous analogues, and this follows the trend established with $\text{Y}\{\text{N}(\text{SiMe}_3)_2\}_3$ grafted on SBA-15.^{6c} Significantly, both scandium and yttrium catalysts as well as both interfacial

and solution-phase conditions provide the bicyclized product with equivalent diastereoselectivity.

For example, the substrate 2-allyl-2-phenylpent-4-en-1-amine (**10a**) is bicyclized to cis-**10c**:trans-**10c** (2:1) over 2 h either at room temperature with **1** or **2**·THF or over 12 h at 60 °C using the supported $\text{Ln}\{\text{N}(\text{SiHMe}_2)\text{tBu}\}_n\text{@MSN}$ (entry 11-14, Table 3.4). The ^1H NMR of the bicyclized product shows two isomers cis(exo,exo)²⁹ and trans(endo,exo) and the diastereomeric ratio is 2:1(cis:trans). The cis and trans pyrrolidine intermediates (cis and trans-**10b**) were observed in the catalytic mixtures prior to quantitative conversion to the **10c**. Unfortunately, the ^1H NMR signals for the intermediates and final products overlapped, so only the selectivity for the final product is reported. Note that the final product **10c** forms with the equivalent diastereomeric ratio, regardless of catalyst (Sc or Y), support vs. unsupported species, support pretreatment temperature and surface-bonded structure, and at least minor variation of the reaction conditions.

Despite this limitation, we investigated a possible relationship between the cis:trans ratio of pyrrolidine intermediate and the final product. Note that the 4C is a stereogenic center in 4-allyl-2-methyl-4-phenylpyrrolidine and trans-**10b**, but that carbon is located on a mirror plane in cis-**10b**. However, starting with 4-allyl-2-methyl-4-phenylpyrrolidine, prepared with a cis:trans ratio of 3.3:1 (% ee of both diastereomers is 96%) by zirconium-catalyzed monocyclization of 2-allyl-2-phenylpent-4-enylamine,⁹ **10c** is obtained with an equivalent cis:trans ratio (2:1) to that obtained directly from bicyclization of the amino dialkene. We conclude that the 4C stereogenic center does not affect the stereoselectivity of pyrrolizidine formation.

Interestingly, substitutions on the phenyl ring, such as 2-allyl-(4-bromophenyl)pent-4-en-1-amine (**11a**), 2-allyl-(p-tolyl)pent-4-en-1-amine (**12a**), and 2-allyl-2-mesitylpent-4-en-1-amine (**13a**) provide diastereoselectivities of 2:1, 2.5:1, and 7:1 respectively. More forcing conditions (**1** or **2**·THF, 60 °C; Ln@MSN, 80 °C) are needed to obtain the bicyclic product **14c** (cis:trans =1:1), whereas lower temperatures provide the pyrrolidine as a mixture of cis and trans isomers (1:1.2). In contrast, the dialkene **15a** is cyclized exclusively to 2-methyl-piperidine **15b** even after heating at 120 °C. Unlike the previously reported {PhB(Ox^{iPr,Me2})₂C₅H₄}Zr(NMe₂)₂ catalyzed cyclizations,⁹ in which the diastereoselectivity is dependent on the concentration of substrate, these scandium and yttrium-based catalysts provide the products with a cis:trans ratio that is independent of concentration of substrate varying from 43.5 mM to 348 mM while the catalyst concentration kept constant (8.7 mM).

The supported catalytic materials were recovered and reused three times for the hydroamination cyclization, although the product yield diminished after second and third cycles. One possible explanation for this behavior is catalyst leaching. Only trace quantities of yttrium were detected in the supernatant from ICP-OES analysis, and conversion stopped after the supported catalyst was separated (by filtration) from the substrate, product, silazane and solvent. We conclude that catalyst leaching is not responsible for the apparent deactivation.

Conclusion

Synthesis, characterization including spectroscopy and structural properties and reactivity of the complexes Ln{N(SiHMe₂)tBu}₃L_n have been presented in this work with their promising applications as catalysts and synthetic precursors. Ln{N(SiHMe₂)tBu}₃L_n was synthesized

from the reaction of three equiv. of $\text{Li}[\text{N}(\text{SiHMe}_2)\text{tBu}]$ and LnCl_3 , $\text{LnCl}_3\text{THF}_n$, or LnI_3THF_n in tetrahydrofuran and diethyl ether. The formation of rare earth amides was confirmed by various spectroscopic techniques including NMR, infrared spectroscopy and X-ray crystallography. The Si-H coupling constants of diamagnetic complexes vary depending on the rare earth elements and coordinating solvents, but are generally low compared to silylamine ligand and suggest that the formation of multinuclear bonds is between the Si-H unit of ligand and Ln metal center. In addition, Si-H bands in the infrared spectra of rare earth amides appeared at lower energy compared to silazane and lithium silazide. This indicates that the interaction is between Si-H and metal centers. Finally, X-ray crystallography confirms the Si-H interaction is with the metal center, with all three Si-H groups pointing towards the metal center.

The homoleptic rare earth silylamides can be transformed into heterogeneous equivalents by the reaction of $\text{Ln}\{\text{N}(\text{SiHMe}_2)\text{tBu}\}_3\text{L}_n$ and calcined mesoporous silica, providing $\text{Ln}\{\text{N}(\text{SiHMe}_2)\text{tBu}\}_n@\text{MSN}$. The surface species formed in the reactions were characterized by multinuclear NMR and infrared spectroscopy. Infrared spectroscopy, solid state NMR and elemental analysis allowed the assignment of $\text{Ln}\{\text{N}(\text{SiHMe}_2)\text{tBu}\}_n@\text{MSN}$ and $\equiv\text{SiOSiHMe}_2$ as the dominant products on the silica surface. Thermal treatment of silica supports has a significant effect on the distribution of surface silanol groups and the formation of mono and/or bi-podal surface complexes. The use of silica pretreated under vacuum at 550 °C results in the formation of mono and bi-podal complexes on the surface. On the other hand, the use of silica pretreated at 700 °C results in the formation of only mono-podal surface complexes. This approach can be used for the effective synthesis of

heterogeneous mono-podal derivatives containing Y, Sc, and Ln metals, which are catalytically active.

We examined the catalytic activity of soluble and supported precatalysts in intramolecular hydramination/cyclization of aminoalkenes and bicyclization of aminodialkenes. The formation of $\text{HN}(\text{SiHMe}_2)t\text{Bu}$ was observed in the hydroamination catalysis by protonolytic substitution, leading to the generation of active species. The soluble and supported amides proved to be catalytically active in intramolecular hydroamination of aminoalkenes and aminodialkenes. Compared to the homogenous equivalents of rare earth amides $\text{Ln}\{\text{N}(\text{SiHMe}_2)t\text{Bu}\}_3\text{L}$, the heterogeneous equivalents $\text{Ln}\{\text{N}(\text{SiHMe}_2)t\text{Bu}\}_n@\text{MSN}$ display slower activity and require more vigorous conditions. Because grafting on the mesoporous silica supports leads to the formation of a single type of grafted species, which can lead to the development of more active catalysts. We are currently investigating the reactivity of the heterogeneous rare earth amide with hydride sources to access surface supported hydrides for new applications in catalysis.

Experimental

General. All reactions were performed under a dry argon atmosphere using standard Schlenk techniques or under a nitrogen atmosphere in a glovebox, unless otherwise indicated. Dry, oxygen-free solvents were used throughout. Benzene, toluene, pentane, methylene chloride, diethyl ether and tetrahydrofuran were degassed by sparging with nitrogen, filtered through activated alumina columns, and stored under nitrogen. Benzene-*d*₆, toluene-*d*₈ and tetrahydrofuran-*d*₈ were heated to reflux over Na/K alloy, vacuum-transferred, and stored over 4 Å molecular sieves in the glovebox prior to use. Anhydrous YCl₃ was purchased from Strem and used as received. ScCl₃(THF)₃,³⁰ LuCl₃(THF)₃,³¹ LaI₃(THF)₃, CeI₃(THF)₃, NdI₃(THF)₃, PrI₃(THF)₃,³² and LiN(SiHMe₂)*t*Bu,³³ were prepared according to literature procedures. ¹H, ¹³C{¹H}, and ²⁹Si{¹H} NMR spectra were collected on a Bruker Avance III 600 spectrometer. ¹⁵N chemical shifts were determined by ¹H-¹⁵N HMBC experiments on a Bruker Avance III 600 spectrometer. ¹⁵N chemical shifts were originally referenced to liquid NH₃ and recalculated to the CH₃NO₂ chemical shift scale by adding -381.9 ppm.

The support, in the form of SBA-15 type MSN characterized by a hexagonal array (*p6mm*) of 9.7 nm diameter pores, was produced by hydrolysis-condensation of tetramethylorthosilicate using the Pluronic P104 template, calcined under vacuum at 550 °C or 700 °C, and subsequently isolated from ambient air and moisture. The material is composed of particles with 385 m²/g surface area. This SiOH group surface concentration of 1.5 mmol/g was determined by measuring the concentration of toluene produced in a titration with Mg(CH₂Ph)₂(O₂C₄H₈)₂ and by quantitative spin counting of Q3-sites using ²⁹Si DP-MAS NMR spectroscopy (1.6 mmol/g).

Sc{N(SiHMe₂)tBu}₃ (1). A solution of LiN(SiHMe₂)tBu (0.422 g, 3.07 mmol, THF) was added to ScCl₃THF₃ (0.371 g, 1.01 mmol) suspended in THF and cooled to -78 °C. The reaction mixture was allowed to stir at -78 °C for 1 h and was then warmed to room temperature and stirring was continued for 12 h. The volatile materials were evaporated under reduced pressure. The residue was extracted with pentane (3 × 5 mL), and the combined extracts were evaporated to afford **1** (0.363 g, 0.833 mmol, 82%) as an analytically pure sticky solid. Recrystallization of Sc{N(SiHMe₂)tBu}₃ at -80 °C from a concentrated pentane solution provided single crystals suitable for X-ray diffraction. ¹H NMR (benzene-*d*₆, 600 MHz): δ 4.19 (br, ¹J_{SiH} = 124.8 Hz, 3 H, SiH), 1.40 (s, 27 H, CMe₃), 0.38 (br, 18 H, SiHMe₂). ¹³C{¹H} NMR (benzene-*d*₆, 151 MHz): δ 55.69 (CMe₃), 36.68 (CMe₃), 3.76 (SiHMe₂). ¹⁵N NMR (benzene-*d*₆, 59.2 MHz): -208.9. ²⁹Si NMR (benzene-*d*₆, 119.2 MHz): δ -22.9. IR (KBr, cm⁻¹): 2963 (s), 2902 (s), 2863 (m), 1893 (s, SiH), 1721 (w), 1463 (s), 1384 (m), 1384 (m), 1357 (s), 1248 (m), 1202 (s), 1048 (s), 1022 (m), 905 (s), 844 (s), 789 (s, br). Anal. Calcd. for C₁₈H₄₈N₃Si₃Sc: C, 49.61; H, 11.10; N, 9.64. Found: C, 49.72; H, 10.66; N, 8.95.

Y{N(SiHMe₂)tBu}₃Et₂O (2·Et₂O). LiN(SiHMe₂)tBu (0.422 g, 3.07 mmol), dissolved in Et₂O, was added to a Et₂O suspension of YCl₃ (0.200 g, 1.02 mmol) cooled to -78 °C. The reaction mixture was allowed to stir at -78 °C for 1 h, and then the solution was warmed to room temperature and stirred for 12 h. The volatile materials were evaporated under reduced pressure. The solid was extracted with pentane (3 × 5 mL). Evaporation of the pentane extracts produced a sticky solid of analytically pure Y{N(SiHMe₂)tBu}₃Et₂O (**2·Et₂O**, 0.523 g, 0.944 mmol, 93%). Y{N(SiHMe₂)tBu}₃Et₂O was recrystallized at -80 °C from a concentrated pentane solution to provide single crystals suitable for X-ray diffraction. ¹H

NMR (benzene-*d*₆, 600 MHz): δ 4.30 (br, $^1J_{\text{SiH}} = 126$ Hz, 3 H, SiH), 3.31 (q, $^3J_{\text{HH}} = 7.2$ Hz, 4 H, OCH₂CH₃), 1.39 (s, 27 H, CMe₃), 1.07 (t, $^3J_{\text{HH}} = 7.3$ Hz, 18 H, OCH₂CH₃) 0.39 (br, 6 H, SiHMe₂). $^{13}\text{C}\{^1\text{H}\}$ NMR (benzene-*d*₆, 151 MHz): δ 66.23 (OCH₂CH₃), 54.85 (CMe₃), 36.92 (CMe₃), 15.59 (OCH₂CH₃), 4.24 (SiHMe₂). ^{15}N NMR (benzene-*d*₆, 59.2 MHz): δ -221.9. ^{29}Si NMR (benzene-*d*₆, 119.2 MHz): δ -25.9. IR (KBr, cm⁻¹): 2959 (s), 2901 (s), 2860 (m), 2116 (w, SiH), 1865 (s, SiH), 1720 (w), 1463 (s), 1382 (m), 1356 (s), 1247 (s), 1210 (s, br), 1057 (s), 1022 (m), 865 (s), 844 (s), 785 (s, br). Anal. Calcd. for C₂₂H₅₈N₃OSi₃Y: C, 47.71; H, 10.56; N, 7.59. Found: C, 47.04; H, 9.87; N, 8.00.

Y{N(SiHMe₂)*t*Bu}₃THF (2·THF). A THF solution of LiN(SiHMe₂)*t*Bu (0.422 g, 3.07 mmol) was added to a THF suspension of YCl₃ (0.200 g, 1.01 mmol) cooled to -78 °C. The solution was allowed to stir at -78 °C for 1 h and then was warmed to room temperature and stirred for 12 h. Evaporation of the reaction mixture left a solid residue, which was extracted with pentane (3 × 5 mL). Evaporation of the pentane extracts under reduced pressure provided a pure sticky solid of Y{N(SiHMe₂)*t*Bu}₃THF (0.511 g, 0.926 mmol, 92%). Y{N(SiHMe₂)*t*Bu}₃THF was recrystallized at -30 °C from a concentrated pentane solution to provide single crystals suitable for X-ray diffraction. ^1H NMR (benzene-*d*₆, 600 MHz): δ 4.59 (br, $^1J_{\text{SiH}} = 142.9$ Hz, 3 H, SiH), 3.73 (t, $^3J_{\text{HH}} = 6.3$ Hz, 4 H, OCH₂CH₂), 1.48 (s, 27 H, CMe₃), 1.26 (t, $^3J_{\text{HH}} = 6.3$ Hz, 4 H, OCH₂CH₂) 0.46 (d, $^3J_{\text{HH}} = 3.0$ Hz, 18 H, SiHMe₂). $^{13}\text{C}\{^1\text{H}\}$ NMR (benzene-*d*₆, 151 MHz): δ 71.27 (OCH₂CH₂), 54.92 (CMe₃), 37.19 (CMe₃), 25.60 (OCH₂CH₂), 4.72 (SiHMe₂). ^{15}N NMR (benzene-*d*₆, 59.2 MHz): δ -231.0. ^{29}Si NMR (benzene-*d*₆, 119.2 MHz): δ -30.5. IR (KBr, cm⁻¹): 2960 (s), 2898 (s), 2861 (m), 2019 (s, SiH), 1967 (s, SiH), 1762 (w), 1464 (s), 1381 (m), 1355 (s), 1244 (s), 1199 (s, br), 1058 (s),

884 (s), 839 (s), 782 (s, br). Anal. Calcd. for $C_{22}H_{56}N_3OSi_3Y$: C, 47.88; H, 10.23; N, 7.61. Found: C, 47.27; H, 9.68; N, 7.32.

Lu{N(SiHMe₂)tBu}₃THF (3·THF). A THF solution of LiN(SiHMe₂)tBu (0.422 g, 3.07 mmol) was added to a suspension of LuCl₃THF₃ (0.503 g, 1.01 mmol) that was cooled to -78 °C. The solution was allowed to stir at that temperature for 1 h and then was warmed to room temperature and stirred for 12 h. The volatile materials were removed in vacuo, the residue was extracted with pentane (3 × 5 mL), and the extracts were combined and evaporated to dryness to provide Lu{N(SiHMe₂)tBu}₃THF (0.596 g, 0.934 mmol, 92%) as a sticky, yet analytically pure solid. Lu{N(SiHMe₂)tBu}₃THF was recrystallized at -30 °C from a concentrated pentane solution to provide single crystals suitable for X-ray diffraction. ¹H NMR (benzene-*d*₆, 600 MHz): δ 4.63 (sept, ³J_{HH} = 3.0 Hz, ¹J_{SiH} = 137.4 Hz, 3 H, SiH), 3.82 (br, 4 H, OCH₂CH₂), 1.47 (s, 27 H, CMe₃), 1.29 (br, 4 H, OCH₂CH₂) 0.49 (d, ³J_{HH} = 3.1 Hz, 18 H, SiHMe₂). ¹³C{¹H} NMR (benzene-*d*₆, 151 MHz): δ 71.91 (OCH₂CH₂), 55.11 (CMe₃), 37.29 (CMe₃), 25.71 (OCH₂CH₂), 4.58 (SiHMe₂). ¹⁵N NMR (benzene-*d*₆, 59.2 MHz): δ -231.5. ²⁹Si NMR (benzene-*d*₆, 119.2 MHz): δ -28.7. IR (KBr, cm⁻¹): 2961 (s), 2899 (s), 2862 (s), 1989 (s, SiH), 1751 (w), 1464 (s), 1382 (m), 1355 (s), 1245 (s), 1199 (s, br), 1036 (s), 868 (s), 842 (s), 785 (s, br). Anal. Calcd. for $C_{22}H_{56}N_3OSi_3Lu$: C, 41.42; H, 8.85; N, 6.59. Found: C, 41.62; H, 8.43; N, 6.88.

La{N(SiHMe₂)tBu}₃THF (4·THF). A THF solution of LiN(SiHMe₂)tBu (0.422 g, 3.07 mmol) was added to a suspension of LaI₃THF₄ (0.816 g, 1.01 mmol, THF) at -78 °C. The mixture was allowed to stir at that temperature for 1 h. The reaction vessel was warmed to room temperature, and the reaction mixture was allowed to stir for 12 h. The volatile components were removed under vacuum, the solid residue was extracted with pentane (3 ×

5 mL), and $\text{La}\{\text{N}(\text{SiHMe}_2)t\text{Bu}\}_3\text{THF}$ (0.568 g, 0.943 mmol, 93%) was isolated as a sticky solid upon evaporation of the pentane. ^1H NMR (benzene- d_6 , 600 MHz): δ 4.66 (br, $^1J_{\text{SiH}} = 145.6$ Hz, 3 H, SiH), 3.60 (t, $^3J_{\text{HH}} = 6.1$ Hz, 4 H, THF), 1.51 (s, 27 H, CMe_3), 1.22 (t, $^3J_{\text{HH}} = 6.1$ Hz, 4 H, THF) 0.46 (d, $^3J_{\text{HH}} = 3.2$ Hz, 18 H, SiHMe_2). $^{13}\text{C}\{^1\text{H}\}$ NMR (benzene- d_6 , 151 MHz): δ 70.35 (THF), 55.12 (CMe_3), 36.77 (CMe_3), 25.57 (OCH_2CH_2), 3.89 (br, SiHMe_2). ^{15}N NMR (benzene- d_6 , 59.2 MHz): δ -195.6. ^{29}Si NMR (benzene- d_6 , 119.2 MHz): δ -33.7. IR (KBr, cm^{-1}): 2968 (s), 2898 (s), 2859 (m), 2003 (s, SiH), 1941 (s, SiH), 1744 (w), 1464 (s), 1380 (m), 1354 (s), 1243 (s), 1208 (s, br), 1063 (s), 1027 (m), 872 (s), 837 (s), 779 (s, br). Anal. Calcd. for $\text{C}_{22}\text{H}_{56}\text{LaN}_3\text{OSi}_3$: C, 43.90; H, 9.38; N, 6.98. Found: C, 44.21; H, 9.65; N, 6.82.

$\text{Ce}\{\text{N}(\text{SiHMe}_2)t\text{Bu}\}_3\text{THF}$ (5·THF). A THF solution of $\text{LiN}(\text{SiHMe}_2)t\text{Bu}$ (0.102 g, 0.743 mmol) was added to CeI_3THF_4 (0.200 g, 0.247 mmol) suspended in THF cooled to -78 °C. The reaction mixture was allowed to stir at -78 °C for 1 h and was then warmed to room temperature and stirred for 12 h. The reaction mixture was evaporated to dryness. The residue was extracted with pentane (3×5 mL), and evaporation of the pentane provided a sticky solid of analytically pure $\text{Ce}\{\text{N}(\text{SiHMe}_2)t\text{Bu}\}_3\text{THF}$ (0.129 g, 0.214 mmol, 86%). ^1H NMR (benzene- d_6 , 600 MHz): δ 12.18 (br), 5.61, 3.74, 2.02 (br), 0.86. IR (KBr, cm^{-1}): 2958 (s), 2899 (s), 2859 (m), 2112 (w), 2004 (s, SiH), 1738 (w), 1463 (s), 1380 (m), 1355 (s), 1243 (s), 1212 (s, br), 1051 (m), 1027 (s), 873 (s), 837 (s), 780 (s). UV-Vis: λ_{max} , 394 nm (ϵ 483.18 $\text{L}\times\text{mol}^{-1}\text{cm}^{-1}$). Anal. Calcd. for $\text{C}_{22}\text{CeH}_{56}\text{N}_3\text{OSi}_3$: C, 43.82; H, 9.36; N, 6.97. Found: C, 43.62; H, 8.95; N, 7.36.

$\text{Pr}\{\text{N}(\text{SiHMe}_2)t\text{Bu}\}_3\text{THF}$ (6·THF). A THF solution of $\text{LiN}(\text{SiHMe}_2)t\text{Bu}$ (0.279 g, 2.03 mmol) was added to PrI_3THF_3 (0.501 g, 0.679 mmol) cooled to -78 °C. The temperature was

maintained for 1 h at $-78\text{ }^{\circ}\text{C}$, the reaction vessel was then warmed to room temperature, and the reaction mixture was stirred for 15 h. THF was removed under reduced pressure, and the residue was extracted with pentane ($3 \times 5\text{ mL}$). The pentane extracts were combined and evaporated to yield $\text{Pr}\{\text{N}(\text{SiHMe}_2)\text{tBu}\}_3\text{THF}$ (0.327 g, 0.541 mmol, 80%). ^1H NMR (benzene- d_6 , 600 MHz, $25\text{ }^{\circ}\text{C}$): δ 29.3, 24.7, 8.28, 1.43, 1.22, 0.39, 0.31, 0.14, -1.20 (s), -5.00 (br, s), -33.5 (s). IR (KBr, cm^{-1}): 2964, 2897 (s), 2119 (s, SiH), 2011 (br), 1464, 1377, 1355, 1243, 1203 (s), 1050, 1026, 974 (br), 914, 885, 837, 779, 751, 693, 634, 512, 490, (s), 418 (br). UV-Vis: λ_{max} , 442 nm (ϵ 64.66 $\text{L}\times\text{mol}^{-1}\text{cm}^{-1}$). Anal. Calcd. for $\text{C}_{22}\text{H}_{56}\text{N}_3\text{PrOSi}_3$: C, 43.72; H, 9.35; N, 6.96. Found: C, 43.86; H, 9.28; N, 6.88.

$\text{Nd}\{\text{N}(\text{SiHMe}_2)\text{tBu}\}_3\text{THF}$ (7·THF). A THF solution of $\text{LiN}(\text{SiHMe}_2)\text{tBu}$ (0.201 g, 1.47 mmol) and solid NdI_3THF_3 (0.363 g, 0.489 mmol) were separately cooled to $-78\text{ }^{\circ}\text{C}$. The reactants were mixed and allowed to stir at $-78\text{ }^{\circ}\text{C}$ for one h, and then the reaction mixture was warmed to room temperature and stirred for 15 h. The solvent was evaporated, and the residue was extracted with pentane ($3 \times 5\text{ mL}$). The pentane extracts were evaporated to dryness to obtain $\text{Nd}\{\text{N}(\text{SiHMe}_2)\text{tBu}\}_3\text{THF}$ (0.201g, 0.332 mmol, 82%). ^1H NMR (benzene- d_6 , 600 MHz, $25\text{ }^{\circ}\text{C}$): δ 6.81, 5.30, 3.68 (br s), 1.46 (s), 1.38, 1.12 (s), 0.43 (br, s). IR (KBr, cm^{-1}): 2965, 2898 (s), 2131 (s, SiH), 2010, 1934 (br), 1462, 1376, 1356, 1245, 1201 (s), 1051, 1026, 972 (br), 913, 886, 838, 780, 751, 695, 635, 490, 457, 419, (s). UV-Vis: ϵ 103.04 $\text{Lmol}^{-1}\text{cm}^{-1}$ (λ_{max} 593.0 nm). Anal. Calcd. for $\text{C}_{22}\text{H}_{56}\text{N}_3\text{NdOSi}_3$: C, 43.52; H, 9.30; N, 6.92. Found: C, 43.35; H, 9.51; N, 6.82

$\text{Sc}\{\text{N}(\text{SiHMe}_2)\text{tBu}\}_n@ \text{MSN}_{550}$. A pentane solution of $\text{Sc}\{\text{N}(\text{SiHMe}_2)\text{tBu}\}_3$ (0.140 g, 0.321 mmol, 5 mL) was added to MSN_{550} (0.200 g, 0.30 mmol of $-\text{OH}$ groups) suspended in pentane (5 mL). The suspension was stirred for 20 h at room temperature, the solid was

allowed to settle in a centrifuge, and the supernatant was decanted. Unreacted, physisorbed $\text{Sc}\{\text{N}(\text{SiHMe}_2)t\text{Bu}\}_3$ was removed from the solid material by washing with pentane (3×5 mL). The solid material was dried under vacuum yielding a white solid (0.234 g). IR (DRIFT): 2964 (m) 2907 (m) 2869 (w), 2149 (s), 1946 (br m), 1867 (br m), 1572 (m), 1470 (m), 1084 (s, $\nu_{\text{Si-O}}$), 950 (m). Elemental analysis: Found: C, 7.34; H, 1.34; N, 1.05; Sc(ICP-OES), 2.5 wt % (0.556 mmol/g).

$\text{Sc}\{\text{N}(\text{SiHMe}_2)t\text{Bu}\}_n@MSN_{550}$. A pentane solution of $\text{Sc}\{\text{N}(\text{SiHMe}_2)t\text{Bu}\}_3$ (0.110 g, 0.252 mmol, 5 mL) was added to MSN_{700} (0.20 g, 0.18 mmol of $-\text{OH}$ groups) suspended in pentane (5 mL). The suspension was stirred for 20 h at ambient temperature, the solid was allowed to settle in a centrifuge, and the supernatant was decanted. Unreacted, physisorbed $\text{Sc}\{\text{N}(\text{SiHMe}_2)t\text{Bu}\}_3$ was removed from the solid material by washing with pentane (3×5 mL). The solid material was dried under vacuum yielding a white solid (0.219 g). IR (DRIFT): 2963 (m) 2907 (m) 2872 (w), 2151 (s), 1951 (br m), 1867 (br m), 1574 (m), 1467 (m), 1084 (s, $\nu_{\text{Si-O}}$), 950 (m). Elemental analysis: Found: C, 5.19; H, 1.13; N, 0.89; Sc(ICP-OES), 1.5 wt % (0.334 mmol/g).

$\text{Y}\{\text{N}(\text{SiHMe}_2)t\text{Bu}\}_n@MSN_{550}$. A pentane solution of $\text{Y}\{\text{N}(\text{SiHMe}_2)t\text{Bu}\}_3\text{THF}$ (0.180 g, 0.326 mmol, 5 mL) was added to MSN_{550} (0.200 g, 0.30 mmol of $-\text{OH}$ groups) suspended in pentane (5 mL). The suspension was stirred for 20 h at ambient temperature, the solid was allowed to settle in a centrifuge, and the supernatant was decanted. Unreacted, physisorbed $\text{Y}\{\text{N}(\text{SiHMe}_2)t\text{Bu}\}_3\text{THF}$ was removed from the solid material by washing with pentane (3×5 mL). The solid material was dried under vacuum yielding a white solid (0.241 g). IR

(DRIFT): 2962 (m) 2904 (m) 2874 (w), 2149 (s), 2016 (m), 1924 (m), 1591 (m), 1466 (m), 1084 (s, $\nu_{\text{Si-O}}$), 950 (m). Elemental analysis: Found: C, 7.67; H, 1.60; N, 1.21; Y(ICP-OES), 4.2 wt % (0.467 mmol/g).

Y{N(SiHMe₂)tBu}₃THF@MSN₇₀₀. A pentane solution of Y{N(SiHMe₂)tBu}₃THF (0.140 g, 0.253 mmol, 5 mL) was added to MSN₇₀₀ (0.200 g, 0.18 mmol of –OH groups) suspended in pentane (5 mL). The suspension was stirred for 20 h at ambient temperature, the solid was allowed to settle in a centrifuge, and the supernatant was decanted. Unreacted, physisorbed Y{N(SiHMe₂)tBu}₃THF was removed from the solid material by washing with pentane (3 × 5 mL). The solid material was dried under vacuum yielding a white solid (0.220 g). IR (KBr, cm^{-1}): 2964 (m) 2907 (m) 2869 (w), 2149 (s), 1946 (m), 1867 (m), 1589 (m), 1465 (m), 1084 (s, $\nu_{\text{Si-O}}$), 950 (m). Elemental analysis: Found: C, 4.12; H, 0.97; N, 0.75; Y(ICP-OES), 2.3 wt % (0.259 mmol/g).

Me₂HSi@MSN₅₅₀. A pentane solution of HN(SiHMe₂)tBu (0.040 g, 0.304 mmol, 5 mL) was added to MSN₅₅₀ (0.200 g, 0.30 mmol of –OH groups) suspended in pentane (5 mL). The suspension was stirred for 20 h at ambient temperature, and then the mixture was centrifuged, and the solvent was decanted. The unreacted HN(SiHMe₂)tBu was removed from the solid material by washing with pentane (3 × 5 mL). The solid material was dried under vacuum yielding a white solid (0.215 g). IR (DRIFT):^{4a,24} 2966 (m) 2908 (w), 2152 (s), 1868 (m), 1634 (m), 1423 (m), 1084 (s, $\nu_{\text{Si-O}}$), 950 (m).

General procedure for hydroamination/cyclization (homogeneous).

A Schlenk flask was charged with the catalyst (0.100 mmol), the appropriate aminoalkene (2.00 mmol), and benzene (5 mL). The solution was stirred for 3 h at room temperature. The products were isolated by removing the solvent and followed by purified using flash column chromatography (silica gel, EtOAc:Et₃N = 100:1).

General procedure for hydroamination/cyclization (surface supported).

A Schlenk flask was charged with the catalyst (0.100 mmol), the appropriate aminoalkene (2.00 mmol), and benzene (5 mL). The solution was stirred for 12 h at 60 °C. The reaction mixture was filtered and the products were isolated by removing the solvent and followed by purified using flash column chromatography (silica gel, EtOAc:Et₃N = 100:1).

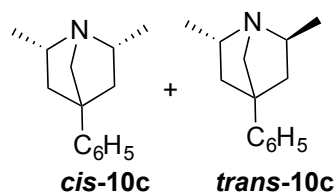
2-Allyl-2-(*p*-tolyl)pent-4-en-1-amine. A flame-dried Schlenk flask was charged with diisopropylamine (7.36 mL, 52.51 mmol) and 50 mL of THF. The flask was cooled to -78 °C and *n*BuLi (21.02 mL, 52.51 mmol, 2.5 M solution in hexanes) was added in a dropwise fashion. The resulting solution was stirred for 60 min at 0 °C. 40 mL of this solution of lithium diisopropylamide (LDA) was transferred to a dropping funnel, fitted with a dried 3-neck flask with a water condenser containing *p*-tolylacetonitrile (3.35 gm, 25.50 mmol) in THF (60 mL). The flask was cooled to -78 °C and the LDA solution was added dropwise over 20 minutes. The resultant deep yellow solution was stirred for 90 min at this temperature and was then treated with allyl bromide (2.16 mL, 24.99 mmol) dropwise and the solution became dark orange. The solution was stirred for another 15 min at -78 °C and was then allowed to warm to room temperature. After stirring for 90 minutes at rt, the solution was cooled back to -78 °C, and the second part of LDA was added over 20 min. The

solution was allowed to warm to 0 °C and was stirred for 1 h and the solution became dark green. After cooling back to -78 °C, the solution was treated with allyl bromide (2.65 mL, 30.6 mmol). The resultant deep orange reaction mixture was allowed to warm slowly to room temperature and stirred overnight. The reaction was quenched by addition of water (10 mL), and the solvent was removed in vacuo. The residue was taken up with Et₂O (200 mL), washed with water (2 × 50 mL) and brine (1 × 50 mL), and dried over Na₂SO₄. Concentration in vacuo gave a yellow oil, which was sufficiently pure for the next step and was used without any purification.

An oven-dried two-neck Schlenk flask fitted with a reflux condenser was charged with LiAlH₄ (0.500 g, 13.2 mmol). The flask was cooled to 0 °C and diethyl ether (100 mL) was added. Dropwise addition of 2-Allyl-2-(*p*-tolyl)pent-4-enenitrile (0.920 g, 4.35 mmol) to the LiAlH₄ suspension at 0 °C gave a mixture that was stirred overnight at room temperature. Then, the solution was cooled to 0 °C and 2 mL of dionized water was slowly added. This mixture was stirred 1 h at room temperature. The ether solution was decanted, and the white precipitation was extracted with diethyl ether (3 × 50 mL). All the organic solutions were combined, dried with Na₂SO₄ and filtered. The solvent was removed under vacuo to give crude 2-Allyl-2-(*p*-tolyl)pent-4-enenitrile. Vacuum distillation (110 °C, 0.01 mm Hg) of the crude product afforded the pure 2-allyl-2-(*p*-tolyl)pent-4-en-1-amine as a colorless oil (0.810 g, 3.76 mmol, 86%), which was stored in glovebox with activated molecular sieves. ¹H NMR (benzene-*d*₆, 600 MHz): δ 7.09 (d, ³J_{H-H} = 7.7 Hz, 2 H, ortho-C₆H₄), 7.02 (d, ³J_{H-H} = 7.8 Hz, 2 H, meta-C₆H₄), 5.63-5.76 (dq, ³J_{H-H} = 16.7 Hz, 7.9 Hz, 2 H, CH=CH₂), 5.04-5.00 (dd, ³J_{H-H} = 34.3 Hz, 13.7 Hz, 4 H, CH=CH₂), 2.77 (s, 2 H, NH₂CH₂), 2.42 (m, 4 H, =CHCH₂), 2.16 (s, 3 H, C₆H₄Me), 0.43 (br s, 2 H, NH₂). ¹³C {¹H} NMR

(benzene-*d*₆, 151 MHz): δ 142.47 (*C*₆H₄Me), 138.68 (*C*₆H₄Me), 135.60 (CH=CH₂), 129.63 (*C*₆H₄Me), 127.51 (*C*₆H₄Me), 117.65 (CH=CH₂), 49.27 (CH₂NH₂), 45.79 (*C*(*C*₆H₄Me)), 40.48 (=CHCH₂), 21.25 (*C*₆H₄Me). IR (KBr, cm⁻¹): 3391 (m), 3324 (w), 3074 (s), 3005 (m), 2977 (s), 2922 (s), 2862 (s), 1899 (w), 1638 (s), 1612 (m), 1515 (m), 1444 (s), 1415 (m), 1330 (w), 1296 (w), 1259 (w), 1195 (m), 1118 (w), 1068 (s), 998 (s), 913 (s), 864 (s), 814 (w), 768 (s), 703 (w), 670 (w). MS (ESI) exact mass calcd for C₁₅H₂₁N: *m/z* 216.1747 ([M⁺+H⁺]), Found: 216.1751 (Δ 0.5 ppm).

2,6-dimethyl-4-phenyl-1-azabicyclo[2,2,1]heptane. (cis:trans = 2:1).

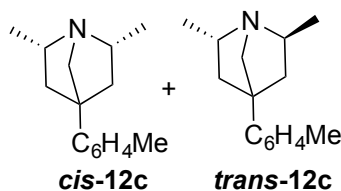


Isolated yield: 88 - 90 %

¹H and ¹³C NMR data identical to the previously reported.¹⁰

¹⁵N NMR (benzene-*d*₆, 61 MHz): δ -293.9 ppm.

4-(4-bromophenyl)-2,6-dimethyl-1-azabicyclo[2.2.1]heptane. (cis:trans = 2:1)

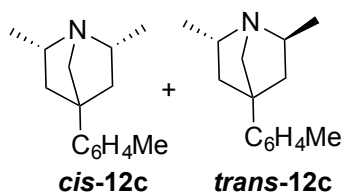


Isolated yield: 85 - 89 %.

¹H NMR (benzene-*d*₆, 600MHz): δ 7.30 (m, 6 H, C₆H₄Br, *cis*+*trans*), 6.74 (m, 6 H, C₆H₄Br, *cis*-*trans*), 3.13 (m, 1 H, *trans*), 3.04 (m, 1 H, *trans*), 2.66 (d, ³*J*_{H-H} = 9.9 Hz, 1 H, *trans*), 2.61

(m, 4 H *cis*), 2.41 (s, 4 H, *cis*), 2.37 (m, $^3J_{\text{H-H}} = 9.4$ Hz, 1 H, *trans*), 1.60 (t, $^3J_{\text{H-H}} = 10.7$ Hz, 1 H, *trans*), 1.42 (t, $^3J_{\text{H-H}} = 10.2$ Hz, 4 H, *cis*), 1.35 (m, 1 H, *trans*), 1.08 (m, 20 H, *cis*), 1.01 (m, 4 H, *cis*), 0.62 (m, 1 H, *trans*). $^{13}\text{C}\{^1\text{H}\}$ NMR (benzene- d_6 , 151 MHz): δ 143.18 ($\text{C}_6\text{H}_4\text{Br}$), 142.64 ($\text{C}_6\text{H}_4\text{Br}$), 131.90 ($\text{C}_6\text{H}_4\text{Br}$), 129.38 ($\text{C}_6\text{H}_4\text{Br}$), 129.35 ($\text{C}_6\text{H}_4\text{Br}$), 129.22 ($\text{C}_6\text{H}_4\text{Br}$), 120.42 ($\text{C}_6\text{H}_4\text{Br}$), 62.96 (NCH), 62.16 (NCH), 60.23 (NCH), 56.56 (PhCCH₂), 56.31 (NCH₂), 55.14 (PhCCH₂), 51.58 (NCH₂), 48.16 (PhCCH₂), 46.23 (PhCCH₂), 45.22 (PhCCH₂), 23.46 (NCHCH₃), 23.36 (NCHCH₃), 17.94 (NCHCH₃). ^{15}N NMR (benzene- d_6 , 61 MHz): δ -293.7 ppm. IR (KBr, cm^{-1}): 3077 (s), 3029 (m), 2965 (s), 2926 (s), 2866 (s), 1639 (s), 1491 (s), 1458 (m), 1395 (m), 1374 (m), 1333 (w), 1298 (w), 1238 (w), 1164 (m), 1110 (w), 1075 (s), 1048 (s), 1010 (m), 971 (s), 910 (s), 860 (s), 816 (w), 793 (s), 714 (w), 698 (w). MS (ESI) exact mass calcd for $\text{C}_{14}\text{H}_{18}\text{BrN}$: m/z 280.0695 ($[\text{M}^+ + \text{H}^+]$), Found: 280.0702 (Δ 0.5 ppm).

2,6-dimethyl-4-(*p*-tolyl)-1-azabicyclo[2.2.1]heptane. (*cis*:*trans* = 2.5:1)

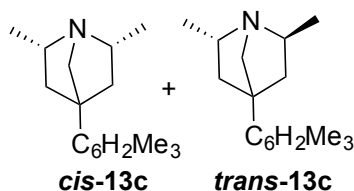


Isolated yield: 83 - 90 %.

^1H NMR (benzene- d_6 , 600MHz): δ 7.10 – 7.04 (m, 15 H, $\text{C}_6\text{H}_4\text{Me}$, *cis*+*trans*), 3.20 (m, 1 H, NCH, *trans*), 3.10 (m, 1 H, NCH, *trans*), 2.84 (d, $^3J_{\text{H-H}} = 9.3$ Hz, 1 H, NCH₂, *trans*), 2.68 (m, 6 H, NCH, *cis*), 2.59 (s, 5 H, NCH₂, *cis*), 2.56 (d, $^3J_{\text{H-H}} = 9.6$ Hz, 1 H, NCH₂, *trans*), 2.19 (s, 12 H, $\text{C}_6\text{H}_4\text{Me}$), 1.81 (td, $^3J_{\text{H-H}} = 10.7$ Hz, $^3J_{\text{H-H}} = 3.5$ Hz, 1 H, PhCCH₂, *trans*), 1.58 (dd, $^3J_{\text{H-H}} = 11.2$ Hz, $^3J_{\text{H-H}} = 7.6$ Hz, 6 H, PhCCH₂, *cis*), 1.52 (t, $^3J_{\text{H-H}} = 9.5$ Hz, 1 H, PhCCH₂, *trans*), 1.26 (m, 1 H, PhCCH₂, *trans*), 1.21 (m, 6 H, PhCCH₂, *cis*) 1.12 (m, 23 H, NCHCH₃,

cis+trans), 0.78 (m, 1 H, PhCCH₂, *trans*). ¹³C{¹H} NMR (benzene-*d*₆, 151 MHz): δ 141.34 (C₆H₄Me), 140.70 (C₆H₄Me), 135.78 (C₆H₄Me), 135.72 (C₆H₄Me), 129.54 (C₆H₄Me), 127.51 (C₆H₄Me), 127.38 (C₆H₄Me), 63.03 (NCH), 62.51 (NCH), 60.30 (NCH), 56.93 (PhCCH₂), 56.55 (NCH₂), 55.41 (PhCCH₂), 51.61 (NCH₂), 48.57 (PhCCH₂), 46.55 (PhCCH₂), 45.63 (PhCCH₂), 23.63 (NCHCH₃), 23.49 (NCHCH₃), 21.43 (C₆H₄Me), 18.10 (NCHCH₃). ¹⁵N NMR (benzene-*d*₆, 61 MHz): δ -293.8 ppm. IR (KBr, cm⁻¹): 3079 (s), 3058 (m), 3027 (m), 2966 (s), 2927 (s), 2866 (s), 1639 (s), 1493 (s), 1448 (m), 1395 (m), 1376 (m), 1333 (w), 1299 (w), 1239 (w), 1165 (m), 1136 (m), 1112 (w), 1075 (s), 1048 (s), 1010 (m), 972 (s), 911 (s), 861 (s), 816 (w), 794 (s), 758 (w), 699 (w). MS (ESI) exact mass calcd for C₁₅H₂₁N: m/z 216.1747 ([M⁺+H⁺]), Found: 216.1751 (Δ 0.5 ppm).

4-mesityl-2,6-dimethyl-1-azabicyclo[2.2.1]heptane. (*cis:trans* = 7:1)

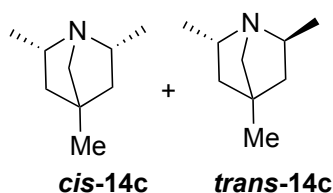


Isolated yield: 86 - 89 %.

¹H NMR (benzene-*d*₆, 600MHz): δ 6.76 (s, 15 H, C₆H₂Me₃, *cis+trans*), 3.23 (d, ³J_{H-H} = 9.4 Hz, 1 H, NCH₂, *trans*), 3.05 (m, 1 H, NCH₂, *trans*), 2.96 (s, 14 H, NCH₂, *cis*), 2.58 (q, ³J_{H-H} = 6.6 Hz, NCHCH₂, *cis*), 2.30 (s, 47 H, C₆H₂Me₃, *cis*), 2.14 (s, 24 H, C₆H₂Me₃, *cis*), 2.07 (td, ³J_{H-H} = 11.7 Hz, 8.0 Hz, 15 H, NCHCH₂, *cis*), 1.70 (t, ³J_{H-H} = 10.7 Hz, NCHCH₂, *trans*), 1.10 (m, 46 H, NCHCH₃, *cis+trans*), 1.01 (m, 15 H, NCH *cis*). ¹³C{¹H} NMR (benzene-*d*₆, 151 MHz): δ 138.24 (C₆H₂Me₃), 137.58 (C₆H₂Me₃), 137.55 (C₆H₂Me₃), 137.49 (C₆H₂Me₃), 135.15 (C₆H₂Me₃), 132.25 (C₆H₂Me₃), 63.90 (NCH), 61.37 (NCH), 59.47 (NCH), 59.04 (PhCCH₂), 57.91 (NCH₂), 57.52 (PhCCH₂), 49.73 (NCH₂), 46.04 (PhCCH₂), 43.93

(PhCCH₂), 43.58 (PhCCH₂), 25.76 (C₆H₂Me₃), 25.78 (C₆H₂Me₃), 23.49 (NCHCH₃), 23.38 (NCHCH₃), 23.07 (C₆H₂Me₃), 20.77 (C₆H₂Me₃), 18.09 (NCHCH₃). ¹⁵N NMR (benzene-*d*₆, 61 MHz): δ -298.2 ppm. IR (KBr, cm⁻¹): 3081 (s), 3059 (m), 3027 (m), 2966 (s), 2928 (s), 2866 (s), 1602 (s), 1496 (s), 1447 (m), 1374 (m), 1333 (w), 1298 (w), 1237 (w), 1166 (m), 1135 (m), 1112 (w), 1095 (s), 1073 (s), 1048 (m), 1005 (m), 964 (s), 910 (s), 861 (s), 816 (w), 792 (s), 758 (w), 699 (w). MS (ESI) exact mass calcd for C₁₇H₂₅N: m/z 244.2060 ([M⁺+H⁺]), Found: 244.2066 (Δ 0.5 ppm).

2,4,6-trimethyl-1-azabicyclo[2.2.1]heptane: (cis:trans = 1:1)



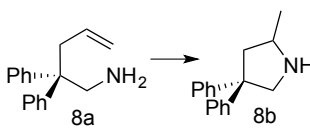
Isolated yield: 81 - 88 %.

¹H NMR (benzene-*d*₆, 600MHz): δ 3.11 (m, 1 H, NCH, *trans*), 3.02 (m, 1 H, NCH, *trans*), 2.59 (m, 2 H, NCH₂, *cis*), 2.34 (d, ³J_{H-H} = 9.4 Hz, 1 H, NCH, *cis*), 2.07 (s, 2 H, NCH₂, *cis*), 2.55 (d, ³J_{H-H} = 9.6 Hz, 1 H, NCH₂, *trans*), 1.36 (t, ³J_{H-H} = 10.5 Hz, 1 H, MeCCH₂, *trans*), 1.17 (t, ³J_{H-H} = 9.6 Hz, 1 H, PhCCH₂, *cis*), 1.08 (m, 18 H, MeCCH₂, NCHCH₃, *cis+trans*), 0.82 (m, 1 H, MeCCH₂, *trans*), 0.76 (m, 2 H, MeCCH₂, *cis*), 0.39 (m, 1 H, MeCCH₂, *trans*).

¹³C {¹H} NMR (benzene-*d*₆, 151 MHz): δ 64.08 (NCH), 63.08 (NCH), 60.39 (NCH), 58.03 (MeCCH₂), 51.59 (NCH₂), 49.01 (MeCCH₂), 48.32 (NCH₂), 47.39 (MeCCH₂), 46.07 (MeCCH₂), 44.83 (MeCCH₂), 23.66 (NCHCH₃), 23.50 (NCHCH₃), 18.21 (C₆H₄Me), 18.16 (NCHCH₃), 17.55 (CH₃C). ¹⁵N NMR (benzene-*d*₆, 61 MHz): δ -291.2 ppm. IR (KBr, cm⁻¹): 2966 (s), 2927 (s), 2866 (s), 1639 (s), 1493 (s), 1448 (m), 1395 (m), 1376 (m), 1333 (w), 1299 (w), 1239 (w), 1165 (m), 1136 (m), 1112 (w), 1075 (s), 1048 (s), 1010 (m), 972 (s), 911

(s), 861 (s), 816 (w), 794 (s), 758 (w), 699 (w). MS (ESI) exact mass calcd for $C_7H_{17}N$: m/z 140.1434 ($[M^+ + H^+]$), Found: 140.1432 (Δ 0.5 ppm)

Table 3.5. Catalytic hydroamination of aminoalkenes.^a

Reaction	Catalyst	Temp (°C)	Time (min)			
			30	60	90	120
	1@MSN ₅₅₀	60	32 ^a	47 ^a	81 ^a	96 ^a
	2•THF@MSN ₅₅₀	60	35 ^a	49 ^a	77 ^a	95 ^a
	1@MSN ₇₀₀	60	33 ^a	51 ^a	75 ^a	96 ^a
	2•THF@MSN ₇₀₀	60	36 ^a	52 ^a	83 ^a	96 ^a

^aNMR yield obtained by integrating product signal in comparison to $Si(SiMe_3)_4$ as an internal standard

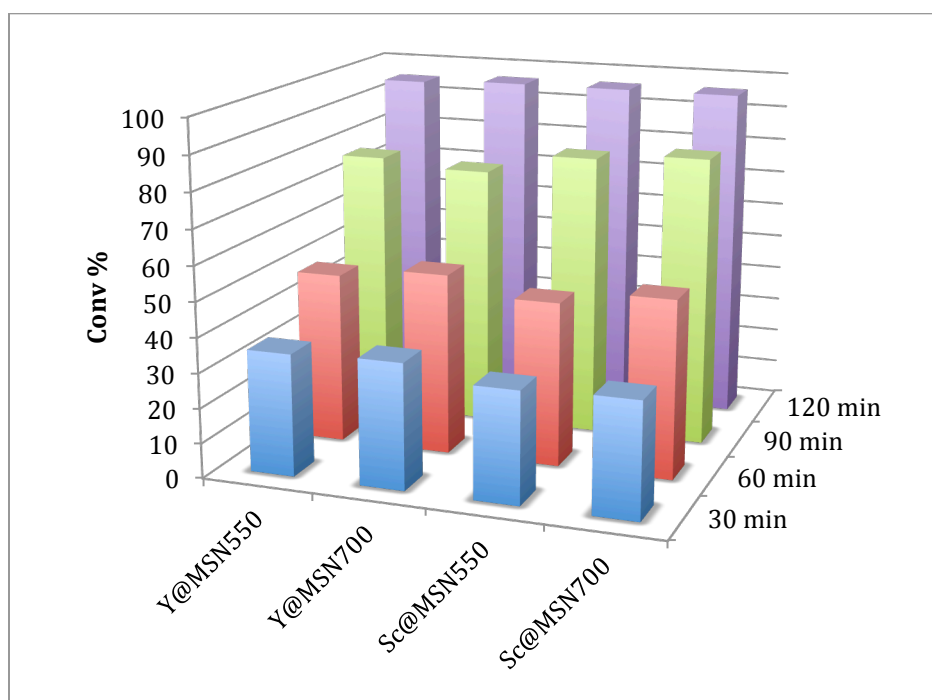


Figure 3.7. NMR yield comparison at 30 min intervals under heterogeneous catalytic conditions

References.

- (a) Kleinhenz, S.; Pfennig, V.; Seppelt, K., *Chem. – A Eur. J.* **1998**, *4*, 1687-1691; (b) Vaid, T. P.; Veige, A. S.; Lobkovsky, E. B.; Glassey, W. V.; Wolczanski, P. T.; Liable-Sands, L. M.; Rheingold, A. L.; Cundari, T. R., *J. Am. Chem. Soc.* **1998**, *120*, 10067-10079; (c) Avent, A. G.; Caro, C. F.; Hitchcock, P. B.; Lappert, M. F.; Li, Z. N.; Wei, X. H., *J. Chem. Soc., Dalton Trans.* **2004**, 1567-1577; (d) Hitchcock, P. B.; Lappert, M. F.; Smith, R. G.; Bartlett, R. A.; Power, P. P., *J. Chem. Soc., Chem. Commun.* **1988**, 1007-9.
- Zimmermann, M.; Anwander, R., *Chem. Rev.* **2010**, *110*, 6194-6259.
- (a) Bradley, D. C.; Ghotra, J. S.; Hart, F. A., *J. Chem. Soc., Chem. Commun.* **1972**, 349-350; (b) Bradley, D. C.; Ghotra, J. S.; Hart, F. A., *J. Chem. Soc., Dalton Trans.* **1973**, 1021-1023; (c) Ghotra, J. S.; Hursthouse, M. B.; Welch, A. J., *J. Chem. Soc., Chem. Commun.* **1973**, 669-670.
- (a) Anwander, R.; Runte, O.; Eppinger, J.; Gerstberger, G.; Herdtweck, E.; Spiegler, M., *J. Chem. Soc., Dalton Trans.* **1998**, 847-858; (b) Bienfait, A. M.; Schadle, C.; Maichle-Mossmer, C.; Tornroos, K. W.; Anwander, R., *Dalton Trans.* **2014**, *43*, 17324-17332.
- (a) Kawaoka, A. M.; Douglass, M. R.; Marks, T. J., *Organometallics* **2003**, *22*, 4630-4632; (b) Yu, X.; Seo, S.; Marks, T. J., *J. Am. Chem. Soc.* **2007**, *129*, 7244-7245; (c) Burgstein, M. R.; Berberich, H.; Roesky, P. W., *Chem.-A Eur. J.* **2001**, *7*, 3078-3085; (d) Seo, S.; Marks, T. J., *Org. Lett.* **2008**, *10*, 317-319.
- (a) Gauvin, R. M.; Delevoye, L.; Hassan, R. A.; Keldenich, J.; Mortreux, A., *Inorg. Chem.* **2007**, *46*, 1062-1070; (b) Gauvin, R. M.; Chenal, T.; Hassan, R. A.; Addad, A.; Mortreux, A., *J. Mol. Catal. A: Chemical* **2006**, *257*, 31-40; (c) Roux, E. L.; Liang, Y.; Storz, M. P.; Anwander, R., *J. Am. Chem. Soc.* **2010**, *132*, 16368-16371; (d) Gerstberger, G.; Palm, C.; Anwander, R., *Chem. – A Eur. J.* **1999**, *5*, 997-1005.
- Woodman, T. J.; Sarazin, Y.; Fink, G.; Hauschild, K.; Bochmann, M., *Macromolecules* **2005**, *38*, 3060-3067.
- Müller, T. E.; Hultsch, K. C.; Yus, M.; Foubelo, F.; Tada, M., *Chem. Rev.* **2008**, *108*, 3795-3892.
- Manna, K.; Eedugurala, N.; Sadow, A. D., *J. Am. Chem. Soc.* **2015**, *137*, 425-435.
- (a) Wang, X.; Chen, Z.; Sun, X.-L.; Tang, Y.; Xie, Z., *Org. Lett.* **2011**, *13*, 4758-4761; (b) Zhang, Y.; Sun, Q.; Wang, Y.; Yuan, D.; Yao, Y.; Shen, Q., *RSC Advances* **2016**, *6*, 10541-10548.
- (a) Hultsch, K. C.; Hampel, F.; Wagner, T., *Organometallics* **2004**, *23*, 2601-2612; (b) Stanlake, L. J. E.; Schafer, L. L., *Organometallics* **2009**, *28*, 3990-3998; (c) Huynh, K.; Livinghouse, T.; Lovick, H. M., *Synlett* **2014**, *25*, 1721-1724; (d) Kim, J. Y.; Livinghouse, T., *Org. Lett.* **2005**, *7*, 4391-4393.
- Sardina, F. J.; Rapoport, H. *Chem. Rev.* **1996**, *96*, 1825-1872.
- (a) Piotrowski, D. W.; Rolph, M.; Wei, L. *Tetrahedron Letters* **2012**, *53*, 1009-1012; (b) Slowinski, F.; Ben Ayad, O.; Vache, J.; Saady, M.; Leclerc, O.; Lochead, A. *Org. Lett.* **2010**, *12*, 5004-5007; (c) D'hooghe, M.; Vervisch, K.; Törnroos, K. W.; Verhaeghe, T.; Desmet, T.; Lategan, C.; Smith, P. J.; Chibale, K.; De Kimpe, N. *Bioorganic & Medicinal Chemistry Letters* **2013**, *23*, 1507-1510.

14. Eppinger, J.; Spiegler, M.; Hieringer, W.; Herrmann, W. A.; Anwander, R., *J. Am. Chem. Soc.* **2000**, *122*, 3080-3096.
15. Yuen, H. F.; Marks, T. J., *Organometallics* **2008**, *27*, 155-158.
16. (a) Procopio, L. J.; Carroll, P. J.; Berry, D. H., *J. Am. Chem. Soc.* **1994**, *116*, 177-185; (b) Procopio, L. J.; Carroll, P. J.; Berry, D. H., *Organometallics* **1993**, *12*, 3087-3093.
17. (a) Yan, K.; Duchimaza Heredia, J. J.; Ellern, A.; Gordon, M. S.; Sadow, A. D., *J. Am. Chem. Soc.* **2013**, *135*, 15225-15237; (b) Yan, K.; Sadow, A. D., *Chem. Commun.* **2013**, *49*, 3212-3214; (c) Yan, K.; Pindwal, A.; Ellern, A.; Sadow, A. D., *Dalton Trans.* **2014**, *43*, 8644-8653; (d) Chen, F.; Fan, S.; Wang, Y.; Chen, J.; Luo, Y., *Organometallics* **2012**, *31*, 3730-3735.
18. Rees, W. S.; Just, O.; Schumann, H.; Weimann, R., *Angew. Chem., Int. Ed.* **1996**, *35*, 419-422.
19. (a) Procopio, L. J.; Carroll, P. J.; Berry, D. H., *J. Am. Chem. Soc.* **1991**, *113*, 1870-1872; (b) Procopio, L. J.; Carroll, P. J.; Berry, D. H., *Polyhedron* **1995**, *14*, 45-55; (c) Yan, K.; Ellern, A.; Sadow, A. D., *J. Am. Chem. Soc.* **2012**, *134*, 9154-9156.
20. Goldfuss, B.; Schleyer, P. v. R.; Handschuh, S.; Hampel, F.; Bauer, W., *Organometallics* **1997**, *16*, 5999-6003.
21. Yan, K.; Pawlikowski, A. V.; Ebert, C.; Sadow, A. D., *Chem. Commun.* **2009**, 656-658.
22. Champion, B. K.; Heyn, R. H.; Tilley, T. D., *Organometallics* **1993**, *12*, 2584-2590.
23. Sadow, A. D.; Tilley, T. D., *J. Am. Chem. Soc.* **2005**, *127*, 643-656.
24. Wang, X.; Chertihin, G. V.; Andrews, L., *J. Phys. Chem. A* **2002**, *106*, 9213-9225.
25. Fjeldberg, T.; Andersen, R. A., *J. Mol. Struct.* **1985**, *128*, 49-57.
26. Deschner, T.; Liang, Y.; Anwander, R., *J. Phys. Chem. C* **2010**, *114*, 22603-22609.
27. McDonald, R. S., *J. Phys. Chem.* **1958**, *62*, 1168-1178.
28. (a) Quignard, F.; Lecuyer, C.; Bougault, C.; Lefebvre, F.; Choplin, A.; Olivier, D.; Basset, J. M., *Inorg. Chem.* **1992**, *31*, 928-930; (b) Morrow, B. A.; McFarlan, A. J., *Langmuir* **1991**, *7*, 1695-1701.
29. Martínez, P. H.; Hultsch, K. C.; Hampel, F., *Chem. Commun.* **2006**, 2221-2223.
30. Deacon, G. B.; Feng, T.; Junk, P. C.; Meyer, G.; Scott, N. M.; Skelton, B. W.; White, A. H., *Aus. J. Chem.* **2000**, *53*, 853-865.
31. Hazin, P. N.; Huffman, J. C.; Bruno, J. W., *Organometallics* **1987**, *6*, 23-27.
32. Karraker, D. G., *Inorg. Chim. Acta* **1987**, *139*, 189-191.
33. Kim, J.; Bott, S. G.; Hoffman, D. M., *Inorg. Chem.* **1998**, *37*, 3835-3841.

CHAPTER 4
**CYCLOPENTADIENYL-BIS(OXAZOLINE) MAGNESIUM AND ZIRCONIUM
 COMPLEXES IN AMINOALKENE HYDROAMINATION**

Modified from a published paper in *Organometallics*, **2015**, *34*, 5566 – 5575

Naresh Eedugurala, Megan Hovey, Hung-An Ho, Barun Jana, Nicole L. Lampland, Arkady Ellern, and Aaron D. Sadow

US Department of Energy Ames Laboratory and Department of Chemistry, Ames IA 50011

Abstract. A new class of cyclopentadiene-bis(oxazoline) compounds and their piano-stool-type organometallic complexes have been prepared as catalysts for hydroamination of aminoalkenes. The two compounds $\text{MeC}(\text{Ox}^{\text{Me}_2})_2\text{C}_5\text{H}_5$ ($\text{Bo}^{\text{M}}\text{CpH}$; Ox^{Me_2} = 4,4-dimethyl-2-oxazoline) and $\text{MeC}(\text{Ox}^{\text{Me}_2})_2\text{C}_5\text{Me}_4\text{H}$ ($\text{Bo}^{\text{M}}\text{Cp}^{\text{tet}}\text{H}$) are synthesized from $\text{C}_5\text{R}_4\text{HI}$ ($\text{R} = \text{H}, \text{Me}$) and $\text{MeC}(\text{Ox}^{\text{Me}_2})_2\text{Li}$. These cyclopentadienebis(oxazolines) are converted into ligands that support a variety of metal centers in piano-stool-type geometries, and here we report the preparation of Mg, Tl, Ti, and Zr compounds. $\text{Bo}^{\text{M}}\text{CpH}$ and $\text{Bo}^{\text{M}}\text{Cp}^{\text{tet}}\text{H}$ react with $\text{MgMe}_2(\text{O}_2\text{C}_4\text{H}_8)_2$ to give the magnesium methyl complexes $\{\text{Bo}^{\text{M}}\text{Cp}\}\text{MgMe}$ and $\{\text{Bo}^{\text{M}}\text{Cp}^{\text{tet}}\}\text{MgMe}$. $\text{Bo}^{\text{M}}\text{CpH}$ and $\text{Bo}^{\text{M}}\text{Cp}^{\text{tet}}\text{H}$ are converted to $\text{Bo}^{\text{M}}\text{CpTl}$ and $\text{Bo}^{\text{M}}\text{Cp}^{\text{tet}}\text{Tl}$ by reaction with TlOEt . The thallium derivatives react with $\text{TiCl}_3(\text{THF})_3$ to provide $[\{\text{Bo}^{\text{M}}\text{Cp}\}\text{TiCl}(\mu\text{-Cl})]_2$ and $[\{\text{Bo}^{\text{M}}\text{Cp}^{\text{tet}}\}\text{TiCl}(\mu\text{-Cl})]_2$, the former of which is crystallographically characterized as a dimeric species. $\text{Bo}^{\text{M}}\text{CpH}$ and $\text{Zr}(\text{NMe}_2)_4$ react to eliminate dimethylamine and afford $\{\text{Bo}^{\text{M}}\text{Cp}\}\text{Zr}(\text{NMe}_2)_3$, which is crystallographically characterized as a monomeric four-legged piano-stool compound. $\{\text{Bo}^{\text{M}}\text{Cp}\}\text{Zr}(\text{NMe}_2)_3$, $\{\text{Bo}^{\text{M}}\text{Cp}\}\text{MgMe}$, and $\{\text{Bo}^{\text{M}}\text{Cp}^{\text{tet}}\}\text{MgMe}$ are efficient catalysts for the hydroamination/cyclization of aminoalkenes under mild conditions.

Introduction

Early metal piano-stool compounds of the type $(\eta^5\text{-C}_5\text{R}_5)\text{MX}_n$ are important for stabilizing reactive moieties such as alkylidenes and dinitrogen compounds,¹ and this class of compounds also provide catalytic sites for olefin polymerization.² The constrained-geometry class of catalysts $\{\text{Me}_2\text{Si}(\text{C}_5\text{R}_4)\text{NR}'\}\text{MX}$ exemplify the applications of piano-stool compounds in catalysis (Chart 4.1). These compounds suggest that strained systems can have further enhanced catalytic properties.³ Recently we showed that oxazolinyborate-substituted cyclopentadienyl ligands provide highly active and enantioselective piano-stool zirconium and hafnium hydroamination/cyclization catalysts.⁴ This reactivity contrasts with that reported for constrained-geometry group 4 catalysts in hydroamination, which require more forcing conditions.⁵ Trivalent rare earth catalysts supported by constrained-geometry-type ligands are highly reactive for hydroamination/ cyclization reactions,⁶ in contrast to the group 4 examples. Monoanionic constrained-geometry-like cyclopentadienyl phosphazene or 2,2-bis(pyrazol-1-yl)ethyl lutetium dialkyl compounds $(\text{bpzcp})\text{Lu}(\text{CH}_2\text{SiMe}_3)_2$ ($\text{bpzcp} = 2\text{-}[2,2\text{-bis}(3,5\text{-dimethylpyrazol-1-yl})\text{-1,1-diphenylethyl}]\text{-1,3-cyclopentadiene}$) also catalyze the cyclization of aminoalkenes to 2-alkylpyrrolidines.⁷ However, group 4 piano-stool-type compounds supported by monoanionic cyclopentadienyl ligands have not been explored in catalytic hydroamination.

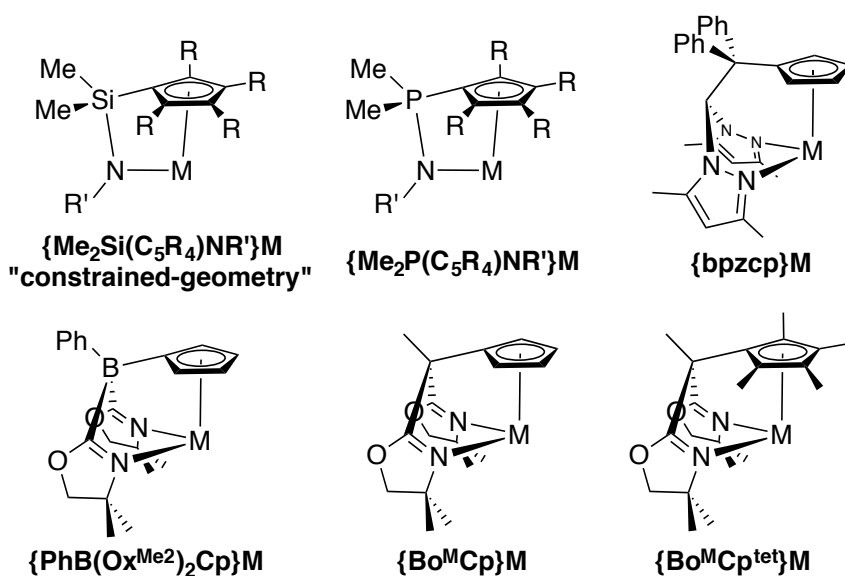


Chart 4.1. Linked cyclopentadienyl-donor ligand complexes providing piano-stool geometry compounds.

The closest examples are dianionic ligands noted above, namely, the constrained-geometry class and our examples involving cyclopentadienyl-bis(oxazolinyl)borates.^{5,8} High oxidation state d^0 group 4 compounds are distinguished from rare earth catalysts by the valence of the metal center, with the latter class of compounds having one fewer valence, assuming the ancillary ligands' valence are equivalent. Thus, another approach to controlling the available reactive valence is through modification of the ancillary ligands' valence requirements. Given the high activity of group 4 compounds supported by these dianionic $[\text{PhB}(\text{Ox}^{\text{R}})_2\text{C}_5\text{H}_4]^{2-}$ ligands,^{4a,c,d} we targeted corresponding monoanionic $[\text{RC}(\text{Ox}^{\text{R}'})_2\text{C}_5\text{R}''_4]^-$ ligands, which might impart high reactivity upon group 4 metal sites in hydroamination and allow further comparisons in the series of compounds $\{\text{PhB}(\text{Ox}^{\text{R}})_2\text{C}_5\text{H}_4\}\text{LnX}$, $\{\text{PhB}(\text{Ox}^{\text{R}})_2\text{C}_5\text{H}_4\}\text{MX}_2$, $\{\text{RC}(\text{Ox}^{\text{R}'})_2\text{C}_5\text{R}''_4\}\text{LnX}_2$, and $\{\text{RC}(\text{Ox}^{\text{R}'})_2\text{C}_5\text{R}''_4\}\text{MX}_3$ (Ln = trivalent group 3 or lanthanide element, M = tetravalent group 4 metal center, X = monovalent ligand). Typically, cyclopentadienyl ligand derivatives are synthesized by reaction of a

nucleophilic C_5R_4H anion and an electrophile such as a halosilane. The monoanionic cyclopentadienylphosphazene ligands are also synthesized through the reaction of $C_5R_4H^-$ and R_2PCl .⁹ Alternatively, reactions of fulvene derivatives with nucleophiles provide a CR_2 linker between the cyclopentadiene and donor groups, such as in bis(pyrazolyl)ethylcyclopentadienyl ligands (bpzcp).¹⁰

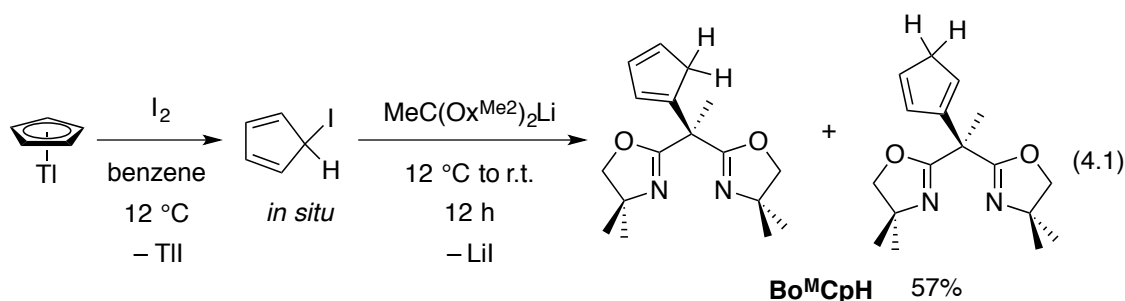
The above routes imply that preparation of one-carbon linked analogues of $[PhB(Ox^R)_2C_5H_4]^{2-}$ would involve coupling of two typically nucleophilic cyclopentadienide and $[RC(Ox^{R'})_2]^-$ species. Instead, we investigated a strategy for coupling the stabilized anions of bis(oxazolines) with electrophilic cyclopentadienyl groups.¹¹ The reaction of deprotonated bis(oxazoline) and organic electrophiles has been very useful to obtain tris(oxazoliny)ethane (tris-ox) ligands¹² or side-arm containing bis(oxazolines) that show improved enantioselectivity in a host of catalytic conversions.¹³ Recently, we reported the synthesis of the tetramethylcyclopentadienyl ligand $MeC(Ox^{Me_2})_2C_5Me_4H$ (Ox^{Me_2} = 4,4-dimethyl-2-oxazoline) and a series of lutetium compounds coordinated by this ligand.¹⁴

Here we describe the full synthesis of achiral monoanionic cyclopentadienyl bis(oxazoline) compounds, magnesium and thallium main group compounds, and titanium and zirconium compounds. We also report an initial study of the magnesium and zirconium compounds' reactivity in hydroamination of aminoalkenes. Comparisons between the parent $CpZr(NMe_2)_3$, the new bis(oxazoline)-substituted cyclopentadienyl zirconium derivative, and previously reported bis(oxazoliny)borate substituted zirconium catalysts suggest trends in hydroamination activity corresponding to cyclopentadienyl substitution and the metal center's reactive valence number.

Results and discussion

Synthesis and Characterization of Bis(4,4-dimethyl-2-oxazoline)cyclopentadiene ($\text{Bo}^{\text{M}}\text{CpH}$) and Bis(4,4-dimethyl-2-oxazoline)tetramethylcyclopentadiene ($\text{Bo}^{\text{M}}\text{Cp}^{\text{tet}}\text{H}$).

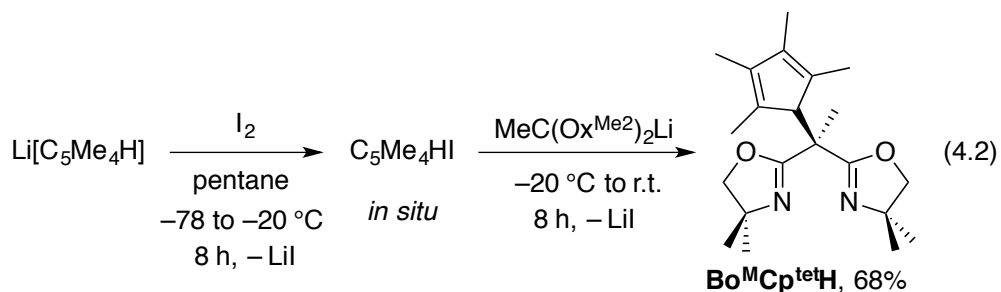
The desired mixed cyclopentadiene-bis(2-oxazoline) proligands are synthesized by reaction of nucleophilic lithium bis(2-oxazolynyl)methylcarbide and iodocyclopentadiene reagents. In the first example, reaction of $\text{C}_5\text{H}_5\text{I}$ and $\text{MeC}(\text{Ox}^{\text{Me}_2})_2\text{Li}$ provides $\text{MeC}(\text{Ox}^{\text{Me}_2})_2\text{C}_5\text{H}_5$ ($\text{Bo}^{\text{M}}\text{CpH}$, eq 4.1). For this reaction, iodocyclopentadiene is generated from thallium cyclopentadienide and iodine in benzene at 12 °C and used *in situ*.¹¹



At least three isomers of $\text{Bo}^{\text{M}}\text{CpH}$ are possible, the structures of which are related by the position of the unique H on the C_5H_5 group. The ^1H NMR spectrum acquired in benzene- d_6 contained two $\text{MeC}(\text{Ox}^{\text{Me}_2})_2\text{C}_5\text{H}_5$ resonances at 2.10 and 2.04 ppm (normalized to 6 H total) that appeared in a 1.15:1 integrated ratio. In addition, two singlets at 3.46 and 2.73 ppm (4 H total) were assigned to sp^3 -hybridized portions of the C_5H_5 , whereas the signals assigned to sp^2 -hybridized cyclopentadienyl group integrated to a total of 6 H. From these data, two isomers are present that contain C–C connectivities with the bis(oxazoline) group bonded to an sp^2 -hybrid carbon on the C_5H_5 unit. The IR spectrum of $\text{Bo}^{\text{M}}\text{CpH}$ contained a band at 1656 cm^{-1} assigned to the oxazoline ν_{CN} , and this is the only band in this region. Interestingly, the IR spectrum of the borato compound $\text{H}[\text{PhB}(\text{Ox}^{\text{Me}_2})_2\text{C}_5\text{H}_5]$, which is isolated as a mixture of three isomers and contains a H that is likely bonded to one or both

oxazolines, also contained only one ν_{CN} band, but that band was red-shifted by ca. 60 cm^{-1} in comparison to $\text{Bo}^{\text{M}}\text{CpH}$.^{4a} We attribute this significant change in energy of the ν_{CN} to the substitution of a four-coordinate anionic boron in $\text{PhB}(\text{Ox}^{\text{Me}2})_2\text{Cp}$ for a neutral carbon linker in $\text{Bo}^{\text{M}}\text{Cp}$, and this may hint at inequivalent coordination properties of the oxazoline donors in the two ligands.

The generality of this synthetic approach is supported by the synthesis of the bulkier tetramethylcyclopentadienyl derivative. $\text{C}_5\text{Me}_4\text{HI}$ ¹⁵ is allowed to react with $\text{MeC}(\text{Ox}^{\text{Me}2})_2\text{Li}$ to provide $\text{MeC}(\text{Ox}^{\text{Me}2})_2\text{C}_5\text{Me}_4\text{H}$ ($\text{Bo}^{\text{M}}\text{Cp}^{\text{tet}}\text{H}$) as a white solid in 68% yield (eq 4.2). As noted above, we recently reported the application of $\text{Bo}^{\text{M}}\text{Cp}^{\text{tet}}\text{H}$ in the synthesis of piano-stool lutetium compounds,¹⁴ while the synthesis and characterization of the organic compound are reported here.



In contrast to $\text{Bo}^{\text{M}}\text{CpH}$, $\text{Bo}^{\text{M}}\text{Cp}^{\text{tet}}\text{H}$ was isolated as only one isomer from this reaction, although a second isomer crystallized from a hydrolyzed organometallic compound (see below). This formulation was suggested by the diagnostic signal from $\text{MeC}(\text{Ox}^{\text{Me}2})_2\text{C}_5\text{Me}_4\text{H}$ that appeared at 1.61 and 16.41 ppm in the ^1H and $^{13}\text{C}\{^1\text{H}\}$ NMR spectra. Two singlet and two coupled doublet ^1H NMR signals were assigned to diastereotopic methyl and methylene oxazoline moieties, indicating that the oxazoline groups are equivalent. These data indicate that $\text{Bo}^{\text{M}}\text{Cp}^{\text{tet}}\text{H}$ is Cs symmetric, placing the proton on the sp^3 -hybridized C12 (identified in Figure 4.1). The infrared spectrum of $\text{Bo}^{\text{M}}\text{Cp}^{\text{tet}}\text{H}$ contained

two bands at 1661 and 1640 cm^{-1} , which were assigned to symmetric and asymmetric ν_{CN} . These two bands for a single isomer contrast the single ν_{CN} signal observed for the multiple isomers of $\text{Bo}^{\text{M}}\text{CpH}$ and $\text{H}[\text{PhB}(\text{Ox}^{\text{Me}2})_2\text{C}_5\text{H}_5]$ noted above. X-ray-quality crystals of $\text{Bo}^{\text{M}}\text{Cp}^{\text{tet}}\text{H}$ were obtained from a pentane solution at $-30\text{ }^\circ\text{C}$ (Figure 4.1).

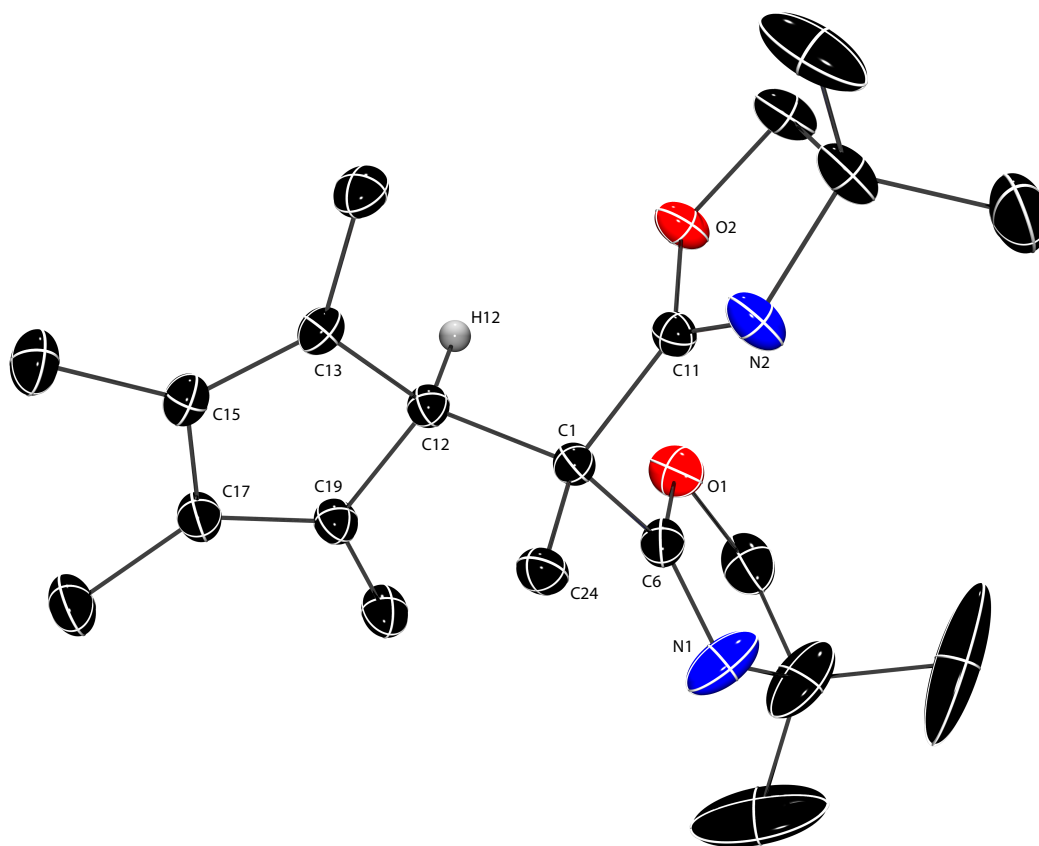
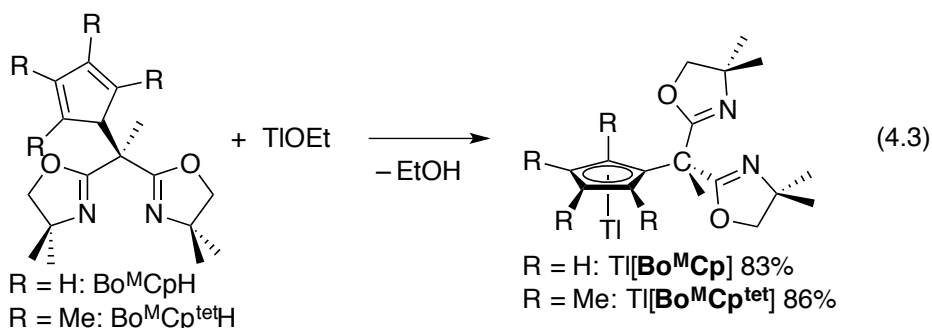


Figure 4.1. Rendered thermal ellipsoid diagram of $\text{MeC}(\text{Ox}^{\text{Me}2})_2\text{C}_5\text{Me}_4\text{H}$ ($\text{Bo}^{\text{M}}\text{Cp}^{\text{tet}}\text{H}$) with ellipsoids plotted at 35% probability. H atoms were placed in calculated positions, refined isotopically using the riding model, and were excluded from the illustration for clarity, with the exception of the H atom on C12. Selected interatomic distances (\AA): C1-C12, 1.567(2); C1-C6, 1.521(1); C1-C11, 1.521(1); C1-C24, 1.532(2); C12-C13, 1.521(2); C12-C19, 1.521(2); C13-C15, 1.346(2); C15-C17, 1.477(2); C17-C19, 1.350(2); C6-N1, 1.247(2); C11-

N2, 1.260(2). Selected interatomic angles (deg): C1-C12-C13, 112.7(1); C1-C12-C19, 114.8(1); C13-C12-C19, 103.0(1).

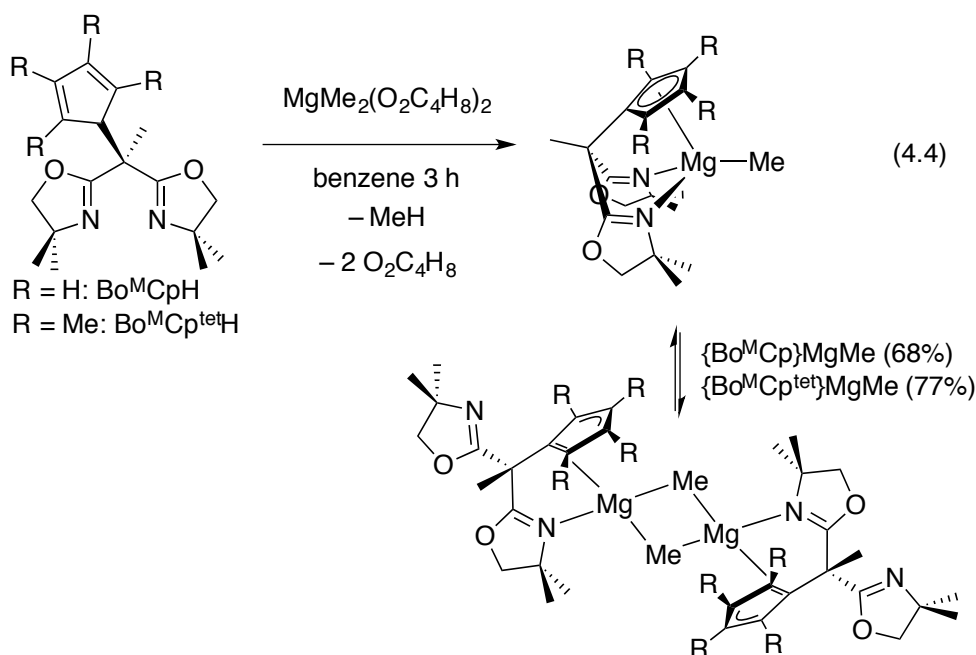
The single-crystal diffraction study confirms the connectivity and the electronic configuration of the cyclopentadiene group in $\text{Bo}^{\text{M}}\text{Cp}^{\text{tet}}\text{H}$. Thus, the C1 connects two oxazoline, a methyl, and a tetramethylcyclopentadienyl group. Moreover, the cyclopentadienyl C12 linked to the bis(oxazoline) unit is sp^3 -hybridized, determined on the basis of single bonds to neighboring carbons ($\sim 1.5 \text{ \AA}$), the sum of C–C12–C angles of 335° , and the C–C distances in the diene portion of the $\text{C}_5\text{Me}_4\text{HR}$ ring. Interestingly, the molecule adopts a conformation that gives a noncrystallographical pseudomirror plane, which contains the C1, C12, H12, and C24, bisects the C_5Me_4 moiety, and relates the two oxazolines. A second X-ray-quality crystal of $\text{Bo}^{\text{M}}\text{Cp}^{\text{tet}}\text{H}$ was obtained from the hydrolysis of a magnesium complex (see below) that proved to be an isomer in which the H atom bonded to the cyclopentadiene is located on the C13 rather than C12. This second isomer was not detected in the NMR spectra of characterized material.

Main Group Compounds $\{\text{Bo}^{\text{M}}\text{Cp}\}\text{M}$ and $\{\text{Bo}^{\text{M}}\text{Cp}^{\text{tet}}\}\text{M}$ ($\text{M} = \text{Mg}, \text{Tl}$). Metalation of $\text{Bo}^{\text{M}}\text{CpH}$ and $\text{Bo}^{\text{M}}\text{Cp}^{\text{tet}}\text{H}$ is achieved through protonolysis of Brønsted basic X-type ligands in MX_n compounds. This route provides access to thallium reagents that are useful for transmetalation. Reactions of $\text{Bo}^{\text{M}}\text{CpH}$ or $\text{Bo}^{\text{M}}\text{Cp}^{\text{tet}}\text{H}$ and thallium ethoxide provide $\text{Bo}^{\text{M}}\text{CpTl}$ or $\text{Bo}^{\text{M}}\text{Cp}^{\text{tet}}\text{Tl}$ (eq 4.3). The formation of $\text{Bo}^{\text{M}}\text{CpTl}$ occurs over 2 h in diethyl ether at room temperature and is significantly faster than the synthesis of $\text{Bo}^{\text{M}}\text{Cp}^{\text{tet}}\text{Tl}$, which requires 10 days in THF.



The ^1H and $^{13}\text{C}\{^1\text{H}\}$ NMR spectra of $\text{Bo}^{\text{M}}\text{CpTl}$ and $\text{Bo}^{\text{M}}\text{Cp}^{\text{tet}}\text{Tl}$ indicate that each compound is a single C_s -symmetric isomer. The ^1H NMR spectra of $\text{Bo}^{\text{M}}\text{CpTl}$ and $\text{Bo}^{\text{M}}\text{Cp}^{\text{tet}}\text{Tl}$ did not show evidence of coupling to the thallium (^{203}Tl and ^{205}Tl are $I = 1/2$). The cyclopentadienyl resonances in the $^{13}\text{C}\{^1\text{H}\}$ NMR spectrum of $\text{Bo}^{\text{M}}\text{CpTl}$ also did not contain evidence for J_{TlC} ; however, the spectrum of $\text{Bo}^{\text{M}}\text{Cp}^{\text{tet}}\text{Tl}$ contained two broad signals at 114.8 ppm (38 Hz at half-height) and 114.1 ppm (and 30 Hz at half-height) and one sharper signal at 115.94 ppm (8 Hz at half-height). In addition, the C_5Me_4 methyl groups appeared as doublets at 12.6 ppm ($J_{\text{TlC}} = 57.4$ Hz) and 11.1 ppm ($J_{\text{TlC}} = 44.8$ Hz). For comparison, the methyl groups in $\text{C}_5\text{Me}_5\text{Tl}$ provided a doublet ($J_{\text{TlC}} = 79.4$ Hz), as did the cyclopentadienyl carbons (114.6 ppm, $J_{\text{TlC}} = 102.2$ Hz).¹⁶ The ^{15}N NMR chemical shifts, determined by ^1H - ^{15}N HMBC experiments (at ^{15}N natural abundance) are -130 and -128 ppm, respectively, and these are in the region of noncoordinated oxazoline (e.g., 2H-4,4-dimethyl-2-oxazoline: -128 ppm).¹⁷ The IR spectra (acquired in a KBr matrix) of $\text{Bo}^{\text{M}}\text{CpTl}$ and $\text{Bo}^{\text{M}}\text{Cp}^{\text{tet}}\text{Tl}$ contained one (1647 cm^{-1}) and two (1654 and 1637 cm^{-1}) bands, respectively, assigned to the ν_{CN} . Thus, both $\text{Bo}^{\text{M}}\text{CpH}$ and $\text{Bo}^{\text{M}}\text{CpTl}$ each produced one similar ν_{CN} IR band, while the spectra for both $\text{Bo}^{\text{M}}\text{Cp}^{\text{tet}}\text{H}$ and $\text{Bo}^{\text{M}}\text{Cp}^{\text{tet}}\text{Tl}$ contained two ν_{CN} bands. The IR bands for the Tl derivatives were slightly redshifted in comparison to the protonated ligands.

Magnesium cyclopentadienyl compounds are also reagents for transmetalation, and oxazoline-coordinated magnesium compounds have applications as catalysts.¹⁸ The reactions of $\text{MgMe}_2(\text{O}_2\text{C}_4\text{H}_8)_2$ and $\text{Bo}^{\text{M}}\text{CpH}$ or $\text{Bo}^{\text{M}}\text{Cp}^{\text{tet}}\text{H}$ give the magnesium methyl complexes $\{\text{Bo}^{\text{M}}\text{Cp}\}\text{MgMe}$ and $\{\text{Bo}^{\text{M}}\text{Cp}^{\text{tet}}\}\text{MgMe}$ (eq 4.4). These compounds are isolated as off-white solids and are best stored at $-30\text{ }^\circ\text{C}$ to avoid thermal decomposition. In addition, we note that the carbon combustion analyses of both $\{\text{Bo}^{\text{M}}\text{Cp}\}\text{MgMe}$ and $\{\text{Bo}^{\text{M}}\text{Cp}^{\text{tet}}\}\text{MgMe}$ are consistently low, while hydrogen and nitrogen values are close to the expected values. In general, isolation of the magnesium compounds was challenging, and typically their reactivity was surveyed by in situ generated species and later repeated and verified with isolated materials.



These magnesium compounds are pseudo- C_s symmetric at room temperature, as determined by ^1H and $^{13}\text{C}\{^1\text{H}\}$ NMR spectra acquired of benzene- d_6 solutions. However, the structures are more complicated than pentahapto cyclopentadienyl and bidentate oxazoline

coordination as suggested by several pieces of data including an X-ray crystal structure of $\{\text{Bo}^{\text{M}}\text{Cp}^{\text{tet}}\}\text{MgMe}$ (see below). For example, the ^1H NMR signals of $\{\text{Bo}^{\text{M}}\text{Cp}\}\text{MgMe}$ were sharp for in situ generated samples that contained dioxane, but broad signals were obtained from samples dried by evaporation of all volatiles and redissolution in benzene- d_6 . The spectra of isolated, exhaustively dried $\{\text{Bo}^{\text{M}}\text{Cp}^{\text{tet}}\}\text{MgMe}$ were broad as well. Addition of THF to the samples that gave broad NMR signals resulted in reproducibly sharp ^1H NMR signals, equivalent to spectra obtained from in situ samples. We conclude that drying removes coordinated ethers and affects the appearance of NMR spectra, but drying does not result in demetalation or protonation of the cyclopentadienyl ligands. Moreover, the ^1H and ^{13}C NMR chemical shifts of dioxane, THF, or Et_2O in the presence of the cyclopentadienylmagnesium compounds were identical or nearly identical to the ethers' resonances in only benzene- d_6 .

The NMR data discussed here describe dioxane-containing samples (<1 equiv). Two C_5H_4 signals at 6.44 and 6.33 ppm and two C_5Me_4 methyls at 2.33 and 2.24 ppm were observed in the ^1H NMR spectra of $\{\text{Bo}^{\text{M}}\text{Cp}\}\text{MgMe}$ and $\{\text{Bo}^{\text{M}}\text{Cp}^{\text{tet}}\}\text{MgMe}$, respectively, as were the typical two oxazoline methyl signals and two coupled diastereotopic CH_2 resonances associated with Cs structures. The magnesium methyl resonances appeared as broad singlets at -0.05 and -0.9 in the ^1H NMR spectra of $\{\text{Bo}^{\text{M}}\text{Cp}\}\text{MgMe}$ and $\{\text{Bo}^{\text{M}}\text{Cp}^{\text{tet}}\}\text{MgMe}$, respectively. At the same time, the cyclopentadienylbis(oxazoline) signals were sharp, further indicating complex structures. Moreover, the ^1H NMR spectrum of $\{\text{Bo}^{\text{M}}\text{Cp}^{\text{tet}}\}\text{MgMe}$ acquired at -63 °C contained four methyl resonances and four coupled diastereotopic CH_2 resonances assigned to inequivalent oxazoline groups, and four signals were observed for cyclopentadienyl methyl groups. Thus, the low-temperature structure is C1

symmetric. The magnesium methyl and 2-C of the oxazoline were difficult to observe in the $^{13}\text{C}\{^1\text{H}\}$ NMR spectra of these compounds, either generated in situ or of isolated materials. However, with small amounts of dioxane, the MgMe resonance was observed at -11 ppm. Interestingly, ^{15}N NMR signals were observed as weak cross-peaks at -146 ppm for $\{\text{Bo}^{\text{M}}\text{Cp}^{\text{tet}}\}\text{MgMe}$ and -147 ppm for $\{\text{Bo}^{\text{M}}\text{Cp}\}\text{MgMe}$ using $^1\text{H}-^{15}\text{N}$ HMBC experiments (room temperature), and these chemical shifts are ca. 20 ppm upfield of 4,4-dimethyl-2-oxazoline (-128 ppm) referenced in the above discussion.

In addition, the infrared spectra (in KBr) of powdered samples of $\{\text{Bo}^{\text{M}}\text{Cp}\}\text{MgMe}$ and $\{\text{Bo}^{\text{M}}\text{Cp}^{\text{tet}}\}\text{MgMe}$, obtained by evaporation of frozen benzene solutions, each contained a single band in the region associated with the C=N stretch of the oxazoline group at 1658 cm^{-1} . The observation of one IR band contrasts the spectra of $\text{Bo}^{\text{M}}\text{Cp}^{\text{tet}}\text{H}$ and $\text{Bo}^{\text{M}}\text{Cp}^{\text{tet}}\text{Ti}$, which contained two ν_{CN} bands. One IR band is commonly observed in tridentate tris(oxazolanyl)borate compounds, and we attribute this to weak intensity of the asymmetric mode. For example, $\text{To}^{\text{M}}\text{MgMe}$ ($\text{To}^{\text{M}} = \text{tris}(4,4\text{-dimethyl-2-oxazolanyl})\text{-phenylborate}$) is C_{3v} symmetric, all three oxazolines are coordinated to magnesium(II), its ^{15}N NMR chemical shift is -157 ppm, and the ν_{CN} absorption appears at 1592 cm^{-1} in the IR spectrum.^{18a} A similar effect may account for the single ν_{CN} in $\{\text{Bo}^{\text{M}}\text{Cp}\}\text{MgMe}$ and $\{\text{Bo}^{\text{M}}\text{Cp}^{\text{tet}}\}\text{MgMe}$.

Support for a dimeric structure is obtained in the solid state from an X-ray diffraction study on $\{\text{Bo}^{\text{M}}\text{Cp}^{\text{tet}}\}\text{MgMe}$. The results indicate that only one oxazoline ring coordinates per magnesium, and the methyl groups bridge between the two magnesium centers (Figure 4.2). The cyclopentadienyl group coordinates to the magnesium center through a $\eta^2\text{-C}_5\text{Me}_4\text{R}$ interaction in which the magnesium-carbon distances are inequivalent. The short Mg-C distances involve the bis(oxazoline)-substituted carbon (Mg1-C13, $2.384(2)\text{ \AA}$) and the

adjacent carbon (Mg1–C14, 2.400(2) Å). The next shorter distances of Mg1–C16 and Mg1–C20, 2.681(2) and 2.658(2) Å, respectively, are significantly longer. The magnesium–carbon distances of the bridging methyl groups are similar but unequal (Mg1–C22, 2.267(2) and Mg1–C22#, 2.271(2) Å) and similar to the shortest distance in the magnesiumcyclopentadienyl interaction. The bridging Mg–C distances are similar to those in $[(C_5Me_4Et)Mg(\mu-Me)THF]_2$.¹⁹ This structure is distinguished from the monomeric structures obtained with $\kappa^2-\eta^5-\{HC(PZ^{Me_2})_2(Ph_2CC_5H_4)\}MgR$ (PZ^{Me_2} = 3,5-dimethylpyrazolyl; R = CH_2SiMe_3 , *t*Bu),²⁰ although a number of cyclopentadienyl magnesium piano-stool compounds have been crystallographically characterized to contain monohapto to pentahapto coordination modes, including $(\eta^1-C_5H_5)(\eta^5-C_5H_5)MgTHF_2$.²¹

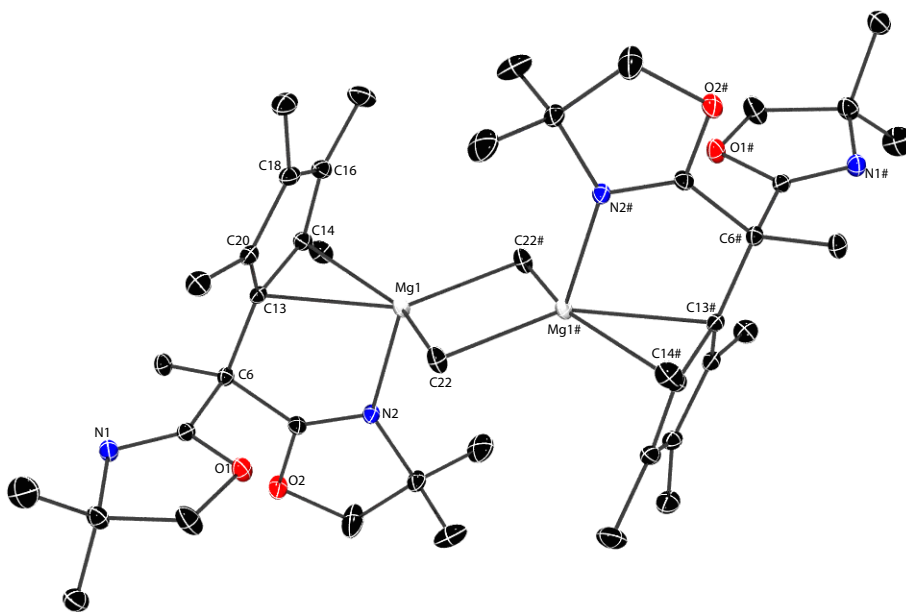


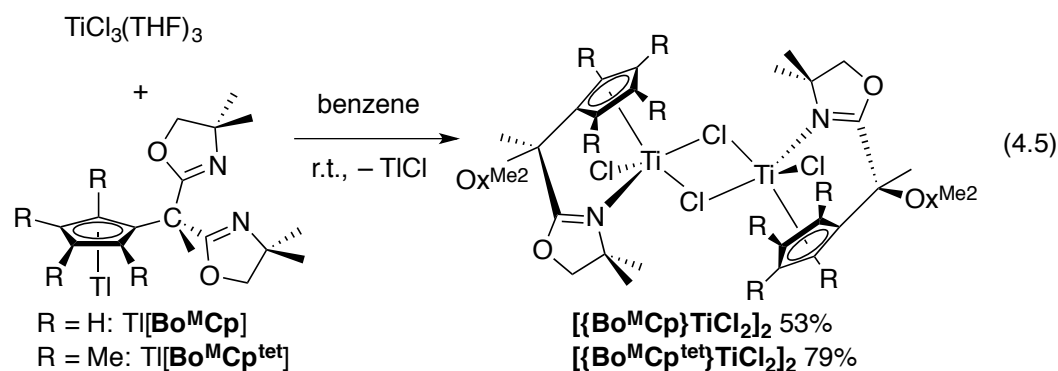
Figure 4.2. Rendered thermal ellipsoid plot of $[\{Bo^{M}Cp^{tet}\}MgMe]_2$ at 35% probability. H atoms are not included in the representation. Atoms marked with # are crystallographic symmetry generated positions. Selected interatomic distances (Å): Mg1–C22, 2.267(2); Mg1–

C22#, 2.271(2); Mg1-N2, 2.214(1); Mg1-C13, 2.284(2); Mg1-C14, 2.400(2); Mg1-C16, 2.681(2); Mg1-C18, 2.821(2); Mg1-C20, 2.658(2); C13-C14, 1.437(2); C14-C16, 1.412(2); C16-C18, 1.404(2); C18-C20, 1.410(2), C13-C20, 1.421(2).

Notably, the solid-state IR spectrum of amorphous material suggests equivalent oxazolines. Therefore, crystallized $\{\text{Bo}^{\text{M}}\text{Cp}^{\text{tet}}\}\text{MgMe}$ was subjected to IR analysis, which revealed two ν_{CN} peaks at 1657 and 1628 cm^{-1} . The two bands in this spectrum are consistent with expectations based on the X-ray diffraction study, with the lower energy band assigned to the coordinated oxazoline.

The solution-phase structure might involve formation of a dimeric species, so the diffusion rate was measured by ^1H DOSY experiments and compared to known monomeric magnesium species. The diffusion constant for $\{\text{Bo}^{\text{M}}\text{Cp}^{\text{tet}}\}\text{MgMe}$ (392.25 amu as a monomer) is $7.9 \times 10^{-10} \text{ m}^2/\text{s}$ (at 23.5 mM), whereas the diffusion constants of monomeric $\text{To}^{\text{M}}\text{MgSi}(\text{SiHMe}_2)_3$ (611.29 amu) and $\text{To}^{\text{M}}\text{MgMe}$ (421.24 amu) are 6.95×10^{-10} and $8.5 \times 10^{-10} \text{ m}^2/\text{s}$,²² respectively. The value of $\{\text{Bo}^{\text{M}}\text{Cp}^{\text{tet}}\}\text{MgMe}$ is between these two compounds, suggesting an averaged molecular weight of rapidly exchanging monomer and dimers.

Group 4 $\{\text{Bo}^{\text{M}}\text{Cp}\}\text{M}$ and $\{\text{Bo}^{\text{M}}\text{Cp}^{\text{tet}}\}\text{M}$ ($\text{M} = \text{Ti, Zr}$) Compounds. The reactions of $\text{TiCl}_3(\text{THF})_3$ with $\text{Bo}^{\text{M}}\text{CpTi}$ or $\text{Bo}^{\text{M}}\text{Cp}^{\text{tet}}\text{Ti}$ provide paramagnetic $[\{\text{Bo}^{\text{M}}\text{Cp}\}\text{TiCl}(\mu\text{-Cl})_2]$ or $[\{\text{Bo}^{\text{M}}\text{Cp}^{\text{tet}}\}\text{TiCl}(\mu\text{-Cl})_2]$ (eq 4.5).



The infrared spectrum of $[\{\text{Bo}^{\text{M}}\text{Cp}\}\text{TiCl}(\mu\text{-Cl})]_2$ acquired in a KBr matrix contained two signals at 1662 and 1635 cm^{-1} , which were assigned to CN stretching modes of non-coordinated and coordinated oxazoline groups. Similarly, the infrared spectrum of $[\{\text{Bo}^{\text{M}}\text{Cp}^{\text{tet}}\}\text{TiCl}(\mu\text{-Cl})]_2$ contained ν_{CN} bands at 1661 and 1641 cm^{-1} . The structures of these two compounds were assigned based on the correspondence of the IR data to the dimeric structure of $[\{\text{Bo}^{\text{M}}\text{Cp}\}\text{TiCl}(\mu\text{-Cl})]_2$ indicated by a single-crystal X-ray diffraction study (see below) and EPR data.

Although the ^1H NMR signals appeared in the typical region at 0–7 ppm, the spectra of $[\{\text{Bo}^{\text{M}}\text{Cp}\}\text{TiCl}(\mu\text{-Cl})]_2$ or $[\{\text{Bo}^{\text{M}}\text{Cp}^{\text{tet}}\}\text{TiCl}(\mu\text{-Cl})]_2$ were not initially useful for assigning structure or monitoring reaction progress because of the d1 Ti(III) centers. The ^1H NMR spectrum of $[\{\text{Bo}^{\text{M}}\text{Cp}\}\text{TiCl}(\mu\text{-Cl})]_2$ contained three broad aliphatic resonances at 0.5, 0.8, and 1 ppm likely from methyl groups present in the $\text{Bo}^{\text{M}}\text{Cp}$ ligand, and these were the most intense signals in the spectrum. Cyclopentadienyl signals were barely detected. In the ^1H NMR spectrum of $[\{\text{Bo}^{\text{M}}\text{Cp}^{\text{tet}}\}\text{TiCl}(\mu\text{-Cl})]_2$, ca. 20 signals at 0.5–2.0 ppm were observed. Despite the complex spectrum, multiple preparations provided reproducible ^1H NMR spectra with these signals assigned to methyl groups in C_5Me_4 and Ox^{Me_2} moieties. All these signals were weak with respect to the residual benzene- d_6 signal, but unlike monomeric Cp^*TiCl , these methyl signals are not paramagnetically shifted.²³ In addition, we note that carbon combustion analyses were consistently lower than expected, although hydrogen and nitrogen match calculated values.

The room-temperature magnetic susceptibility values (measured by Evan's method) were $1.60 \mu_{\text{B}}$ ($0.886 e^-$) and $1.25 \mu_{\text{B}}$ ($0.69 e^-$) per Ti center. Electron paramagnetic resonance (EPR) experiments on point samples measured at room temperature provided g-values of

1.98 and 1.99 for $[\{\text{Bo}^{\text{M}}\text{Cp}\}\text{TiCl}(\mu\text{-Cl})]_2$ and $\{\text{Bo}^{\text{M}}\text{Cp}^{\text{tet}}\}\text{TiCl}(\mu\text{-Cl})_2$, respectively. Moreover, EPR spectra of glassed 9 mM toluene solutions of $[\{\text{Bo}^{\text{M}}\text{Cp}\}\text{TiCl}(\mu\text{-Cl})]_2$ and $[\{\text{Bo}^{\text{M}}\text{Cp}^{\text{tet}}\}\text{TiCl}(\mu\text{-Cl})]_2$ measured at 10 K contained a signal at half-field that indicated the presence of a triplet diradical in the samples. The triplet signal is also observed for $(\text{Cp}_2\text{TiCl})_2$,²⁴ and that compound also exhibits weak antiferromagnetic coupling of the two d1 Ti(III) centers.²⁵ Thus, the EPR spectrum provides additional evidence for dimeric structures of the two titanium(III) compounds. In contrast, the triplet EPR signal was not observed in glassed 2-methyltetrahydrofuran at 10 K.

X-ray-quality crystals of $[\{\text{Bo}^{\text{M}}\text{Cp}\}\text{TiCl}(\mu\text{-Cl})]_2$ were obtained from a toluene/pentane solution cooled at $-30\text{ }^\circ\text{C}$ (Figure 4.3). The compound crystallizes as a dimer with each Ti coordinated in a four-legged piano-stool geometry, with two bridging chloride ligands, a terminal chloride, the cyclopentadienyl group, and one oxazoline ligand. The two $\{\text{Bo}^{\text{M}}\text{Cp}\}\text{Ti}$ groups in the dimer are related by a crystallographically imposed inversion center. The Ti–Ti distance is 3.844(2) Å, which is slightly smaller than the distances of 3.943(2) and 3.926(3) Å in $[\text{Cp}_2\text{Ti}(\mu\text{-Cl})]_2$ and $[(\text{C}_5\text{H}_4\text{Me})_2\text{Ti}(\mu\text{-Cl})]_2$.²⁵ Only one oxazoline ring coordinates per titanium center, and a similar pentahapto-monodentate coordination is observed for the zirconium compound $\{\text{Bo}^{\text{M}}\text{Cp}\}\text{Zr}(\text{NMe}_2)_3$ described below.

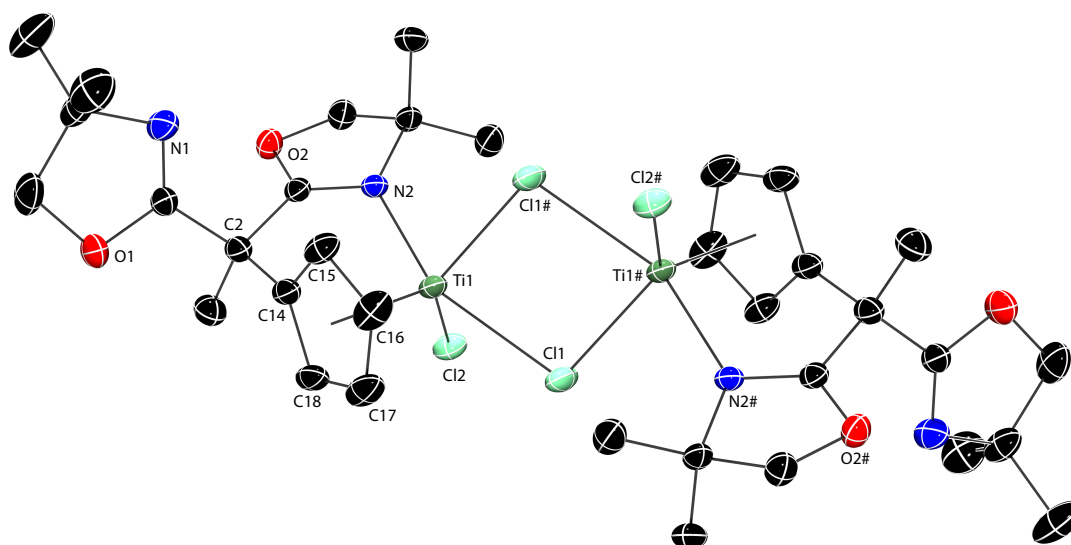
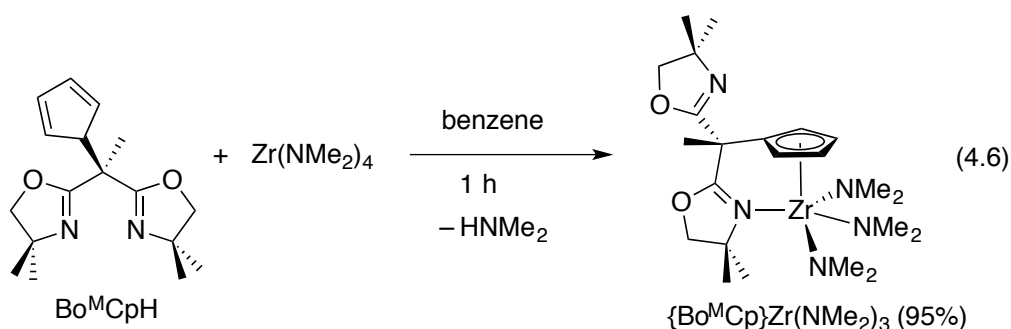


Figure 4.3. Rendered thermal ellipsoid plot of $[\{\text{Bo}^{\text{M}}\text{Cp}\}\text{TiCl}(\mu\text{-Cl})]_2$. Ellipsoids are plotted at 35% probability, and H atoms are not illustrated for clarity. Selected interatomic distances (Å): Ti1–Cl1, 2.435(1); Ti1–Cl1#, 2.570(1); Ti1–Cl2, 2.366(1); Ti1–N2, 2.238(2); Ti1–C14, 2.328(3); Ti1–C15, 2.312(4); Ti1–C16, 2.339(4); Ti1–C17, 2.396(4); Ti1–C18, 2.404(4); Ti1–Ti1#, 3.844(2); C14–C15, 1.429(5); C15–C16, 1.415(4); C16–C17, 1.424(6); C17–C18, 1.393(6); C18–C14, 1.418(4).

The terminal Ti1–Cl2 is the shortest distance (2.366(1) Å) of the three Ti–Cl bonds, and the two bridging Ti1–Cl1–Ti1# interactions have inequivalent Ti–Cl distances (Ti1–Cl1, 2.435(1); Ti1–Cl1#, 2.570(1) Å). The unequal bridging Ti–Cl distances also contrast the molecular structures of $[\text{Cp}_2\text{Ti}(\mu\text{-Cl})]_2$ and $[(\text{C}_5\text{H}_4\text{Me})_2\text{Ti}(\mu\text{-Cl})]_2$, which contain similar internal distances (e.g., in the latter, Ti–Cl = 2.566(2), 2.526(2), 2.535(2), and 2.562(2) Å).

The reaction of $\text{Bo}^{\text{M}}\text{CpH}$ and $\text{Zr}(\text{NMe}_2)_4$ in benzene at room temperature yields $\{\text{Bo}^{\text{M}}\text{Cp}\}\text{Zr}(\text{NMe}_2)_3$ with the loss of dimethylamine (eq 4.6). However, $\text{Bo}^{\text{M}}\text{Cp}^{\text{tet}}\text{H}$ does not

react with $\text{Zr}(\text{NMe}_2)_4$ in benzene or THF, even at elevated temperatures up to 120 °C over 2 days.



A ^1H NMR spectrum of a micromolar-scale reaction showed that $\{\text{Bo}^{\text{M}}\text{Cp}\}\text{Zr}(\text{NMe}_2)_3$ forms within 10 min at room temperature. A singlet resonance at 3.08 ppm (18 H) in the ^1H NMR spectrum was assigned to the apparently equivalent NMe_2 groups. In addition, one set of oxazoline signals, with two signals corresponding to inequivalent methyl and two doublets assigned to diastereotopic methylenes, was observed in the spectrum acquired at room temperature. At -70 °C, the oxazolines were inequivalent and revealed four methyl resonances. Four cyclopentadienyl signals also appeared. The NMe_2 signal broadened from its sharp nature at room temperature to a broad signal that overlapped with oxazoline methylene signals at -78 °C. Thus, at room temperature, the coordinated and noncoordinated oxazolines exchange rapidly. The exchange process is slowed at low temperature, while a second process that affects the NMe_2 on the order of the ^1H NMR time scale occurs at -78 °C.

As in the magnesium compounds described above, the νCN features in the infrared spectra varied between solution phase, amorphous material obtained from fast evaporation of solvent, and crystalline material. In benzene solution, two bands at 1659 and 1641 cm^{-1} were observed, while amorphous material (in a KBr matrix) provided a spectrum with only one νCN at 1646 cm^{-1} . $\{\text{Bo}^{\text{M}}\text{Cp}\}\text{Zr}(\text{NMe}_2)_3$ that was crystallized from a mixture of

pentane and toluene provided an IR spectrum that contained two bands at 1657 and 1636 cm^{-1} . In spectra from the crystal or solution-phase samples, the low-energy band was assigned to coordinated oxazoline, and the high-energy stretch was assigned to a noncoordinated group. Presumably, both oxazolines are coordinated in the amorphous material.

A single-crystal X-ray diffraction study of $\{\text{Bo}^{\text{M}}\text{Cp}\}\text{Zr}(\text{NMe}_2)_3$ showed one coordinated and one noncoordinated oxazoline. The zirconium center adopts a four-legged pianostool geometry, an open site *trans* to the cyclopentadienyl group. The Zr1-N1 distance of 2.536(1) Å is significantly longer than the distances to the amides (Zr1-N3, 2.071(2); Zr1-N4, 2.092(1); Zr1-N5, 2.101(2) Å).

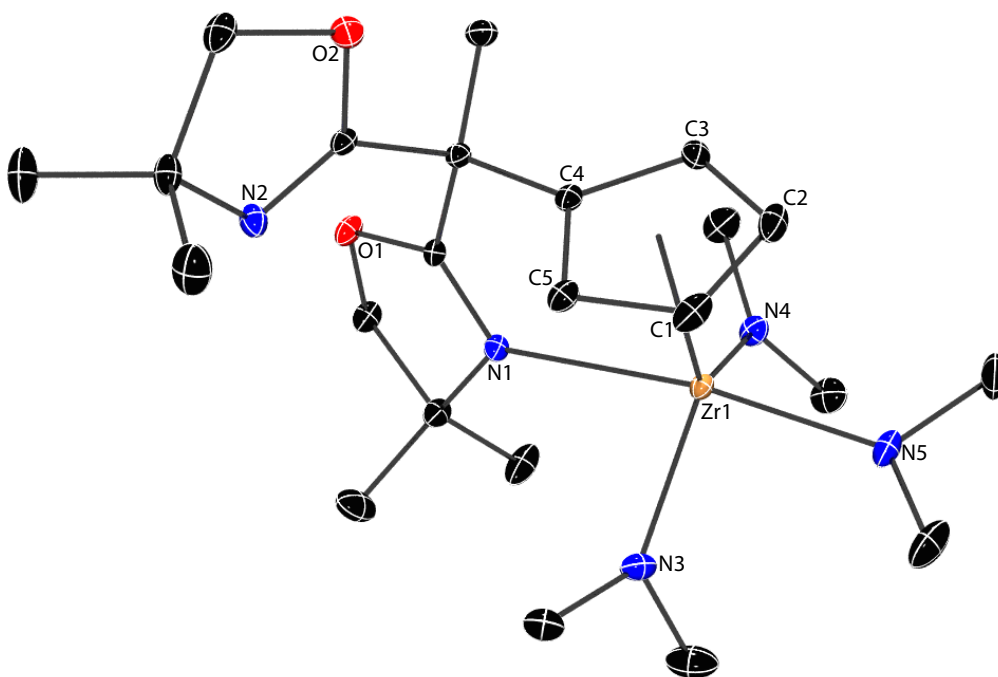


Figure 4.4. Rendered thermal ellipsoid plot of $\text{Bo}^{\text{M}}\text{CpZr}(\text{NMe}_2)_3$. H atoms are not depicted for clarity. Selected interatomic distances (Å): Zr1-C1, 2.573(2); Zr1-C2, 2.580(2); Zr1-C3,

2.617(2); Zr1-C4, 2.641(2); Zr1-C5, 2.599(2); Zr1-N1, 2.536(1); Zr1-N3, 2.071(2); Zr1-N4, 2.092(1); Zr1-N5, 2.101(2). Selected angles (deg): N1-Zr1-N5, 163.36(6), N3-Zr1-N4, 120.40(6).

The cyclopentadienyl is coordinated to zirconium through a pentahapto motif, but the Zr–C distances are not equivalent. Interestingly, the longest Zr–C distance is Zr1-C4, which is the carbon bonded to the bis(oxazoline) moiety. This coordination mode contrasts the bonding to $\{\text{Bo}^{\text{M}}\text{Cp}^{\text{tet}}\}\text{MgMe}$, in which the shortest Mg–C distance involves that carbon. Clearly, there are significant differences between Zr and Mg in terms of polarity and the availability of d orbitals for bonding, and these factors likely affect the cyclopentadienyl coordination. The N1-Zr1-N5 angle ($163.36(6)^\circ$) is larger than the N3-Zr1-N4 angle ($120.40(6)^\circ$), and the more open angle may partly result from constraints imposed by the coordination of cyclopentadienyl and oxazoline donor in a chelate.

The mutually *trans* dimethylamide ligands of N3 and N4 are planar (\sum angles around N3 and N4 are 360°), while the dimethylamide of N5 (pseudo *trans* to the oxazoline) is slightly pyramidalized (\sum angles around N5 are 356°). In addition, the N5 dimethylamide is oriented with both methyls equidistant from the Cp centroid, whereas N3 and N4 dimethylamide planes are roughly orthogonal to the cyclopentadienyl plane.

Catalytic Hydroamination/Cyclization of Aminoalkenes. Catalytic cyclization reactions of aminoalkenes provide an initial test of the reactivity of the magnesium and group 4 compounds supported by these cyclopentadienyl-bis(oxazoline) ligands. These reactions also provide means for comparing reactivity with previously reported $\text{To}^{\text{M}}\text{MgMe}$,^{18a} $\text{To}^{\text{M}}\text{Zr}(\text{NMe}_2)_3$,²⁶ and $\{\text{PhB}(\text{Ox}^{\text{Me}_2})_2\text{Cp}\}\text{Zr}(\text{NMe}_2)_2$,^{4a} as well as the unsubstituted piano-stool

compound $\text{CpZr}(\text{NMe}_2)_3$. It is worth noting that the amide groups in $\text{To}^{\text{M}}\text{Zr}(\text{NMe}_2)_3$ are not readily substituted and that the compound is not a good catalyst for cyclization of aminoalkenes.²⁶ $\text{CpZr}(\text{NMe}_2)_3$ is isoelectronic with $\text{To}^{\text{M}}\text{Zr}(\text{NMe}_2)_3$, but to our knowledge, the former compounds' reactivity in catalytic hydroamination/ cyclization has not previously been described.

Table 4.1. Catalytic hydroamination of aminoalkenes.

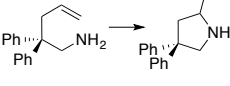
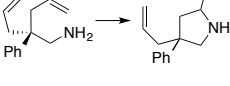
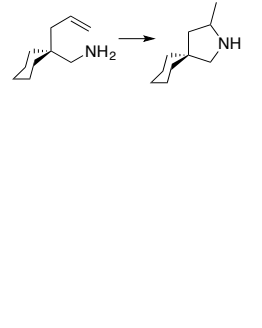
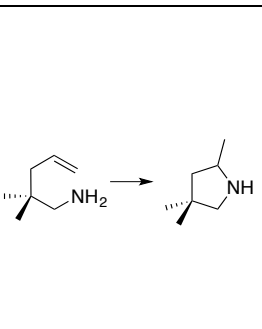
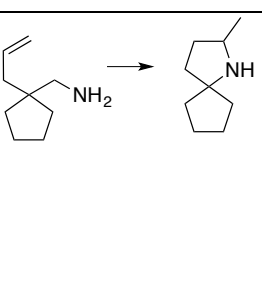
Substrate	Catalyst (10 mol%)	Temp. (°C)	Time (h)	Conv. (%)	N_t	Yield (%) ^c
	$\{\text{Bo}^{\text{M}}\text{Cp}\}\text{MgMe}$	25	0.75	>99	13	95
	$\{\text{Bo}^{\text{M}}\text{Cp}^{\text{tet}}\}\text{MgMe}$	25	1.5	>99	6.7	96
	$\text{To}^{\text{M}}\text{MgMe}^a$	50	12	99	0.83	99 ^d
	$\{\text{Bo}^{\text{M}}\text{Cp}\}\text{Zr}(\text{NMe}_2)_3$	25	36	>99	0.28	86
	$\text{CpZr}(\text{NMe}_2)_3$	25	36	20	0.05	n.a.
	$\text{CpZr}(\text{NMe}_2)_3$	60	20	>99	0.5	80
	$\{\text{Bo}^{\text{M}}\text{Cp}\}\text{Zr}(\text{NMe}_2)_3$	60	2.5	>99	4	86
	$\{\text{PhB}(\text{Ox}^{\text{Me}_2})_2\text{Cp}\}\text{Zr}(\text{NMe}_2)_2^b$	23	11	90	0.8	84
	$\{\text{Bo}^{\text{M}}\text{Cp}\}\text{MgMe}$	25	2	>99	5	95
	$\{\text{Bo}^{\text{M}}\text{Cp}^{\text{tet}}\}\text{MgMe}$	25	2	>99	5	94
	$\{\text{Bo}^{\text{M}}\text{Cp}\}\text{Zr}(\text{NMe}_2)_3$	25	42	>99	0.2	88
	$\text{CpZr}(\text{NMe}_2)_3$	25	42	20	0.05	n.a.
	$\text{CpZr}(\text{NMe}_2)_3$	60	24	>99	0.4	82
	$\{\text{Bo}^{\text{M}}\text{Cp}\}\text{Zr}(\text{NMe}_2)_3$	60	3	>99	3.3	88

Table 4.1. Continued

	$\{\text{Bo}^{\text{M}}\text{Cp}\}\text{MgMe}$	25	2	>99	5	94
	$\{\text{Bo}^{\text{M}}\text{Cp}^{\text{tet}}\}\text{MgMe}$	25	1.5	>99	6.7	94
	$\text{To}^{\text{M}}\text{MgMe}^a$	50	15	>99	0.67	99 ^d
	$\{\text{Bo}^{\text{M}}\text{Cp}\}\text{Zr}(\text{NMe}_2)_3$	25	36	>99	0.28	88
	$\{\text{PhB}(\text{Ox}^{\text{Me}_2})_2\text{Cp}\}\text{Zr}(\text{NMe}_2)_2^b$	23	11	92	0.84	87
	$\{\text{Bo}^{\text{M}}\text{Cp}\}\text{MgMe}$	25	12	12	0.1	10 ^d
	$\{\text{Bo}^{\text{M}}\text{Cp}^{\text{tet}}\}\text{MgMe}$	80	1.5	50	3.3	46 ^d
	$\text{To}^{\text{M}}\text{MgMe}^a$	50	72	20	0.03	20 ^d
	$\{\text{Bo}^{\text{M}}\text{Cp}\}\text{Zr}(\text{NMe}_2)_3$	60	12	50	0.4	41 ^d
	$\{\text{PhB}(\text{Ox}^{\text{Me}_2})_2\text{Cp}\}\text{Zr}(\text{NMe}_2)_2^b$	23	11	85	0.8	85
	$\{\text{Bo}^{\text{M}}\text{Cp}\}\text{MgMe}$	25	2	>99	5	95
	$\{\text{Bo}^{\text{M}}\text{Cp}^{\text{tet}}\}\text{MgMe}$	25	2	>99	5	97
	$\{\text{Bo}^{\text{M}}\text{Cp}\}\text{Zr}(\text{NMe}_2)_3$	25	36	>99	0.3	87
	$\{\text{PhB}(\text{Ox}^{\text{Me}_2})_2\text{Cp}\}\text{Zr}(\text{NMe}_2)_2^b$	23	11	87	0.8	80

^a See reference 16a. ^b See reference 4a. ^c Isolated yield. ^d NMR yield.

$\{\text{Bo}^{\text{M}}\text{Cp}\}\text{MgMe}$, $\{\text{Bo}^{\text{M}}\text{Cp}^{\text{tet}}\}\text{MgMe}$, and $\{\text{Bo}^{\text{M}}\text{Cp}\}\text{Zr}(\text{NMe}_2)_3$ are precatalysts for the cyclization of aminoalkenes to heterocyclic amines as reported in Table 4.1. Upon addition of primary amines to the magnesium methyl or zirconium dimethylamide compounds, methane or dimethylamine is observed, indicating that a metal amide is formed. Comparison of Mg and Zr catalysts with the same ancillary ligand shows that magnesium catalysts are generally more reactive than zirconium, i.e., $\text{To}^{\text{M}}\text{MgMe} > \text{To}^{\text{M}}\text{Zr}(\text{NMe}_2)_3$ and $\{\text{Bo}^{\text{M}}\text{Cp}\}\text{MgMe} > \{\text{Bo}^{\text{M}}\text{Cp}\}\text{Zr}(\text{NMe}_2)_3$. In the magnesium series, relative reaction rates

show $\{\text{Bo}^{\text{M}}\text{Cp}\}\text{MgMe} \sim \{\text{Bo}^{\text{M}}\text{Cp}\}\text{MgMe} > \text{To}^{\text{M}}\text{MgMe}$ as catalysts for aminoalkene cyclization. Notably, both $\{\text{Bo}^{\text{M}}\text{Cp}\}\text{MgMe}$ and $\{\text{Bo}^{\text{M}}\text{Cp}^{\text{tet}}\}\text{MgMe}$ readily afford pyrrolidine at room temperature. The diastereoselectivity for cyclization of amino dialkene by $\{\text{Bo}^{\text{M}}\text{Cp}\}\text{MgMe}$ or $\{\text{Bo}^{\text{M}}\text{Cp}^{\text{tet}}\}\text{MgMe}$ is 1:1.

In the zirconium series, the relative reactivity follows the trend $\{\text{PhB}(\text{Ox}^{\text{Me}_2})_2\text{Cp}\}\text{Zr}(\text{NMe}_2)_2 > \{\text{Bo}^{\text{M}}\text{Cp}\}\text{Zr}(\text{NMe}_2)_3 > \text{CpZr}(\text{NMe}_2)_3 \gg \text{To}^{\text{M}}\text{Zr}(\text{NMe}_2)_3$. At room temperature under equivalent conditions, the turnover rate for cyclization to 2-methyl-4,4-diphenylpyrrolidine by $\{\text{Bo}^{\text{M}}\text{Cp}\}\text{Zr}(\text{NMe}_2)_3$ is approximately $5\times$ faster than $\text{CpZr}(\text{NMe}_2)_3$ but $3\times$ slower than $\{\text{PhB}(\text{Ox}^{\text{Me}_2})_2\text{Cp}\}\text{Zr}(\text{NMe}_2)_3$. Although $\text{CpZr}(\text{NMe}_2)_3$ is the least reactive of the cyclopentadienyl-coordinated precatalysts, catalytic conversion is observed at room temperature. This activity is perhaps surprising given the few examples of zirconium complexes that catalyze hydroamination/cyclization at room temperature. For example, the N_t for constrained-geometry $\{\text{Me}_2\text{Si}(\text{C}_5\text{R}_4)\text{NR}'\}\text{ZrMe}_2$ is 0.07 h^{-1} at $100 \text{ }^\circ\text{C}$ in a conversion that gives 4,4-dimethyl-2-methylpyrrolidine, whereas the N_t for $\{\text{Bo}^{\text{M}}\text{Cp}\}\text{Zr}(\text{NMe}_2)_3$ is 0.4 h^{-1} at $60 \text{ }^\circ\text{C}$. Interestingly, a slightly faster conversion is catalyzed by $\{\text{Me}_2\text{Si}(\text{C}_5\text{R}_4)\text{NR}'\}\text{ZrCl}(\text{NMe}_2)$ with an N_t of 0.14 h^{-1} at $100 \text{ }^\circ\text{C}$.⁵ As noted above, $\text{To}^{\text{M}}\text{Zr}(\text{NMe}_2)_3$, which is isoelectronic with $\text{CpZr}(\text{NMe}_2)_3$, is not a catalyst for cyclization of aminoalkenes, and this inactivity may relate to its six-coordinate zirconium center and substitutionally inert coordination sphere.

Conclusions:

These new monoanionic cyclopentadienyl-bis(oxazoline) ligands provide chelating piano-stool compounds of Ti, Mg, Ti, and Zr. The syntheses of the ligands described here employ

the combination of electrophilic cyclopentadienyl derivatives with nucleophilic, stabilized bis(oxazoline) carbanions. This cyclopentadienyl ligand construction is opposite to the synthesis of ansa-type dimethylsilyl-bis(cyclopentadiene) or constrained geometry-type dimethylsilyl-cyclopentadiene-amido ligands that employ nucleophilic cyclopentadienide derivatives that react with electrophilic silicon centers.^{3b} Likewise, the synthesis of the optically active dianionic cyclopentadienyl-bis(oxazoliny)borate ligands $[\text{PhB}(\text{Ox}^{\text{R}})_2\text{C}_5\text{H}_4]^{2-}$ involves the reaction of cyclopentadienide nucleophile NaC_5H_5 and electrophilic borane $\text{PhB}(\text{Ox}^{\text{R}})_2$.^{4a-c} Here, we have shown that reversing the electrophilic and nucleophilic components in this alternative synthetic approach has some generality in terms of varying steric properties on the cyclopentadienyl group. The synthetic approach, then, lends itself to a range of combinations through the variation of groups on the cyclopentadienyl ring as well as the substituents on the oxazoline ring. Because oxazolines are readily prepared in enantiopure chiral form with a number of substituents in the 4 and 5 positions, optically active piano-stool compounds may readily be prepared for application in asymmetric catalysis, including hydroamination. We are currently synthesizing a range of derivatives of this ligand class. Moreover, this approach may be generally useful for the synthesis of cyclopentadienyl ligands with new substitution patterns and substituents derived from nucleophiles rather than electrophiles.

In this context, it is interesting to note that the combination of the bis(oxazoline) and cyclopentadienyl ligands on zirconium gives more reactive catalytic species than the oxazoline-free $\text{CpZr}(\text{NMe}_2)_3$ catalyst precursor. We are not aware of prior studies of the parent piano-stool compound $\text{CpZr}(\text{NMe}_2)_3$ as a catalyst for cyclization of aminoalkenes, and this compound is surprisingly reactive under catalytic conditions. In contrast, the compound

To^MZr(NMe₂)₃,²⁴ which is isoelectronic with CpZr(NMe₂)₃, is inert toward substitution of dimethylamide groups by amines and is not an active catalyst for hydroamination/cyclization. That is, the introduction of oxazoline donors does not inherently enhance the reactivity of dimethylamido zirconium sites in hydroamination. However, the combination of cyclopentadienyl and oxazoline ligands on zirconium leads to more reactive catalytic sites than parent cyclopentadienyl or tris(oxazolinyl)borate ligands. Moreover, the comparison of zwitterionic borate complex {PhB(Ox^{Me2})₂Cp}Zr(NMe₂)₂ with {Bo^MCp}Zr(NMe₂)₃ reveals that the divalent ancillary ligand gives more reactive zirconium sites. We are continuing to study and compare these ligand classes in catalytic chemistry to further discover systematic trends of reactivity and selectivity.

Experimental

General. All reactions were performed under a dry argon atmosphere using standard Schlenk techniques or under a nitrogen atmosphere in a glovebox, unless otherwise indicated. Dry, oxygen-free solvents were used throughout. Benzene, toluene, pentane, methylene chloride, diethyl ether and tetrahydrofuran were degassed by sparging with nitrogen, filtered through activated alumina columns, and stored under nitrogen. Benzene-*d*₆, toluene-*d*₈ and tetrahydrofuran-*d*₈ were heated to reflux over Na/K alloy and vacuum-transferred. Anhydrous TiCl₃(THF)₃ and TiOEt were purchased from Aldrich and used as received. HCMe(Ox^{Me2})₂,²⁵ MgMe₂(diox)₂,²⁶ Zr(NMe₂)₄,²⁷ TiC₅H₅,²⁸ C₅Me₄H₂,²⁹ Bo^MCp^{tet}H,¹² 2,2-diphenyl-4-penten-1-amine,³⁰ 2,2-dimethyl-4-penten-1-amine,³¹ (1-allylcyclohexyl)methylamine,³² and C-(1-allyl-cyclopentyl)-methylamine³² were prepared according to the literature. ¹H and ¹³C{¹H} NMR spectra were collected either on a Bruker DRX-400 spectrometer, Bruker Avance III 600 spectrometer, or an Agilent MR 400

spectrometer. ^{15}N chemical shifts were determined by ^1H - ^{15}N HMBC experiments on a Bruker Avance III 600 spectrometer. ^{15}N chemical shifts were originally referenced to liquid NH_3 and recalculated to the CH_3NO_2 chemical shift scale by adding -381.9 ppm.

$\text{MeC}(\text{Ox}^{\text{Me}_2})_2\text{Li}$. $\text{HCMe}(\text{Ox}^{\text{Me}_2})_2$ (2.000 g, 8.92 mmol) was dissolved in pentane (50 mL), the solution was cooled -78 °C, and $n\text{BuLi}$ in hexane (9.0 mmol, 3.6 mL) was added. The mixture was stirred at this temperature for 2 h, and then the solution was warmed to room temperature and stirred for 12 h. The solvent was removed by filtration, and the solid product was washed with pentane (50 mL). Evaporation of residual solvent under reduced pressure provided white solid $\text{MeC}(\text{Ox}^{\text{Me}_2})_2\text{Li}$ in good yield (1.912 g, 8.3 mmol, 93%). ^1H NMR ($\text{THF-}d_8$, 600 MHz): δ 3.59 (s, 4 H, $\text{CNCMe}_2\text{CH}_2\text{O}$), 1.69 (s, 3 H, $\text{MeC}(\text{Ox}^{\text{Me}_2})_2$), 1.13 (s, 12 H, $\text{CNCMe}_2\text{CH}_2\text{O}$). $^{13}\text{C}\{^1\text{H}\}$ NMR ($\text{THF-}d_8$, 151 MHz): δ 170.51 ($\text{CNCMe}_2\text{CH}_2\text{O}$), 77.84 ($\text{CNCMe}_2\text{CH}_2\text{O}$), 65.39 ($\text{CNCMe}_2\text{CH}_2\text{O}$), 57.01 ($\text{MeC}(\text{Ox}^{\text{Me}_2})_2$), 30.04 ($\text{CNCMe}_2\text{CH}_2\text{O}$), 12.41 ($\text{MeC}(\text{Ox}^{\text{Me}_2})_2$). $^{15}\text{N}\{^1\text{H}\}$ NMR ($\text{THF-}d_8$, 61 MHz): δ -211.3 ($\text{CNCMe}_2\text{CH}_2\text{O}$). IR (KBr , cm^{-1}): 2964 s, 2928 m, 2867 m, 1671 w, 1615 s, 1590 s, 1543 m, 1509 s, 1460 m, 1397 m, 1361 m, 1293 m, 1245 w, 1189 m, 1070 m, 1019 s, 980 m, 922 w, 828 w, 767 w, 732 w. Anal. Calcd for $\text{C}_{12}\text{H}_{19}\text{LiN}_2\text{O}_2$: C, 62.6; H, 8.32; N, 12.17. Found C, 62.29; H, 8.55; N, 12.06.

$\text{Bo}^{\text{M}}\text{CpH}$. $\text{Ti}[\text{C}_5\text{H}_5]$ (1.44 g, 5.35 mmol) was slurried in benzene (10 mL) in a 100 mL Schlenk flask. The flask was fitted with an addition funnel, and the solution was cooled to 12 °C using a dioxane/dry ice bath. A solution of iodine (1.24 g, 4.86 mmol) in benzene (50 mL) was added to the slurry in a dropwise fashion over 1.5 h while maintaining the temperature at 12 °C to form a cloudy yellow solution of $\text{C}_5\text{H}_5\text{I}$. $\text{MeC}(\text{Ox}^{\text{Me}_2})_2\text{Li}$ (1.12 g, 4.86 mmol) dissolved in THF (20 mL) was added to the iodocyclopentadiene mixture via cannula. The

solution was then warmed to room temperature and stirred overnight. The solution was filtered in air, and the solvent was evaporated on a rotovapor at 100 mTorr. The crude oily product was purified by silica gel chromatography in ethyl acetate to give a brown oil, which was dissolved in benzene and stirred over phosphorus pentoxide for 6 h to remove any water. The solution was filtered and the solvent was removed under reduced pressure to provide brown, oily $\text{Bo}^{\text{M}}\text{CpH}$ as a mixture of two isomers (0.789 g, 2.753 mmol, 57%). ^1H NMR (benzene- d_6 , 600 MHz): δ 7.04 (m, 1 H, $\text{H}_2\text{C}_5\text{H}_3$), 6.58 (s, 1 H, $\text{H}_2\text{C}_5\text{H}_3$), 6.41 (m, 1 H, $\text{H}_2\text{C}_5\text{H}_3$), 6.35 (m, 2 H, $\text{H}_2\text{C}_5\text{H}_3$), 6.31 (m, 1 H, $\text{H}_2\text{C}_5\text{H}_3$), 3.66-3.58 (m, 8 H, $\text{CNCMe}_2\text{CH}_2\text{O}$), 3.46 (s, 2 H, $\text{H}_2\text{C}_5\text{H}_3$), 2.73 (s, 2 H, $\text{H}_2\text{C}_5\text{H}_3$), 2.10 (s, 3 H, $\text{MeC}(\text{Ox}^{\text{Me}_2})_2$), 2.04 (s, 3 H, $\text{MeC}(\text{Ox}^{\text{Me}_2})_2$), 1.11 (v t, 24 H, $\text{CNCMe}_2\text{CH}_2\text{O}$). $^{13}\text{C}\{^1\text{H}\}$ NMR (benzene- d_6 , 151 MHz, two isomers observed): δ 166.56 ($\text{CNCMe}_2\text{CH}_2\text{O}$), 166.23 ($\text{CNCMe}_2\text{CH}_2\text{O}$), 148.24 ($\text{H}_2\text{C}_5\text{H}_3$), 147.17 ($\text{H}_2\text{C}_5\text{H}_3$), 135.26 ($\text{H}_2\text{C}_5\text{H}_3$), 133.46 ($\text{H}_2\text{C}_5\text{H}_3$), 132.55 ($\text{H}_2\text{C}_5\text{H}_3$), 132.18 ($\text{H}_2\text{C}_5\text{H}_3$), 129.60 ($\text{H}_2\text{C}_5\text{H}_3$), 128.92 ($\text{H}_2\text{C}_5\text{H}_3$), 79.55 ($\text{CNCMe}_2\text{CH}_2\text{O}$), 79.53 ($\text{CNCMe}_2\text{CH}_2\text{O}$), 67.72 ($\text{CNCMe}_2\text{CH}_2\text{O}$), 67.66 ($\text{CNCMe}_2\text{CH}_2\text{O}$), 45.31 ($\text{H}_2\text{C}_5\text{H}_3$), 44.68 ($\text{H}_2\text{C}_5\text{H}_3$), 43.21 ($\text{MeC}(\text{Ox}^{\text{Me}_2})_2$), 41.42 ($\text{MeC}(\text{Ox}^{\text{Me}_2})_2$), 28.60 ($\text{CNCMe}_2\text{CH}_2\text{O}$), 28.55 ($\text{CNCMe}_2\text{CH}_2\text{O}$), 28.51 ($\text{CNCMe}_2\text{CH}_2\text{O}$), 24.48 ($\text{MeC}(\text{Ox}^{\text{Me}_2})_2$), 23.83 ($\text{MeC}(\text{Ox}^{\text{Me}_2})_2$). ^{15}N NMR (benzene- d_6 , 61 MHz): δ -132.5 ($\text{CNCMe}_2\text{CH}_2\text{O}$). IR (KBr, cm^{-1}): 2968 s, 2930 m, 2890 m, 1656 s (C=N), 1462 m, 1364 m, 1286 m, 1249 w, 1193 m, 1084 m, 974 m, 933 w, 900 w, 732 w. Anal. Calcd for $\text{C}_{17}\text{H}_{24}\text{N}_2\text{O}_2$: C, 70.80; H, 8.39; N, 9.71. Found: C, 70.30; H, 8.78; N, 9.69.

$\text{Bo}^{\text{M}}\text{Cp}^{\text{tet}}\text{H}$.¹² A 500 mL Schlenk flask was charged with 2,3,4,5-tetramethylcyclopentadienyllithium (1.12 g, 8.74 mmol). Dry pentane (400 mL) was added, and the mixture was cooled to -78 °C. Solid iodine (2.21 g, 8.73 mmol) was added to the flask. The mixture was stirred at -78 °C for 8 h and then was warmed to -20 °C and stirred

for 12 h until all LiC_5Me_4 reacted. Over the course of the reaction, the solution turned dark yellow, and the mixture gave a white precipitate. $\text{MeC}(\text{Ox}^{\text{Me}_2})_2\text{Li}$ (2.00 g, 8.73 mmol) was placed in a 100 mL Schlenk flask and dissolved in THF (30 mL). The THF solution was added via cannula to the pentane mixture at $-20\text{ }^\circ\text{C}$. The solution was warmed to room temperature and was stirred for 8 h. The reaction mixture was then filtered in air, and the solvent was removed using a rotovapor. The crude oily product was purified by silica gel chromatography in ethyl acetate to give the product as a white solid (2.04 g, 5.90 mmol, 68%). The solid was dissolved in benzene and dried over with phosphorus pentoxide for 6 h. Crystallization from pentane at $-35\text{ }^\circ\text{C}$ gave X-ray quality crystals. ^1H NMR (benzene- d_6 , 600 MHz): δ 4.17 (s, 1 H, CHMe_4), 3.74 (d, 2 H, $^2J_{\text{HH}} = 8.1\text{ Hz}$, $\text{CNCMe}_2\text{CH}_2\text{O}$), 3.65 (d, 2 H, $^2J_{\text{HH}} = 8.1\text{ Hz}$, $\text{CNCMe}_2\text{CH}_2\text{O}$), 1.95 (s, 6 H, C_5HMe_4), 1.70 (s, 6 H, C_5HMe_4), 1.61 (s, 3 H, $\text{MeC}(\text{Ox}^{\text{Me}_2})_2$), 1.17 (s, 6 H, $\text{CNCMe}_2\text{CH}_2\text{O}$), 1.13 (s, 6 H, $\text{CNCMe}_2\text{CH}_2\text{O}$). $^{13}\text{C}\{^1\text{H}\}$ NMR (benzene- d_6 , 151 MHz): δ 166.88 ($\text{CNCMe}_2\text{CH}_2\text{O}$), 138.22 (C_5HMe_4), 134.43 (C_5HMe_4), 79.45 ($\text{CNCMe}_2\text{CH}_2\text{O}$), 67.62 ($\text{CNCMe}_2\text{CH}_2\text{O}$), 59.80 (C_5HMe_4), 44.35 ($\text{MeC}(\text{Ox}^{\text{Me}_2})_2$), 29.05 ($\text{CNCMe}_2\text{CH}_2\text{O}$), 28.08 ($\text{CNCMe}_2\text{CH}_2\text{O}$), 16.41 ($\text{MeC}(\text{Ox}^{\text{Me}_2})_2$), 14.20 (C_5HMe_4), 11.67 (C_5HMe_4). ^{15}N NMR (benzene- d_6 , 61 MHz): δ -131.2 ($\text{CNCMe}_2\text{CH}_2\text{O}$). IR (KBr, cm^{-1}): 3287 w, 3010 m, 2963 s, 2930 s, 2890 s, 2860 s, 2734 w, 1661 s (C=N), 1640 m (C=N), 1463 s, 1446 s, 1376 s, 1363 m, 1346 m, 1301 m, 1253 m, 1195 m, 1170 m, 1094 m, 1068 m, 1036 m, 1011 m, 994 m, 975 s, 945 s, 926 m, 892 w, 852 m, 769 m, 733 w, 654 s, 615 w. Anal. Calcd for $\text{C}_{21}\text{H}_{32}\text{N}_2\text{O}_2$: C, 73.22; H, 9.36; N, 8.13. Found: C, 73.16; H, 9.31; N, 8.12. mp 109–111 $^\circ\text{C}$.

$\text{Bo}^{\text{M}}\text{CpTi}$. $\text{Bo}^{\text{M}}\text{CpH}$ (0.375 g, 1.31 mmol) was dissolved in diethyl ether. Thallium ethoxide (102 μL , 1.44 mmol) was added, and brown precipitate immediately formed. The solution

was stirred at room temperature for 2 h. The mixture was centrifuged, and the solvent was decanted. The solid was washed with pentane (3×) and was then extracted with benzene, filtered, and dried under reduced pressure to give the product as a brown solid (0.537 g, 1.09 mmol, 83%). ^1H NMR (benzene- d_6 , 600 MHz): δ 6.56 (s, 2 H, C_5H_4), 6.29 (s, 2 H, C_5H_4), 3.65 (d, 2 H, $^2J_{\text{HH}} = 8$ Hz, $\text{CNCMe}_2\text{CH}_2\text{O}$), 3.59 (d, 2 H, $^2J_{\text{HH}} = 8$ Hz, $\text{CNCMe}_2\text{CH}_2\text{O}$), 2.14 (s, 3 H, $\text{MeC}(\text{Ox}^{\text{Me}_2})_2$), 1.03 (s, 6 H, $\text{CNCMe}_2\text{CH}_2\text{O}$), 1.01 (s, 6 H, $\text{CNCMe}_2\text{CH}_2\text{O}$). $^{13}\text{C}\{^1\text{H}\}$ NMR (benzene- d_6 , 151 MHz): δ 170.92 ($\text{CNCMe}_2\text{CH}_2\text{O}$), 124.22 (C_5H_4), 107.90 (C_5H_4), 107.52 (C_5H_4), 80.14 ($\text{CNCMe}_2\text{CH}_2\text{O}$), 67.31 ($\text{CNCMe}_2\text{CH}_2\text{O}$), 44.21 ($\text{MeC}(\text{Ox}^{\text{Me}_2})_2$), 28.46 ($\text{CNCMe}_2\text{CH}_2\text{O}$), 28.39 ($\text{CNCMe}_2\text{CH}_2\text{O}$), 25.17 ($\text{MeC}(\text{Ox}^{\text{Me}_2})_2$). ^{15}N NMR (benzene- d_6 , 61 MHz): δ -130 ($\text{CNCMe}_2\text{CH}_2\text{O}$). IR (KBr, cm^{-1}): 3075 m, 2966 s, 2930 m, 2887 s, 1647 s (C=N), 1463 m, 1383 w, 1365 m, 1349 w, 1276 m, 1248 m, 1200 m, 1080 s, 1042 vw, 1028 w, 975 m. Anal. Calcd for $\text{C}_{17}\text{H}_{23}\text{N}_2\text{O}_2\text{Ti}$: C, 41.52; H, 4.71; N, 5.70. Found: C, 41.14; H, 4.61; N, 5.67. mp 168–171 °C, dec.

Bo^MCp^{tet}Ti. TIOEt (84.9 μL , 1.20 mmol) was added to a THF solution of Bo^MCp^{tet}H (0.377 g, 1.09 mmol), and the reaction mixture was stirred at room temperature for 10 days. The volatile materials were evaporated, and the solid was washed with pentane (3×). The residue was extracted with benzene and dried under reduced pressure to give the product as a green solid (0.512 g, 0.933 mmol, 85.5%). ^1H NMR (benzene- d_6 , 600 MHz): δ 3.65 (d, $^2J_{\text{HH}} = 8.1$ Hz, 2 H, $\text{CNCMe}_2\text{CH}_2\text{O}$), 3.63 (d, $^2J_{\text{HH}} = 8.1$ Hz, 2 H, $\text{CNCMe}_2\text{CH}_2\text{O}$), 2.36 (s, 6 H, C_5Me_4), 2.24 (s, 6 H, C_5Me_4), 2.20 (s, 3 H, $\text{MeC}(\text{Ox}^{\text{Me}_2})_2$), 1.11 (s, 6 H, $\text{CNCMe}_2\text{CH}_2\text{O}$), 1.10 (s, 6 H, $\text{CNCMe}_2\text{CH}_2\text{O}$). $^{13}\text{C}\{^1\text{H}\}$ NMR (benzene- d_6 , 151 MHz): δ 170.23 ($\text{CNCMe}_2\text{CH}_2\text{O}$), 115.94 (C_5Me_4), 114.8 (C_5Me_4), 114.1 (br, C_5Me_4), 79.83 ($\text{CNCMe}_2\text{CH}_2\text{O}$), 67.62 ($\text{CNCMe}_2\text{CH}_2\text{O}$), 46.53 ($\text{MeC}(\text{Ox}^{\text{Me}_2})_2$), 28.76 ($\text{CNCMe}_2\text{CH}_2\text{O}$), 28.26 ($\text{CNCMe}_2\text{CH}_2\text{O}$),

26.65 ($\text{MeC}(\text{Ox}^{\text{Me}_2})_2$), 12.63 (d, $J_{\text{TIC}} = 57.4$ Hz, C_5Me_4), 11.14 (d, $J_{\text{TIC}} = 44.8$ Hz, C_5Me_4). ^{15}N NMR (benzene- d_6 , 61 MHz): δ -128.1 ($\text{CNCMe}_2\text{CH}_2\text{O}$). IR (KBr, cm^{-1}): 2971 s, 2961 m, 2923 m, 2889 m, 2855 m, 1654 m (C=N), 1637 s (C=N), 1457 w, 1381 m, 1362 w, 1343 w, 1267 m, 1246 m, 1194 m, 1091 m, 1075 m, 1042 w, 993 m, 973 m, 936 w, 897 w. Anal. Calcd for $\text{C}_{21}\text{H}_{31}\text{N}_2\text{O}_2\text{Ti}$: C, 46.04; H, 5.70; N, 5.11. Found: C, 46.21; H, 5.79; N, 5.06. mp 162-164 °C (dec).

{Bo^MCp}MgMe. $\text{MgMe}_2(\text{dioxane})_2$ (0.049 g, 0.230 mmol) was added to a benzene solution of $\text{Bo}^{\text{M}}\text{CpH}$ (0.066 g, 0.230 mmol), and the reaction mixture was stirred at room temperature for 1.5 h. Gas formation was observed over the course of the reaction. The solution was filtered, and the filtrate was evaporated under reduced pressure to give a pink oil. The oil was washed with pentane (3×) and dried under reduced pressure to give a white solid that was stored at -30 °C (0.051 g, 0.157 mmol, 68.3%). Exhaustive evaporation to remove residual dioxane and diethyl ether gives broad spectra, and data given here contains residual ethers, the 2C and magnesium methyl signals were not detected in the $^{13}\text{C}\{^1\text{H}\}$ NMR spectrum or through 2D correlation spectroscopy, and C analysis were systematically lower than calculated values. ^1H NMR (benzene- d_6 , 600 MHz): δ 6.44 (s, 2 H, C_5H_4), 6.33 (s, 2 H, C_5H_4), 3.66 (d, 2 H, $^2J_{\text{HH}} = 8.1$ Hz, $\text{CNCMe}_2\text{CH}_2\text{O}$), 3.55 (d, 2 H, $^2J_{\text{HH}} = 8.1$ Hz, $\text{CNCMe}_2\text{CH}_2\text{O}$), 2.06 (s, 3 H, $\text{MeC}(\text{Ox}^{\text{Me}_2})_2$), 1.16 (6 H, $\text{CNCMe}_2\text{CH}_2\text{O}$), 1.13 (6 H, $\text{CNCMe}_2\text{CH}_2\text{O}$), -0.05 (br s, MgMe). $^{13}\text{C}\{^1\text{H}\}$ NMR (benzene- d_6 , 151 MHz): δ 118.46 (C_5H_4), 108.54 (C_5H_4), 102.46 (C_5H_4), 81.16 ($\text{CNCMe}_2\text{CH}_2\text{O}$), 66.94 ($\text{CNCMe}_2\text{CH}_2\text{O}$), 44.89 ($\text{MeC}(\text{Ox}^{\text{Me}_2})_2$), 28.29 ($\text{CNCMe}_2\text{CH}_2\text{O}$), 28.22 ($\text{CNCMe}_2\text{CH}_2\text{O}$), 22.20 ($\text{MeC}(\text{Ox}^{\text{Me}_2})_2$). ^{15}N NMR (benzene- d_6 , 61 MHz): δ -147.4 ($\text{CNCMe}_2\text{CH}_2\text{O}$). IR (KBr, cm^{-1}): 2968 s, 2931 m, 2897 m, 1658 s (C=N), 1547 w, 1463 m, 1366 m, 1309 w, 1292 w, 1255 w, 1202 w, 1192

m, 1084 s sh, 1041 s, 974 w, 960 w, 934 w, 874 m, 809 w, 750 m. Anal. Calcd for $C_{18}H_{26}MgN_2O_2$: C, 66.17; H, 8.02; N, 8.57. Found: C, 63.34; H, 7.61; N, 8.67. mp 145–147 °C, dec.

$\{Bo^M Cp^{tet}\}MgMe$. A benzene solution of $Bo^M Cp^{tet}H$ (0.129 g, 0.373 mmol) was allowed to react with $MgMe_2(dioxane)_2$ (0.080 g, 0.373 mmol) at room temperature for 4 h. Gas formation was observed over the course of the reaction. The reaction mixture was filtered and evaporated to dryness under reduced pressure to give a yellow oil. The oil was washed with pentane (3×) and dried under reduced pressure to give a white solid that was stored at -30 °C (0.110 g, 0.286 mmol, 76.9%). 1H NMR (600 MHz, benzene- d_6): 3.70 (d, 2 H, $^2J = 8.3$ Hz, $CNCMe_2CH_2O$), 3.58 (d, 2 H, $^2J = 8.3$ Hz, $CNCMe_2CH_2O$), 2.33 (s, 6 H, C_5Me_4), 2.24 (s, 6 H, C_5Me_4), 2.11 (s, 3 H, $MeC(Ox^{Me_2})_2$), 1.08 (s, 6 H, $CNCMe_2CH_2O$), 1.05 (s, 6 H, $CNCMe_2CH_2O$), -0.91 (s, 3 H, $MgMe$). $^{13}C\{^1H\}$ NMR (151 MHz, benzene- d_6): δ 173.8 ($CNCMe_2CH_2O$), 113.66 (C_5Me_4), 108.19 (C_5Me_4), 107.47 (C_5Me_4), 80.81 ($CNCMe_2CH_2O$), 66.51 ($CNCMe_2CH_2O$), 46.69 ($MeC(Ox^{Me_2})_2$), 28.61 ($CNCMe_2CH_2O$), 27.73 ($CNCMe_2CH_2O$), 24.11 ($MeC(Ox^{Me_2})_2$), 14.01 (C_5Me_4), 11.97 (C_5Me_4), -10.84 ($MgMe$). ^{15}N NMR (benzene- d_6 , 61 MHz): δ -145.7 ($CNCMe_2CH_2O$). IR (powdered sample, KBr, cm^{-1}): 2996 s, 2928 s, 2866 s, 2726 w sh, 1658 s (C=N), 1496 m, 1467 m, 1304 m, 1306 m, 1283 m, 1252 m, 1192 m, 1087 m, 1024 w, 991 w, 974 m, 962 m, 934 m, 893 w, 829 w. IR (crystallized sample, KBr, cm^{-1}): 2966 s, 2928 s, 2897 s, 2867 s, 1657 s, 1627 s, 1462 m, 1365 m, 1307 m, 1253 w, 1190 m, 1088 s, 1024 w, 961 m, 935 m, 831 w. Anal. Calcd for $C_{22}H_{34}MgN_2O_2$: C, 69.02; H, 8.95; N, 6.95. Found: C, 67.48; H, 9.35; N, 6.95. mp 145–146 °C, dec.

{Bo^MCp}TiCl₂. TiCl₃(THF)₃ (0.194 g, 0.523 mmol) was dissolved in benzene (10 mL) and added to a benzene solution of Bo^MCpTi (0.257 g, 0.523 mmol) to produce a cloudy green solution. The reaction mixture was stirred for 8 h. The solution was filtered, and the filtrate was evaporated to dryness under reduced pressure to give a brown solid. The solid was recrystallized at -30 °C in a mixture of toluene and pentane to give green, paramagnetic X-ray quality crystals (0.113 g, 0.278 mmol, 53.1%). IR (KBr, cm⁻¹): 3117 w, 2970 m, 1662 s (C=N), 1635 s (C=N), 1461 m, 1368 s, 1323 s, 1290 m, 1258 m, 1190 m, 1109 s, 1090 s, 1050 w, 1036 w, 982 s, 960 s, 935 m, 874 w, 822 s 808 s, 773 w. Anal. Calcd for C₁₇H₂₃Cl₂N₂O₂Ti: C, 50.27; H, 5.71; N, 6.90. Found: C, 49.92; H, 5.64; N, 6.84. mp 140–142 °C, dec.

Magnetic susceptibility was measured using Evan's method at room temperature using a Bruker 400 MHz NMR spectrometer. A sample of Bo^MCpTiCl₂ (5.7 mg, 0.014 mmol) was dissolved in benzene-*d*₆ (0.90 mL) to give a 15.6 mM solution. The solution (0.60 mL) was placed in an NMR tube. A capillary was charged with benzene-*d*₆ and placed in the NMR tube. The ¹H NMR spectrum showed a paramagnetic shift in the benzene-*d*₆ peak. Using Evan's method, the following values were obtained: Δδ = 0.070 ppm, χ_{mol} = 1.07 × 10⁻³ cm³/mol, μ = 1.60 μ_B, n = 0.885 electrons. The data is consistent with a d¹ Ti(III) complex.

{Bo^MCp^{tet}}TiCl₂. TiCl₃(THF)₃ (0.071 g, 0.192 mmol) was dissolved in benzene (5 mL) and added to a benzene solution of Bo^MCp^{tet}Ti (0.257 g, 0.523 mmol) resulting in a cloudy green solution. The reaction mixture was stirred for 18 h. The solution was filtered, and the filtrate was evaporated to dryness under reduced pressure. The solid was then extracted with benzene and dried under reduced pressure to give a green solid (0.070 g, 0.151 mmol, 79%). IR (KBr, cm⁻¹): 2964 s, 2927 m, 2871 w, 1661 m sh (C=N), 1641 s (C=N), 1570 w, 1463 m,

1366 m, 1322 m, 1285 w, 1253 w, 1190 m, 1170 m, 1096 m, 1029 w, 973 m, 956 m, 935 w, 832 w. $n = 0.69$ by Evan's method. Anal. Calcd for $C_{21}H_{31}Cl_2N_2O_2Ti$: C, 54.56; H, 6.76; N, 6.06. Found: C, 53.82; H, 6.75; N, 5.84. mp 141–143 °C, dec.

$\{Bo^M Cp\}Zr(NMe_2)_3$. Benzene solutions of $Bo^M CpH$ (0.100 g, 0.347 mmol) and $Zr(NMe_2)_4$ (0.093 g, 0.347 mmol) were mixed, allowed to stir for 1 h at room temperature, and then filtered. Evaporation of the filtrate to dryness under reduced pressure provided a yellow gel that was washed with pentane (3×5 mL). Further drying under vacuum yielded $\{Bo^M Cp\}Zr(NMe_2)_3$ as a yellow, analytically pure solid (0.168 g, 0.329 mmol, 94.9%). X-ray quality single crystals were obtained from a toluene and pentane solution of the product at -30 °C. 1H NMR (600 MHz, benzene- d_6): 6.24 (t, 2 H, $^3J_{HH} = 2.2$ Hz, C_5H_4), 6.20 (t, 2 H, $^3J_{HH} = 2.2$ Hz, C_5H_4), 3.63 (d, 2 H, $^2J_{HH} = 8.1$ Hz, $CNCMe_2CH_2O$), 3.52 (d, 2 H, $^2J_{HH} = 8.1$ Hz, $CNCMe_2CH_2O$), 3.09 (s, 18 H, NMe_2), 1.92 (s, 3 H, $MeC(Ox^{Me_2})_2$), 1.02 (s, 6 H, $CNCMe_2CH_2O$), 0.97 (s, 6 H, $CNCMe_2CH_2O$). $^{13}C\{^1H\}$ NMR (151 MHz, benzene- d_6): δ 170.42 ($CNCMe_2CH_2O$), 126.30 (*ipso*- C_5H_4), 109.36 (C_5H_4), 108.98 (C_5H_4), 80.73 ($CNCMe_2CH_2O$), 67.81 ($CNCMe_2CH_2O$), 47.36 (NMe_2), 43.92 ($MeC(Ox^{Me_2})_2$), 27.33 ($CNCMe_2CH_2O$), 27.03 ($CNCMe_2CH_2O$), 22.42 ($MeC(Ox^{Me_2})_2$). ^{15}N NMR (benzene- d_6 , 61 MHz): δ -138 ($CNCMe_2CH_2O$); $Zr(NMe_2)_3$ was not detected. IR (KBr, cm^{-1} , amorphous solid): 2965 s, 2930 m, 2890 m, 2865 m, 2819 m, 2759 m, 2736 m, 1645 s (C=N), 1460 m, 1364 m, 1314 m, 1288 m, 1235 m, 1203 m, 1139 s, 1122 m, 1102 m, 1083 m, 1046 s, 975 s, 957 m, 938 m, 875 m, 786 s, 715 m, 712 s. Anal. Calcd. for $C_{23}H_{41}N_5O_2Zr$: C, 54.08; H, 8.09; N, 13.71. Found: C, 53.63; H, 7.57; N, 13.30. mp 129–132 °C.

General procedure for catalytic hydroamination.

Micromolar-scale catalysis. In a typical small-scale hydroamination experiment, a J. Young style NMR tube was charged with 100 μmol of aminoalkene substrate, 10 μmol of catalyst, and 0.5 mL of solvent (benzene- d_6). The J. Young tube was sealed with a Teflon valve, and the reaction progress was monitored by ^1H NMR spectroscopy at regular intervals to determine the conversion.

Scaled up hydroamination catalysis. A Schlenk flask was charged with the catalyst $\{\text{Bo}^{\text{M}}\text{Cp}\}\text{MX}$ or $\{\text{Bo}^{\text{M}}\text{Cp}^{\text{tet}}\}\text{MX}$ (0.200 mmol), the appropriate aminoalkene (2.00 mmol), and benzene (10 mL). The solution was stirred for 4 h to 48 h at room temperature. The products were isolated by evaporation of the solvent and purified using flash column chromatography (silica gel, $\text{CH}_2\text{Cl}_2:\text{MeOH} = 9.5:0.5$).

References:

1. (a) Fryzuk, M. D.; Mao, S. S. H.; Zaworotko, M. J.; MacGillivray, L. R. *J. Am. Chem. Soc.* **1993**, *115*, 5336–7. (b) Hirotsu, M.; Fontaine, P. P.; Epshteyn, A.; Sita, L. R. *J. Am. Chem. Soc.* **2007**, *129*, 9284–9285. (c) Hirotsu, M.; Fontaine, P. P.; Zavalij, P. Y.; Sita, L. R. *J. Am. Chem. Soc.* **2007**, *129*, 12690–12692. (d) Shima, T.; Hu, S.; Luo, G.; Kang, X.; Luo, Y.; Hou, Z. *Science* **2013**, *340*, 1549–1552.
2. (a) Arndt, S.; Okuda, J. *Chem. Rev.* **2002**, *102*, 1953–1976. (b) Gibson, V. C.; Spitzmesser, S. K. *Chem. Rev.* **2002**, *103*, 283–316.
3. (a) Okuda, J. *Chem. Ber.* **1990**, *123*, 1649–1651. (b) Shapiro, P. J.; Bunel, E.; Schaefer, W. P.; Bercaw, J. E. *Organometallics* **1990**, *9*, 867–869. (c) Stevens, J. C. InsiteTM Catalysts Structure/Activity Relationships for Olefin Polymerization. In *Catalyst Design for Tailor-Made Polyolefins: Proceedings of the International Symposium on Catalyst Design for Tailor-Made Polyolefins*; Kanazawa, March 10–12, 1994, Soga, K.; Terano, M., Eds.; Elsevier: Tokyo, 1994; Vol. 89, pp 277–284. (d) Chen, Y.-X.; Marks, T. J. *Organometallics* **1997**, *16*, 3649–3657.
4. (a) Manna, K.; Ellern, A.; Sadow, A. D. *Chem. Commun.* **2010**, *46*, 339–341. (b) Manna, K.; Kruse, M. L.; Sadow, A. D. *ACS Catal.* **2011**, *1*, 1637–1642. (c) Manna, K.; Xu, S.; Sadow, A. D. *Angew. Chem., Int. Ed.* **2011**, *50*, 1865–1868. (d) Manna, K.; Everett, W. C.; Schoendorff, G.; Ellern, A.; Windus, T. L.; Sadow, A. D. *J. Am. Chem. Soc.* **2013**, *135*, 7235–72504.
5. Stubbert, B. D.; Marks, T. J. *J. Am. Chem. Soc.* **2007**, *129*, 6149–6167

6. Tian, S.; Arredondo, V. M.; Stern, C. L.; Marks, T. J. *Organometallics* **1999**, *18*, 2568–2570.
7. (a) Hangaly, N. K.; Petrov, A. R.; Rufanov, K. A.; Harms, K.; Elfferding, M.; Sundermeyer, J. *Organometallics* **2011**, *30*, 4544–4554. (b) Otero, A.; Lara-Sánchez, A.; Najera, C.; Fernández-Baeza, J.; Mañriquez-Segovia, I.; Castro-Osma, J. A.; Martínez, J.; Sánchez-Barba, L. F.; Rodríguez, A. M. *Organometallics* **2012**, *31*, 2244–2255
8. Bertolasi, V.; Boaretto, R.; Chierotti, M. R.; Gobetto, R.; Sostero, S. *Dalton Trans.* **2007**, 5179–5189.
9. Rufanov, K. A.; Petrov, A. R.; Kotov, V. V.; Laquai, F.; Sundermeyer, J. *Eur. J. Inorg. Chem.* **2005**, 3805–3807.
10. (a) Otero, A.; Fernandez-Baeza, J.; Antinolo, A.; Tejada, J.; Lara-Sanchez, A.; Sanchez-Barba, L.; Rodriguez, A. M.; Maestro, M. A. *J. Am. Chem. Soc.* **2004**, *126*, 1330–1331. (b) Otero, A.; Fernandez-Baeza, J.; Antinolo, A.; Tejada, J.; Lara-Sanchez, A.; Sanchez-Barba, L. F.; Sanchez-Molina, M.; Rodriguez, A. M.; Bo, C.; Urbano-Cuadrado, M. *Organometallics* **2007**, *26*, 4310–4320.
11. Breslow, R.; Canary, J. W. *J. Am. Chem. Soc.* **1991**, *113*, 3950–3952.
12. (a) Gade, L. H.; Bellemin-Laponnaz, S. *Chem. - Eur. J.* **2008**, *14*, 4142–4152. (b) Bellemin-Laponnaz, S.; Gade, L. H. *Chem. Commun.* **2002**, 1286–1287.
13. Liao, S.; Sun, X.-L.; Tang, Y. *Acc. Chem. Res.* **2014**, *47*, 2260–2272.
14. Lampland, N. L.; Zhu, J.; Hovey, M.; Jana, B.; Ellern, A.; Sadow, A. D. *Inorg. Chem.* **2015**, *54*, 6938–6946.
15. Bauer, A.; Hilbig, H.; Hiller, W.; Hinterschwepfinger, E.; Köhler, F. H.; Neumayer, M. *Synthesis* **2001**, 778–782.
16. Werner, H.; Otto, H.; Kraus, H. J. *J. Organomet. Chem.* **1986**, *315*, C57–C60.
17. Pawlikowski, A. V.; Gray, T. S.; Schoendorff, G.; Baird, B.; Ellern, A.; Windus, T. L.; Sadow, A. D. *Inorg. Chim. Acta* **2009**, *362*, 4517–4525.
18. (a) Dunne, J. F.; Fulton, D. B.; Ellern, A.; Sadow, A. D. *J. Am. Chem. Soc.* **2010**, *132*, 17680–17683. (b) Mukherjee, D.; Ellern, A.; Sadow, A. D. *Chem. Sci.* **2014**, *5*, 959–964. (c) Sibi, M. P.; Shay, J. J.; Liu, M.; Jasperse, C. P. *J. Am. Chem. Soc.* **1998**, *120*, 6615–6616.
19. Westerhausen, M.; Makropoulos, N.; Wieneke, B.; Karaghiosoff, K.; Nöth, H.; Schwenk-Kircher, H.; Knizek, J.; Seifert, T. *Eur. J. Inorg. Chem.* **1998**, 965–971.
20. Garceś, A.; Sánchez-Barba, L. F.; Alonso-Moreno, C.; Fajardo, M.; Fernández-Baeza, J.; Otero, A.; Lara-Sánchez, A.; López-Solera, I.; Rodríguez, A. M. *Inorg. Chem.* **2010**, *49*, 2859–2871.
21. Jaenschke, A.; Paap, J.; Behrens, U. *Organometallics* **2003**, *22*, 1167–1169.
22. Mukherjee, D.; Lampland, N. L.; Yan, K.; Dunne, J. F.; Ellern, A.; Sadow, A. D. *Chem. Commun.* **2013**, *49*, 4334–4336.
23. Pattiasina, J. W.; Heeres, H. J.; Van Bolhuis, F.; Meetsma, A.; Teuben, J. H.; Spek, A. L. *Organometallics* **1987**, *6*, 1004–1010.
24. Samuel, E.; Harrod, J. F.; Gourrier, D.; Dromzee, Y.; Robert, F.; Jeannin, Y. *Inorg. Chem.* **1992**, *31*, 3252–3259.
25. Jungst, R.; Sekutowski, D.; Davis, J.; Luly, M.; Stucky, G. *Inorg. Chem.* **1977**, *16*, 1645–1655.
26. Dunne, J. F.; Su, J.; Ellern, A.; Sadow, A. D. *Organometallics* **2008**, *27*, 2399–2401.

27. Dagonne, S.; Bellemin-Laponnaz, S.; Welter, R. *Organometallics* **2004**, *23*, 3053–3061.
28. Tobia, D.; Baranski, J.; Rickborn, B. *J. Org. Chem.* **1989**, *54*, 4253–4256.
29. Diamond, G. M.; Jordan, R. F.; Petersen, J. L. *J. Am. Chem. Soc.* **1996**, *118*, 8024–8033.
30. Corey, E. J.; Koelliker, U.; Neuffer, J. *J. Am. Chem. Soc.* **1971**, *93*, 1489–1490.
31. Fendrick, C. M.; Schertz, L. D.; Day, V. W.; Marks, T. J. *Organometallics* **1988**, *7*, 1828–1838.
32. Hong, S.; Tian, S.; Metz, M. V.; Marks, T. J. *J. Am. Chem. Soc.* **2003**, *125*, 14768–83.
33. Bender, C. F.; Widenhoefer, R. A. *J. Am. Chem. Soc.* **2005**, *127*, 1070–1071.
34. Riegert, D.; Collin, J.; Meddour, A.; Schulz, E.; Trifonov, A. *J. Org. Chem.* **2006**, *71*, 2514–2517.

CHAPTER 5

**SYNTHESIS AND CHARACTERIZATION OF TRIS(OXAZOLINYL)BORATO
COPPER(II) AND COPPER(I) COMPLEXES**

Naresh Eedugurala, Zhuoran Wang, Arkady Ellern, Marek Pruski, and Aaron D. Sadow

US Department of Energy Ames Laboratory and Department of Chemistry, Ames IA 50011

Abstract. The reaction of $To^M Tl$ (To^M = tris(4,4-dimethyl-2-oxazolinyl)phenylborate) and $CuBr_2$ in benzene at 60 °C provides $To^M CuBr$. NMR, FT-IR, and EPR spectroscopies are used to determine electronic and structural properties of copper(II) compounds and the structures were confirmed by X-ray crystallography. $To^M CuBr$ is a precursor for the new tris(oxazolinyl)phenylborato copper chemistry, $To^M CuOtBu$ and $To^M CuOAc$ were prepared by the reaction of $To^M CuBr$ with $KOtBu$ and $NaOAc$. $To^M CuOtBu$ is transformed into $[To^M CuOH]_2$ dimer through the hydrolysis. Reduction of copper is observed in our attempt to synthesize monomeric copperhydride by treatment of $To^M CuOR$ with phenylsilane. $To^M Cu$ and $To^M_2 Cu$ were independently synthesized and characterized for the comparison.

Introduction

Tris(pyrazolyl)borates (Tp),¹ a family of *fac*-coordinating tripodal monoanionic ligands, are known for stabilizing reactive first row metal complexes, including metal alkyls containing β -hydrogen,^{2,3,4} peroxides and alkyl peroxides, imido,⁵ and hydrides^{6,7} due to their ability to shield the metal center.⁸ Thus, these scorpionates have been studied extensively as models for metal sites in enzymes and in organometallic chemistry,^{1,8,9,10} because the ligand modifications readily influence structural and electronic properties, as well as reactivity, needed to compare with natural systems and develop new catalytic chemistry.¹¹

For example, copper(I) centers coordinated by three imidazole from histidine residues mediate oxygen transport or catalytic oxidations in metalloenzymes and metalloproteins.^{12,13} Tris(pyrazolyl)borate ligands have been used to prepare peroxo dinuclear copper(II) complexes, which show structural similarities to sites in oxyhemocyanin and oxytyrosinase,¹⁴ which form by oxidation of Cu(I) upon O₂ coordination. Both sites must undergo reduction, either by O₂ dissociation in O₂-transport proteins or through chemical means in tyrosinase.

Reduction chemistry, in fact, is common in copper-catalyzed hydrosilylations, in which copper(I) hydride is proposed as the active species.^{15,16} For example, copper(I) hydride complexes related to Stryker's reagent $\{(\text{Ph}_3\text{P})\text{CuH}\}_6$ ^{17,18} which has a range of applications in catalysis such as the conjugative reduction of α,β -unsaturated carbonyl compounds,¹⁹ may be formed by in situ reduction of Cu(II) acetate in the presence of a neutral ligand by an organosilane,²⁰ or by conversion of copper(I) alkoxides to the hydride by hydrogen¹⁷ or silanes.^{21,22,23,24} Notably, copper(II) hydrides, particularly those supported in tetrahedral environments are not isolable species. These species might have a role in hydrosilylation catalysis, or other catalytic processes involving Cu(I)/Cu(II) interconversions.

In contrast, the neighboring tetrahedral zinc hydride congeners are known as isolable scorpionate-supported species,^{25,26,27,28,29} and even as an NHC-supported dihydride.³⁰ Some of these compounds are inert, for example to O₂, and other are highly reactive in catalytic chemistry, such as dehydrocoupling of silanes and alcohols,^{31,26} or hydrosilylation.^{32,33}

We were curious if a similar synthetic strategy could allow the synthesis of a monomeric copper(II) hydride, and whether tetrahedral Cu(II) would allow access to hydrosilylation-type catalysis. On one hand, tris(pyrazolyl)borate copper(I) compounds form multimetallic structures,³⁴ based on the instability of monomeric TpCu that would be forced

to form an unfavorable pyramidal geometry. The multimetallic structures observed with TpCu(I) might be disfavored by the non-planar oxazoline donors of To^M and instead favor Cu(II) complexes. To test this idea, we have attempted to synthesize monomeric copper(II) hydride supported by tris(4,4-dimethyl-2-oxazoliny)phenylborato (To^M) ligand. In this pursuit, we have synthesized $To^M CuX$ ($X = Br, OtBu, OAc$), studied their reactions with silanes, and tested their capabilities to initiate hydrosilylation catalysis.

Results and discussion

Synthesis and reactivity of $To^M CuX$ ($X = Br, OtBu, OAc, OH, To^M$) compounds. The entry-point into tris(4,4-dimethyl-2-oxazoliny)phenylborate copper(II) chemistry, orange colored $To^M CuBr$ (**1**), is prepared through a salt metathesis reaction of $TiTo^M$ and $CuBr_2$ in benzene at 60 °C (eq 5.1). Compound **1** was analyzed by 1H and ^{11}B NMR spectroscopy, IR spectroscopy, X-ray diffraction, elemental analysis, and magnetic measurements through Evans method and EPR spectroscopy (Table 5.1). The signals in the 1H NMR spectrum of **1** were broad as expected for the paramagnetic compound and appeared at 10.39 (6 H, CH_2) and -1.15 ppm (18 H, CH_3) readily assigned to equivalent oxazoline groups. $^{13}C\{^1H\}$ NMR spectroscopy also suggested a C_{3v} symmetric species, based on chemical shifts observed for methylene groups at 265.9 ppm and methyl groups at 21.9 ppm. In addition, the ^{11}B NMR spectrum contained a singlet at -9.6 ppm. Even though ^{11}B NMR spectroscopy is not structurally informative, it proves useful here to count and distinguish paramagnetic and diamagnetic species, as well as to identify formation of new compounds. In the infrared spectrum, a single C=N stretching band was observed at 1590 cm^{-1} (cf. $TiTo^M$: $\nu_{CN} = 1600\text{ cm}^{-1}$). This part of the IR spectrum suggests tridentate coordination of To^M to the copper(II)

center, as non-coordinated oxazoline groups in To^M typically show ν_{CN} bands at 1630 cm^{-1} .

35,36

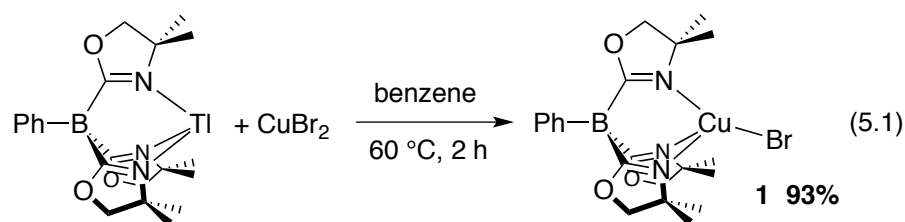
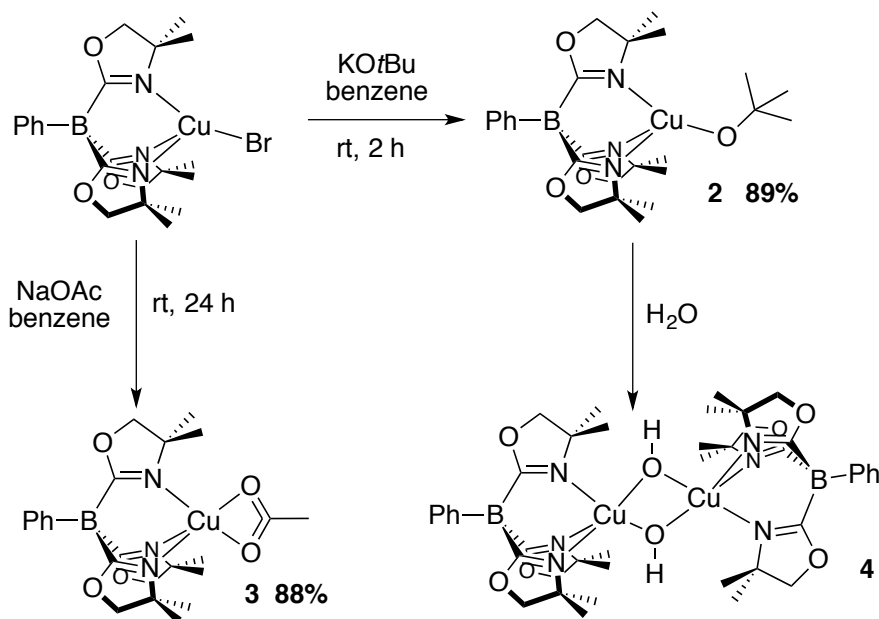


Table 5.1. Spectroscopic data for the copper(I) and copper(II) compounds

Compound	$\nu_{C=N}$ (cm^{-1})	EPR (g)	μ_{eff} (μ_B)	^{15}N (ppm)	^{11}B (ppm)
$To^M\text{CuBr}$	1591	2.40, 2.35, 2.17	1.650	-----	-9.6
$To^M\text{CuOtBu}$	1576	2.37, 2.15	1.922	-----	-15.7
$To^M\text{CuOAc}$	1602, 1527 (ν_{COO})	2.30, 2.08	1.548	-----	-14.8
$[\text{To}^M\text{CuOH}]_2$	1574, 3686(ν_{OH})	2.33, 2.08	-----	-----	-19.3
$To^M_2\text{Cu}$	1604, 1560	2.37, 2.14	1.666	-----	-30.0
$To^M\text{Cu}$	1581	-----	-----	-150.1	-15.9
$To^M\text{ZnBr}$	1596	-----	-----	-161.2	-18.0

Alkoxide and acetate compounds of Cu(I) and Cu(II) are precursors for copper hydrides and are precatalysts for hydrosilylation,^{37,13,38} and $To^M\text{ZnOtBu}$ reacts with organosilanes to give $To^M\text{ZnH}$. Therefore, we targeted $To^M\text{CuOtBu}$ (**2**) and $To^M\text{CuOAc}$ (**3**) as possible precursors to $To^M\text{CuH}$ or as catalyst for hydrosilylation. These complexes are synthesized through salt metathesis reactions of **1** and KOtBu or NaOAc (Scheme 5.1). The

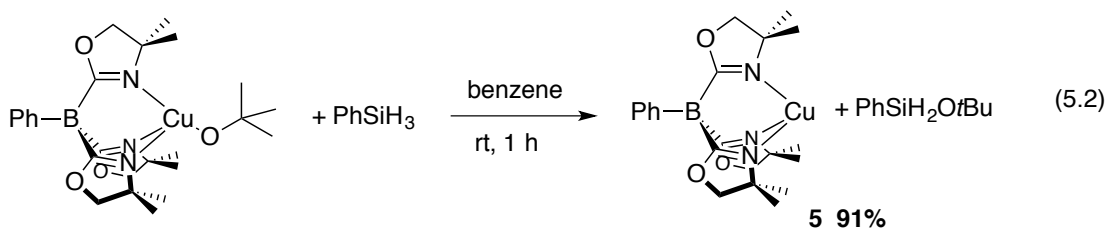
^1H NMR spectrum of **2** contained a characteristic signal at 1.31 ppm (9 H) assigned to the butyl group as well as resonances from the methylene (6.10 ppm, 6 H) and methyl (−0.82 ppm, 18 H) in the To^{M} ligand. Likewise, a ^1H NMR signal at 6.89 ppm was assigned to the acetate in compound **3**. The ^{11}B NMR spectra of **2** and **3** contained singlets at −15.7 and −14.8 ppm, respectively which are upfield compared to **1** and surprisingly close to the range of To^{M} signals in diamagnetic compounds (e.g. the ^{11}B NMR signal for $\text{To}^{\text{M}}\text{ZnBr}$ appeared at −18 ppm). Tripodal coordination of To^{M} was supported by IR bands at 1564 and 1602 cm^{-1} assigned to oxazoline C=N stretching mode in **2** and **3**, respectively. The IR spectrum of **3** also contained signals at 1530 and 1471 cm^{-1} assigned to the acetate group. These signals are similar to those reported for $\text{Tp}^{\text{tBu}}\text{CuOAc}$,³⁹ and in the range expected for bidentate coordinated carboxylates.⁴⁰



Scheme 5.1. Synthesis of $\text{To}^{\text{M}}\text{CuOtBu}$ (**2**) and $\text{To}^{\text{M}}\text{CuOAc}$ (**3**).

Compound **2** is very sensitive to water, and it reacts over days in benzene- d_6 solutions or in the solid state with trace amounts of water to give the green hydroxyl bridged dimeric compound $[\text{To}^{\text{M}}\text{CuOH}]_2$ (**4**). Attempts to impede the hydrolysis with multiply-distilled solvents, surface-silylated, teflon-sealed glassware, and cooling solutions could slow, but not stop the formation of **4**. A ^1H NMR spectrum of **4** in methylene chloride- d_2 revealed signals in the region typical to diamagnetic compounds, at 4.32 ppm (6 H) and 1.55 ppm (18 H), assigned to the methylene and methyl groups on a symmetrical To^{M} ligand. A broad signal at -15.67 ppm was assigned to the bridging hydroxyl group. The ^{11}B NMR spectrum contained a singlet peak at -19.35 ppm. These NMR properties may be rationalized by antiferromagnetic coupling between two Cu(II) centers in a dimeric structure for **4**, which was supported by X-ray diffraction studies (see below). Additional support for the structure of **4** was provided by its infrared spectrum, which contained a band at 1602 cm^{-1} assigned to the the C=N stretching mode of tridentate-coordinated To^{M} , as well as a band at 3682 cm^{-1} assigned to a ν_{OH} .¹⁴

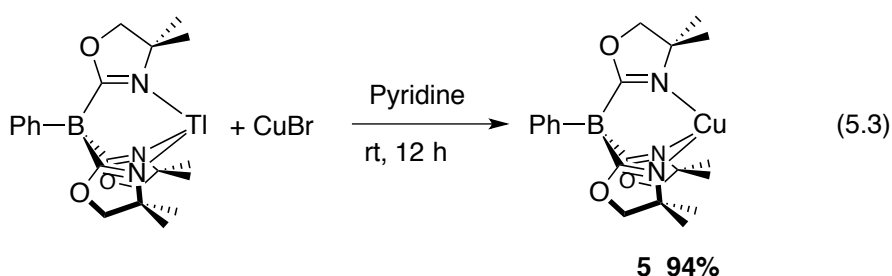
Compounds **2**, **3**, or **4** and the organosilanes PhSiH_3 or PhMeSiH_2 (room temperature or $-78\text{ }^\circ\text{C}$), were allowed to react toward the desired $\text{To}^{\text{M}}\text{CuH}$. $\text{PhSiH}_2(\text{O}t\text{Bu})$ and a light yellow precipitate are formed over 1 h upon addition of PhSiH_3 to **2**. In contrast to the preparation of Stryker's catalyst from $\text{CuCl}/\text{KO}t\text{Bu}$ and H_2 , no reaction observed upon addition of hydrogen (1 atm) to **2** in benzene.



The yellow precipitate (**5**), later identified as $\text{To}^{\text{M}}\text{Cu}$, is insoluble in aliphatic and aromatic

hydrocarbon solvents, tetrahydrofuran, and acetonitrile, but soluble in pyridine. The ^1H and ^{11}B NMR spectra of **5** contained To^{M} signals with typical diamagnetic shifts at 3.78 (6 H, CH_2) and 1.15 ppm (18 H, Me), and at -15.9 ppm, respectively. Interestingly, the solid-state ^{13}C NMR spectrum (see SI) of **5** shows equivalent oxazoline groups based on methylene groups at 76.7 ppm and methyl groups at 27.5 ppm. The infrared spectrum of **5** contained a band at 1582 cm^{-1} ; this and its solubility properties ruled out its identity as compounds **1-4**. The compound $\text{To}^{\text{M}}_2\text{Cu}$ (**6**) was synthesized and characterized for comparison, but its solubility, magnetic properties, and spectroscopy did not match those of **5**. The desired compound $\text{To}^{\text{M}}\text{CuH}$ could exist as a dimeric antiferromagnetically coupled species. While the dimer **4**, showed diamagnetic NMR chemical shifts in solution and a weak EPR signal as a toluene glass, it exhibited a strong EPR signal in 2-methyltetrahydrofuran attributed to formation monomeric Cu(II) species (see below). Thus, its apparent diamagnetic behavior upon dissolution in pyridine seems to conflict with the possibility that **5** is antiferromagnetically-coupled dimeric $(\text{To}^{\text{M}}\text{CuH})_2$.

Instead, we independently prepared $\text{To}^{\text{M}}\text{Cu}$ by the reaction of TiTo^{M} and copper(I) iodide in pyridine (eq 5.3) for comparison with **5**.



The solubility properties, solution-phase NMR data in pyridine- d_5 , infrared spectrum, and elemental analysis data for $\text{To}^{\text{M}}\text{Cu}$ matched those of the material obtained from reaction of **2** and PhSiH_3 . Although mass balance of the reaction of **2** and PhSiH_3 shown in equation 2

implies that two hydrogen atoms should be a byproduct of the reaction, H₂ could not be detected by ¹H NMR spectroscopy nor could the fate of the H be determined. We thought, however, that support for the existence of To^MCuH might be obtained from its in situ generation and trapping in the presence of excess organic carbonyl, or it might be used in situ in a catalytic carbonyl hydrosilylation. However, catalytic hydrosilylation of acetophenone (167 mM) with phenylsilane (185 mM) or phenylmethylsilane(180 mM) in the presence of 10 mol% of **2** (16.7 mM) or **3** (16.7 mM) as precatalysts at room temperature results in precipitation of **5**. Moreover, catalytic addition products were not detected in ¹H NMR spectra of these reaction mixtures. The formation of To^MCu was observed in the experiments to trap To^MCuH with 10 equiv. of acetone or acetophenone upon addition of PhSiH₃ to **2** and no insertion of carbonyl was observed. In the attempt to make the dimethylsulfide adduct To^MCuSMe₂ from the reaction of To^MTl and CuBr.SMe₂ in benzene, To^MCu was precipitated by the dissociation of dimethyl sulfide. No soluble species was observed upon addition of CO (1 atm) gas in benzene. Moreover, addition of CO gas to **5** didn't result in changes to the ¹H NMR in pyridine-*d*₅ and identified no soluble species in benzene-*d*₆. When **5** was exposed to oxygen (1 atm), the solution changed color from yellow to green. As a result, three peaks are observed in the ¹¹B NMR at -15.1 and -19.0 ppm including the starting material at -15.9 ppm. We were unable to detect paramagnetic compounds in the ¹H NMR and ¹¹B NMR. The reaction of oxygen(1 atm) with phenylsilane (185 mM), in the presence of 10 mol% of **5** (18.5 mM) as precatalysts, results in a brown precipitate and no desired product was observed.

X-ray crystallography. Recrystallization of **1** from methylene chloride and pentane provides crystals for a single crystal X-ray diffraction study (Figure 5.1), which shows that $\text{To}^{\text{M}}\text{CuBr}$ is distorted from the pseudo- C_{3v} symmetric structure observed for divalent main group tetra-coordinated tris(oxazolanyl)borate compounds $\{\kappa^3\text{-To}^{\text{M}}\}\text{MX}$ ($\text{M} = \text{Mg}, \text{Zn}$) in a pseudo- C_s coordination sphere.^{28,41} In contrast to the typical “flattening” of a T_d symmetric species into a D_{2d} structure that reduces the values of two dihedral angles from 90° , the three dihedral angles of **1** are $88.13(6)$, $90.02(6)$, and $94.10(6)^\circ$. Instead, a pseudo- C_s symmetric coordination geometry for the Cu center is observed, with the interatomic angle defined by B1-Cu1-Br1 as 160.5° . The N1-Cu1-Br1 angle $142.75(4)^\circ$ is much larger than the N2-Cu1-Br1 and N3-Cu1-Br1 angles of $112.92(4)$ and $112.79(4)^\circ$. That is, the Br is displaced off the pseudo- C_3 axis away from the oxazoline of N1 and wedged between the other two coordinated oxazoline groups (of N2 and N3). The Cu1-N1 distance is $1.937(2) \text{ \AA}$, which is associated with the oxazoline with the most obtuse N-Cu-Br angle, is slightly shorter than the distances (Cu1-N2, $2.081(2)$ and Cu1-N3, $2.000(2) \text{ \AA}$) of the two oxazoline rings coordinated with the narrower N-Cu-Br angles. A related distortion is reported for $\text{Tp}^{t\text{Bu,Me}}\text{CuCl}$ (B-Cu-Cl, 159.3°),⁴² $\text{Tp}^{t\text{Bu},i\text{Pr}}\text{CuCl}$ (162.7°),⁴³ and $\text{Ttz}^{t\text{Bu,Me}}\text{CuCl}$ (B-Cu-Cl, 157.0°),⁴⁴ whereas C_{3v} symmetric structures are reported for $\text{Tp}^{\text{Ph}_2}\text{CuCl}$ (B-Cu-Cl, 180°),⁴⁵ $\text{Tp}^{i\text{Pr}_2}\text{CuCl}$ (B-Cu-Cl, 178.7°),⁴⁶ and $\text{Tp}^{\text{Ad}}\text{CuCl}$ (170.4°).⁴³ Interestingly $\text{MeTp}^{\text{Mes}}\text{CuCl}$ co-crystallizes with two conformers containing B-Cu-Cl angles of 160.1 and 171.1° ,⁴⁷ suggesting relatively small energy changes accompany the distortion. Also for comparison, the B-Zn-Cl angle in $\text{To}^{\text{M}}\text{ZnCl}$ is 174.3° ,²⁸ and the B-Zn-Br angle in $\text{To}^{\text{M}}\text{ZnBr}$ is 174.2° ($\text{To}^{\text{M}}\text{ZnBr}$ is prepared through the reaction of TiTo^{M} with ZnBr_2 in benzene at room temperature).

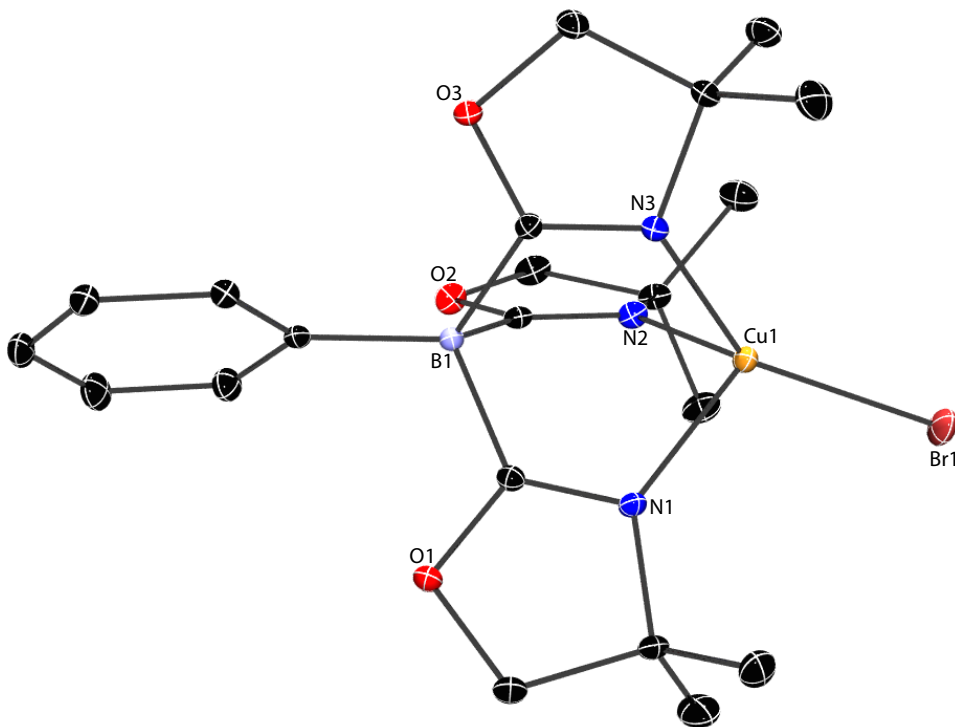


Figure 5.1. Thermal ellipsoid plot of $To^M CuBr$ (**1**). H atoms are not shown for clarity. Selected interatomic distances (Å): Cu1-Br1, 2.292(4); Cu1-N1, 1.937(2); Cu1-N2, 2.081(2); Cu1-N3, 2.000(2). Selected interatomic angles (°): N1-Cu1-Br1, 142.75(4); N2-Cu1-Br1, 112.92(4); N3-Cu1-Br1, 112.79(4), N1-Cu1-N2, 89.71(6); N1-Cu1-N3, 92.59(6); N2-Cu1-N3, 96.01(6).

X-ray quality crystals of **2** and **3** were obtained by recrystallization from toluene and pentane, and X-ray diffraction studies show their structures are distinct from **1**. While **2** (Figure 5.2) is four-coordinate, distorted from ideal pseudo- C_{3v} (B1-Cu1-O4 angle (158.4°), and the dihedral angles are close to 90° : $89.30(7)$, $88.81(7)$, and $90.46(7)^\circ$ like in **1**, the distortions for the two compounds are different. In particular the N2-Cu1-O4 angle ($104.92(7)^\circ$) is much smaller than N1-Cu1-O4 and N3-Cu1-O4 ($132.88(7)$ and $131.73(7)^\circ$, respectively). The N3-Cu1 distance ($2.216(2)$ Å) is much longer than N1-Cu1 and N2-Cu1

(1.964(2) and 1.991(2) Å, respectively). The Cu center is only 0.168(1) Å displaced from a plane defined by N1, N3, and O4, and the sum of the angles of these atoms with Cu1 is 357.5°. Thus, the N2 is the axial ligand in a trigonal monopyramidal geometry.

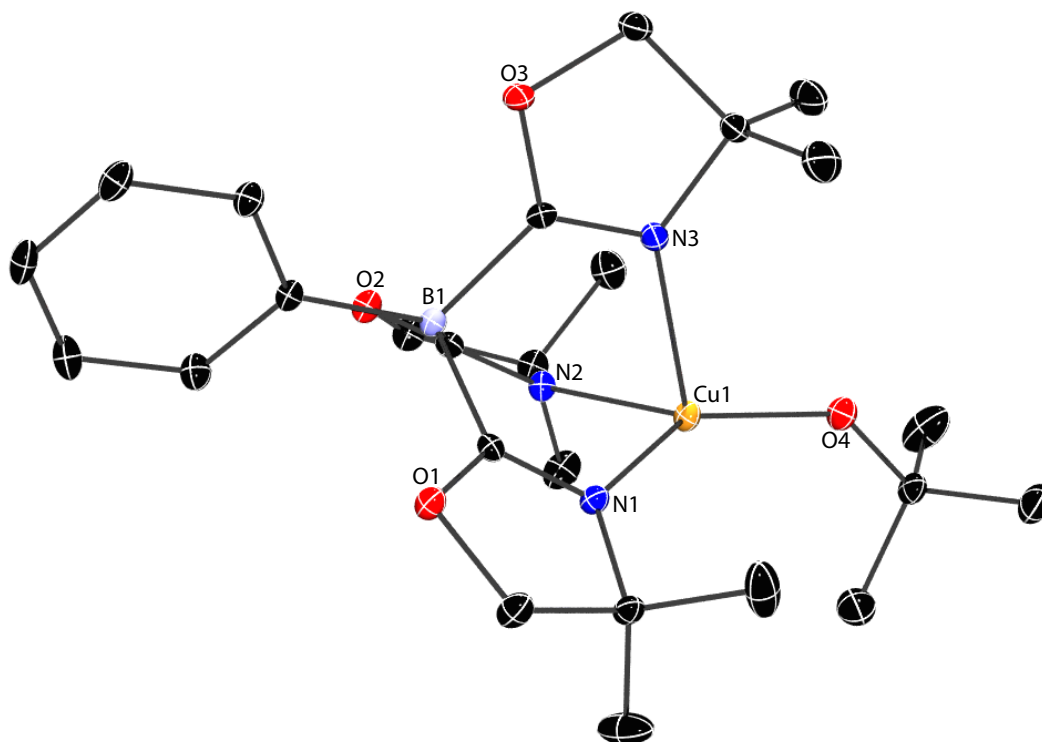


Figure 5.2. ORTEP diagram of $\text{To}^{\text{M}}\text{CuOtBu}$ (**2**). H atoms are not shown for clarity. Selected interatomic distances (Å): Cu1-O4, 1.792(2); Cu1-N1, 1.964(2); Cu1-N3, 2.216(2); Cu1-N2, 1.991(2). Selected interatomic angles (°): N1-Cu1-O4, 132.90(7); N2-Cu1-O4, 104.91(7); N3-Cu1-O4, 131.70(7), N1-Cu1-N2, 88.77(7); N1-Cu1-N3, 92.86(7); N2-Cu1-N3, 87.83(7).

The Cu1-O4 and Cu1-O5 distances in **3** (Figure 5.3) of 2.035(2) and 2.034(2) Å (are longer than in **2** (1.792(2) Å) and shorter than the Co-O distances in $\text{To}^{\text{M}}\text{CoOAc}$ (2.098(2) and 2.089(2) Å). In addition, the pair of largest angles (O-Cu-N) in **3** are nearly equal, which is consistent with nearly square pyramidal geometry around the copper center that is present in $\text{Tp}^{\text{iPr}_2}\text{Cu}(\text{mCBA})$ ⁴⁸ and $[\text{B}(3\text{-iPrpz})\text{CuOAc}]$ ⁴⁹ The ligand arrangement at the metal center

has two nitrogens of To^M and two oxygens of the acetate in the same plane and the other nitrogen of the To^M is in the apical group in the square-pyramidal geometry. The distance between copper and apical nitrogen (N3-Cu1; 2.146(2) Å) is longer than N1-Cu1 and N2-Cu1 (1.996(2) and 1.973(2) Å, respectively).

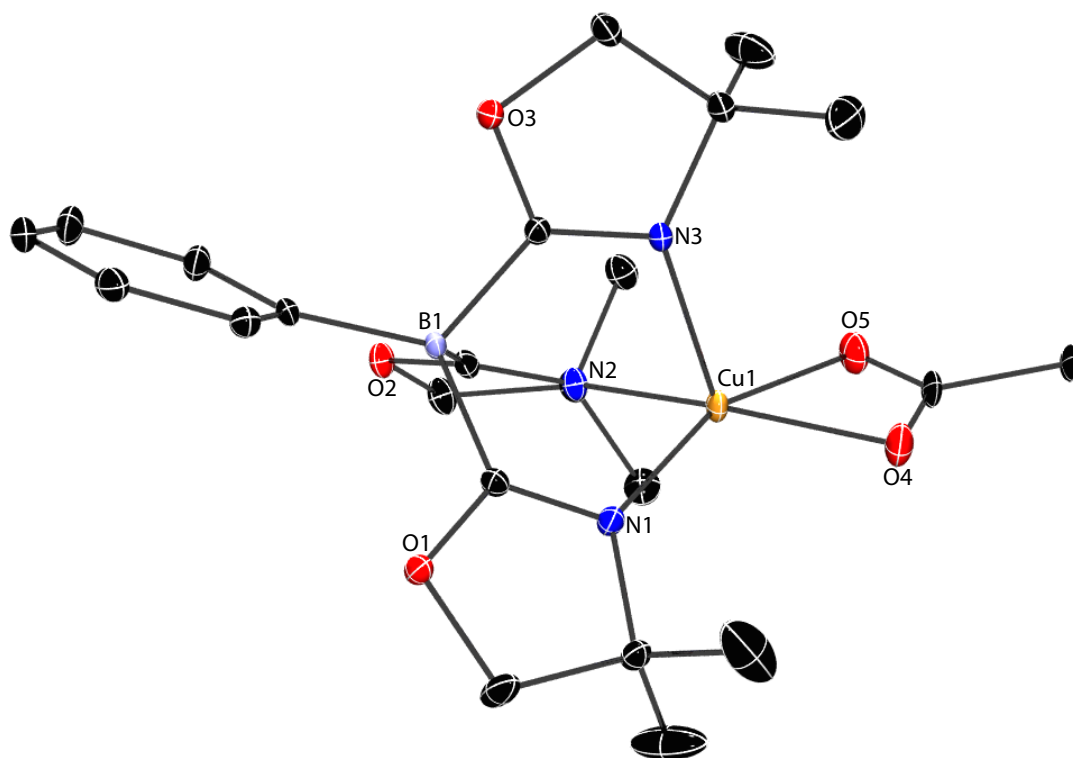


Figure 5.3. ORTEP diagram of $To^M CuOAc$ (**3**). H atoms are not shown for clarity. Selected interatomic distances (Å): Cu1-O4, 2.035(2); Cu1-O5, 2.034(2); Cu1-N1, 2.146(2); Cu1-N2, 1.996(2); Cu1-N3, 1.973(2). Selected interatomic angles (°): N1-Cu1-O4, 104.43(9); N2-Cu1-O4, 101.83(8); N3-Cu1-O4, 161.34(9), N1-Cu1-O5, 106.32(9); N2-Cu1-O5, 159.23(9); N3-Cu1-O5, 100.68(9), N1-Cu1-N2, 91.53(8); N1-Cu1-N3, 89.68(8); N2-Cu1-N3, 89.73(9).

For compound **4** two $[CuTo^M]^+$ units are bridged by two hydroxyl groups to form a dimeric structure (Figure 5.4). The Cu-O bonds 1.962(2), 1.982(2) are longer than the Cu-O bond (1.792(2) Å) in compound **2** and shorter than the Cu-O bonds (2.035(2) and 2.034(2) Å)

in **3**. Similar to compound **3**, **4** has the square-pyramidal geometry at the each metal center where two nitrogens (N1 and N2 or N1' and N2') of To^M and two oxygens of the hydroxyl groups are in the same plane and the other nitrogen (N3 or N3') of the To^M is in the apical position in the square-pyramidal arrangement. The distance between copper and apical nitrogen is considerably longer than copper and nitrogens in equatorial positions. In comparison, $[Cu(HB(3,5-Me_2pz)_3)]_2(OH)_2$ has the similar structure of square-pyramidal geometry at each metal center including one nitrogen of the each Tp ligand in the apical position.^{48,50} The distance between copper and copper in compound **4** is slightly larger than the distance between Cu-Cu in $[Cu(HB(3,5-Me_2pz)_3)]_2(OH)_2$.

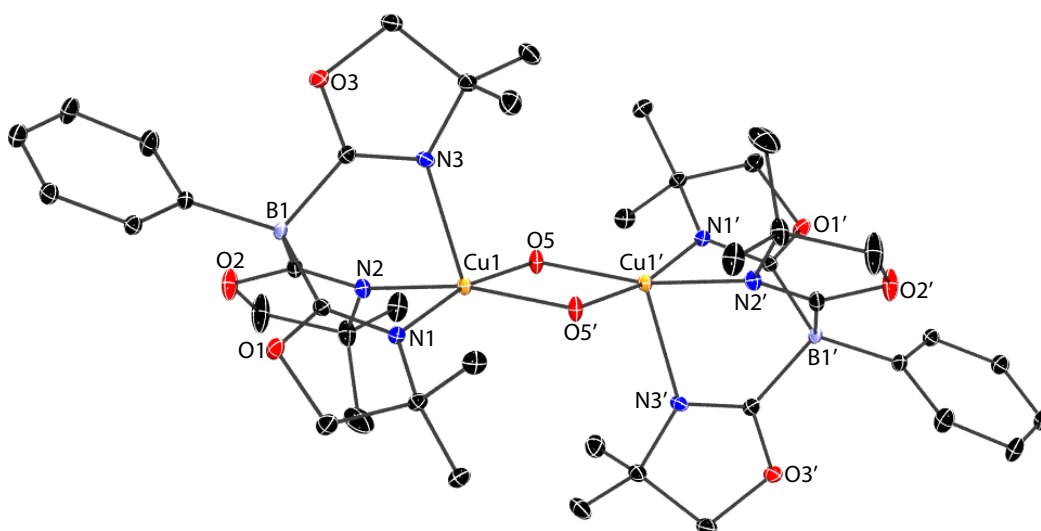


Figure 5.4. ORTEP diagram of $[To^M CuOH]_2$ (**4**). H atoms are not shown for clarity. Selected interatomic distances (Å): Cu1-O5, 1.969(2); Cu1-O5', 1.982(2); Cu1-N1, 2.042(2); Cu1-N3, 2.275(2); Cu1-N1, 2.033(2). Selected interatomic angles (°): N1-Cu1-O4, 95.35(8); N2-Cu1-O4, 104.22(8); N3-Cu1-O4, 168.83(8), N1-Cu1-O5', 162.86(8); N2-Cu1-O5', 106.92(8); N3-Cu1-O5', 97.93(8), N1-Cu1-N2, 89.28(8); N1-Cu1-N3, 88.50(8); N2-Cu1-N3, 86.27(7).

EPR spectra and magnetic measurements. The room temperature magnetic moment (1.650 μ_B) measured by Evan's method in benzene- d_6 is consistent with one unpaired electron ($S = \frac{1}{2}$), as expected for the spin-only value of a d^9 metal center. EPR spectra of **1** measured in 2-methyltetrahydrofuran, glassed at 10 K (Figure 5.5) or in toluene 10 K are broad, but qualitatively similar, and these data suggest that Cu(II) is four coordinate in both the solvents, even at low temperature (in contrast to $\text{Tp}^{i\text{Pr}_2}\text{CuCl}$ which coordinates THF at low temperature).⁴⁸ A g-value at 2.40 (see Table 5.1) was assigned at the center of a broad four-line pattern from copper-hyperfine coupling (68 G) that overlaps with a broad feature. The assignment was facilitated by comparison with $\text{To}^{\text{M}}\text{CuOtBu}$ (**2**), the spectrum of which is better resolved (see below). The fourth peak of that signal overlaps with a broad feature with a g-value of 2.17, which likely represents both g_{xx} and g_{yy} (rather than g_z) since the coordination sphere in the solid-state structure is pseudo- C_s symmetric. The solid-state geometry of $\text{Tp}^{i\text{Pr}_2}\text{CuCl}$ is described as an elongated tetrahedron, and that gives a broad, but distinct EPR spectrum with rhombic site symmetry.⁴⁶

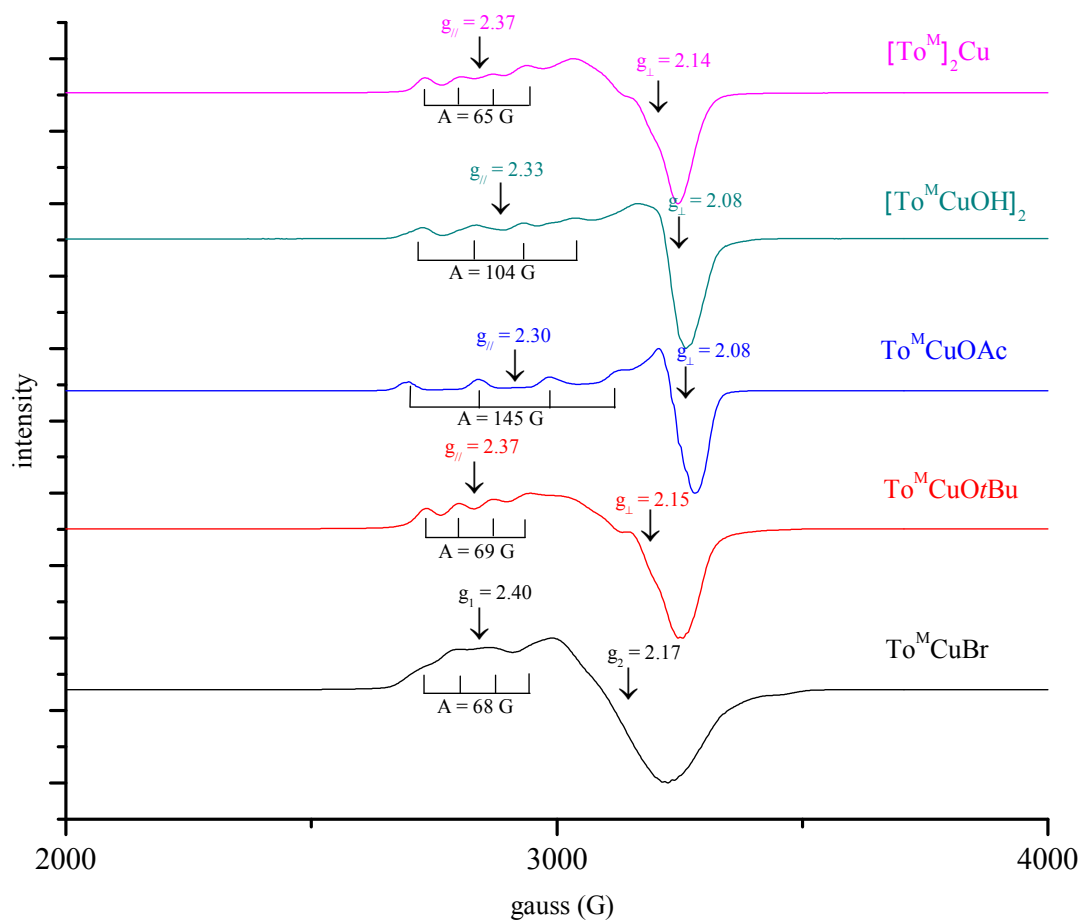


Figure 5.5. EPR spectra of $\text{To}^{\text{M}}\text{CuBr}$, $\text{To}^{\text{M}}\text{CuOtBu}$, $\text{To}^{\text{M}}\text{CuOAc}$, $[\text{To}^{\text{M}}\text{CuOH}]_2$ and $\text{To}^{\text{M}}_2\text{Cu}$ acquired in 2-methyltetrahydrofuran at 10 K.

The magnetic moment values for **2** and **3**, measured by Evan's method at room temperature, were $1.922 \mu_{\text{B}}$ and $1.548 \mu_{\text{B}}$ ($1.167 e^-$) per Cu center. Electron paramagnetic resonance (EPR) experiments for **2** and **3** were performed with coordinating and non-coordinating solvents. The spectra indicate a $d_{x^2-y^2}$ ground state, which is consistent with the tetragonally elongated four-coordinated Cu(II) complexes.⁵¹ In non-coordinating solvent dichloromethane, the spectrum is obtained at 10K showed poorly resolved hyperfine splitting. However, the hyperfine splitting is resolved in the presence of a coordinating

solvent such as 2-Methyltetrahydrofuran (Figure 5.5) resulting in the formation of penta-coordinated adduct. The g_{\parallel} and g_{\perp} values are greater than 2.0023, which indicates that the compounds **2** and **3** are in an axial symmetry.⁵²

Electron paramagnetic resonance (EPR) measurements of **4** in methylene chloride solution at 10K resulted a spectrum with very low intensity peaks indicating the presence of an antiferromagnetic dimeric compound in solution. In contrast, a very strong EPR spectrum is observed in the presence of coordinating solvent such as 2-Methyltetrahydrofuran indicating the formation of a monomeric penta-coordinated adduct that is similar to the EPR spectrum of **2** obtained in 2-Methyltetrahydrofuran (Figure 5.5). The g_{\parallel} and g_{\perp} values are greater than 2.0023, which indicates that the compound **4** in an axial symmetry with ground state of $d_x^2-y^2$ and consistent with pentacoordinated Cu(II) complexes.

Conclusion

We successfully synthesized the compound $To^M CuBr$ from $TITO^M$ and $CuBr_2$ through salt metathesis. This compound is a starting material for the synthesis of various compounds such as $To^M CuOtBu$, $To^M CuOAc$, $To^M Cu$, $To^M_2 Cu$ and $[To^M CuOH]_2$. NMR, FT-IR, UV-VIS and EPR spectroscopies were used to determine the structures of these compounds and these were confirmed by X-ray crystallography. We observed the reduction of copper(II) to copper(I) in our attempt to synthesize monomeric copper hydride from the reaction of $To^M CuOtBu$ with phenylsilane. $To^M Cu$ and $To^M_2 Cu$ were independently synthesized and characterized for the comparison. Since we observed reduction with silanes, there seemed to be a possibility of redox catalysis. Thus, we are currently studying the reactivity of copper(I) complexes with molecular oxygen.

Experimental

General. All reactions were performed under a dry argon atmosphere using standard Schlenk techniques or under a nitrogen atmosphere in a glovebox, unless otherwise indicated. Dry, oxygen-free solvents were used throughout. Benzene, toluene, pentane, methylene chloride, pyridine and tetrahydrofuran were degassed by sparging with nitrogen, filtered through activated alumina columns, and stored under nitrogen. Benzene- d_6 , toluene- d_8 , and tetrahydrofuran- d_8 were heated to reflux over Na/K alloy and vacuum-transferred. Pyridine- d_5 stored over 4 Å mol. sieves in the glovebox prior to use. Anhydrous CuBr_2 and CuBr were purchased from Aldrich and used as received. $\text{KO}t\text{Bu}$ and NaOAc were purified by sublimation before use. PhSiH_3 was distilled and stored over 4 Å mol. sieves in the glovebox prior to use. TiTo^{M} ^{35,36} were synthesized following the reported procedure. ^1H , $^{13}\text{C}\{^1\text{H}\}$, and ^{11}B , spectra were collected either on a Bruker DRX-400 spectrometer, Bruker Avance III 600 spectrometer or an Agilent MR 400 spectrometer. Pyridine- d_5 was referenced in the ^1H NMR spectrum by residual 2H to 8.74 ppm and ^{13}C to the 2C at 150.35 ppm. ^{15}N chemical shifts were determined by ^1H - ^{15}N HMBC experiments on a Bruker Avance III 600 spectrometer. ^{15}N chemical shifts were originally referenced to liquid NH_3 and recalculated to the CH_3NO_2 chemical shift scale by adding -381.9 ppm. ^{11}B NMR spectra were referenced to an external sample of $\text{BF}_3 \cdot \text{Et}_2\text{O}$. EPR were obtained on an X-band Elexsys 580 FT- EPR spectrometer. Elemental analyses were performed using a Perkin-Elmer 2400 Series II CHN/S.

To^MCuBr(1): A solution of TiTo^{M} (0.500 g, 0.852 mmol) in benzene (15 mL) was added to CuBr_2 (0.20 g, 0.90 mmol) suspended in benzene (5 mL). The solution instantaneously became yellow. This mixture was stirred for 2 h at 60 °C and then was filtered. The filtrate

was evaporated to dryness providing an orange solid that was washed with pentane (3×5 mL) and further dried under vacuum yielding orange crystalline, analytically pure $\text{To}^{\text{M}}\text{CuBr}$ (0.416 g, 0.791 mmol, 92.8%). Recrystallization of $\text{To}^{\text{M}}\text{CuBr}$ at -30 °C from concentrated methylene chloride/pentane solution provided single crystals suitable for X-ray diffraction. ^1H NMR (600 MHz, benzene- d_6): δ 10.45 (br, s, 6 H, $\text{CNCMe}_2\text{CH}_2\text{O}$), 8.79 (br, s, 2 H, *ortho*- C_6H_5), 7.95 (br, s, 2 H, *meta*- C_6H_5), 7.10 (br, s, 1 H, *para*- C_6H_5), -1.19 (br, s, 18 H, $\text{CNCMe}_2\text{CH}_2\text{O}$). $^{13}\text{C}\{^1\text{H}\}$ NMR (151 MHz, benzene- d_6): δ 265.84 ($\text{CNCMe}_2\text{CH}_2\text{O}$), 147.55 (C_6H_5), 129.73 (C_6H_5), 128.92 (C_6H_5), 126.15 (C_6H_5), 114.58 ($\text{CNCMe}_2\text{CH}_2\text{O}$), 21.91 ($\text{CNCMe}_2\text{CH}_2\text{O}$). ^{11}B NMR (192.63 MHz, benzene- d_6): δ -9.6 . IR (KBr, cm^{-1}): 3073 (m), 3047 (m) 2967 (s), 2897 (m), 2871 (m), 1590 (s, ν_{CN}), 1493 (w), 1461 (m), 1443 (m), 1387 (m), 1368 (m), 1352 (m), 1274 (m), 1253 (m), 1194 (s), 1160 (m), 1000 (m), 953 (s), 892 (m), 842 (m), 815 (m), 770 (m), 749 (s). Evans method: $\mu_{\text{eff}}(\text{C}_6\text{D}_6) = 1.650 \mu_{\text{B}}$. UV-Vis: λ_{max} , 437 nm (ϵ 3047.12 $\text{L}\times\text{mol}^{-1}\text{cm}^{-1}$); λ_{max} , 279 nm (ϵ 2801.05 $\text{L}\times\text{mol}^{-1}\text{cm}^{-1}$). Anal. Calcd. for $\text{C}_{21}\text{H}_{29}\text{BBrN}_3\text{O}_3\text{Cu}$: C, 47.98; H, 5.56; N, 7.99. Found: C, 47.81; H, 5.54; N, 7.73. Mp 220-223 °C.

$\text{To}^{\text{M}}\text{ZnBr}$: A solution of TiTo^{M} (0.500 g, 0.852 mmol) in benzene (15 mL) was added to ZnBr_2 (0.192 g, 0.852 mmol) suspended in benzene (5 mL). The solution instantaneously became turbid. This mixture was stirred for 12 h at room temperature and then was filtered. The filtrate was evaporated to dryness providing a white solid that was washed with pentane (3×5 mL) and further dried under vacuum yielding white crystalline, analytically pure $\text{To}^{\text{M}}\text{ZnBr}$ (0.426 g, 0.808 mmol, 95%). Recrystallization of $\text{To}^{\text{M}}\text{ZnBr}$ at -30 °C from a concentrated toluene solution provided single crystals suitable for X-ray diffraction studies.

^1H NMR (600 MHz, benzene- d_6): δ 8.25 (d, $^3J_{\text{HH}} = 7.5$ Hz, 2 H, *ortho*- C_6H_5), 7.51 (vt,

$^3J_{\text{HH}} = 7.5$ Hz, 2 H, *meta*-C₆H₅), 7.34 (t, $^3J_{\text{HH}} = 7.3$ Hz, 1 H, *para*-C₆H₅), 3.44 (s, 6 H, CNCMe₂CH₂O), 1.10 (s, 18 H, CNCMe₂CH₂O). $^{13}\text{C}\{^1\text{H}\}$ NMR (151 MHz, benzene-*d*₆): δ 190.93 (br, CNCMe₂CH₂O), 141.26 (*ipso*-C₆H₅), 136.26 (*ortho*-C₆H₅), 127.39 (*meta*-C₆H₅), 126.60 (*para*-C₆H₅), 81.51 (CNCMe₂CH₂O), 65.83 (CNCMe₂CH₂O), 28.16 (CNCMe₂CH₂O). ^{11}B NMR (192.63 MHz, benzene-*d*₆): δ -18.0. ^{15}N NMR (60.9 MHz, benzene-*d*₆): δ -161.2. IR (KBr, cm⁻¹): 3076 (m), 3049 (m) 2968 (s), 2898 (m), 2871 (m), 1594 (s, ν_{CN}), 1495 (w), 1462 (m), 1434 (m), 1388 (m), 1369 (m), 1353 (m), 1273 (m), 1195 (s), 1163 (m), 1016 (m), 956 (s), 894 (m), 844 (m), 819 (m), 750 (m), 711 (s). Anal. Calcd. for C₂₁H₂₉BBN₃O₃Zn: C, 47.81; H, 5.54; N, 7.96. Found: C, 47.97; H, 5.25; N, 7.42. Mp: 296-300 °C (dec).

To^MCuOtBu(2): A benzene solution of To^MCuBr (0.150 g, 0.285 mmol, 8 mL) was added to KOtBu (0.032 g, 0.285 mmol) and dissolved in benzene (3 mL). The reaction mixture was stirred for 3 hours at room temperature. The KBr by-product was removed by filtration to provide a brown solution. Evaporation of the benzene provided a brown solid, which was washed with pentane (3 × 5 mL) and dried under vacuum affording brown crystalline, pure To^MCuOtBu (0.134 g, 0.258 mmol, 89%). Recrystallization of To^MCuOtBu at -30 °C from concentrated solution of toluene was suitable for X-ray. ^1H NMR (600 MHz, benzene-*d*₆): δ 7.71 (2 H), 7.79 (1 H), 6.92 (1 H), 6.10 ppm (6 H), 1.31 ppm (9 H), -0.82 ppm (18 H). ^{11}B NMR (192.63 MHz, benzene-*d*₆): δ -15.7. IR (KBr, cm⁻¹): 3070 (m), 3044 (m) 2967 (s), 2892 (m), 1564 (s, ν_{CN}), 1532 (m), 1463 (w), 1433 (m), 1359 (m), 1281 (m), 1249 (m), 1197 (s), 1183 (m), 1154 (m), 1025 (m), 966 (s), 905 (m), 838 (m). Evans method: μ_{eff} (C₆D₆) = 1.922 μ_{B} . UV-Vis: λ_{max} , 431 nm (ϵ 1516.58 L×mol⁻¹cm⁻¹); λ_{max} , 283 nm (ϵ 966.32 L×mol⁻¹cm⁻¹). Anal. Calcd for C₂₅H₃₈BN₃O₄Cu: C, 57.86; H, 7.38; N, 8.10. Found: C, 57.98; H, 6.94; N,

8.12. Mp 205-208 °C.

To^MCuOAc (3): A benzene solution of To^MCuBr (0.150 g, 0.285 mmol, 8 mL) was added to NaOAc (0.024 g, 0.292 mmol) suspension in benzene (3 mL). The reaction mixture was stirred for 12 h at room temperature. The NaBr by-product was removed by filtration to provide a green solution. Evaporation of the benzene provided a green solid, which was washed with pentane (3 × 5 mL) and dried under vacuum affording crystalline, analytically pure To^MCuOAc (0.127 g, 0.251 mmol, 88%). Recrystallization of To^MCuOAc at -30 °C from concentrated solution of toluene/pentane was suitable for X-ray. ¹H NMR (600 MHz, benzene-*d*₆): δ 7.75 (2 H), 7.46 (6 H), 7.29 (2 H), 6.89 (3 H), 0.65 (21 H). ¹¹B NMR (192.63 MHz, benzene-*d*₆): δ -14.8. IR (KBr, cm⁻¹): 3068 (m), 3046 (m), 2968 (s), 2929 (w), 2894 (m), 1603 (s), 1530 (s), 1471 (s), 1460 (m), 1367 (m), 1353 (s), 1275 (s), 1195 (s), 1162 (m), 958 (s), 895 (w), 814 (w), 745 (s), 705 (s). Evans method: μ_{eff} (C₆D₆) = 1.5474 μ_B. UV-Vis: λ_{max}, 280 nm (ε 6962.25 L×mol⁻¹cm⁻¹). Anal. Calcd for C₂₃H₃₂BN₃O₅Cu: C, 54.72; H, 6.39; N, 8.32. Found: C, 54.66; H, 6.23; N, 7.85. Mp 182-184 °C.

[To^MCuOH]₂(4): A solution of To^MCuOtBu (0.134 g, 0.258 mmol) in benzene (5mL) left in a vial at room temperature in the glove box for few days. To^MCuOtBu decomposes slowly to hydroxyl bridged dimer of [To^MCuOH]₂ (0.107 g, 0.115 mmol, 90 %) which crystalized out of the solution as green compound. The crystals were suitable for X-ray. ¹H NMR (600 MHz, benzene-*d*₆): 7.53 (2 H), 7.36 (1 H), 7.26 (1 H), 7.13 (1 H), 4.33 (6 H), 1.56 (9 H), 1.26 (9 H), -15.67 (br, 1 H, OH). ¹¹B NMR (192.63 MHz, methylene chloride-*d*₂): δ -19.3. IR (KBr, cm⁻¹): 3682 (m), 3067 (m), 3048 (m) 2968 (s), 2928 (m), 2882 (m), 1602 (s), 1579 (s, ν_{CN}), 1492 (w), 1462 (m), 1434 (m), 1383 (m), 1365 (m), 1272 (m), 1178 (s), 1145 (m), 992 (s), 890 (m), 813. UV-Vis: λ_{max}, 341 nm (ε 4067.13 L×mol⁻¹cm⁻¹); λ_{max}, 265 nm (ε 6875.13

$L \times \text{mol}^{-1} \text{cm}^{-1}$). Anal. Calcd for $\text{C}_{42}\text{H}_{60}\text{B}_2\text{N}_6\text{O}_8\text{Cu}_2$: C, 54.50; H, 6.53; N, 9.08. Found: C, 55.01; H, 6.49; N, 8.90. Mp 258-261°C (dec).

Synthesis of $\text{To}^{\text{M}}\text{Cu}(5)$: A solution of $\text{Ti}\{\text{To}^{\text{M}}\}$ (0.500 g, 0.852 mmol) in pyridine (15 mL) was added to CuBr (0.122 g, 0.852 mmol) suspended in pyridine (10 mL). The solution instantaneously became yellow and turbid. This mixture was stirred for 12 h at ambient temperature and then was filtered. The filtrate was evaporated to dryness providing a light yellow solid that was washed with pentane (3×5 mL) and further dried under vacuum yielding $\text{To}^{\text{M}}\text{Cu}$ (0.358 g, 802 μmol , 94%) as a light yellow solid. **Alternative synthesis of $\text{To}^{\text{M}}\text{Cu}$ from $\text{To}^{\text{M}}\text{CuO}t\text{Bu}$.** PhSiH_3 (0.021 g, 0.193 mmol) was added to $\text{To}^{\text{M}}\text{CuO}t\text{Bu}$ (0.1 g, 0.193 mmol) dissolved in benzene (10 mL). A light yellow precipitate formed, which was isolated by filtration. The solid was washed with pentane (3×5 mL) and dried under vacuum yielding light yellow amorphous, analytically pure $\text{To}^{\text{M}}\text{Cu}$ (0.079 g, 0.177 mmol, 91 %). ^1H NMR (600 MHz, pyridine- d_5): δ 8.35 (d, $^3J_{\text{HH}} = 7.3$ Hz, 2 H, *ortho*- C_6H_5), 7.41 (vt, $^3J_{\text{HH}} = 7.4$ Hz, 2 H, *meta*- C_6H_5), 7.23 (t, $^3J_{\text{HH}} = 7.3$ Hz, 1 H, *para*- C_6H_5), 3.78 (s, 6 H, $\text{CNCMe}_2\text{CH}_2\text{O}$), 1.15 (s, 18 H, $\text{CNCMe}_2\text{CH}_2\text{O}$). $^{13}\text{C}\{^1\text{H}\}$ NMR (151 MHz, pyridine- d_5): δ 185.18 (br, $\text{CNCMe}_2\text{CH}_2\text{O}$), 135.21 (*ortho*- C_6H_5), 127.42 (*meta*- C_6H_5), 125.31 (*para*- C_6H_5), 77.62 ($\text{CNCMe}_2\text{CH}_2\text{O}$), 67.44 ($\text{CNCMe}_2\text{CH}_2\text{O}$), 29.14 ($\text{CNCMe}_2\text{CH}_2\text{O}$). ^{11}B NMR (192.63 MHz, pyridine- d_5): δ -15.9. ^{15}N NMR (60.9 MHz, pyridine- d_5): δ -150.1. IR (KBr, cm^{-1}): 3068 (m), 3046 (m), 2963 (m), 2929 (m), 2876 (m), 1582 (s, νCN), 1488 (m), 1462 (m), 1431 (m), 1383 (m), 1365 (m), 1346 (m), 1262 (m), 1195 (s), 1131 (m), 1000(m), 973 (s), 926 (m), 886 (m), 834 (m), 768 (m), 731 (m), 704 (s). Anal. Calcd. for $\text{C}_{21}\text{H}_{29}\text{BN}_3\text{O}_3\text{Cu}$: C, 56.57; H, 6.56; N, 9.43. Found: C, 56.54; H, 6.25; N, 9.41. Mp 271-275°C (dec).

To^M₂Cu(6): A solution of 2 equivalents of Tl{To^M} (0.500 g, 0.852 mmol) in tetrahydrofuran (10 mL) was added to CuBr₂ (0.20 g, 0.90 mmol) suspended in tetrahydrofuran (5 mL). The solution instantaneously became yellow and turbid. This mixture was stirred for 2 h at ambient temperature and then filtered. The filtrate was evaporated to dryness providing a yellow solid that was washed with pentane (3 × 5 mL) and further dried under vacuum yielding crystalline, analytically pure {To^M}₂Cu (0.416 g, .791 mmol, 92%). Recrystallization of {To^M}₂Cu at -30 °C from concentrated solution of toluene was suitable for X-ray. ¹H NMR contains several peaks at 14.75, 7.63, 7.34, 6.74, 6.66, 3.72, 1.95, 1.33, 1.30, 0.20, -0.25 and -1.18 ppm. ¹¹B NMR (192.63 MHz, benzene-*d*₆): δ -30.1. IR (KBr, cm⁻¹): 3069 (m), 3045 (m), 2966 (m), 2930 (m), 2882 (m), 1605 (m), 1561 (s, νCN), 1530 (m), 1490 (m), 1463 (m), 1433 (m), 1370 (m), 1359 (m), 1285 (m), 1249 (m), 1198 (s), 1153 (m), 1068 (m), 1026 (m), 1004 (m), 965 (s), 837 (s), 810 (s), 738 (m), 712 (s). Evans method: μ_{eff} (C₆D₆) = 1.666 μ_B. UV-Vis: λ_{max}, 424 nm (ε 486.63 L×mol⁻¹cm⁻¹); λ_{max}, 375 nm (ε 541.98 L×mol⁻¹cm⁻¹); λ_{max}, 260 nm (ε 1400.32 L×mol⁻¹cm⁻¹). Anal. Calcd. for C₄₂H₅₈B₂N₆O₆Cu: C, 47.98; H, 5.56; N, 7.99. Found: C, 47.55; H, 5.37 ; N, 7.81. Mp 233-236°C (dec).

Calculation of magnetic moment using Evan's method.

Magnetic susceptibility measurements were measured by the Evans method at room temperature and calculated using the following equation.

$$\chi_{mol} = \frac{3\Delta\delta}{400\pi C}$$

where χ_{mol} is the magnetic susceptibility of the solute, C the concentration of the solute and $\Delta\delta$ chemical shift difference. The magnetic moment (μ) and number of unpaired electrons (n)

were calculated by following equations.

$$\mu = 2.828(\chi_{mol}T)^{1/2}$$

$$n = (1 + \mu^2)^{1/2} - 1$$

References:

1. Trofimenko, S. *J. Am. Chem. Soc.* **1966**, *88*, 1842-844.
2. Kunishita, A.; Gianetti, T. L.; Arnold, J. *Organometallics* **2012**, *31*, 372-380.
3. Shirasawa, N.; Akita, M.; Hikichi, S.; Moro-oka, Y. *Chem. Commun.* **1999**, 417-418.
4. Jové, F. A.; Pariya, C.; Scoble, M.; Yap, G. P. A.; Theopold, K. H. *Chemistry - A European Journal* **2011**, *17*, 1310-1318.
5. Shay, D. T.; Yap, G. P. A.; Zakharov, L. N.; Rheingold, A. L.; Theopold, K. H. *Angew. Chem., Int. Ed.* **2005**, *44*, 1508-1510
6. Jewson, J. D.; Liable-Sands, L. M.; Yap, G. P. A.; Rheingold, A. L.; Theopold, K. H. *Organometallics* **1999**, *18*, 300-305.
7. Han, R.; Gorrell, I. B.; Looney, A. G.; Parkin, G. *J. Chem. Soc., Chem. Commun.* **1991**, 717-719
8. Trofimenko, S. *Scorpionates; The Coordination Chemistry of Polypyrazolylborate Ligands*; Imperial College Press: London, UK, **1999**
9. Trofimenko, S. *J. Am. Chem. Soc.* **1970**, *92*, 5118-5126.
10. Trofimenko, S. *Chem. Rev.* **1993**, *93*, 943-980
11. Egan, J. W.; Haggerty, B. S.; Rheingold, A. L.; Sendlinger, S. C.; Theopold, K. H. *J. Am. Chem. Soc.* **1990**, *112*, 2445-2446.
12. Que, L.; Tolman, W. B. *Nature* **2008**, *455*, 333-340.
13. Fontecave, M.; Pierre, J.-L. *Coord. Chem. Rev.* **1998**, *170*, 125-140.
14. Kitajima, N.; Fujisawa, K.; Fujimoto, C.; Morooka, Y.; Hashimoto, S.; Kitagawa, T.; Toriumi, K.; Tatsumi, K.; Nakamura, A. *J. Am. Chem. Soc.* **1992**, *114*, 1277-1291.
15. Yun, J.; Kim, D.; Yun, H. *Chem. Commun.* **2005**, 5181-5183.
16. Lee, D.-w.; Yun, J. *Tetrahedron Letters* **2004**, *45*, 5415-5417.
17. Brestensky, D. M.; Huseland, D. E.; McGettigan, C.; Stryker, J. M. *Tetrahedron Letters* **1988**, *29*, 3749-3752.
18. Mahoney, W. S.; Brestensky, D. M.; Stryker, J. M. *J. Am. Chem. Soc.* **1988**, *110*, 291-293.
19. Appella, D. H.; Moritani, Y.; Shintani, R.; Ferreira, E. M.; Buchwald, S. L. *J. Am. Chem. Soc.* **1999**, *121*, 9473-9474.
20. Lee, D.-w.; Yun, J. *Tetrahedron Letters* **2005**, *46*, 2037-2039.
21. Mori, A.; Fujita, A. *Chem. Commun.* **1997**, 2159-2160.
22. Ito, H.; Ishizuka, T.; Arimoto, K.; Miura, K.; Hosomi, A. *Tetrahedron Letters* **1997**, *38*, 8887-8890.
23. Lipshutz, B. H.; Keith, J.; Papa, P.; Vivian, R. *Tetrahedron Letters* **1998**, *39*, 4627-4630.
24. Chiu, P.; Li, Z.; Fung, K. C. M. *Tetrahedron Letters* **2003**, *44*, 455-457.

25. Rauch, M.; Rong, Y.; Sattler, W.; Parkin, G. *Polyhedron* **2016**, *103*, 135-140.
26. Sattler, W.; Parkin, G. *J. Am. Chem. Soc.* **2011**, *133*, 9708.
27. Nyder, C. J.; Heeg, M. J.; Winter, C. H. *Inorg. Chem.* **2011**, *50*, 9210-9212.
28. Mukherjee, D.; Ellern, A.; Sadow, A. D. *J. Am. Chem. Soc.* **2010**, *132*, 7582-7583.
29. Xu, S.; Magoon, Y.; Reinig, R. R.; Schmidt, B. M.; Ellern, A.; Sadow, A. D. *Organometallics* **2015**, *34*, 3508-3519.
30. Rit, A.; Zanardi, A.; Spaniol, T. P.; Maron, L.; Okuda, J. *Angew. Chem., Int. Ed.* **2014**, *53*, 13273-13277.
31. Mukherjee, D.; Thompson, R. R.; Ellern, A.; Sadow, A. D. *ACS Catal.* **2011**, *1*, 698-702.
32. Sattler, W.; Parkin, G. *J. Am. Chem. Soc.* **2012**, *134*, 17462-17465.
33. Sattler, W.; Rucolo, S.; Rostami Chaijan, M.; Nasr Allah, T.; Parkin, G. *Organometallics* **2015**, *34*, 4717-4731.
34. Mealli, C.; Arcus, C. S.; Wilkinson, J. L.; Marks, T. J.; Ibers, J. A. *J. Am. Chem. Soc.* **1976**, *98*, 711-718.
35. Dunne, J. F.; Su, J.; Ellern, A.; Sadow, A. D. *Organometallics* **2008**, *27*, 2399-2401.
36. Ho, H.-A.; Dunne, J. F.; Ellern, A.; Sadow, A. D. *Organometallics* **2010**, *29*, 4105-4114.
37. Zhang, L.; Cheng, J.; Hou, Z. *Chem. Commun.* **2013**, *49*, 4782-4784.
38. Zhang, L.; Hou, Z. *Chem. Sci.* **2013**, *4*, 3395-3403.
39. Tolman, W. B. *Inorg. Chem.* **1991**, *30*, 4877-4880.
40. Deacon, G. *Coord. Chem. Rev.* **1980**, *33*, 227-250.
41. Dunne, J. F.; Fulton, D. B.; Ellern, A.; Sadow, A. D. *J. Am. Chem. Soc.* **2010**, *132*, 17680-17683.
42. Yoon, K.; Parkin, G. *Polyhedron* **1995**, *14*, 811-821.
43. Fujisawa, K.; Tada, N.; Ishikawa, Y.; Higashimura, H.; Miyashita, Y.; Okamoto, K.-i. *Inorg. Chem. Commun.* **2004**, *7*, 209-212.
44. Bongiovanni, J. L.; Rowe, B. W.; Fadden, P. T.; Taylor, M. T.; Wells, K. R.; Kumar, M.; Papish, E. T.; Yap, G. P. A.; Zeller, M. *Inorg. Chim. Acta* **2010**, *363*, 2163-2170.
45. Higashimura, H.; Kubota, M.; Shiga, A.; Fujisawa, K.; Moro-oka, Y.; Uyama, H.; Kobayashi, S. *Macromolecules* **2000**, *33*, 1986-1995.
46. Kitajima, N.; Fujisawa, K.; Morooka, Y. *J. Am. Chem. Soc.* **1990**, *112*, 3210-3212.
47. Dias, H. V. R.; Wang, X.; Rajapakse, R. M. G.; Elsenbaumer, R. L. *Chem. Commun.* **2006**, 976-978.
48. Kitajima, N.; Fujisawa, K.; Moro-oka, Y. *Inorg. Chem.* **1990**, *29*, 357-358.
49. Kitano, T.; Sohrin, Y.; Hata, Y.; Mukai, H.; Wada, H.; Ueda, K. *Polyhedron* **2004**, *23*, 283-289.
50. Kitajima, N.; Koda, T.; Hashimoto, S.; Kitagawa, T.; Morooka, Y. *J. Am. Chem. Soc.* **1991**, *113*, 5664-5671.
51. Chen, P.; Fujisawa, K.; Solomon, E. I. *J. Am. Chem. Soc.* **2000**, *122*, 10177-10193.
52. Shaban, S. Y.; Ramadan, A. E.-M. M.; Ibrahim, M. M.; Mohamed, M. A.; van Eldik, R. *Dalton Trans.* **2015**, *44*, 14110-14121.

CHAPTER 6: GENERAL CONCLUSION

The developments of monocyclopentadienyl systems with an additional donor ligand have been very effective with various metal centers. These systems are attracting increased interest in the chemistry of early transition metals because of their potential applications in catalysis. In this context, new monoanionic cyclopentadienyl-bis(oxazoline) ligands have been synthesized and their metal complexes have been used in the hydroamination catalysis. Interestingly, the cyclopentadienyl-bis(oxazoline) ligands on zirconium gives more active catalytic species than $\text{CpZr}(\text{NMe}_2)_3$ catalyst. Varying the substituents on the oxazoline ring provides a chiral ligands and their metal complexes can be used in asymmetric catalysis, including hydroamination. Future work will be continued in synthesizing chiral ligands by varying the substituents on the oxazoline ring.

Surface organometallic chemistry (SOMC) is a powerful approach in heterogeneous catalyst development and making an impact in industrial process. The reaction of early transition metal amides or rare earth silazides with partially dehydroxylated supports results in the formation of amine and heterogeneous catalysts. These surface organometallic compounds were characterized by NMR, IR and elemental analysis (CHN and ICP-OES). The surface-supported zirconium amide is an efficient catalyst for the reduction of carbonyl containing compounds using pinacolborane as hydride source. The surface supported rare earth silazides are efficient catalysts for the hydroamination of amino alkenes and bicyclization of aminodialkenes. Additionally, future work will be continued in grafting bis(oxazoline)zirconium amides of bis(oxazoline) rare earth silazide complexes on

mesoporous silica for developing heterogeneous catalysts for the asymmetric hydroboration and hydroamination catalysis.